Formulation and stabilization of colloidal polyelectrolyte complexes of chitosan and siRNA

Tim Delas

université de BORDEAUX

THÈSE PRÉSENTÉE

POUR OBTENIR LE GRADE DE

DOCTEUR DE

L'UNIVERSITÉ DE BORDEAUX

ÉCOLE DOCTORALE DES SCIENCES CHIMIQUES

SPÉCIALITÉ POLYMÈRES

Par Tim DELAS

Formulation et stabilisation de complexes colloïdaux de polyélectrolytes à base de chitosane et de siRNA

Formulation and stabilization of colloidal polyelectrolyte complexes of chitosan and siRNA

Sous la direction de : Christophe SCHATZ

Co-directeur : Olivier SANDRE

Soutenue le 22 mars 2021

Membres du jury :

Mme. CRAUSTE-MANCIET, Sylvie	Professeure, Université de Bordeaux	Examinatrice
M. CHRISTENSEN, Bjørn E.	Professeur, NTNU, Norway	Rapporteur
M. MÜLLER, Martin	Senior Scientist, Leibniz-IPF Dresden, Germany	Rapporteur
M. HILLAIREAU, Hervé	Professeur, Université Paris-Saclay	Examinateur
M. TROMBOTTO, Stéphane	Maître de conférences, Univ. Claude Bernard Lyon 1	Examinateur
M. CHAPEL, Jean-Paul	Directeur de recherche, CNRS, Université de Bordeaux	Président
M. SCHATZ, Christophe	Maître de conférences, Bordeaux INP	Directeur de thèse
M. SANDRE, Olivier	Directeur de recherche, CNRS, Université de Bordeaux	Co-directeur

Titre : Formulation et stabilisation de complexes de polyélectrolytes à base de chitosane et de siRNA

Résumé : La présence de fortes interactions électrostatiques entre les acides nucléiques tel que l'ADN, l'ARN et des polycations permet l'élaboration de particules colloïdales appelées complexes de polyélectrolytes (PECs). Cette approche permettant la formation de vecteurs non-viraux pour la délivrance de matériel génétique a fait l'objet de nombreuses études basées sur l'utilisation de chitosane comme polycation. Dans le cadre de cette thèse, ce dernier a été étudié pour ses propriétés de complexation avec des petits ARN interférents (small interfering RNA, siRNA).

Dans un premier temps, des oligosaccharides de chitosane (COS) ont fait l'objet d'une étude quant à leurs propriétés en solution et de complexation avec des siRNA. L'effet de longueur de chaîne sur la solubilité du chitosane et leur comportement complexant a pu être étudié. Par la suite, la stabilité colloïdale en conditions physiologiques des PECs formés à partir de chitosane et de siRNA a été abordée. La déprotonation du chitosane étant un élément rédhibitoire quant à la stabilité des complexes, l'introduction d'ions zinc lors de la formulation des complexes a permis une amélioration de la stabilité à pH physiologique. De plus, l'augmentation du degré d'acétylation du chitosane a également permis une nette amélioration de la stabilité des complexes à des concentrations physiologiques en sel. Avec l'introduction de zinc, une étude portant sur les interactions entre des ions métalliques et le siRNA a également été menée. Finalement, une nouvelle synthèse menant à la formation d'un nouveau copolymère à base de chitosane a été réalisée, permettant d'obtenir des structures encore inexplorées à base de chitosane telles que des micelles ou des structures de type conjugués.

Mots clés : chitosane, oligosaccharide, siRNA, interactions électrostatiques, complexes de polyélectrolytes, stabilité colloïdale, conjugué

Title: Formulation and stabilization of colloidal polyelectrolyte complexes of chitosan and siRNA

Abstract: The presence of strong electrostatic interactions between nucleic acids such as DNA, RNA and polycations leads to the formation of colloidal particles called polyelectrolyte complexes (PECs). This approach, which allows the formation of non-viral vectors for genetic material delivery, has been the subject of numerous studies based on the use of chitosan as polycation. In the framework of this thesis, the latter was studied for its complexing properties towards small interfering RNA (siRNA).

First, chitosan oligosaccharides (COS) were studied for their solution properties and complexation properties with siRNA. The effect of chain length on the solubility of chitosan and their complexing behaviour was demonstrated. Subsequently, the colloidal stability of PECs formed between chitosan and siRNA under physiological conditions was addressed. As the deprotonation of chitosan is redhibitory for the stability of the complexes, it was shown that the introduction of zinc ions in the formulation of complexes allowed to improve their stability at physiological pH. Moreover, the increase in the degree of acetylation of chitosan also allowed a clear improvement in the stability of the complexes at physiological salt conditions. With the introduction of zinc, a study of the interactions between metal ions and siRNA was also carried out and was able to highlight the strong interactions involved between metal ions and siRNA. Finally, a new synthesis leading to the formation of a new chitosan-based copolymer was carried out, making it possible to obtain as yet unexplored chitosan-based structures such as micelles or conjugate-type structures.

Keywords: chitosan, oligosaccharide, siRNA, electrostatic interaction, polyelectrolyte complexes, colloidal stability, conjugates

Unité de recherche

Laboratoire de Chimie des Polymères Organiques,
Équipe Polymer Self Assembly and Life Sciences,
UMR 5629, Unité mixte de recherche Université de Bordeaux/CNRS/Bordeaux INP

16 Avenue Pey-Berland 33607

Pessac Cedex France

Acknowledgements – Remerciements

Bien qu'il s'agisse d'un travail personnel, une thèse s'effectue entouré de beaucoup de monde sans qui rien ne serait possible.

A commencer par les membres jury de cette thèse qui ont accepté de prendre le temps d'évaluer ce travail et de participer à une riche discussion lors de la soutenance, malgré les conditions à distance auxquelles il a fallu faire face.

Également, il est impossible d'effectuer une thèse et de la recherche sans soutien financier, apporté par l'ANR pour le projet TANGO, Campus France qui a financé les divers déplacements à Prague ainsi que le réseau TGIR qui a permis un déplacement à Lyon pour l'utilisation du 1 GHz.

Cet ambitieux projet a pu voir le jour grâce à l'investissement de différents laboratoires impliqués dans le projet TANGO : l'IMP à Lyon avec l'implication de Thierry Delair, Stéphane Trombotto, Agnès Crepet, Jimmy Faivre et Maxime Mock-Joubert et l'IGPS à Paris avec la collaboration d'Hervé Hillaireau, Elias Fattal et Franceline Reynaud. Ce projet a également bénéficié de l'expertise du CRPP à Bordeaux avec l'aide de François Dole et Jean-Paul Chapel. Je remercie énormément Jiří Pánek de l'IMC à Prague qui nous a si gentiment accueillis à plusieurs reprises, a pris énormément de son temps pour réaliser les mesures de FCS avec nous mais qui nous a aussi fait découvrir la ville, la bière locale et m'a fait partager la fête de Noël de son laboratoire. Je remercie chaleureusement tous ces collaborateurs pour leur implication dans le projet TANGO et les riches discussions.

Je remercie mes directeurs de thèse, à commencer par Olivier Sandre, qui malgré son implication à distance dans le projet, a toujours été présent, prêt à échanger, à suggérer ses idées et à signer mes papiers... Merci de partager ton puit de savoir sans fin et des informations toujours à point nommé.

Christophe Schatz, mon directeur de thèse qui m'a fait confiance avec le lancement de ce nouveau projet au laboratoire, toujours apportant un regard critique sur les résultats, un optimisme scientifique rafraichissant tout au long de ma thèse et une grande disponibilité pour discuter de résultats, de nouveaux papiers, d'idées… Un des rares directeur de thèse qui parvient à se dégager du temps ici et là pour effectuer des manips et que l'on a le plaisir de parfois retrouver à un coin de sa paillasse. J'espère avoir su capter les éléments essentiels de ton enseignement et la physicochimie pragmatique de terrain à laquelle tu m'as formé au cours de ces 3 ans et demi.

Jean-Paul Chapel, mon maître de stage de M1 et M2 grâce à qui j'ai pu me retrouver en thèse au LCPO et que j'ai eu le plaisir de retrouver régulièrement pendant ma thèse jusqu'à ma soutenance.

Je remercie également tous les spécialistes qui m'ont formé et aidé tout au long de ma thèse. François Dole du CRPP qui m'a formé sur l'ITC, qui a pris le temps de remettre en état une ITC un peu poussiéreuse et qui m'a permis d'être autonome très rapidement sur cet appareil. Les spécialistes du LCPO : Amélie, toujours très réactive que ce soit pour trouver un créneau rapidement pour passer quelques échantillons en SEC ou pour aider à retrouver une commande en cours… Anne-Laure, qui s'est rendu disponible une semaine pour m'accompagner faire des manips à Lyon au 1 GHz, qui parvient à se rendre disponible pour discuter de résultats, passer les échantillons de beaucoup de monde et…à faire une thèse en même temps !! Un grand merci à toutes les deux. Merci à Sylvain, efficace bras droit d'Amélie pour la SEC et pour son travail titanesque entreprit pour le rangement des produits chimiques, bon courage pour la fin ! Merci à Paul pour son aide sur l'infrarouge, à mettre au point cette technique à breveter pour analyser l'ARN… Merci également à Manu et sa grande maîtrise de l'AFM associée à sa méticulosité qui m'ont permis de compléter ma thèse avec de belles images de microscopie.

Un grand merci à Charlotte Cabanne du CBMN, qui s'est rendue extrêmement disponible au retour du confinement pour mettre en œuvre les manips de la dernière chance de cette thèse qui seront très profitables par la suite.

J'ai eu la chance de faire un bout de chemin avec plusieurs stagiaires qui ont contribué à l'avancement de ce projet. Merci à Myriam et Mirjam et bien sûr à Victor.

Merci au personnel administratif du LCPO : Corinne, Dominique, Séverine et Claude qui font de ce labo une machine bien huilée, toujours disponibles pour répondre aux interrogations des jeunes du laboratoire et réagir rapidement aux requêtes de dernière minute des chercheurs.

J'ai pu intégrer une équipe de recherche dirigée par Sébastien Lecommandoux portant également la responsabilité de directeur de laboratoire, que je remercie pour m'avoir accueilli dans cette équipe et ce laboratoire mais également pour sa gestion par ces temps de pandémie qui a permis de privilégier le travail expérimental des doctorants et post-doctorants. J'ai eu la chance d'intégrer une équipe de recherche dont les permanents sont impliqués dans les différents travaux de recherches, partageant leur expertise et leur bonne humeur et qui font de « l'étage N2 » un endroit si agréable où travailler. Merci à Sébastien, Colin, Angela, Elisabeth et Jean-François. Un grand merci également à Bertrand pour son temps, ses explications et discussions sur la bio tout au long de ma thèse mais aussi sa surfeur-positivo attitude inébranlable qui peut mettre la pêche pour toute une journée lorsqu'on y est exposé dès le matin.

Cette équipe est complétée par plein de monde qui y maintient la bonne ambiance et que je tiens à remercier : Manon, Florian, Megi, Sophie, Marie Haddou, Léa, Guillaume C., Romane, Boris, Mostafa, Fanny et Clémence. Merci à tous ceux que j'ai pu retrouver dans le bureau N2-29 et qui m'y ont accueilli : Louis et toutes ses anecdotes et casses-têtes, Julien le doyen, le papa du bureau et son café qui met de bons coups de fouets, Michèle avec toujours une énergie débordante, merci à Marie Rosselin (la maman du bureau ?) pour sa sérénité et tous ses bons conseils, merci pour ces bons moments dans le bureau (avec ces surprises dans les tiroirs) comme en dehors. Et Quentin S., dont je me souviendrai en réalité comme un N2 ! Thank you Tingting for your good mood and all these joyful discussions in the lab. Thank you Hang for your wisdom, these shared moments (and beers) and discussions. Thank you

Ye machine, Vangelis and Vusala to contribute to the good atmosphere in the office. And thank you Diana ! (and your loud music 😉)

Merci aux autres anciens qui m'ont accueilli dans l'équipe, Coralie, Guillaume G., qui avec Martin et Michèle formaient un sacré groupe rythmé d'aller-retours au RU, d'escalade et de pauses au labo.

Le récemment renommé « labo des bests », le N2-21, a vu du monde pendant mon séjour et chaque membre justifie ce nouveau nom du labo. Mon ancienne voisine de paillasse Monica – l'unique partenaire chitosane –, la plus récente Nadia et ces questions à se poser entre non-chimistes… Et encore plus récemment Clémence. Merci au duo de choc Pierre-Anouk pour cette ambiance renouvelée dans le labo, cette organisation impeccable et tous ces échanges ! Et bien sûr Martin, un pilier qui est resté pendant ces années et qui a porté plusieurs casquettes : DJ, grand sage, partenaire CAES/pauses café/jogger/grimpeur et surtout ami.

Merci à Pedro, toujours partant pour une bière (ou une partie de CS en ligne), pour discuter et partager sa philosophie.

J'aimerais remercier également les anciens ou actuels dont j'ai croisé la route dans le laboratoire et qui rendent l'expérience si enrichissante, faisant du LCPO une très grande famille composée de doctorants, post-docs et stagiaires.

Cette thèse fut rythmée de sorties vélos et de « quelques » bières grâce à l'Adoc, les amis de master, merci à Thomas le président, Simon, Iñaki, Lara, David et bien d'autres !

Je remercie Sven, un ami formidable toujours présent depuis trèèèèès longtemps, optimiste et combatif de la vie qui va jusqu'au bout de ses plans et dont la détermination restera toujours un exemple pour moi. Raphaël, la surprise de ta connexion à ma soutenance… Loïc, un très cher ami parfois perdu de vue mais que je retrouve toujours avec tellement de plaisir. Dorian, merci également de répondre toujours présent pour partager un moment.

Je finirai par remercier toute ma famille, en particulier bien sûr mes parents, Eric et Stéphanie, qui ont toujours soutenu leurs enfants dans ce qu'ils ont entrepris que ce soit dans les bons ou mauvais moments, que ce soit financièrement ou moralement et qui nous ont toujours encouragés et enveloppés de bienveillance. Mon frère et ma sœur, Gaston et Marie, qui m'ont fait l'énorme plaisir de se déplacer pour cette soutenance et qui m'impressionnent constamment par leur volonté pour affronter l'adversité. Benjamin, merci pour ton soutien et ta gentillesse. Merci à Marty et Titou. Et enfin merci à Anna sans qui je ne serai jamais allé aussi loin, qui a été présente quotidiennement pour traverser les mauvais moments mais surtout avec qui j'ai pu partager les meilleurs moments depuis six ans qui remplissent ma vie de bonheur.

« Il ne sert à rien à l'homme de gagner la Lune s'il vient à perdre la Terre. »

François Mauriac (1885-1970)

« Nous sommes faits d'un étrange mélange d'acides nucléiques et de souvenirs, de rêves et de protéines, de cellules et de mots. »

François Jacob, Prix Nobel de médecine et de physiologie (1920-2013)

Résumé

Le développement des nanotechnologies pour la médecine a amélioré considérablement toutes sortes de traitements et de techniques d'imagerie médicale. En particulier, la vectorisation de médicaments et biomolécules biologiquement actives a été l'objet de beaucoup de recherches. En effet, le domaine de l'auto-assemblage de chaînes de polymère basé sur leur nanostructuration, induite par diverses interactions telles qu'hydrophobes ou électrostatiques a permis l'encapsulation de diverses molécules thérapeutiques dans des objets nanométriques. Ces objets présentant diverses morphologies peuvent se présenter sous forme de vésicules, de micelles ou de complexes nanométriques appelés complexes de polyélectrolytes. En particulier, la délivrance de gène (ADN, ARN) – pouvant être considéré comme un polymère portant des charges négatives (polyanion) – a été très développée sur la base d'interactions électrostatiques avec un polymère de charge opposée (polycation). Ainsi, les fortes interactions électrostatiques présentes entre deux polymères de charge opposée peuvent induire la formation de particules appelées PECs (polyelectrolyte complexes). Les propriétés de ces derniers sont définies par de nombreux paramètres tels que la longueur des chaînes polymère, la densité de charge d'une chaîne, le pH et la force ionique de la solution ainsi que la température. De plus, afin d'assurer la protection du gène vectorisé et une certaine stabilité des complexes, il a été démontré qu'il est nécessaire de former les particules hors de la stœchiométrie en charge des espèces, assuré par un excès de polycation (excès de charges positives). La découverte il y maintenant une vingtaine d'années du potentiel d'application de nouvelles formes d'ARN sous forme de court double brin (siRNA) a suscité un nouvel entrain au développement de vecteurs pour application génique. Dans ce contexte, de nombreux polycations synthétiques ont été développés pour former des complexes à base de siRNA pour la délivrance de ces derniers.

Dans le cadre de cette thèse, l'un des seuls polycations biosourcés existant a été étudié : le chitosane. Il s'agit d'un polymère dérivé de la chitine pouvant provenir de sources variées comme la carapace de crustacés ou extrait de champignons. Il s'agit d'un polycation dont les propriétés de complexation avec différents polyanions ont été grandement étudiées que ce soit avec de l'ADN, des protéines ou des polyanions synthétiques. L'utilisation de chitosane fait aujourd'hui l'objet d'un nombre grandissant d'études dans le cadre de ses propriétés de complexation avec du siRNA. En effet, la découverte encore récente du potentiel des siRNA a permis un renouveau dans la recherche sur les propriétés de complexation de ce biopolymère. Cela est en parti dû à la très petite taille des siRNA à vectoriser en comparaison des grandes chaînes de polyanions historiquement étudiées (ADN plasmide, sulfate de dextran, etc.), modifiant ainsi une partie des paramètres physico-chimiques établis précédemment pour l'obtention de complexes stables.

Dans ce projet de thèse, l'étude des propriétés de complexation du chitosane envers du siRNA et la stabilité des complexes obtenus a été privilégiée. En effet, il a été supposé

que de la même manière que pour l'ADN, l'efficacité de la complexation de siRNA par du chitosane va dépendre de nombreux facteurs tels que la longueur des chaînes de polycation, le milieu de complexation ou encore la densité de charge portée par le polycation. Dans un second temps, la stabilisation de complexes chitosane-siRNA a été étudiée et deux voies ont été privilégiées :

- L'introduction d'ions métalliques divalents tel que du zinc dans la formulation
- La modification chimique du chitosane par l'introduction d'un bloc hydrophile stabilisateur, du PEG.

Cette deuxième approche est basée sur une nouvelle voie de synthèse qui permettrait d'obtenir des complexes présentant des structures encore inexplorées à base de chitosane. Ce manuscrit de thèse se compose dans un premier temps d'un chapitre bibliographique (chapitre 1) permettant de positionner l'étude quant aux sujets abordés au cours de cette thèse. Un état de l'art sur les différentes voies de vectorisation du siRNA y est proposé ainsi qu'une discussion quant aux paramètres jouant un rôle dans la formation de complexes de polyélectrolytes à base de chitosane. Ce dernier se termine par une vue d'ensemble des interactions pouvant intervenir entre des ions métalliques et les deux composants des complexes : le chitosane ou le siRNA. Les travaux de recherche effectués faisant l'objet des différents chapitres expérimentaux sont résumés ci-après.

Chapitre 2 : Effets de longueur de chaîne d'oligosaccharides de chitosane sur ses propriétés en solution et de complexation avec du siRNA.

Dans ce chapitre, les propriétés physico-chimiques en solution d'oligosaccharides de chitosane (COS) ont été évaluées ainsi que leurs propriétés de complexation de siRNA. Pour cela, une librairie de COS a été synthétisée par un procédé de dépolymérisation d'un chitosane très faiblement acétylé (DA < 1%) de grande masse molaire. Cette librairie de COS a pu être caractérisée par Résonance Magnétique du Proton (H^1 RMN) et par Chromatographie d'Exclusion Stérique couplée à un détecteur de diffusion statique de la lumière multi-angle (SEC-MALLS). Ce procédé de dépolymérisation a permis l'obtention de COS dont la longueur varie de 5 unités monomériques à 50. Les propriétés de ces COS en solution ont par la suite été évaluées. Il a pu être démontré que la solubilité du chitosane ainsi que ses propriétés électrostatiques sont fortement dépendantes de la longueur des chaînes grâce à l'exploitation de dosages potentiométriques ainsi que la diffusion dynamique de la lumière (DLS). En effet, la solubilité du chitosane dépend de son état de protonation en solution, diminuant avec l'augmentation du pH. Ainsi, il a pu être démontré que le pK_a du chitosane augmente lorsque la longueur de chaîne diminue, se rapprochant du pK_a d'une unité monomérique isolée. De même, la solubilité des chaînes de chitosane se voit améliorée lorsque la taille des chaînes diminue, exprimée par un pH critique de solubilité augmentant avec la diminution de la taille des chaînes.

Dans un second temps, les propriétés de complexation de cette librairie de COS avec du siRNA ont été évaluées. Il a pu être démontré par l'utilisation d'un protocole de déplétion d'un chromophore, que la stœchiométrie de complexation du siRNA par des COS était dépendante de la longueur du COS. En effet, une longueur de chaîne de 13 unités était nécessaire pour atteindre une stœchiométrie de 1 pour 1, conduisant à la complexation totale du siRNA à un rapport N:P = 1. Un COS composé d'uniquement 5 unités complexantes ne présente en revanche qu'une stœchiométrie de 5 pour 1, suggérant un mécanisme de complexation coopératif traduit par une complexation plus efficace avec l'augmentation de la longueur de chaîne du COS. Une analyse de titration calorimétrique isotherme (ITC) a également permis de mettre en lumière la présence de deux phénomènes lors de la complexation de siRNA par de courtes chaînes de chitosane. L'un de ces phénomènes a été attribué à l'appariement ionique entre les chaînes de COS et de siRNA se manifestant par une importante contribution exothermique, indiquant une très forte interaction entre les deux composants. L'autre phénomène observé, de nature endothermique, a été attribué à l'agrégation des complexes formés en début de titration, à faible rapport de charge. Cette dernière analyse a également mis en évidence l'augmentation de la constante de complexation K_b avec la longueur de chaîne du COS de façon linéaire.

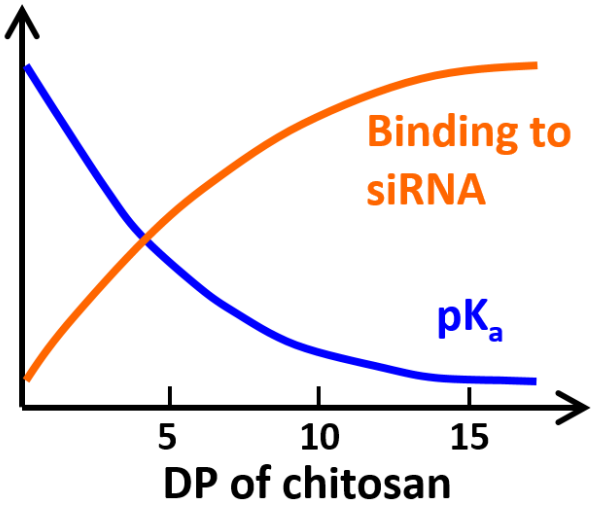

Figure 1. Représentation de la relation entre le comportement des oligosaccharides de chitosane en solution et ses propriétés de complexation associées avec du siRNA en fonction du degré de polymérisation (DP).

Chapitre 3 : Interaction d'ions métalliques avec de petits ARN interférents au niveau moléculaire et colloïdal.

Pour envisager l'introduction d'ions métalliques dans la formulation des complexes chitosane-siRNA, une étude de l'effet de tels ions sur du siRNA seul a été réalisée. L'objectif premier de ce travail était de déterminer quel était le mode d'interaction entre les acides nucléiques et les métaux. En effet, deux types d'interaction entre des ions métalliques et des acides nucléiques sont possibles : une interaction électrostatique entre les ions métalliques chargés positivement et les groupements phosphates chargés négativement qui relient les nucléosides, ou une interaction de type coordination, provenant des atomes des bases azotées pouvant coordonner des ions métalliques. Différentes méthodes ont été employées pour caractériser ces interactions telles que des mesures d'infrarouge par transformée de Fourier (FTIR), des mesures de déplacement d'un intercalant fluorescent et la détermination des températures de dénaturation des duplexes en présence des ions. Il a alors pu être déduit le mode d'interaction préférentiel des ions magnésium, zinc, fer II et fer III. En effet, les ions magnésium semblent préférentiellement interagir de façon électrostatique avec les siRNA alors que le zinc présente un comportement plutôt intermédiaire entre électrostatique et coordination. Le fer II ou III quant à lui semble interagir presque exclusivement en étant coordonné par les bases des siRNA.

Les conséquences de ces modes d'interactions ont également été évaluées à l'échelle colloïdale. En effet, l'interaction des ions magnésium presque exclusivement avec les groupements phosphates du siRNA n'a pas de conséquence sur la stabilité colloïdale des brins d'acide nucléique telle qu'évaluée par diffusion dynamique de la lumière (DLS) ou par électrophorèse sur gel d'agarose. En revanche, l'introduction d'un excès de zinc en présence de siRNA a pu mener à la formation de nanoparticules bien définies qui ont pu être observées en DLS et en microscopie à force atomique (AFM). Ces nanoparticules ont été formées à un rapport Zn:P = 10, correspondant au rapport des ions zinc en solution par rapport au nombre de groupements phosphates. Un excès de zinc supplémentaire mène alors à la formation de particules de taille micrométrique. Quant au fer (II ou III), il a été observé que celui-ci induit la formation de très gros objets conduisant à la précipitation des agrégats formés. Un état colloïdal particulier a également pu être observé avec le fer II avec la formation de nanoparticules pour un ratio Fe:P = 1, mis en évidence par DLS et visualisé par AFM (Figure 2).

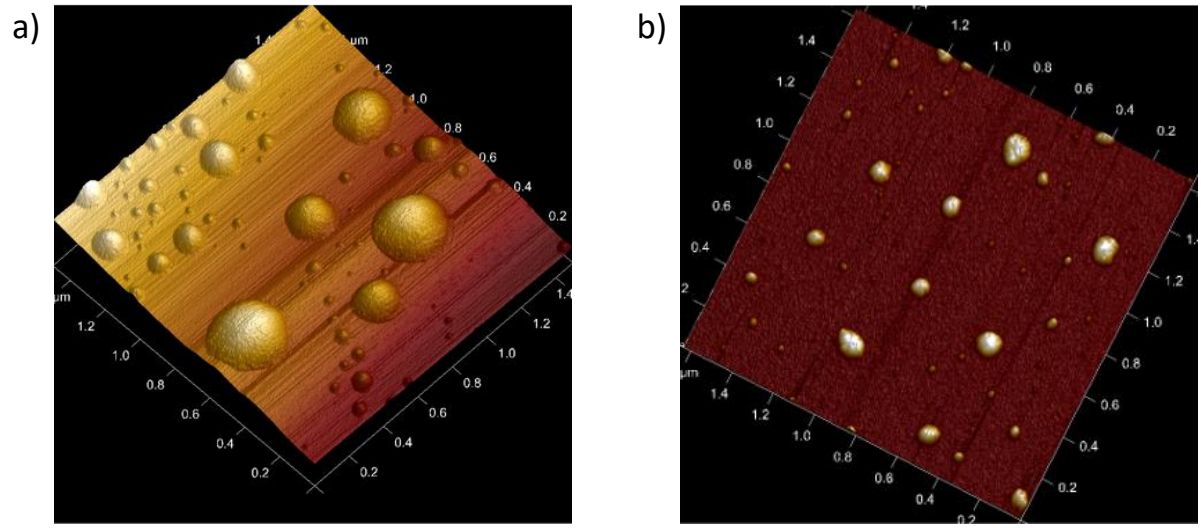

Figure 2. Profil 3D obtenu par AFM des nanoparticules formées en présence a) de zinc et de siRNA (Zn :P = 10) et b) de fer II avec du siRNA (Fe:P = 1).

Complétée par des mesures de dichroïsme circulaire, cette étude a permis de révéler la conservation de l'hélicité du siRNA de type A, malgré les changements d'état à l'échelle colloïdale. La conservation de cette dernière, malgré la complexation des ions zinc avec les siRNA, suggère la formation d'un nouveau type d'hélice décrit dans la littérature comme de type métallique : la « M-forme »

L'évaluation des complexes métaux-siRNA *in vitro* a révélé la cytotoxicité des complexes formés avec du magnésium et du zinc. L'importante toxicité observée en présence de zinc correspond à l'état de nanoparticules obtenues à un rapport Zn:P = 10. En revanche, une cytotoxicité n'a été observée en présence de fer (II ou III) uniquement pour des rapports extrêmement élevés avec le fer III, voire aucune toxicité avec du fer II.

Chapitre 4 : Etude de l'interaction de zinc avec du chitosane, vers une stabilité améliorée des complexes chitosane-siRNA.

La stabilité des complexes formés entre du chitosane et du siRNA en conditions physiologiques est un enjeu majeur quant à l'utilisation de telle formulations pour des applications biologiques. En effet, de tels complexes sont le plus souvent formulés à un pH acide (pH = 4) pour assurer la protonation complète des amines du chitosane, permettant l'interaction électrostatique avec les groupements phosphates du siRNA. L'introduction d'un excès de chitosane permet alors la stabilisation des complexes. Le pH d'un milieu physiologique induisant la déprotonation du chitosane d'une part, ainsi que l'importante force ionique d'un tel milieu limitant la stabilisation des complexes basée sur l'excès de charges cationiques apportées par le chitosane d'autre part, sont souvent les principales limites de l'utilisation de tels complexes.

Dans ce chapitre, cette problématique de stabilité a été abordée par l'introduction d'ions zinc II dans la formulation des complexes. A cet effet, l'interaction entre ces ions et le chitosane a été démontrée dans un premier temps au moyen de techniques telles que des dosages potentiométriques et de l'infrarouge (FTIR). D'après ces mesures, il a pu être établi que ces ions zinc étaient chélatés par les amines du chitosane lors de la déprotonation de ces dernières. De plus, la fixation de ces ions a été trouvée étant maximale à un pH = 6. L'effet de l'introduction de ces ions sur les propriétés en solution du chitosane a ensuite été évalué par des mesures de DLS et de potentiel zeta. Une amélioration de la solubilité face à l'augmentation du pH et la conservation d'une charge cationique à pH physiologique ont été révélées, dans le cas de chitosanes présentant de faibles degrés d'acétylation.

Finalement, la stabilité des complexes formés entre du chitosane et du siRNA en milieu physiologique a été abordée et séparée en deux problématiques : la stabilité en conditions isotoniques (en milieu salin, 0.9% NaCl), et la stabilité à pH physiologique dans un milieu à faible force ionique. Pour répondre à cette première problématique, l'effet du degré d'acétylation (DA) du chitosane sur l'amélioration de la stabilité des complexes en conditions isotoniques a été évalué. D'une part, il a été montré l'effet du DA sur le potentiel zeta des complexes, celui-ci diminuant lorsque le DA du chitosane augmente traduisant une densité de charge moins importante. D'autre part, l'augmentation du DA du chitosane jusqu'à une certaine limite a montré un effet stabilisateur des complexes en conditions isotoniques jusqu'à au moins 20h d'incubation. L'introduction des ions zinc, comme mentionnée précédemment, a été considérée pour répondre à la deuxième problématique, le pH physiologique. Une nouvelle formulation a été mise au point pour favoriser la fixation d'un maximum d'ions zinc dans les complexes par dialyse contre une solution aqueuse ajustée à pH = 6. L'incorporation des ions zinc a été évaluée par Spectrométrie à plasma à couplage inductif (ICP) permettant de mesurer la quantité de zinc fixée dans les complexes. L'évaluation de la stabilité des

complexes formulés avec du zinc à pH physiologique a démontré l'intérêt de l'introduction de tels ions. En effet, l'introduction de ces ions permet la conservation d'un potentiel zeta positif à un pH = 6, une libération diffuse du siRNA illustrée par une expérience d'électrophorèse des complexes sur gel d'agarose et une stabilité améliorée des complexes jusqu'à 16h après incubation dans une solution tampon à pH physiologique. De plus, l'introduction de zinc dans les formulations ne semble pas avoir affecté l'effet du DA sur la stabilité des complexes en conditions isotoniques.

En revanche, ces améliorations sur la stabilité en conditions physiologiques ne semblent pas permettre la stabilité recherchée lorsque les deux problématiques sont associées : une stabilité dans un milieu à force ionique élevée et une stabilité à pH physiologique comme dans un tampon PBS.

Chapitre 5 : Synthèse d'un copolymère à bloc contenant un court bloc chitosane pour une conjugaison non-covalente à du siRNA.

La PEGylation de nanoparticules est une approche souvent utilisée pour améliorer la stabilité et la furtivité de nanoparticules. Dans le cas de polypexes à base de chitosane, l'introduction de motifs PEGylés se fait historiquement par la modification chimique des amines primaires du chitosane. Cette approche permet en effet d'améliorer la stabilité des complexes ainsi que de diminuer leur taille. Elle ne permet pas, en revanche, de contrôler précisément le nombre de motifs introduits. De plus, cette modification supprime des motifs complexant du chitosane, pouvant poser problème lorsque ces derniers sont en nombre limité dans le cas de courtes chaînes de chitosane ou de chitosane fortement acétylés.

Ce chapitre explore une nouvelle voie de modification du chitosane, prenant avantage de l'extrémité réductrice de ce dernier après dépolymérisation. En effet, cette dernière présente une fonction aldéhyde particulièrement réactive comparée à une extrémité réductrice classique de polysaccharides sous leur forme hemiacétal-aldéhyde. Cette voie très avantageuse a par conséquence fait l'objet de différentes études dans le cadre de conjugaisons de molécules par amination réductrice. Dans ce chapitre, cette réaction a été utilisée avec pour objectif de conjuguer un bloc PEG à un court chitosane, appelé COS. Cette approche encore inexplorée permettrait pour la première fois l'obtention d'un copolymère à base de chitosane par conjugaison directe d'un bloc PEG à l'extrémité réductrice, sans étape intermédiaire. L'obtention d'un tel polymère permettrait alors l'étude de structures pour la délivrance de siRNA encore inexplorées à base de chitosane telles que des polyion complex (PIC) micelles ou des structures de type conjugués.

La réaction, permettant des conversions importantes, mène à un milieu réactionnel particulièrement difficile à purifier et ainsi, des rendements très faibles. La complexation d'un tel polymère avec du siRNA a pu être étudiée par DLS et par spectroscopie de corrélation de fluorescence (FCS) mettant en évidence l'obtention de deux structures en fonction de la composition du copolymère introduit. En effet, une structure agrégée de type micelle a pu être observée pour un copolymère contenant un court bloc PEG stabilisant de 2kDa. En revanche, pour des copolymères contenant un bloc stabilisant de 5kDa, des complexes présentant une structure de type conjugué d'une taille d'environ 16 nm d'après la FCS ont pu être obtenus (Figure 3).

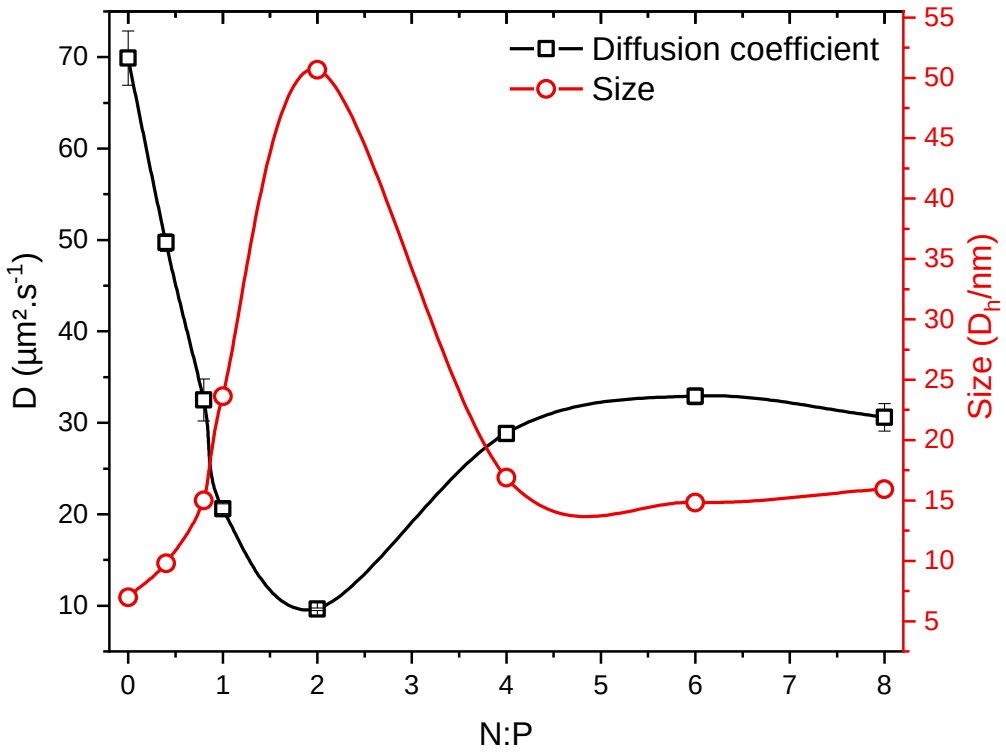

Figure 3. Suivi de l'évolution du coefficient de diffusion (noir) et de la taille correspondante (rouge) d'un siRNA fluorescent (Cy 5.5) par FCS en fonction de l'ajout de copolymère (N:P) présentant un bloc COS d'un degré de polymérisation de 20 et un bloc PEG de 5kDa.

De plus amples investigations ont révélé la présence de COS seul dans le produit final expliquerait la formation des structures agrégées aux ratios N:P proches de la stœchiométrie, due à la diffusion bien plus rapide des courtes chaînes de chitosane comparé aux chaînes de copolymères, menant à la formation de structures agrégées stabilisées par le copolymère.

Les voies de purifications d'un tel produit sont un point central de ce chapitre, la présence d'homopolymère étant un facteur déterminant sur les structures finales obtenues. Une nouvelle voie de purification par chromatographie préparative a donc été développée afin de séparer le copolymère et l'homopolymère de COS restant après la réaction de couplage.

Table of content

General introduction

Nanomedicine is a vast field among which the delivery of therapeutics takes an important place. The development of nanoparticles based on the self-assembly of lipids or polymer chains through weak interactions allows the encapsulation, protection and delivery of active molecules. The delivery of nucleic acids has been a challenge for many years which started with the delivery of DNA for gene therapy [1]. This problematic has been addressed by means of two types of vehicles: the viral vectors, based on hijacked existing viruses [2] and the non-viral vectors. This second approach relies on the encapsulation of the nucleic acids in nanoparticles made of lipids or polymers to protect and deliver these structures. Most of them take advantage of the polyanionic character of the nucleic acids to encapsulate them efficiently in a cationic vehicle. More recently, the discovery of a panel of RNA-based technologies (siRNA, miRNA, mRNA) and their potential therapeutic effect stimulated the research in the domain of gene-based therapies and strengthened the interest for the treatment of a large panel of diseases [3, 4]. For instance, the first two new treatments based on the siRNA technology discovered almost 20 years ago and developed by Alnylam Pharmaceuticals were recently approved for marketing after a long process of clinical trials. Moreover, the interest in these RNA-based technologies is even greater today in the context of the pandemic caused by the COVID-19. For instance, this emerging virus and the worldwide safety concerns have prompted the development of lipid particles as delivering vehicle of the first mRNA-based vaccines.

The typical approach for non-viral gene delivery relies on the electrostatic complexation between the polyanionic nucleic acids and polycations. The mixing of two oppositely charged polyelectrolytes leads to the formation of polyelectrolyte complexes (PECs), also called polyplexes in the field of gene delivery. This type of vehicles which has been studied for all types of nucleic acids is the central to this thesis for the formulation of siRNA-based colloidal polyelectrolyte complexes. The biocompatible and biosourced polysaccharide chitosan was chosen for its cationic character and studied as complexing polycation for the formulation of polyplexes chitosan-siRNA.

In this context, the main goal of this thesis is to study the interaction between chitosan and siRNA. A particular attention is paid to the colloidal stability of the complexes formulated and the approaches available to improve it. Three approaches have been developed to meet the challenge of stability of these colloidal complexes: the modification of the acetylation degree of chitosan, the introduction of metallic ions in the formulation and a new PEGylation approach of the chitosan.

The first chapter of this manuscript is a literature review covering several aspects in the field of siRNA delivery. The current approaches and methods developed for its delivery are addressed. The conjugate approach as well as the development of the various siRNA carriers are discussed. Special attention is paid to the formation of chitosan-based polyplexes and the various parameters influencing the properties of the complexes. Finally, a state of the art regarding the interaction of metallic ions with chitosan or nucleic acids is presented.

A study on the role of the chitosan chain length on the solubility of the polymer and its electrostatic properties is the topic of the second chapter. The complexation of chitosan oligosaccharides with siRNA is also investigated as well as the colloidal properties of the resulting PECs.

The third chapter focuses on the interaction of metallic ions with small interfering RNA. This interaction is described at the molecular and colloidal level. Electrostatic and coordinative bonding of the metallic ions with siRNA is analysed by means of infrared spectroscopy, ethidium bromide displacement and thermal denaturation analysis. In addition, clusters formed in the presence of specific metals are evidenced by dynamic light scattering and imaged with atomic force microscopy.

The chapter 4 focuses on the stability of polyplexes from siRNA and chitosan in physiological conditions by playing with the concentration of zinc ions and the degree of acetylation of chitosan. A first part is dedicated to the characterisation of the interaction of Zn^{2+} ions with chitosan. In the second part, various easy-to-implement improvements are proposed to better stabilize the complexes under physiological conditions. First, the lack of stability at physiological salt concentration (i.e. 0.9% NaCl) is tackled by the increase of the chitosan DA, allowing a better stability of the complexes, as evaluated by DLS. The stability of the complexes at physiological pH is addressed by the incorporation of Zn^{2+} ions in the formulation.

The last chapter deals with the synthesis of a new chitosan-based block copolymer and the resulting assemblies with siRNA. This new synthesis relies on the conjugation of a PEG block to the reducing end of a short chitosan block by means of a reductive amination pathway. The challenging purification steps of the copolymer are discussed as they appear to be central in the obtention of the desired copolymer structure. The complexes obtained from the chitosan-*b*-PEG copolymer and siRNA are characterised by Fluorescence Correlation Spectroscopy and Light Scattering techniques. They were found to be of the micellar type but objects corresponding to a conjugate-like structure were also evidenced.

References

[1] Wirth T, Parker N, Ylä-Herttuala S (2013) History of gene therapy. Gene 525:162–169 . https://doi.org/10.1016/j.gene.2013.03.137

[2] Goswami R, Subramanian G, Silayeva L, Newkirk I, Doctor D, Chawla K, Chattopadhyay S, Chandra D, Chilukuri N, Betapudi V (2019) Gene Therapy Leaves a Vicious Cycle. Front Oncol 9:1–25 . https://doi.org/10.3389/fonc.2019.00297

[3] Uludag H, Ubeda A, Ansari A (2019) At the Intersection of Biomaterials and Gene Therapy: Progress in Non-viral Delivery of Nucleic Acids. Front Bioeng Biotechnol 7:1–21 . https://doi.org/10.3389/fbioe.2019.00131

[4] Challener C (2020) "Can Using RNA Simplify Gene Therapy Development?" BioPharm Int. 33

List of abbreviations

AFM	Atomic Force Microscopy
AGO2	Argonaute 2
AMF (M)	2,5-anhydro-D-mannofurannose
bp	base pair
CD	Circular Dichroism
COS	Chitosan Oligosaccharides
DA	Degree of Acetylation
DAPI	4′,6-diamidino-2-phenylindole
DDA	Degree of Deacetylation
DFT	Density Functional Theory
DHBC	Double Hydrophilic Block Copolymer
DLS	Dynamic Light Scattering
DMEM	Dulbeco's Modified Eagle's Medium
DMSO	Dimethyl sulfoxide
DNA	Deoxyribonucleic Acid
DP	Degree of Polymerization
dRI	Differential Refractive Index
dsRNA	Double Stranded Ribonucleic Acid
EDTA	Ethylenediaminetetraacetic acid (IUPAC: 2,2′,2″,2‴-(Ethane-1,2-diyldinitrilo)tetraacetic acid)
EtBr (EB)	Ethidium Bromide
FBS	Fetal Bovine Serum
FCS	Fluorescence Correlation Spectroscopy
FDA	Food and Drug Administration
FTIR	Fourier Transform Infrared Spectroscopy
GFP	Green Fluorescent Protein
GlcN (D)	D-glucosamine
GlcNAc (A)	N-acetyl-D-glucosamine
^{1}H NMR	Proton Nuclear Magnetic Resonance
HEPES	4-(2-hydroxyethyl)-1-piperazineethanesulfonic acid
HMF	Hydroxymehylfurfural
HPLC	High Performance Liquid Chromatography
Hz	Hydrazide
ICP/OES	Inductively Coupled Plasma / Optical Emission Spectrometry
ITC	Isothermal Titration Calorimetry
MALDI-TOF	Matrix Assisted Laser Desorption Ionization – Time Of Flight
MeOH	Methanol
MES	2-(N-morpholino)ethanesulfonic acid
MNIS	Multiple non-interacting sites

MOPS	3-(N-morpholino)propanesulfonic acid
mPEG	methoxy Poly(ethylene glycol)
mRNA	Messenger Ribonucleic Acid
MTT	3-(4,5-dimethylthiazol-2-yl)-2,5-diphenyltetrazolium bromide
MW	Molecular Weight
ncRNA	Non-coding Ribonucleic Acid
NHS	N-Hydroxysuccinimide
NNLS	Non-negative least squares
OD	Optical Density
PAA	Poly(acrylic acid)
PAN	1-(2-pyridylazo)-2-naphthol
PBS	Phosphate Buffered Saline
PCL	Poly(caprolactone)
PdI	Polydispersity Index
PE	Polyelectrolyte
PEC	Polyelectrolyte Complex
PEG	Poly(Ethylene Glycol)
PEI	Poly(ethylene imine)
PIC	Polyion Complex
PLL	Poly(L-lysine)
PMAA	Poly(methacrylic acid)
PSD	Particle Size Distribution
RNA	Ribonucleic Acid
RNAi	RNA interference
RISC	RNA-Induced Silencing Complex
RT-PCR	Reverse Transcription Polymerase Chain Reaction
RVG	Rabies Virus Glycoprotein
SEC	Size Exclusion Chromatography
SEC-MALLS	Size Exclusion Chromatography-Multiangle Laser Light Scattering
siRNA	Small Interfering Ribonucleic Acid
SLS	Static Light Scattering
TB	Toluidine Blue
TEM	Transmission Electron Microscopy
TPP	Tripolyphosphate
Tris	Tris(hydroxymethyl)aminomethane (IUPAC: 2-Amino-2-(hydroxymethyl)propane-1,3-diol)
uPIC	Unit Polyion Complex
UV	Ultraviolet
UV-vis	Ultraviolet-visible
YBC	Y-shaped Block Catiomer

Notations

α	Degree of dissociation
ΔG	Free energy change ($kJ.mol^{-1}$)
ΔH	Enthalpy change ($kJ.mol^{-1}$)
ΔR	Rayleigh ratio (cm^{-1})
ΔS_h	Entropy change by the hydrophobic interactions ($kJ.K^{-1}.mol^{-1}$)
ΔS_i	Entropy change by the release of counter-ions ($kJ.K^{-1}.mol^{-1}$)
ΔS_p	Entropy change by the fixation of polymer chains ($kJ.K^{-1}.mol^{-1}$)
D	Diffusion coefficient ($\mu m^2.s^{-1}$ or $m^2.s^{-1}$)
D_h	Hydrodynamic diameter (nm)
dn/dc	Refractive index increment ($g.mL^{-1}$)
Đ	Dispersity of a polymer
DP_n	Number-average degree of polymerization
$\boldsymbol{e}$	Elemental electric charge (A.s)
f_h	Hydrophilic mass fraction (%)
γ	Degree of protonation or Protonation rate
I	Ionic strength ($mol.L^{-1}$)
IC_{50}	Half-maximal inhibitory concentration (μM)
K_b	Binding constant ($L.mol^{-1}$)
kDa	kiloDaltons (1 kDA = 1 000 g/mol)
λ	Wavelength (nm)
λ_D	Debye length (nm)
$\boldsymbol{l_B}$	Bjerrum length (nm)
M_n	Number average molar mass ($g.mol^{-1}$)
M_w	Mass average molar mass ($g.mol^{-1}$)
$\boldsymbol{\bar{n}}$	Average number of coordinating molecules fixed per one metal atom
$\boldsymbol{N_a}$	Avogadro's number (mol^{-1})
N_{agg}	Aggregation number
N:P	Amine to phosphate ratio
$pK_{1/2}$	pK_a at $\alpha = 0.5$
$\boldsymbol{\psi_0}$	Surface potential (V)
R_g	Gyration radius (nm)
R_h	Hydrodynamic radius (nm)
TΔS	Entropic contribution to the free energy ($kJ.mol^{-1}$)
T_m	Melting temperature (°C)
ζ-potential	Zeta potential (mV)

Chapter 1:
State of the art

1.1. Introduction

The discovery of gene interference in the *C. Elegans* worm model, in 1998 by Craig C. Mello and al. [1] shook the biological world and opened a new field of research and applications. Indeed, this discovery leads to research on the role of non-coding RNA (ncRNA) in various interference mechanisms like regulating systems operating in the cells, from the cell development and differentiation to the cell integrity thanks to these multiple small transcripts. In this interference mechanism, allowing the regulation of the gene expression, biologists could see the opportunity for the treatment of genetic diseases and other harms from genetic causes. Indeed, these ncRNA can be Post Transcriptional Gene Silencers, suppressing the expression of targeted mRNA by preventing their translation and favouring their degradation, hence justifying the use of the term 'interference'. They found that interference was much more efficient with the double stranded RNAs (dsRNA) than individual ones. This discovery was later supported by the use of this kind of duplexes for interference in mammalian cells [2], confirming their relevance for gene therapy. Importantly, the interference also can take place with small RNA strands (i.e. 21-23 base pairs), known as small interfering RNA (siRNA). Finally, it took several years to confirm the transposition of this technology to human, with the first in-human phase I clinical trial for the delivery of siRNA using a targeting nanoparticle system [3]. Since then, at least two treatments have been successfully approved for marketing: Patisiran (ONPATTRO^{TM}), a lipid-siRNA complex for the treatment of hereditary transthyretin amyloidosis [4] and Givosiran for the treatment of acute hepatic porphyria [5]. These two siRNA-based therapies highlight the tremendous potential of gene interference and also shows that various systems may exist to successfully deliver siRNA to their targeted site.

Nanocarrier systems are needed to overcome the various biological barriers to siRNA delivery. The development of such systems is at the heart of "nanomedicine" which lies at the interface of biology, chemistry, physics, material science and medicine. There are different approaches to deliver oligonucleotides, for instance with lipid vesicles as with the messaging RNA-based vaccines currently used to fight the SARS-Cov2 pandemic. Many of them are also based on macromolecules, which are expected to form more stable complexes with siRNA (thus more protective) than lipids. These systems can be natural or synthetic such as polysaccharides, peptides or synthetic polymers. The broad range of materials available and the development of various chemical pathways lead to various nanocarriers over the years with the common aims to protect siRNA and deliver it safely to its target, a specific site.

An important aspect of these carriers is their colloidal stability, which in many cases is not thoroughly studied or developed as the main goal is often put on the biological evaluation of

the carriers. Nonetheless, this aspect is strongly dependent on the formulation process and deserves more attention.

This chapter will first introduce the discovery of siRNA and the various developments that followed. Mainly, the interference mechanism involving siRNA will be discussed, followed by the barriers encountered by the siRNA delivery and the strategies developed to overcome them. Two strategies are discussed: the chemical modification of siRNA either by the modification of the backbone or the covalent attachment of moieties at the end of the strands, and the development of colloidal carriers. Then, the colloidal stability will be addressed in the context of chitosan-based systems for siRNA delivery. During this work, a particular attention was dedicated to improve the pH-stability of such carriers by using metallic ions. Therefore, the interaction between chitosan and metallic ions as well as the interactions between siRNA and metallic ions will be discussed in this chapter.

1.2. siRNA, promises for the future

1.2.1. Interference mechanism with siRNA

Since the introduction of a chemically synthesized siRNA into mammalian cells and the following successful interference in 2001 [2], the interference mechanism has been the object of various researches. In the natural process discovered initially [1], long double stranded RNA (dsRNA) are degraded through the action of so-called Dicer enzyme and processed into siRNA (Figure 1.2-1.a). However, in the particular case of synthetic siRNA, the Dicer enzyme is not involved (Figure 1.2-1.b) thus avoiding difficulties such as interferon activation pathway [6, 7]. With this degradation step skipped, the introduction of a sequence-defined siRNA into a cell can lead directly to the formation of the RNA-Induced Silencing Complex (RISC). This complex is formed thanks to the association of the siRNA with different proteins including one called Argonaute2 (AGO2) [6, 8]. This particular protein recognizes the antisense strand of the siRNA, used as a guide. The other strand, called the sense strand or the passenger strand (in blue in Figure 1.2-1) will be cleaved and discarded [9]. The association of the antisense strand with AGO2 into the RISC will allow the binding to the corresponding sequence of messenger RNA (mRNA). The targeted sequence is then split between the 10^{th} and the 11^{th} bases from the 5’ end of the guide strand, inhibiting the gene expression and therefore silencing the target gene. The activated RISC can then target another complementary mRNA sequence [10]. This interference mechanism can then propagate until a threshold, where dilution of the guide strand due to cellular division becomes a limitation for the interference mechanism. This high

specificity and potency added to its versatility make siRNA an amazing fighter for a large panel of diseases.

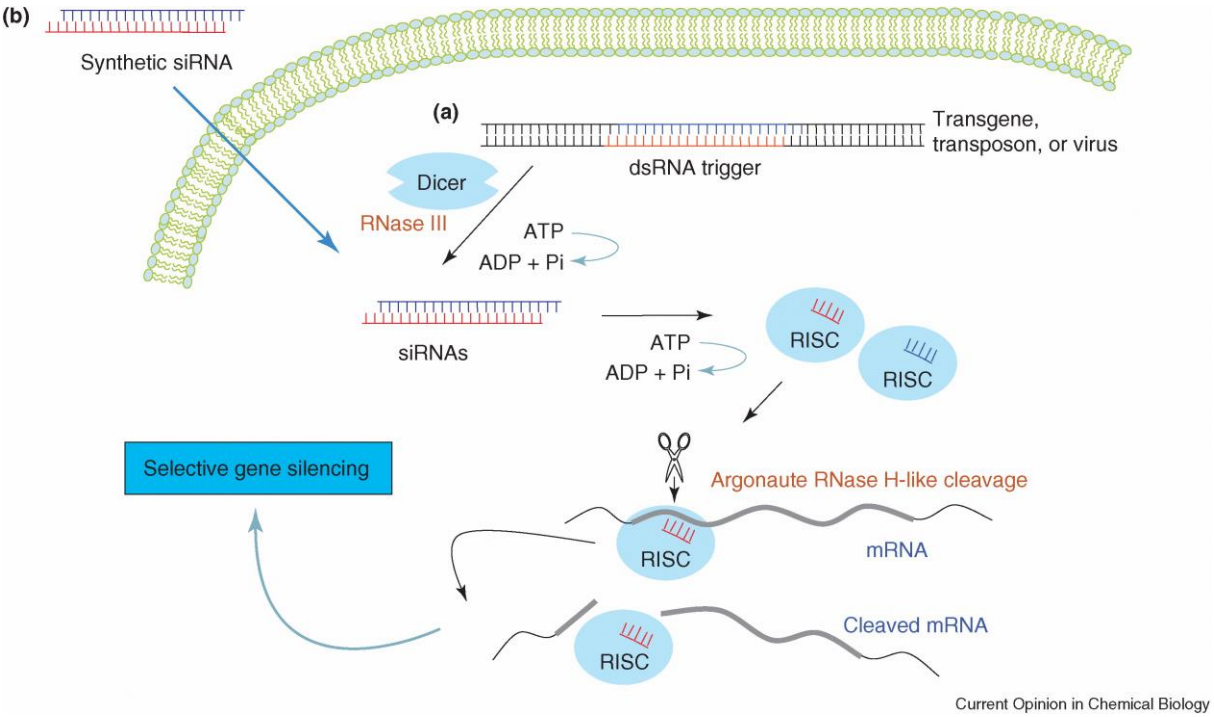

Figure 1.2-1. Interference mechanism for (a) dsRNA and (b) siRNA [11].

1.2.2. Hurdles to siRNA delivery

Despite the tremendous biological properties that siRNA provides, its application has to face various difficulties. The first barrier is its short half-life time in blood. siRNA is indeed a very fragile object which is easily degraded by nuclease enzymes (~ 15 minutes after injection) [12, 13], removing all its activity and specificity. The oligonucleotide being also a rather large molecule (~23 bp, 15 kDa), hydrophilic and polyanionic, it is challenging to ensure its efficient cellular uptake due to the hydrophobicity of the membrane and the presence of anionic groups at cell surface.

Some off-target effects have also been identified with the use of siRNA [14–16]. The most frequent one is the microRNA-like off-target effect resulting from an imperfect pairing between the siRNA guide strand and the mRNA. This behaviour which results from a non-optimal design of the siRNA leads to the downregulation of transcripts. It has also been shown that siRNA could induce an immune response [16], depending on the presence of a pro-inflammatory sequence (all of them have not been identified). In extreme cases, a saturation of

the RNAi machinery has also been observed by a displacement of the endogenous microRNA in the RISC by foreign siRNAs [16, 17].

Various strategies have been developed to overcome these hurdles, which can be split into two approaches: the chemical modification of siRNA and the siRNA immobilization within a carrier.

1.2.3. Modifications of siRNA

1.2.3.1. siRNA structure modifications

The chemical modification of siRNA has been an important research line in the development of siRNA-based therapies. Indeed, it represents a way to improve the biological stability of siRNA by reducing its sensitivity to nucleases, as for example Eri1, a conserved enzyme which induces the cleavage of terminal oligoribonucleotide phosphodiester bonds. Indeed, the coordination of deprotonated Mg^{2+} ions, by water and a Eri1 histidine residue, converts the former into a nucleophile able to cleave the bond [18, 19]. The modification of the siRNA structure was also investigated in order to modify properties like hydrophobicity, temperature stability (duplex melting temperature), recognition in the interference machinery and eventually the duplex conformation [20–22]. Two main modifications have been developed to improve the resistance to nuclease without affecting the interference efficiency: the modification of the 2'-OH in the ribose (Figure 1.2-2.c) and the modification of the phosphate group on the backbone (Figure 1.2-2.b). The biological effect of these various modifications has been thoroughly reviewed, especially on the stability and efficiency of siRNA [20, 21].

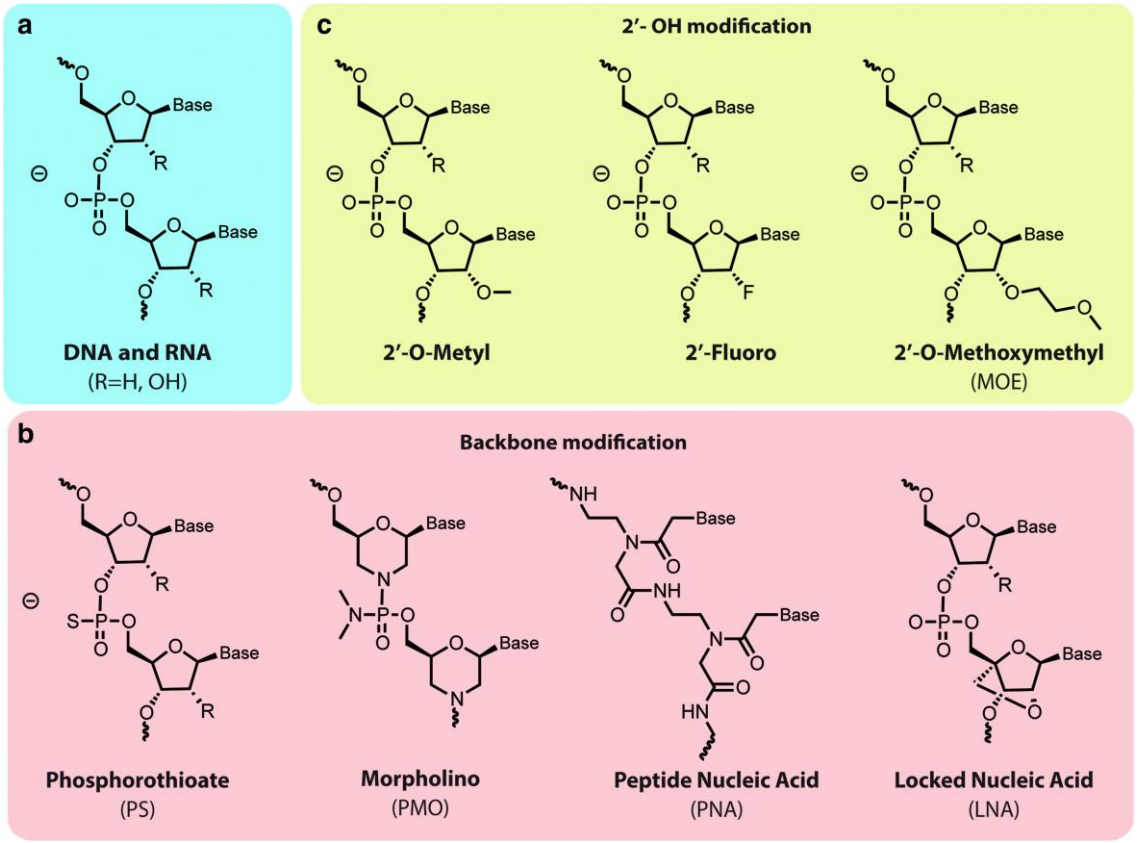

Figure 1.2-2. Chemical modifications of siRNA. a) structure of the backbone of DNA (R = H) and RNA (R = OH). b) Modification of the phosphodiester bond into a phosphorothioate linkage more resistant to nucleases and increasing the hydrophobicity of the backbone, phosphorodiamidate morpholino oligonucleotide (PMO) modification and peptide nucleic acid (PNA) modification providing uncharged backbone and higher stability against nucleases and locked nucleic acid (LNA) modification providing resistance to nucleases and increased hybridization and binding properties. c) Modifications of the ribose 2'OH group, not involved in the RNAi machinery; modification to 2'-O-Me and 2'-F allows the conservation of similar biophysical properties, better stability against nucleases and prevent the activation of the immune system [21].

1.2.3.2. Development of siRNA bioconjugates

Bioconjugation of siRNA has been applied to overcome the natural barriers to siRNA delivery, mentioned previously. It corresponds to the attachment of a molecule presenting biological properties of interest to a terminal end of the siRNA. However, the choice of the strand to modify (sense or antisense) and which end (5' or 3') must be carefully considered as it may affect the activity of the siRNA in the RNAi machinery. In any case, it seems that the modification of the 3'-end of the antisense strand must be avoided to keep the gene silencing properties since it was shown that its modification with fluorescent probes or other moieties abolished gene silencing [11]. The (macro)molecule covalently linked to siRNA allows to improve the binding of the conjugates to the cell surface, their internalization and their blood stability (Figure 1.2-3) [20, 21]. Positively charged or hydrophobic moieties were also introduced to favour the interaction of siRNA with cell surface. Natural molecules like cholesterol have been used in order to help crossing the cell membrane, thanks to hydrophobic interactions [23–25]. Another conjugation available to improve the properties of a naked siRNA is the attachment of a polymer like PEG to improve the blood circulation [26] which can be combined with the addition of a targeting moiety on the PEG end [20].

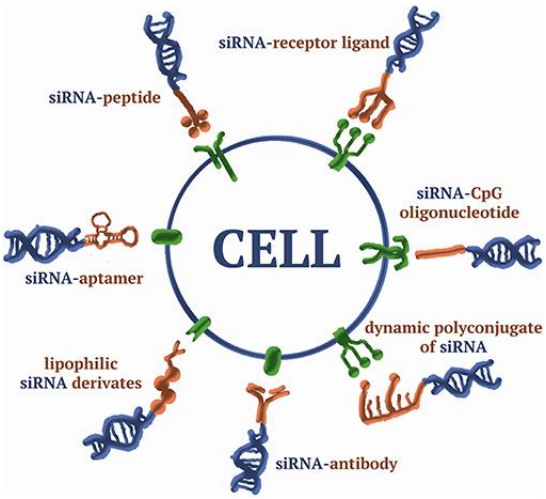

Figure 1.2-3. Various bioconjugates of siRNA [20].

This bioconjugate approach has made its path over the years and successfully lead to the FDA-approved Givosiran [5], a siRNA-based treatment using the bioconjugate approach with three N-acetyl-D-galactosamine units as targeting moieties, that are attached to the 3' end of the sense strand. These galactosamine units were chosen for their great affinity to asialoglycoprotein receptors, almost exlusively expressed on hepatocytes.

1.2.3.3. RNAi therapeutics market

Since the discovery of interference and its potential as a treatment for numerous diseases, the research on this technology has experienced ups and downs. Indeed, after a period of big enthusiasm from the major pharmaceutical companies which were aware of the tremendous potential of such technology, the lack of encouraging results after a few years has been stronger than their patience [27]. Fortunately, several companies stayed on course and have seen their

efforts rewarded after a few years as Alnylam funded in 2002. Indeed, this company offers today two therapies based on siRNA technology approved in the USA and Europe after several years of clinical trials: Patisiran [28] and Givosiran. In addition to these therapies, Alnylam Pharmaceuticals also started to develop a treatment for the COVID-19 based on siRNA technology as an inhalational formulation. Over 350 different siRNA were synthesized among which many showed a real activity against the virus [29]. However, due to their cost and a lack of popularity, this kind of siRNA-based therapy is for now only used as a last resort for the perennial treatment of diseases and not used at the moment against the COVID-19 [30].

The year 2018 was a turning point for the RNAi-based technologies where a few therapies entered phase III of clinical trials, inducing a major new impetus [31] (Figure 1.2-4). These elements combined suggest that "The dawn of a new era" has coming [31].

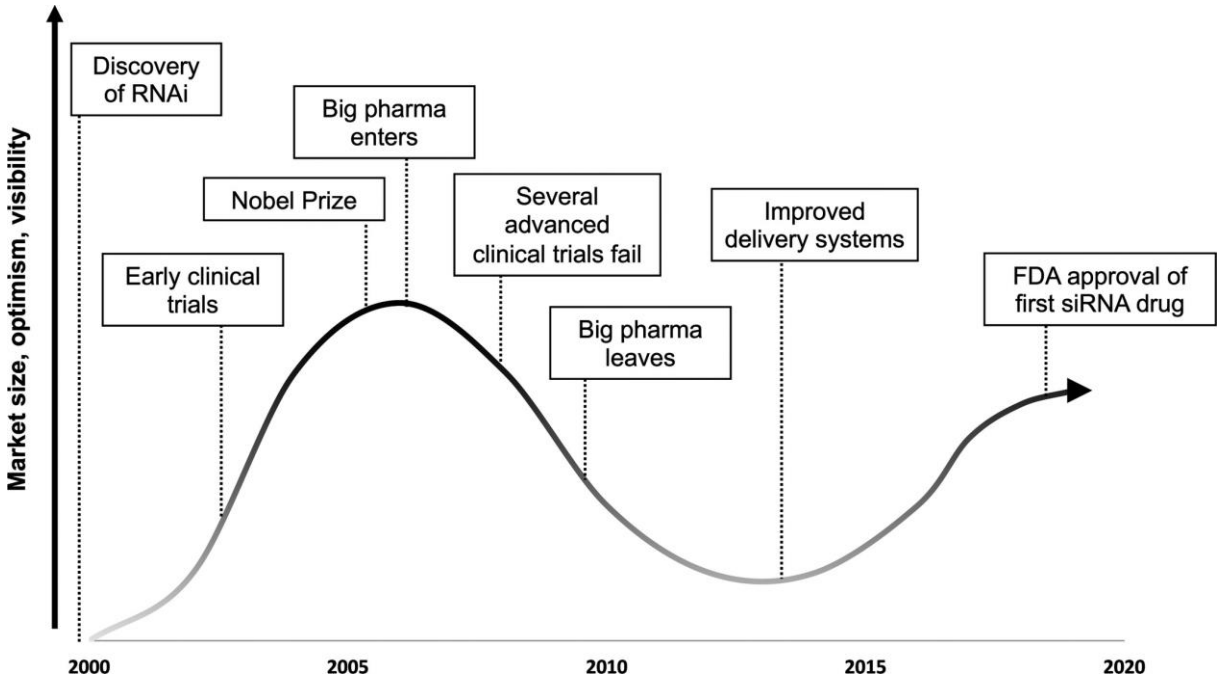

Figure 1.2-4. Major events in the history of the siRNA research and their impact on market size, optimism and visibility. Adapted from [31].

1.3. siRNA encapsulation, a variety of carriers

Vehicles might be essential to overcome the natural barriers of the human body and to protect the cargo from degradation pathways. A general feature of the vehicles used nowadays to deliver siRNA is that a majority of them is based on the electrostatic interaction between the negatively charged siRNA molecules and positively charged lipids or polymers [32], with some exceptions [33, 34]. The electrostatic interaction ensures a high yield of encapsulation which is even more relevant regarding the high cost of siRNA. Among these vehicles, some are totally

artificial, based on synthetic polymers [35–38] while some others are based on natural building blocks such as polysaccharides [39].

1.3.1. Lipid nanoparticles

Liposomes are a very old variety of delivery systems, discovered by Bangham in the early 1960s [40]. Indeed, phospholipids can spontaneously form in water bilayers and vesicles at appropriate concentrations. They are extensively used in the field of drug and gene delivery [34], and more recently for mRNA-based anti-Covid19 vaccines. In order to use them for the delivery of siRNA, the liposomes are usually formed in presence of a cationic lipid and optionally mixed with neutral phospholipids as helpers [41, 42]. The presence of the cationic charge will ensure a high loading of siRNA, otherwise most of the siRNA chains would stay in the outer medium of the liposomes and be wasted. PEGylation of the liposomes has also been used with significant improvements in the blood circulation time after systemic injection and accumulation of the vehicle at the targeted site [43]. The Patisiran, developed by the company Alnylam [4] demonstrated that a PEGylated formulation of liposomes can be effective to deliver siRNA to the hepatocytes and be applied as an efficient nanomedicine for the human body [44].

1.3.2. Polymer-based carriers

1.3.2.1. A large library of polymers

Synthetic polymers

A large variety of polymers has been developed, synthesised and used for siRNA delivery. One of the earliest polymer, known as the “gold standard” in the field of gene delivery is poly(ethyleneimine) (PEI) (Figure 1.3-1.a) [45]. PEI which can have either a branched or linear structure [46] presents a high density of amine groups with pKa values lying between 6 and 8. However, the PEI is cytotoxic due to its high charge number which increases with the molecular weight [47, 48]. This drawback has been partially resolved with the use of reversibly cross-linked bonds between PEI chains. Indeed, the use of reversible disulfide bonds allows the use of high molecular weight-like PEI to efficiently bind and deliver nucleic acids which can then return to its native low molecular weight form once exposed to the cellular reducing environment, limiting the PEI cytotoxicity [49].

Poly(L-lysine) (PLL) (Figure 1.3-1.b) is also a well-known polymer used in gene delivery [35, 36, 50]. However, similarly to PEI, this polymer can induce an important cytotoxicity due to

the important number of charges [47, 51]. To overcome this drawback, various architectures have been developed as well as other copolypeptides with the introduction of other moieties in the PLL or polypeptide backbone such as histidine, aspartic acid, leucine, etc. to tune the charge density or facilitate the cell internalization [52, 53].

Less cytotoxic polycations have been developed over the years such as poly(β-amino esters) (Figure 1.3-1.c) . They are often used after various modifications [54]. For instance, the introduction of various hydrophobic or hydrophilic amines with different alkyl chains lengths has been used in order to tune the hydrophobicity of the polymer to enhance the stability of the formed polyplexes (R_1 in Figure 1.3-1.c). The hydrophilic/hydrophobic balance was also modified with the insertion of hydrophobic molecules such as cholesterol for better cell membrane interaction. Finally, oligopeptides were added as terminal groups of the polymer chains to obtain cell-specific formulations (R_2 in Figure 1.3-1.c) [54].

Poly(amido amine) (Figure 1.3-1.d) is another kind of polymer which has been the subject of important developments. This kind of polymer allows a great versatility of architectures thanks to the numerous amine groups present which allow to tune and control the charge density and introduce functional moieties to the polycationic backbone [55]. Various complex architectures of oligo(amido amines) have been developed to better stabilize the polyplexes by introducing PEG moieties, tyrosine trimers as hydrophobic stabilizers and other ligands [56, 57]. Moreover, PEI-like polymers have been synthesized from various short synthetic amino acids (succinimidyl tetraethylene pentaamine or succinoyl-pentaethylene-hexamine) and their buffering capacity increased by the addition of histidine residues to favour the endosomal escape [56–58]. This polymer family is also suitable for the development of cationic dendrimers [59].

Finally, poly(aspartamides) (Figure 1.3-1.e) have also been synthesised and developed with various amounts of amine groups incorporated as side chains to tune the cationic behaviour of the polymer [60]. These side chains also allowed the modulation of the polymer hydrophobicity with the introduction of alkyl chains to favour specific assemblies such as vesicles [61, 62] when associated as block copolymer with a PEG block (see 1.3.2.2).

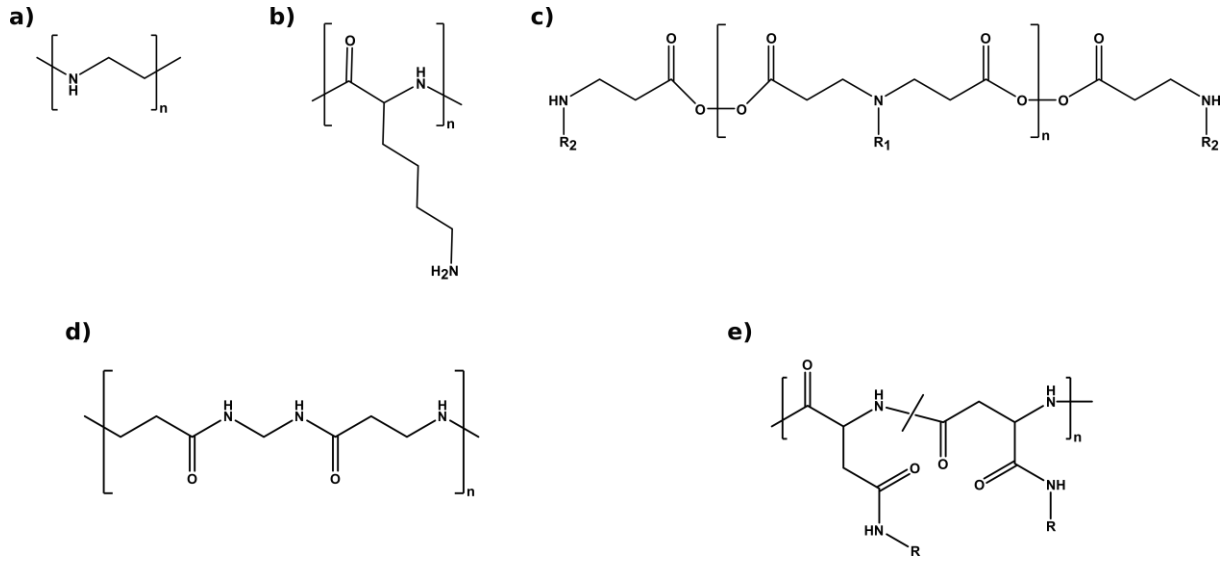

Figure 1.3-1. Chemical structures of a) poly(ethylene imine); b) poly(L-lysine); c) poly(β-amino esters); d) poly(amido amine); e) poly(aspartamides).

Additionally, these polymers have also been endowed with stimuli-responsiveness properties in order to release the cargo after cellular uptake. Indeed, the unpacking of the siRNA is equally important in order to obtain an efficient interference process [63]. Therefore, the use of stimuli-responsive bonds might be required in some situations. For example, cleavable bonds such as disulfide links may be used to degrade the vector [49–51, 55] and release siRNA in the cell. Another approach is the development of pH-responsive polymers. These are polymers which can be degraded under acidic or basic medium [51] and therefore release their cargo. Finally, photocleavable links has also been used to control the release of siRNA in time and space [64].

Finally, many studies have shown that the conjugation of PEG or other hydrophilic polymers to the polycationic backbone could reduce the size of the complexes with siRNA, the cytotoxicity as well as improving the stability of the complexes [57, 65]. Moreover, it showed great improvements in the biocompatibility and blood circulation time of the complexes [66].

Natural polymers

The natural polymers used for siRNA delivery are mostly polysaccharides. Among this large family of polymers, only one present naturally cationic charges to bind to siRNA, the chitosan. The properties of this polymer will be developed in a next part. However, other polysaccharides have also been proposed as complexing agents of siRNA. For this purpose, they have been chemically modified to introduce cationic moieties. The polysaccharides chosen for these approaches are water soluble and neutral such as dextran or pullulan [67] (Figure 1.3-2.a and Figure 1.3-2.b). In a first approach, dextran microgels were formed by copolymerizing dextran modified with hydroxyethyl methacrylate and dimethyl aminoethyl methacrylate to introduce positively charged moieties in order to bind to siRNA [68]. In another approach, pullulan and

dextran were modified by introducing spermine with the same goal to introduce cationised moieties to efficiently bind nucleic acids [69–71] (Figure 1.3-2.c to e). Amine groups of spermine have pKa values above physiological pH (7.4) [72]. Other chemical approaches aim to directly conjugate the siRNA with a cleavable bond on the polysaccharide backbone and promote the self-assembly with chemical or physical crosslinking [73, 74].

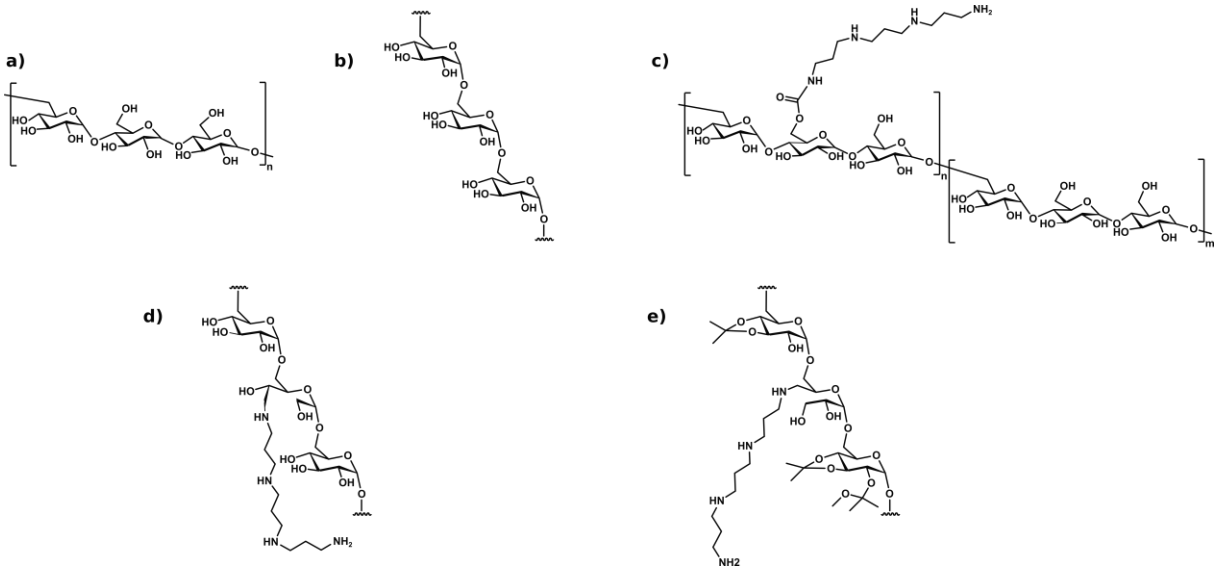

Figure 1.3-2. Chemical structures of a) pullulan, b) dextran, c) spermine-modified pullulan [67, 69] , d) spermine-modified dextran [70], e) spermine-modified acetalated-dextran [71].

1.3.2.2. Polymer carriers for siRNA delivery

Various formulations have been studied as potent carriers for nucleic acids delivery [75, 76]. One of the most studied and used is the polyelectrolyte complex (PEC) approach where two polyelectrolytes of opposite charges are mixed together, forming particles through electrostatic interactions [77] (Figure 1.3-3.a). This strategy will be the most discussed in this chapter. In the case of gene delivery, siRNA is the polyanion and chitosan can be the polycation introduced in excess. The excess of polycation allows the stabilisation of the complex particles and the protection of the cargo [78]. PECs are easy to prepare with only two components to mix together in aqueous solution [79, 80]. However, the electrostatic interaction between the two components can be challenged by other charged species in a biological media which can also interact with the positively charged shell of chitosan in excess.

Another approach is the formation of nanogels which are physically or chemically crosslinked [81, 82] (Figure 1.3-3.b). The physical crosslinking called ionic gelation is achieved with the introduction of an anionic crosslinker such as tripolyphosphate (TPP) to a polycation solution [83–85]. The siRNA is then adsorbed at nanogel surface thanks to the free positive charges left after ionic gelation [86]. Irreversible or reversible chemical crosslinking can be performed as

well. For instance, the introduction of thiolated groups on chitosan chains has shown great potential to form reversible crosslinked chitosan nanogels able to bind siRNA [74]. A more classical approach to form chitosan nanogels consists in the use of a crosslinking agent such as genipin [87], a much less toxic alternative to the historical crosslinking agents glutaraldehyde [88] and epichlorhydrine [89]. The introduction of cationic methacrylic moieties on dextran chains with various degrees of substitution has also been used to photoinitiate the crosslinking of dextran into microgel bearing cationic moieties [68]. The entrapment of siRNA in the nanogels can be achieved by introducing positive charges in the nanogel or thanks to the ones naturally present on the polymer chains.

Micelles are also used a lot for gene delivery as illustrated by the constant number of publications per year with the keywords 'siRNA' and 'micelle' (~ 40 publications each year since 2011, Scopus). In this context, the development of micelles has fostered the research on double hydrophilic block copolymers (DHBCs) composed of a cationic block and a hydrophilic and neutral block like PEG. A non-exhaustive list of polymers developed can be found in reference [90]. Micelles are typically formed in the presence of siRNA through electrostatic interactions between the negatively charged oligonucleotides and a double hydrophilic copolymer polycation-*b*-(PEG or PEG like polymer) [91] (Figure 1.3-3.c). The micelles are composed of a dehydrated core containing the siRNA complexed with the polycation, stabilised by a water-soluble block shell. Additionally, the core can be crosslinked with the introduction of reversible disulfide links, allowing a better stability [35]. Other approaches have also been developed for the use of micelle to co-deliver siRNA and a hydrophobic drug such as doxorubicin or paclitaxel. In that case, the use of an amphiphilic block copolymer such as PEG-*b*-PCL accounts for the formation of micelles where the hydrophobic core can immobilize the drug. The hydrophilic shell can be further modified to introduce cationic moieties to immobilize siRNA at micelle surface [92–94].

Another system used in nanomedicine is based on polymersomes, obtained from amphiphilic block copolymers with a well-defined hydrophilic/hydrophobic balance [95]. In the case of gene delivery, polymersomes have shown promising results to co-encapsulate and deliver siRNA. The membrane of polymersomes is formed thanks to the electrostatic interaction between siRNA and the cationic blocks of a double hydrophilic copolymer polycation-*b*-(PEG or PEG like polymer). The spontaneous self-assembly which results in the formation of either PIC micelles or PICsomes (Polyion complex polymersomes) is governed by the molecular packing of the block copolymers in the same manner as for neutral amphiphilic block copolymers. In the case of neutral amphiphilic block copolymers, it was empirically determined that the morphology of the objects is dependent on the hydrophilic mass fraction (f_H) in such a way that micelles are preferentially obtained when $f_H > 45\%$ while polymersomes are mainly formed when $f_H \approx 35\%$ [96]. However, a lower hydrophilic mass fraction is needed for the

formation of PICsomes (Figure 1.3-3.d) [61, 62, 97]. An active hydrophilic molecule can also be encapsulated inside the vesicles [61]. Polymersomes obtained by complexation of siRNA have been called siRNAsomes.

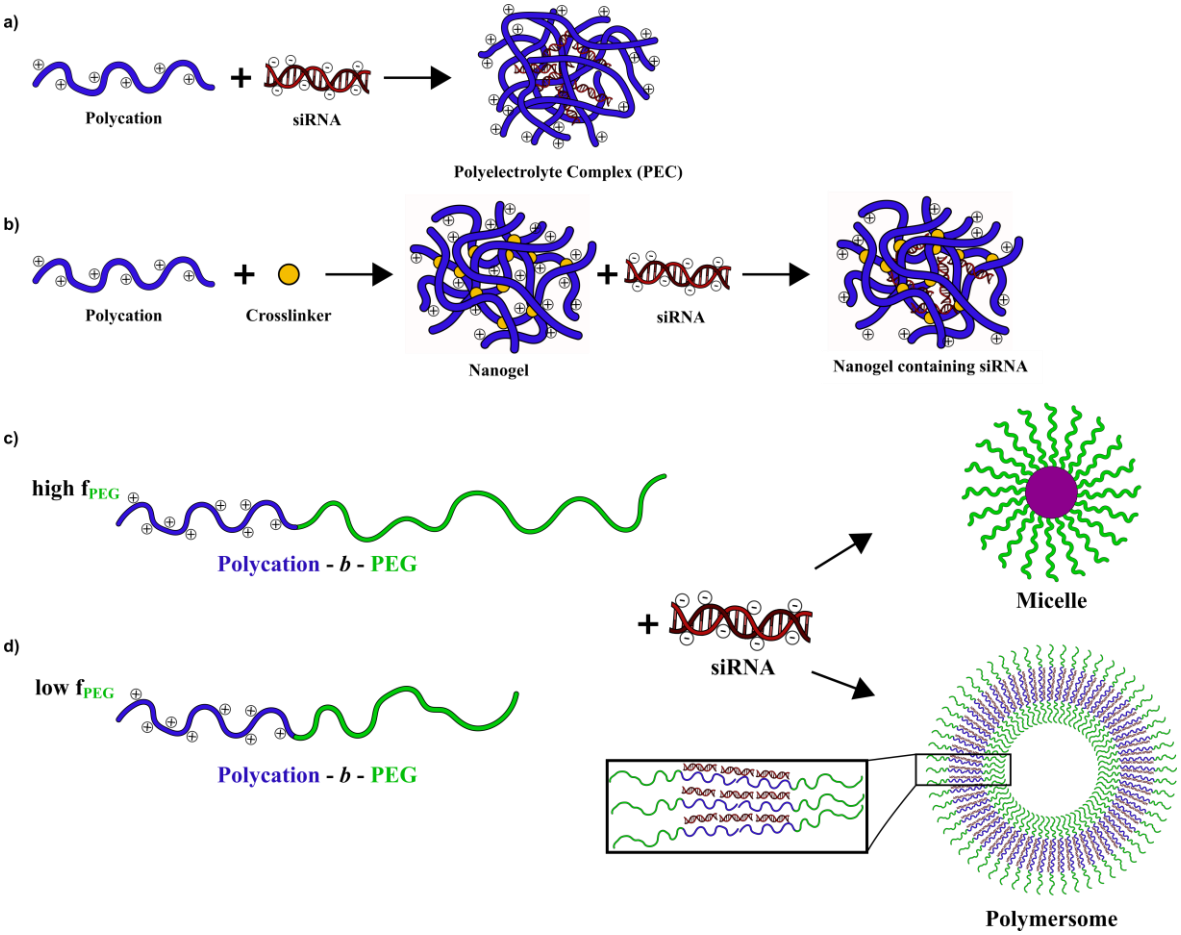

Figure 1.3-3. Formation of various carriers for siRNA delivery a) PECs, b) nanogels, c) polyion complex micelle, d) siRNAsome.

Dendriplexes that are obtained by a complexation approach with charged dendrimers are also a kind of vector suitable for siRNA delivery [59, 98, 99]. Dendrimers have been first reported in the late 70s [100]. Thanks to the design of cationic dendrimers, they have shown a potential to mediate high gene silencing with minor side effect both *in vitro* [101] and *in vivo* [102].

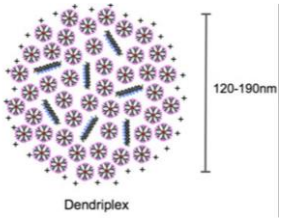

Figure 1.3-4. Structure of a dendriplex, a dendrimer-based PEC [102].

Finally, another type of system has been introduced a few years ago. It combines the conjugate approach as seen in section 1.2.3.2 and the electrostatic one as seen with the formation of polyplexes and PICs which results in the formation of a non-covalent conjugate that can be

referred as unit Polyion Complex (uPIC) [103, 104], monomolecular assembly [36] or nanosized polyplexes [105]. This kind of system is very similar to micelles in the use of a block copolymer polycation-*b*-PEG. However, the obtention of these water-soluble complexes from oppositely charged polyelectrolytes as introduced by Kabanov [106], Dautzenberg [107] and Tsuchida [108] in the 1980s becomes possible thanks to the limited size of the cationic block. Indeed, it should not exceed the length and number of charges of one siRNA strand to avoid intermolecular complexation but be long enough to efficiently bind to the oligonucleotide. The final structure consists of one siRNA molecule electrostatically complexed by one or several copolymers, resulting in a single entity which cannot further aggregate into larger structures (Figure 1.3-5). The conjugates obtained are then supposed to be at a thermodynamic equilibrium and therefore, the number of complexed copolymer chains per siRNA molecule is directly defined by the amount of copolymer chains introduced in presence of siRNA. By doing so, the formation of conjugates becomes much easier and versatile as compared to the chemical approach with the suppression of the laborious synthesis and purification steps where only one end of the dsRNA will be conjugated resulting in reduced affinity. Additionally, it may be possible to play on the copolymer grafting density through the size of cationic block and hence increase the stability of the complexes. One can also benefit from a multivalent targeting effect by increasing the number of targeting ligands at the surface of the complex. This approach leads to several advantages such as the small complex size (< 50 nm) which allows a reduced uptake by the reticuloendothelial system [103, 105], the precise control of the number of siRNA moieties per particle [103, 109], an efficient shielding to protect siRNA [36] and a good stability of the complexes [36].

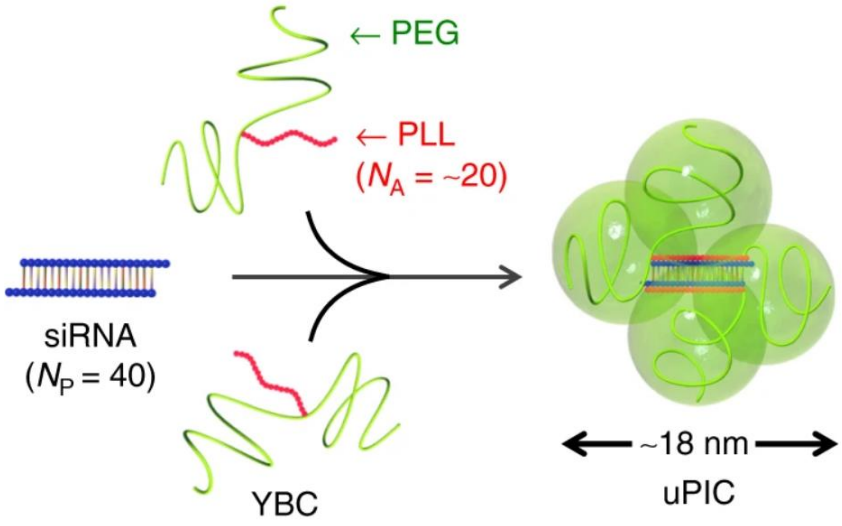

Figure 1.3-5. Scheme of a uPIC, a conjugate-like complex. YBC stands for Y-shaped Block Catiomer [103].

1.4. Chitosan as a natural carrier

1.4.1. Origin of chitosan

Chitosan is obtained from the partial N-deacetylation of chitin under alkaline conditions. If chitin was first isolated from mushrooms [110], it is nowadays mainly produced from various marine seashell wastes and thus available in large amounts in the fishery industry [111]. Chitin and chitosan from fungal origin are also commercially available under the trade name Kitozyme [112]. Chitin and chitosan have the same chemical structure as they are linear copolymers composed of D-glucosamine and N-acetyl-D-glucosamine linked by β-(1→4) glycosidic bonds (Figure 1.4-1). Their solubility properties allow to differentiate them: chitosan is soluble in slightly acid aqueous solutions like 1% acetic acid through the protonation of primary amines whereas chitin is insoluble in water, except for very low degrees of polymerization (DP < 6). Chitosan is therefore obtained when the degree of acetylation (DA) i.e., the molar fraction of acetylated units is sufficiently low so that enough glucosamine units can be protonated to solubilize the polymer chain. This condition is typically achieved when the DA is lower than 60-70% depending on the molar mass and the origin of chitosan.

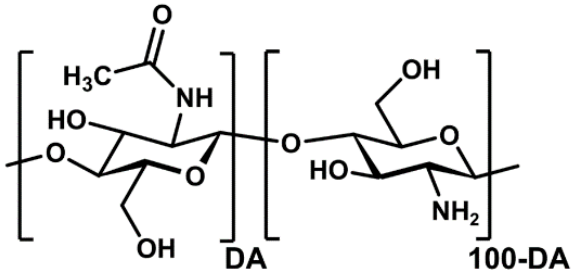

Figure 1.4-1. Chemical structure of chitosan. DA refers to the degree of acetylation.

Controlling the DA and the molar mass is essential with regard to the physicochemical and biological properties of chitosan. The control of the DA is achieved either by heterogeneous deacetylation of chitin with concentrated sodium hydroxide solutions at high temperatures [113] or by homogeneous reacetylation of a highly deacetylated chitosan with acetic anhydride under mild conditions in hydro-alcoholic mixtures [114]. The deacetylation approach tends to favour an irregular structure with a block distribution of acetylated units due to the semi-crystalline nature of the initial chitin which decreases the accessibility of the sodium hydroxide to reactive sites [115]. Conversely, the acetylation method gives a random distribution of the acetylated units along the chain. It is important to know the origin of the chitosan used because the pattern of the acetylated groups can strongly influence the solution properties of chitosan [115, 116] and also the biological activity [117, 118]. For example, a chitosan with DA = 50%

can be only partially soluble in acid solutions when heterogeneously deacetylated whereas it is always fully soluble in neutral aqueous medium when homogeneously acetylated at the same DA. Most commercial chitosans have a DA around 20% and are obtained by heterogeneous deacetylation; therefore, the presence of irregularities in the acetylation pattern cannot be excluded. The control of the molar mass is achieved through hydrolysis of the polymer chain by chemical or enzymatic approaches [119–122] or by means of an ultrasound treatment [123]. The polymer degradation can be monitored by size exclusion chromatography or viscometry. These different approaches allow to prepare chitosan oligosaccharides with a good control of the degree of polymerization [122, 124].

1.4.2. siRNA/chitosan complexes: which factors?

When it comes to the formulation of a delivery system for siRNA, various parameters have to be taken into account. Here, the parameters investigated are mainly related to chitosan, the only polysaccharide able to electrostatically complex siRNA on its native form.

1.4.2.1. Length of the polycation

The length of the polycation chains plays a critical role in the formation and activity of siRNA containing particles. The typical way to have access to a library of chitosan chain length is the controlled depolymerisation of long starting chitosan [122, 125]. It has been shown over the years – first for DNA and now for siRNA – that a critical length of the polymers is required to efficiently bind the nucleic acids in the optimized conditions of chitosan's protonation [126] (Figure 1.4-5). A cooperative binding is expected in the case of a polymer-oligomer interaction, as revealed by the exponential evolution of the binding constant with the polymerization degree of the polymer (Figure 1.4-2)[108]. It has been reported that the binding constant gradually increases with the length of the chitosan in the case of an interaction with DNA [127] but rather linearly than exponentially.

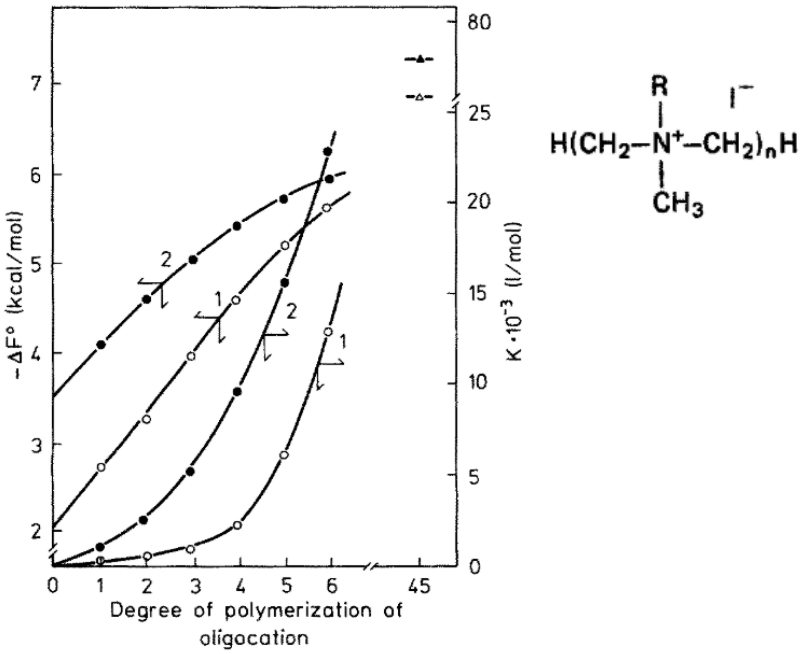

Figure 1.4-2. Dependence of the stability constants (K) and the free energy changes (-ΔF°) in the formation of polyelectrolyte complexes on the degree of polymerization of oligocations. System : polyanion: poly(methacrylic acid) (PMAA; degree of neutralization = 1, M_w = 5.3x10^4 g/mol) – oligocation: (1) R = CH_3 and (2) R = $CH_2C_6H_5$ [108, 128].

In the case of siRNA, a much shorter polyanion, similar findings did not fit properly the assumption of the exponential increase of the binding constant [78]. The length of the polycation will determine the stability of the complex particles (the free parts of chains stabilize the complex) but also the dissociation and release of the nucleic acids (the affinity increases with the chain length) [129, 130]. Efforts have been made to rationalize the effect of chain length of polycation on the particle properties regarding their siRNA content, their stability, cellular uptake etc. It was reported that the size of the particles is determined by the length of the chitosan for the use of low molecular weight chitosan [131, 132] (Figure 1.4-3.a) while no size effect was found with high molecular weight chitosan [78] (Figure 1.4-3.c). In a recent and comprehensive study, Buschmann et al. evidenced an increase of the internalization with the increase of the chitosan M_n with a threshold of 10 kDa. This increase in internalization is accompanied with an increase in the knockdown efficiency [131].

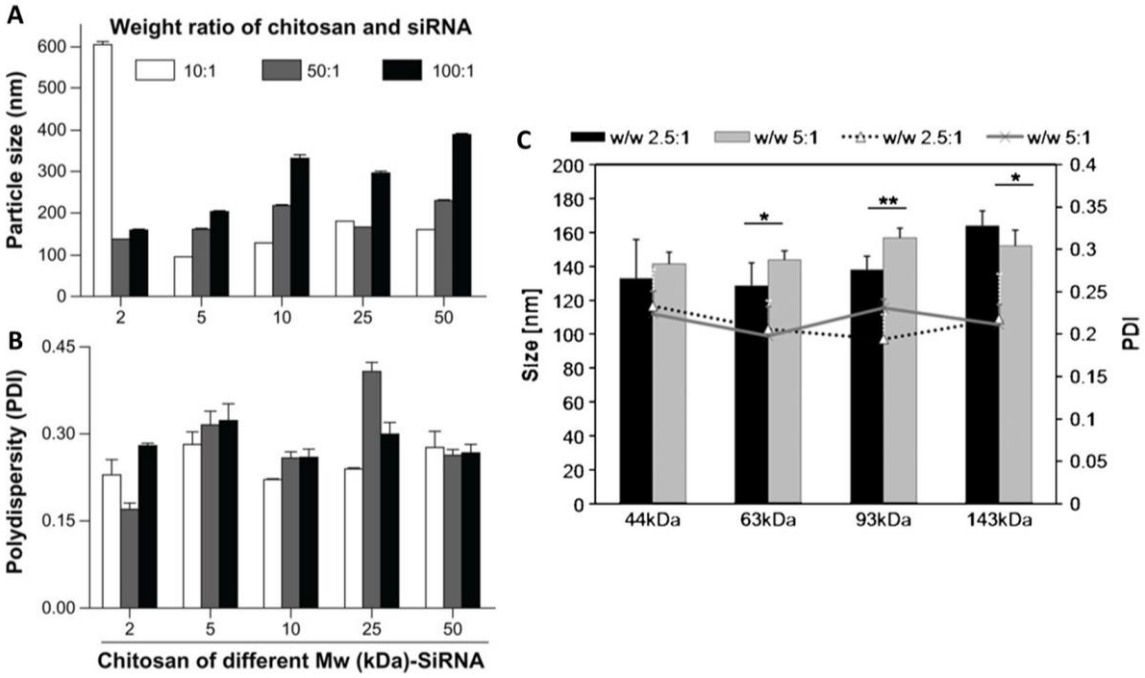

Figure 1.4-3. Size distributions and polydispersities of chitosan/siRNA polyplexes with different weight ratios of chitosan and siRNA in the case of Low molecular weight chitosans (A, B) [132] and High molecular weight chitosans (C) [78].

1.4.2.2. Acetylation degree of chitosan

The influence of the acetylation degree on the stability and transfection efficiency of the complexes has been studied for gene delivery systems. It is first known that the higher DA shows the lower cytotoxicity, the lowest DA involving the lowest charge density of chitosan [133, 134]. The control over the distribution of the acetylated units may also be of importance as it could be statistic or forming blocks depending on the method used to deacetylate as mentioned previously. Studies made on complexes of chitosan with DNA suggest that a fine balance has to be found regarding the DA to lower the affinity between the chitosan and the nucleic acid in order to unpack the DNA intracellularly while keeping it strong enough to protect it from degradation before reaching the target [135]. It was demonstrated that the binding affinity between chitosan and DNA increases with decreasing the DA at constant chitosan chain length which shows that the stability of the particles can be improved by playing with the DA [127, 136]. In the meantime, it was also demonstrated that the stoichiometry of the complexes does not depend on the acetylation degree of the chitosan since only the number of protonated amine groups has to be taken into account [127, 137]. This tendency which has been demonstrated in the case of DNAs was also demonstrated in the case of complexes made from chitosan and microRNAs where the dissociation constant increases with increasing the DA whether the chitosan is long or short [138]. Unfortunately, this parameter was scarcely studied

in the case of complexes with siRNA as compared to the influence of the chain length. However, a recent study suggests that the acetylation degree doesn't affect the size of the particles but it has an influence on the zeta-potential of the particles, the lower the DA, the higher the zeta-potential and the better the internalisation (and the gene knockdown) (Figure 1.4-4). It was also shown that the particles were the most stable with the lowest DA and a rather high N:P ratio of 30 [131]. Another study suggests that a DA of 16% and a N:P ratio of 150 lead to the highest knockdown efficiency [139].

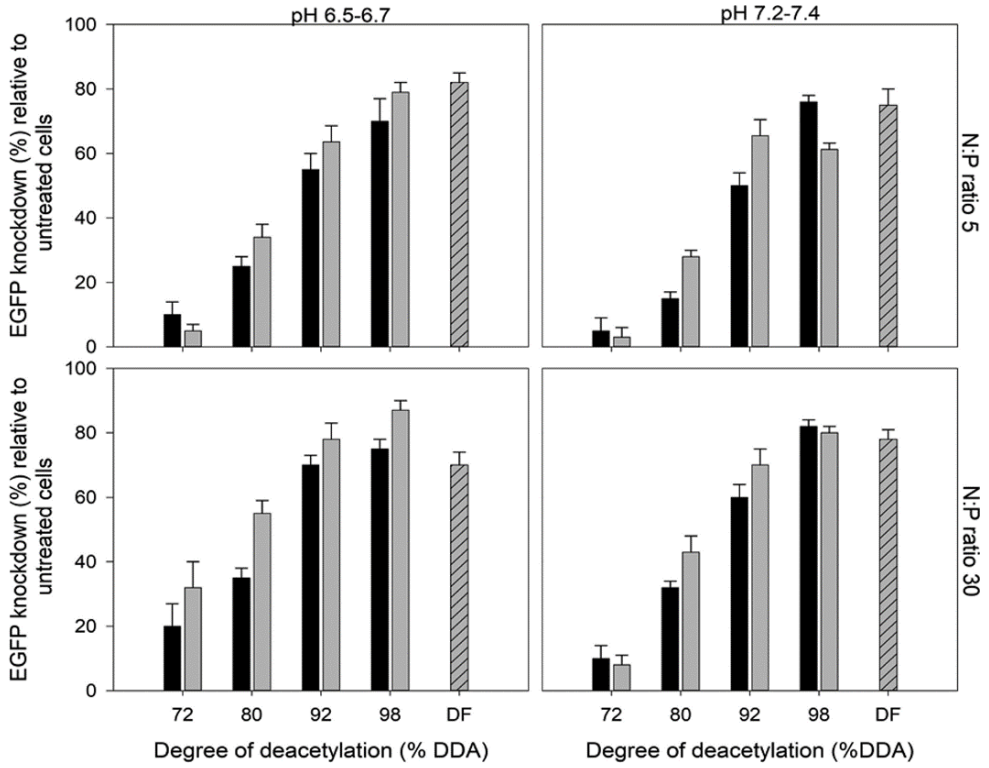

Figure 1.4-4. Effect of DDA (the degree of deacetylation, DDA = 100 – DA), Mn (black: 10kDa, grey: 120kDa), N:P ratio, and pH on the gene knockdown performance of chitosan-siRNA nanoparticles in the presence of 10% FBS. The pH of the cell medium culture was buffered with 20 mM MES to lower the pH to 6.5-6.7 [131].

1.4.2.3. Influence of the pH

The pH of the medium determines the ionization degree of the chitosan which also depends on the intrinsic parameters of the polymer (DA and MW) [140]. Chitosan presents a typical behaviour of polyelectrolytes as its pKa decreases when decreasing the dissociation degree due to the repulsion of neighbouring charged sites along the chain. The ionization of chitosan has also an effect on its solubility. The deprotonation can induce its precipitation above a critical pH value [141]. The ionization state of chitosan is of importance regarding its complexation

efficiency with siRNA. Indeed, the binding affinity decreases with increasing the pH [126, 127, 142], with the strongest affinity being for complete protonation (Figure 1.4-5).

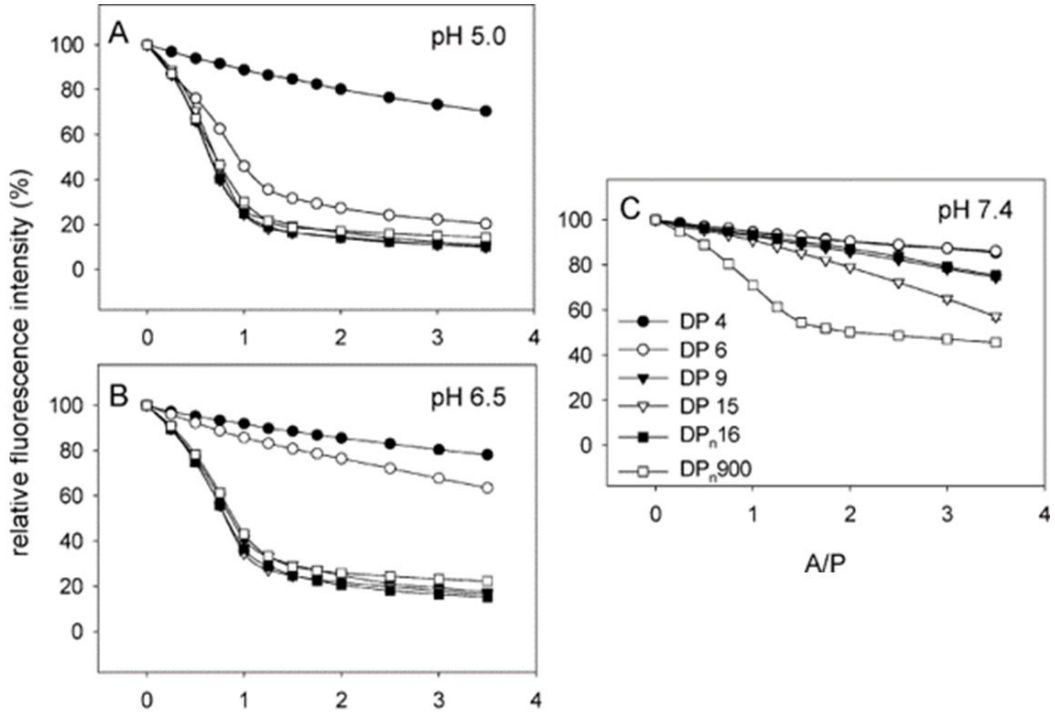

Figure 1.4-5. Titration of DNA-EtBr (Ethidium bromide) solution by fully deacetylated chitosan of various degrees of polymerization (DP). A/P represents the amine to phosphate ratio. A) in acetate buffer (pH = 5, 20 mM), B) in a MOPS buffer adjusted at pH = 6.5 (20 mM), C) in a MOPS buffer adjusted at pH = 7.4 (20 mM). I = 100 mM, adjusted for all the buffers. The decrease in fluorescence intensity is proportional to the fraction of DNA complexed by chitosan (the initial intense flurorescence of EtBr is due to the hydrophobic environment found between base pairs in DNA). From ref. [126].

1.4.2.4. Chemical modifications

Over the years, different approaches have been developed to improve the properties of polysaccharides as building blocks of nucleic acid vectors. One of these approaches is the chemical modification of the polysaccharide structure. First, in order to avoid the pH dependency of the degree of protonation of chitosan, various approaches were developed to quaternize the amine present on the chitosan backbone [143–147] (Figure 1.4-6.b and c). This approach improves the solubility of chitosan at higher pH and its ability to complex siRNA under neutral pH conditions. With the similar goal, chitosan can also be modified by introducing imidazole groups which account for an increase of the pKa of chitosan [148–150] (Figure 1.4-6.d and e). However, one has to be careful with the introduction of this kind of functions since it may induce cytotoxicity due to the large number of cationic groups able to interact with the cell membrane [146].

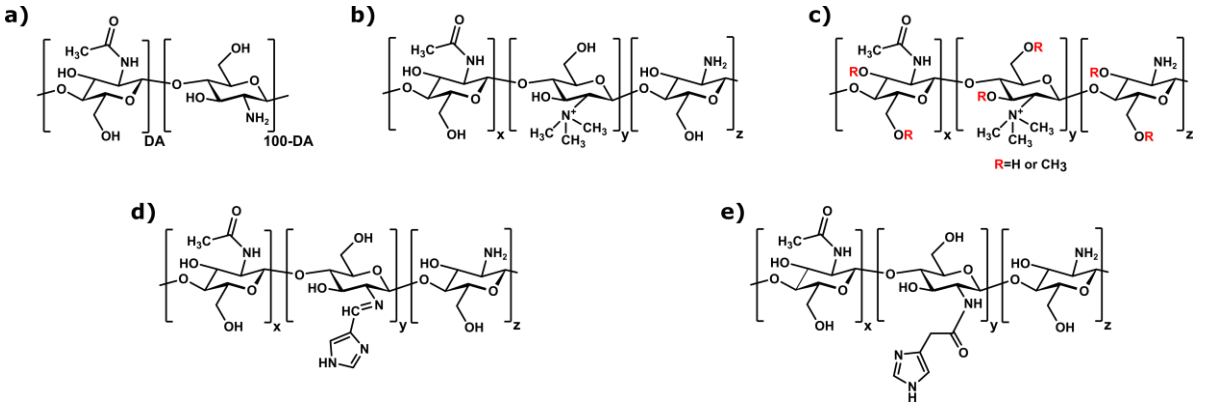

Figure 1.4-6. Chemical structures of a) chitosan, b) quaternized chitosan [143, 146], c) other type of quaternized chitosan [144, 145], d) chitosan modification with imidazole groups [148], e) other type of chitosan modification with imidazole groups [149, 150].

In addition to the modification of the cationicity of chitosan, the introduction of a stabilizing block is of particular interest regarding the improvement of the stability of the nanoparticles. Moreover, this kind of block presents interesting stealth properties that could be transferred to the complexes. Indeed, it was demonstrated that the introduction of a PEG block on the chitosan backbone could reduce the size of the complexes formulated in the same conditions as the non-PEGylated chitosan complexes. It also confers higher stability and lower toxicity to the chitosan/siRNA complex particles [132]. However, the introduction of this moiety is often made through the modification of the primary amine on the chitosan backbone [151, 152] which might be an issue when the number of charged units is low, i.e. for chitosan of high DA and/or of low molecular weight (Figure 1.4-7.a). Moreover, even if the synthesis is done in mild conditions, it does not allow a precise control of the number of units grafted on the chitosan and their distribution on the backbone. To overcome this issue, another synthetic pathway taking advantage of the aldehyde group in equilibrium with its hemiacetalic form at the reducing end of polysaccharides has been developed (Figure 1.4-7.b). It offers new opportunities for the synthesis of linear diblock copolymers with a precise control of their composition [153–156]. This type of macromolecular architecture could allow the access to new structures poorly investigated with polysaccharides such as micelles, PICsomes and conjugate-like structure (see section 1.3.2.2).

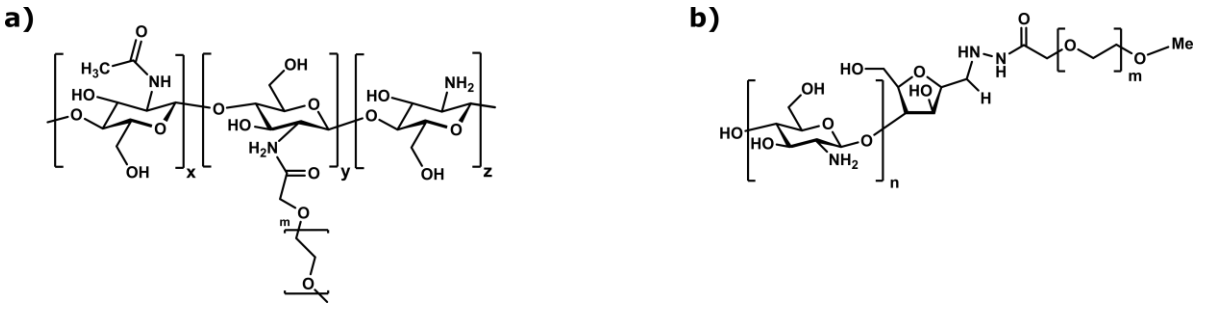

Figure 1.4-7. Chemical structures of PEG-modified chitosans. a) chitosan-g-PEG from the reaction of chitosan with a NHS-methoxy PEG [152] b) chitosan-b-PEG from the reaction of a PEG-hydrazide at the chitosan reducing end [156].

1.4.3. Formulation and analysis of the complexes

In addition to the role played by intrinsic parameters of chitosan on the properties of complexes (charge, size), it is also important to pay attention to the experimental conditions (pH, mixing) used to prepare the complexes. Indeed, they can play an important role on the final morphology and properties of the complexes. Moreover, a particular attention is needed regarding the characterization of the complexes since many aspects involving the size and the stability can be clarified before any costly biological assays. This part will therefore contain a brief discussion regarding the techniques available to characterize the size and stability of the complexes.

1.4.3.1. Medium of complexation

First, since the pH of the solution has an important effect on the ionization degree of the polycation, it can impact the stoichiometry of the complexes formed [137, 157]. Different approaches have been proposed to control the ionization degree:

- the complexation is performed with the chitosan fully protonated (addition of a stoichiometric amount of HCl or use of chitosan under its hydrochloride form) [130, 131].

- the complexation is performed in a buffer adjusted at a certain pH [78, 139].

Another aspect regarding the medium of complexation is the ionic strength. The strength of the interaction decreases with the increase of the ionic strength due to the screening effect of the ions [40]. Moreover, the formation of the complexes in presence of salt can induce changes and rearrangements of the PECs structure leading to smaller particles at low salt concentration but aggregation at higher salt content, which is specific for each system [158, 159]. With this aspect in mind, the formation of the complexes is usually done at relatively low ionic strength (< 100 mM). However, one has to keep in mind that the ionic strength in a biological media is quite

high (i.e. around 154 mM) and may induce a decrease in the colloidal stability of the system leading to aggregation or decomplexation phenomena [159, 160]. These aspects can be summarized as shown in (Figure 1.4-8) [136].

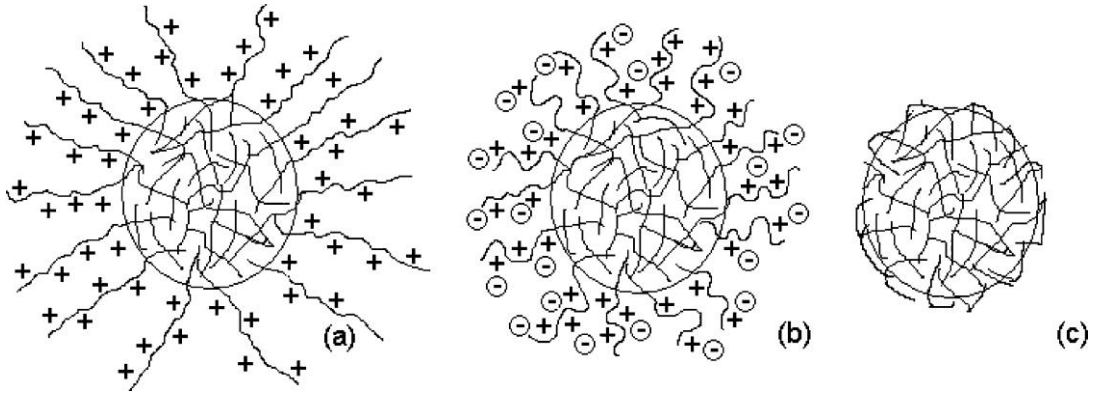

Figure 1.4-8. Mechanism of PEC stabilization: (a) at acid pHs and low ionic strength (electrostatic and steric stabilization occurred), (b) at acid pHs and high ionic strength (steric stabilization only), and (c) at neutral pH (no stabilization) [136].

1.4.3.2. Mixing of the components

Different ways of mixing the chitosan solution with siRNA to form PECs are possible and the variety of the mixing conditions used makes it difficult to rationalize their role on the morphology and properties of PECs.

Indeed, the interaction of the chitosan with siRNA is strong and therefore the association of these two polyelectrolytes is governed by the kinetics rather than the thermodynamics, leading to frozen, out-of equilibrium structures. Accordingly, the reaction time between two oppositely charged polyelectrolytes is in the order of the microsecond which corresponds to the typical diffusion-collision time of PEs in solution [161]. With this aspect in mind, PECs are preferentially obtained with a fast mixing of the two components. Some exceptions remain, as the slow addition of chitosan in siRNA which was found to be also successful in some cases [78]. However, the mixing of the two components was performed under stirring to allow a good homogenization of the two solutions and avoid local over concentration during the complexation step [130, 139]. Unfortunately, this aspect is not always mentioned in the formulation process of the PECs formed with siRNA. It is also important in general to consider the way of addition. It is indeed considered that the most reliable formulation pathway is when the component in default is added in the one in excess to avoid the system to cross the charge neutralization state which favours the aggregation [160, 162] (Figure 1.4-9).

The literature on the subject can provide promising formulation pathway to formulate chitosan-based polyplexes in the most reliable manner. First, the concentration of the starting solutions

has to be considered as it was shown that the size of the PEC particles is strongly concentration dependent [158–160, 162] as shown by the increase of the size, polydispersity and aggregation indexes of complexes with increasing the polymer concentration. In order to obtain stable particles, one of the two components have to be in excess to form a stabilizing shell at the complex surface [160]. This parameter is expressed as the N:P ratio which corresponds to the number of amine groups carried by the chitosan to the number of phosphate groups carried by the siRNA. In the optimised pH conditions (pH ≤ 4 for full ionization of chitosan), this ratio corresponds to the effective charge ratio z = +/- since the pKa of the phosphate groups is closed to 1.5 ensuring a constant anionic charge density of the siRNA over the usual pH range investigated [163]. The N:P ratio is generally at least equal to 5 [131] or even more [139] to ensure that the chitosan is in large excess to stabilize and protect the particles and its cargo. Moreover, it was suggested that the excess of polycation which is non-complexed to the siRNA improves the transfection efficiency [67]. No specific trend of the complex size with the N:P ratio has been evidenced.

The final aspect to consider is the volumes of solution used for the complexation, i.e. microliters or millilitres. Low volumes of solution are usually involved in the preparation of complexes not only because of the cost of siRNA but also to ensure a good homogeneity of the mixture and rapid diffusion of species during the mixing step. Besides, microfluidic has become a promising tool to produce polyplexes in a larger quantity. It allows a better control over the size, polydispersity and ensures a good reproducibility but requires specific equipment and knowledge [164, 165].

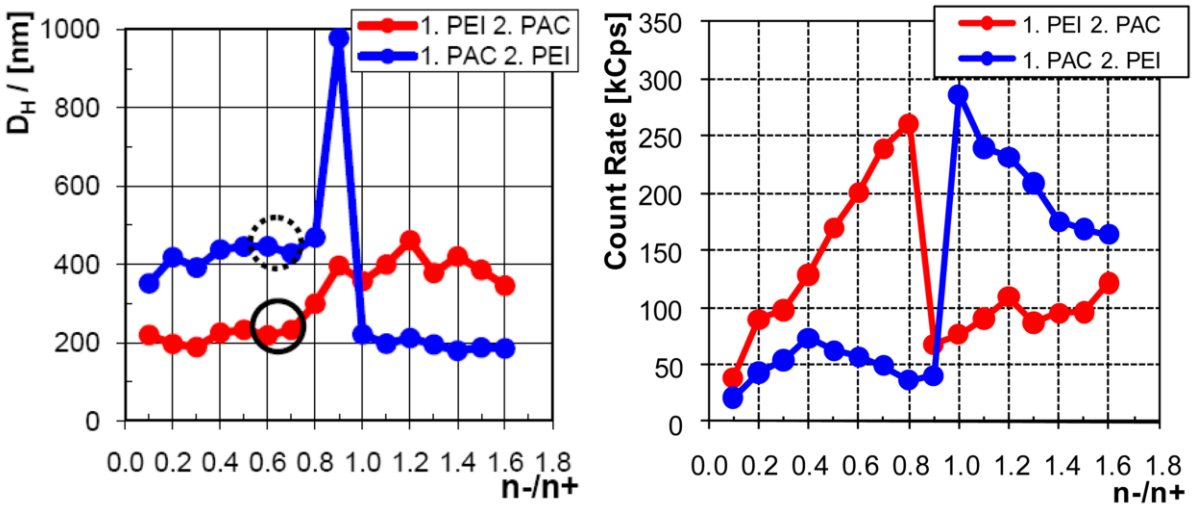

Figure 1.4-9. Size of poly(ethyleneimine)/poly(acrylic acid) complex particles as a function of the charge ratio n-/n+ (left) and count rate values as a function of the mixing ratio (right) (PEI solution at pH = 4 and PAC solution at pH = 10). Two ways of addition of components are considered: PEI in PAC (red) and PAC in PEI (blue) [162].

1.4.3.3. Evaluation of the entrapment efficiency

Once the particles are formed, it is important to assess the loading content of siRNA as the non-complexed siRNA can be degraded or lost. Various techniques are available for the titration of free siRNA after complexation. For instance, a variety of commercial fluorescent molecules are available [71, 131, 146], replacing the well-known but toxic ethidium bromide. Nevertheless, the fluorescent probes need to be used in specific conditions of concentrations and pH in order to obtain a linear and accurate calibration. The same kind of measurement can be done with a fluorescently labelled siRNA by measuring the fluorescence of the supernatant after centrifugation of the complexes. Another approach is the determination of free siRNA in the supernatant with a spectrophotometer since nucleic acids absorb at 260 nm, which allows their direct quantification in solution [86, 166, 167]. However, this technique shows less sensitivity than with fluorescent probes even though it is faster to use.

1.4.3.4. Size assessment of the complexes

Dynamic Light Scattering (DLS) is one of the most common techniques to determine the size of polyplexes. Indeed, it is one of the techniques which is the fastest, easiest and cheapest to implement. However, special care is needed regarding the analysis and the preparation of the samples. First, the analysis of polyelectrolytes by DLS is really specific compared to the analysis of neutral polymers, where an unusual behaviour is observed. Two modes can be observed and have been subject to thorough researches [168]: a “fast-mode” corresponding to the polyelectrolyte chains, and a “slow-mode” attributed to aggregates or compact multi chains structures [169]. The first mode has been explained by the coupling of the counterions with the charges of the polyelectrolyte [169] or a model of Brownian particles accelerated due to interactions between each other [170] and is dependent of the ionic concentration in solution. The higher the salt concentration, the more the size given by this mode corresponds to neutral chain size, due to the electrostatic screening of the interactions [170].

Moreover, chitosan is particularly subject to self-aggregation [171–173]. The aggregates formed are weakly bounded as evidenced by their disruption under low shear stress [174] which suggests that they should disappear during the strong electrostatic interaction with siRNA.

Finally, DLS is a powerful instrument to use in routine for the screening of the conditions and stability but might not be enough to fully characterize a system [175, 176]. Indeed, apart from the hydrodynamic size of the objects, the DLS analysis performed at a single angle does not provide any information on their morphology even though it is often assumed that they are spherical in shape. This can be verified by performing DLS measurements at various angles,

which gives a better determination of the apparent diffusion coefficient and emphasizes the possible formation of anisotropic structures or the presence of internal relaxation modes [176, 177]. DLS is also very sensitive to the presence of large objects in the case of polydisperse samples and to background effects such as the presence of proteins in biological media. Therefore, all conditions cannot be investigated (e.g. behaviour of complexes in a serum) [178]. However, the combination of DLS with Static Light Scattering (SLS) allows a detailed characterization of a system with the access to various parameters of the objects such as the gyration radius (R_g) and the hydrodynamic radius (R_h) to estimate the morphology of the samples and the aggregation number (N_{agg}) [176].

Other techniques can be used to further characterize the system such as microscopy techniques like transmission electron microscopy (TEM) and atomic force microscopy (AFM). TEM can be used in the dry state with a staining agent for the visualization of polymeric materials [176]. However, this can lead to some difficulties to optimize the conditions of staining. Therefore cryo-TEM might be of better use for polymeric objects even though it is also subject to artefacts such as the presence of ice introduced during the sample preparation and is subject to a low signal to noise ratio.

AFM is a promising technique to visualize the three-dimensional profile of the particles and access to their size. However, this is a very time-consuming technique where some physical changes of the sample can occur due to the tip of the cantilever [175] and the spreading of the complexes on the surface of the substrate (silica, mica, graphite) used for the analysis.

Fluorescence Correlation Spectroscopy (FCS) and related techniques are also promising tools based on the analysis of the fluctuations of fluorescence. They are mostly used in the field of biological systems [179] but start also to be used for the study of synthetic self-assembled systems. The measurements which are done in a very low volume can be performed in various media, i.e in presence of proteins, since only fluorescently labelled objects are visualised. It can also be used to follow the intracellular fate of the complexes [38]. Moreover, the technique is usually “limited” to the determination of the diffusion coefficients of the species but tremendous efforts have been made to generalize methods of analysis to access to the distribution of diffusion coefficients [180]. However, it requires the fluorescent labelling of the objects and a particular attention must be paid to the analysis of the experimental data [175].

1.4.4. Biological application of complexes of chitosan-siRNA

Once a gene delivery vector seems to fulfil the previous requirements, it can be biologically evaluated. First *in vitro*, to ensure that the protection of the cargo and the transfection efficiency are effective and then *in vivo*, to assess the potency in real conditions.

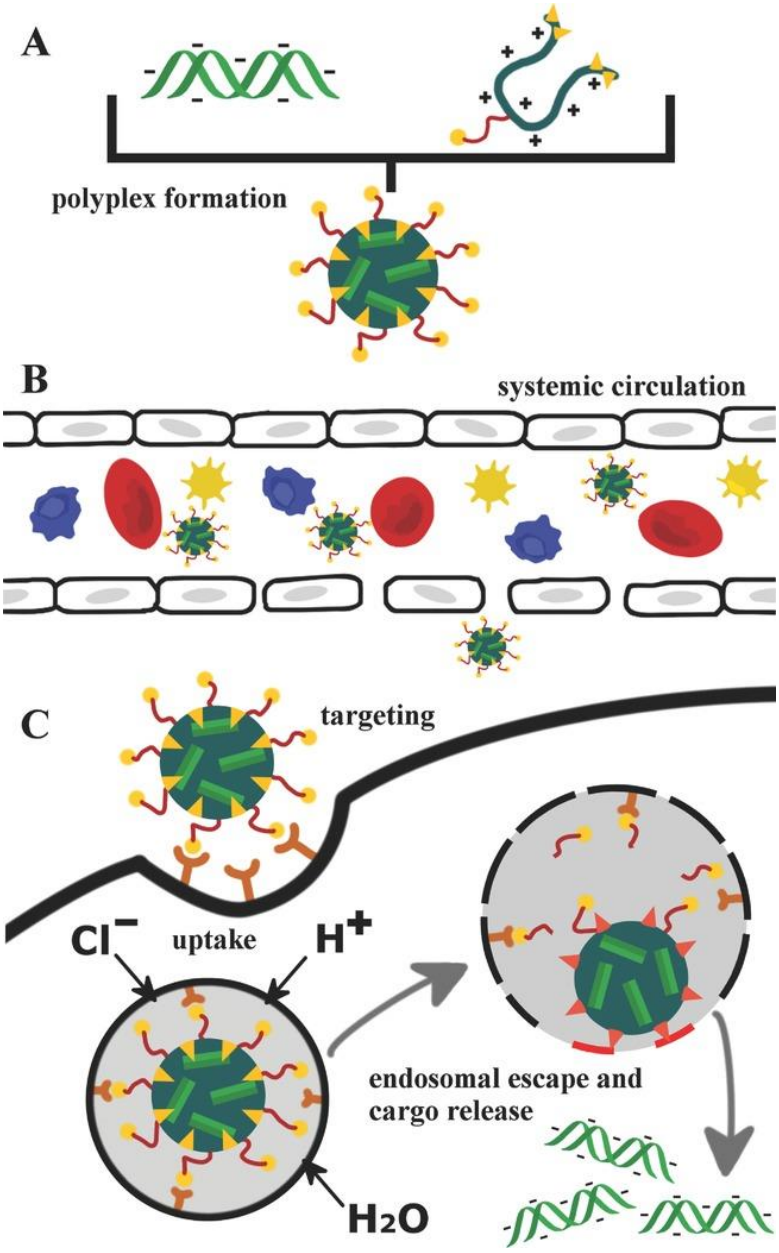

Figure 1.4-10. The various barriers to cross for the nucleic acid delivery from polyplexes. a) Formation of stable polyplexes, b) avoidance of rapid clearance and nonspecific interactions with blood components, c) receptor targeting, endocytosis, endosomal escape and cytosolic cargo release [181].

1.4.4.1. In vitro

The biological evaluation of a non-viral siRNA delivering system starts with the study of its cytotoxicity. Even though chitosan is a biodegradable and biocompatible polymer as shown by its FDA approval for wound dressing purposes, it is a different matter for its use in gene delivery material. Indeed, *in vitro* toxicity of chitosan has been evidenced depending on the acetylation degree and molecular weight of the polymer [133, 182]. The molecular weight will have a prominent cytotoxic effect in the case of high DA, similarly to a polycation presenting a high charge density [47]. Moreover, the chemical modifications of the polycation can also induce cytotoxicity from either the modification itself or the residual chemical compounds. Furthermore, it is necessary to evaluate the cytotoxicity of the complexes themselves in addition to the components alone since their behaviour may be different [182]. The mechanism of action of siRNA taking place inside the cells, it is also necessary to ensure that the internalization of the complexes in the cell does really take place. This can be assessed by confocal microscopy [86, 183, 184] or by flow cytometry [131, 185, 186] (Figure 1.4-12). For both techniques, it is necessary to use a fluorescently labelled siRNA and carefully choose the excitation and emission wavelengths to avoid any overlapping of the fluorescent signals. If the cellular uptake and internalization of complexes are successful, the complexes have yet to escape the endosomes/lysosomes. This escape can be achieved thanks to the buffering capacity of the nanocarrier system which can trigger a proton sponge mechanism where the osmotic pressure inside the lysosome increases, leading to its rupture [45, 187] (Figure 1.4-10.c). Chitosan as well as PEI present this proton sponge behaviour due to their relatively low pKa [188] and could therefore benefit from this lysosomal escape pathway. This hypothesis could also be verified by adding chloroquine as a lysosomotropic agent; the latter has little influence on the transfection efficiency, indicating that the endosomal escape from the system is primarily due to the buffering capacity of the carrier [184, 189]. Finally, the gene interference needs to be evaluated by using, for example, a cell line expressing the luciferase gene [78, 83] or the (enhanced) green fluorescent protein ((e)GFP) [68, 73, 86, 131, 139, 146, 152, 184, 185] or a combination of the two [165] and measuring the relative decrease in photon emission (from the bioluminescence of luciferase or the fluorescence of eGFP) due to the gene expression knockdown after interference (Figure 1.4-11).

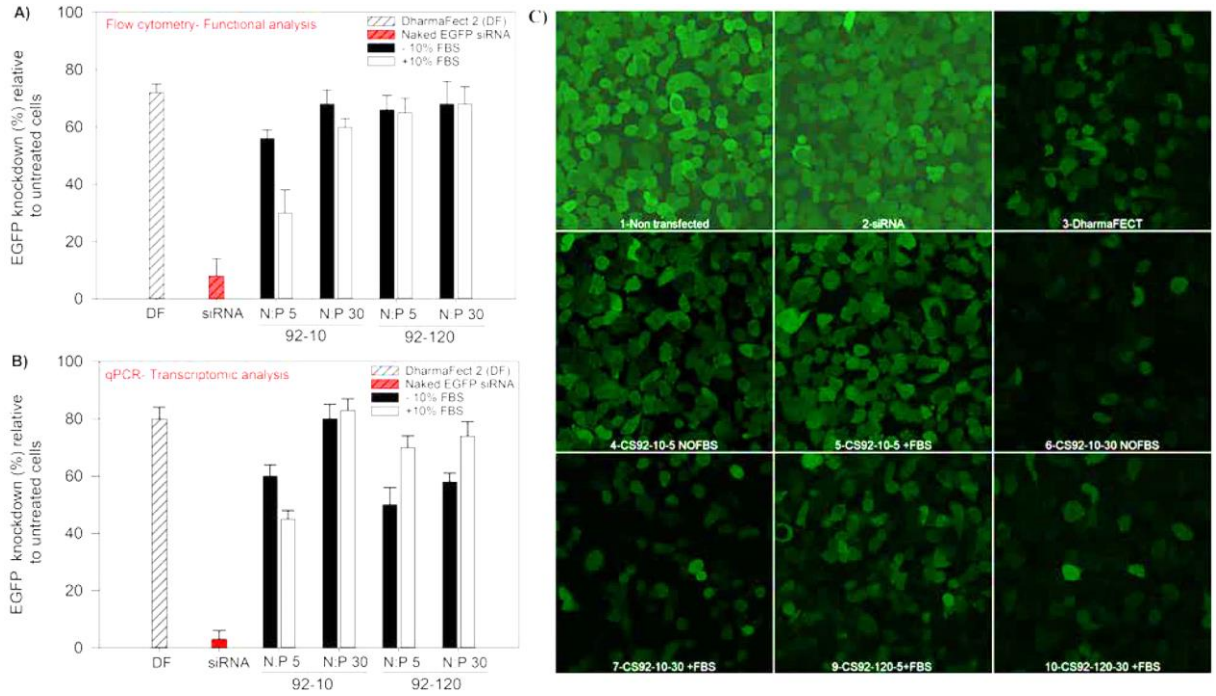

Figure 1.4-11. Effect of FBS, chitosan M_n (10 kDa or 120 kDa), and N:P ratio at 92% deacetylation (DA = 8%) on EGFP knockdown in H1299 cells. (A) EGFP knockdown measured as the average fluorescence intensity (FI) relative to untreated cells 48 h post transfection with siEGFP. EGFP+ H1299 cells were transfected in the absence or presence of 10% serum for a period of 5 h, media aspirated, replenished with complete RPMI-1640 media (pH 7.2−7.4, 290 mOsm), and incubated for an additional 43 h before analysis. (B) EGFP mRNA knockdown measured using qPCR, normalized using the geometric average of EIF, PUM-1, and GAPDH and calibrated to untreated cells. EGFP+ H1299 cells were treated as described in A. (C) Representative confocal laser scanning microscopy (CLSM) images. EGFP is indicated in green. In all experiments, siRNA was delivered at a final concentration of 100 nM, and data in A and B are expressed as the average values of 3 independent experiments with 2 or 3 technical replicates per experiment (N =3, n =6−9). *p-value < 0.01. From ref. [131].

In the case of a specific application using a targeted gene, the mRNA can directly be quantified by quantitative RT-PCR and hence the interference efficiency evaluated [92, 132, 145, 186, 190, 191]. Finally, the interference levels can also be deduced from the quantification of the proteins coded by the targeted gene [74, 145, 150, 151, 164, 186, 192–194]. In any cases, the experiments are done with a positive control ensuring the highest levels of transfection (e.g. Lipofectamine) and an appropriate negative control.

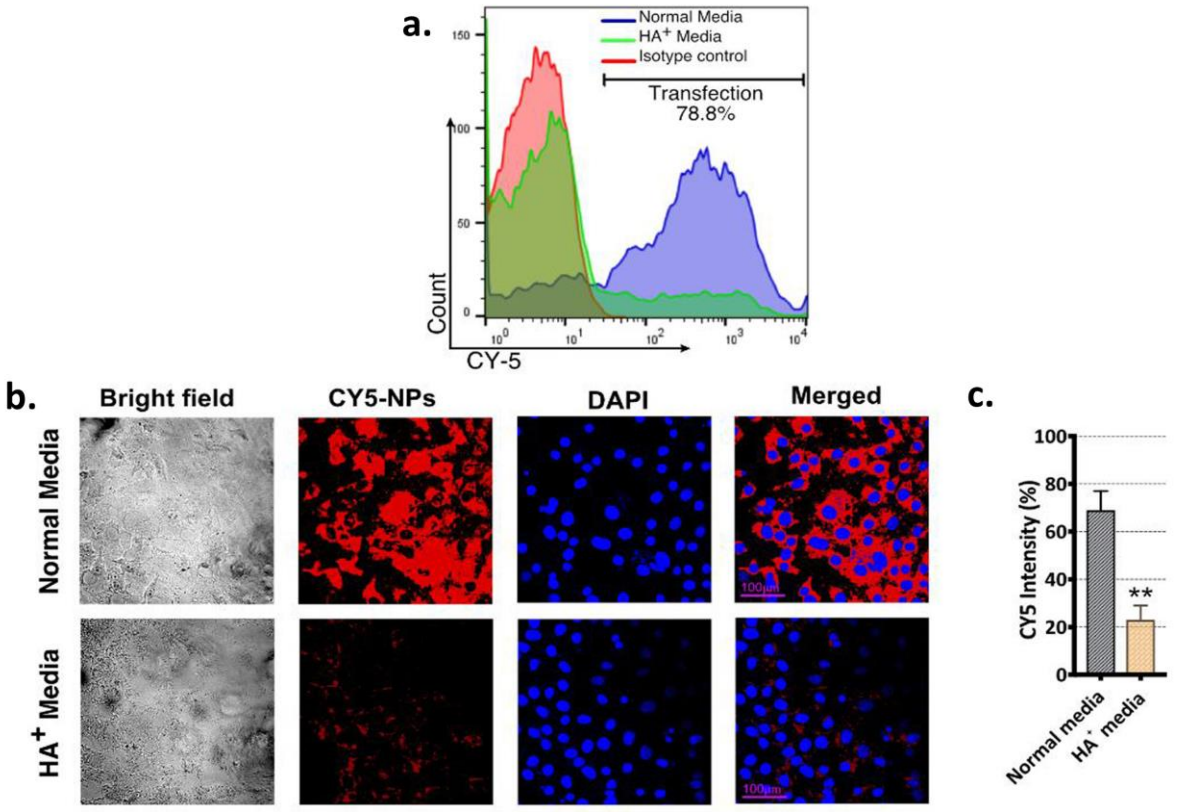

Figure 1.4-12. Uptake of a PEG-quaternized chitosan-hyaluronic acid complex encapsulating a Cy5 labelled siRNA. (a) assay by flow cytometry, (b) & (c) assay by confocal microscopy with and without hyaluronic acid. DAPI is used for nuclear staining [145].

1.4.4.2. In vivo

Different administration pathways are used in order to assay the *in vivo* behaviour of the particles depending on the expression's site of the disease. The material can be injected intravenously, usually in the tail of the mice [74, 92, 131, 186, 193–195] or even directly into the tumour [196]. The complexes are administered via intranasal route [184, 197] or through oral route [192, 198]. The biodistribution is evaluated after administration, *in vivo* with the help of fluorescent probes (in the near-infrared region) [74, 92, 194] or sometimes ex vivo [131, 186, 192, 193] after sacrifice of the mice. The common *in-vivo* behaviour observed with the nano vectors is their accumulation in the kidney, due to the fast renal clearance of such objects [74, 131, 193]. The accumulation in the liver is also a typical behaviour of the complexes and one of the major barrier to overcome [74, 131, 186, 190]. Similarly to the *in vitro* analysis, the interference efficiency can be evaluated in vivo through the quantification of the encoded proteins [74, 186, 192, 196] or the mRNA [197, 198] of the targeted genes. Other more visual methods can also be applied to assay the efficiency of siRNA vectors by monitoring the tumour size in case of a targeted cancer [74, 92, 186, 194–196] or by targeting a fluorescent protein

expressed by the mice and measure the possible decrease in the fluorescence intensity in the same manner as *in vitro* [73, 184, 194].

1.4.4.3. Improvements of the vectors

In the vast field of drug delivery, one of the main obstacles is to transfer a technology from *in vitro* to the *in vivo* application. With this aspect in mind, major improvements and developments have been made to overcome the accumulation of the vehicles in the liver or in the kidneys. The use of various ligands at the vector surface, in order to specifically target some receptors overexpressed on cells, has gained a lot of interest [199] (Figure 1.4-10.c). This specific targeting approach has also been used for chitosan-based siRNA delivery systems and has shown encouraging results regarding their specificity and efficiency [200]. The various ligands of choice to specifically target the cells of interest can be antibodies, peptides or smaller molecules [199]. Sugars can be efficient and cheap ligands, such as hyaluronic acid [145] (Figure 1.4-12.b and c), mannose [186] or galactose [192] to specifically target the cells of interest (e.g. cancer cells). Another targeting ligand for cancer cells is the folic acid which enhances the cellular uptake [148] and the interference effect [132, 196, 201]. A peptide derived from the rabies virus glycoprotein (RVG) has also been studied to target brain cells *in vivo* and has shown encouraging silencing effect *in vitro* [193]. Finally, chitosan-based particles with antibodies has also shown good results for the specific targeting of T cells [191]. Another efficient approach to enhance the effects of a chitosan-based nanocarrier is the co-delivery of two active moieties [200]. The delivery of two active species can indeed benefit from the synergistic effect of the two components. For example, the co-delivery of siRNA and doxorubicin has gained some interest regarding the treatment of cancers [92, 202–204]. The co-delivery of two different siRNAs has also been investigated to silence the expression of cancer specific proteins [145, 186].

1.5. Chitosan and metals

Chitin and chitosan have started to be the subject of thorough researches regarding their chelating properties during the 70's [205]. Since then, the researchers kept their interest on the subject to characterize chitosan and its chelating behavior in presence of metals. Various parameters have been studied such as the acetylation degree of the polymer, the intrinsic properties of metals, the influence of the pH and concentration of each species, etc. The interest of this topic grew with the aim to use chitosan and derivatives as sustainable materials for water treatment. More recently, the chelating properties of chitosan have been applied to the

stabilization of colloids such as polyelectrolyte complexes (PECs) which is here our point of interest.

1.5.1. Interaction of chitosan with metal ions

1.5.1.1. Highlights on the chitosan-metal interaction

The fundamental study of the interaction between chitosan and metals has been investigated over the years by means of different approaches. One of the most simple and common technique used to evidence the chitosan-metal interaction is potentiometry. In 1983, Joon Woo Park and al. [206] proposed a straightforward approach to show the mechanism of interaction between $-NH_2$ groups of chitosan and copper ions by comparing the titration curves obtained with D-glucosamine and the one obtained with chitosan. Alain Domard [207] demonstrated the same interaction between chitosan and copper ions thanks to titration methods and was able to evidence the structure of the complexes thanks to circular dichroism, suggesting a complex of the type [Cu $NH_2(OH)_2$]. M. Rhazi et al. later completed the potentiometric study on the interaction between chitosan and copper ions [208] and found that two types of complexes could be obtained, depending on the pH of the solution: $\{[Cu(-NH_2)]^{2+}, 2OH^-, H_2O\}$ for a pH between 5.3 and 5.8 and $\{[Cu(-NH_2)_2]^{2+}, 2OH^-\}$ when the pH is above 5.8, which corresponds to a threshold in the fraction of deprotonated amino groups. Further studies also used potentiometric titrations to characterize similar compounds, based on other metallic ions such as iron [209], cobalt and zinc [210] and others [211]. Infrared spectroscopy has also been used to evidence the interaction between the chelating groups of chitosan and metallic ions. Indeed, infrared spectroscopy of chitosan has been thoroughly studied over the years to determine the DA of chitosan [212, 213] and therefore most of the vibration bands have been assigned. In another study A. Domard et al. [214] could show the disappearance of the characteristic peak of the $-NH_2$ group after complexation of chitosan with uranyl ions as well as the appearance of new peaks. Other observations were also made in presence of metallic ions like zinc where the bending vibration of $-NH_2$ groups at 1617 cm^{-1} shifted to higher wavenumber upon chelation with metallic ions [215, 216]; new peaks also appeared and were assigned to stretching vibrations of N-Zn and O-Zn in the 533-534 cm^{-1} range and 472-476 cm^{-1} [215–217] (Figure 1.5-1). The same observations were made in the case of a modified O,N-carboxymethyl chitosan in presence of zinc [218]. Finally, the interaction between iron and chitosan was evidenced in a similar manner [219]. The binding of metallic ions was also studied by Isothermal Titration Calorimetry (ITC), allowing the determination of binding constants and other thermodynamic quantities in the conditions of experimentation [220, 221].

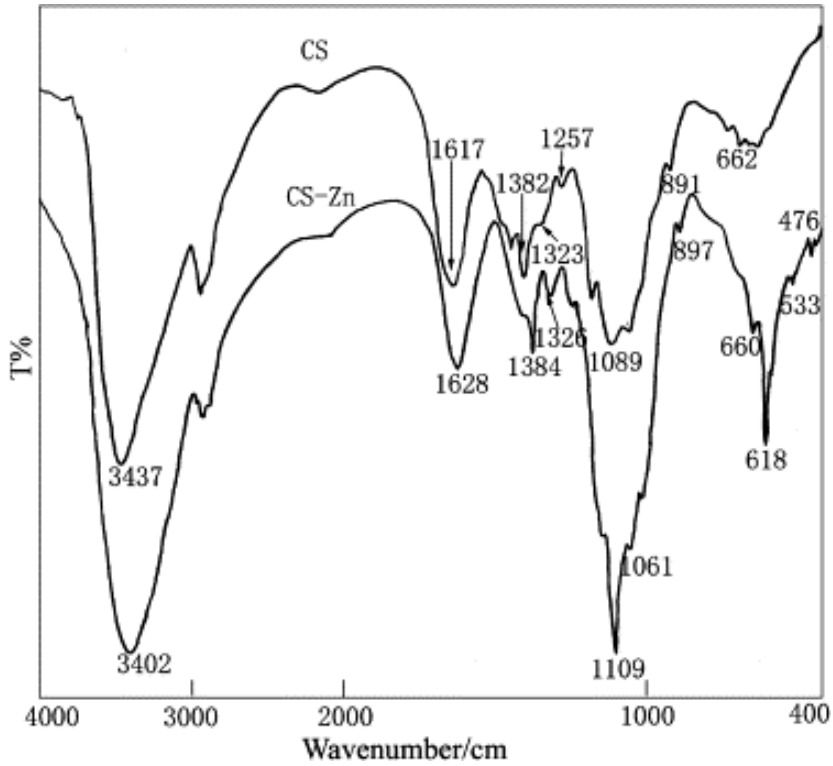

Figure 1.5-1. FTIR spectra of Chitosan and Chitosan–Zn complexes. From ref. [215].

X-ray diffraction experiments were also conducted on the complexes formed from the mixture of chitosan and metals. These experiments inform on the morphology of chitosan in presence of various metals. Indeed, chitosan alone has a typical X-ray diffraction pattern with 2 peaks, at 2θ = 10° corresponding to the orthorhombic "form I" crystal (a = 7.76, b = 10.91, and c = 10.30 Å) and another one around 20° attributed to the orthorhombic "form II" crystal (a = 4.4, b = 10.0, and c = 10.3 Å) [222], a crystallinity originating from the inter- and intra-molecular hydrogen bonds of chitosan [215, 223]. The metallic ions studied had various influence on the morphology depending on their nature. Copper seems to lower the crystallinity of chitosan [224] whereas nickel had little influence [223]. This was explained by the strong affinity that copper presents for the coordinating nitrogen atoms and hydroxyl groups, thus lowering the intensity of hydrogen bonding [223]. A similar behavior seems to take place in presence of Fe^{3+} ions, with also a decrease in crystallinity [209]. Zinc ions allow the conservation of a crystalline phase [223] even though the crystalline phase obtained could be different depending on the zinc salt used, the zinc counterions determining the hydration state of the phase [215, 224].

1.5.1.2. Quantifying the chitosan's chelating potential

The quantification of the chitosan's chelating potential has been a challenge in the early years, depending on the technique used to characterize the interaction metal-chitosan. The

conceptualization of the treatment of titration data has been established in previous years. Harry P. Gregor and al. [225] showed indeed that it was possible to estimate the number of ligands per metallic ion in the case of polyacrylic acid (PAA) and copper. These concepts were also generalized by H. M. Irving and H. S. Rossotti [226] allowing the establishment of common notations for titration experiments that will be more detailed in the chapter 4. Mainly, the term ñ corresponding to the degree of formation of the metal-ligand complex was introduced as following:

$$\tilde{n} = \frac{total\ concentration\ of\ ligand\ bound\ to\ metal}{total\ concentration\ of\ metal} = \frac{([-NH_2]_t - [-NH_2] - [-NH_3^+])}{[M^{2+}]_t}$$

with $[-NH_2]_t$ the total concentration of amine groups; $[-NH_2]$ the concentration of deprotonated amine groups; $[-NH_3^+]$ the concentration of protonated amine groups and $[M^{2+}]_t$ the total concentration of metallic ions.

For instance, it was found that the highest amount of copper ions complexed was about one Cu^{2+} for two $-NH_2$ groups if the chitosan contains a minimum of 6 monomeric units, as seen by spectrophotometric experiments [208]. In the case of cobalt and zinc, chitosan is also a good ligand as shown by the determination of species distribution diagrams [210] (Figure 1.5-2). Depending on the pH conditions, zinc and cobalt can form either [ML] or $[ML_2]$ complexes where M is the metal ions and L the ligand ($-NH_2$ group). In a similar manner, the formation of different complexes with a hexacoordinated form were found for Fe^{3+} depending on the pH of the solution ($[FeNO_2Cl_3]$, $[FeN_2O_2Cl_2]$, $[FeN_3O_3]$ and $[FeN_2O_4]$)[227]. The elemental analysis has been also used to confirm the chelation for various metallic ions. It was found that chitosan could complex up to one zinc atom per monomeric unit of chitosan [215].

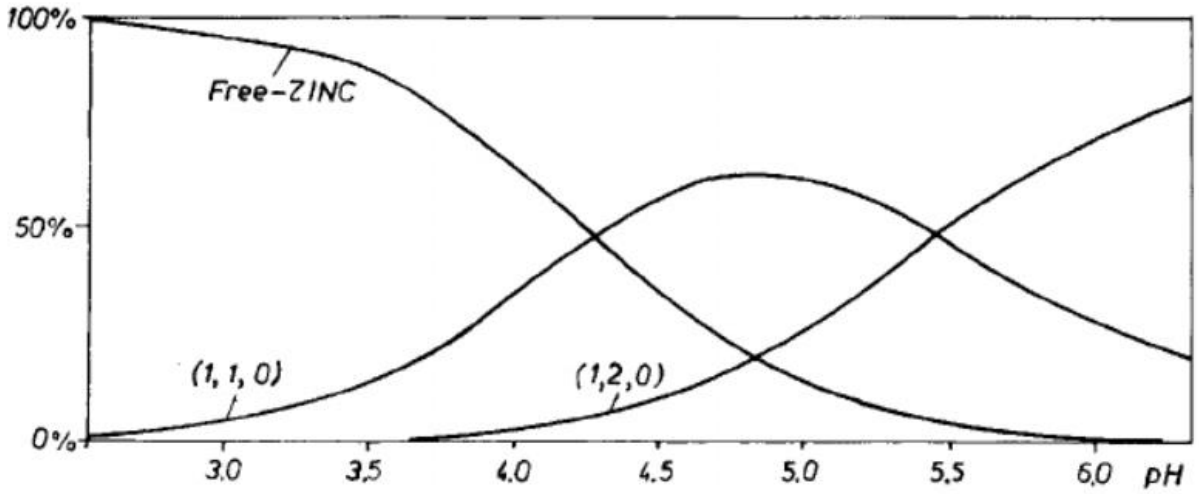

Figure 1.5-2. Species distribution diagram in the Zn (II) - chitosan system. $C_{Zn} = 2.22x10^{-3}$ mol/dm^3; $C_L = 2.22x10^{-2}$ mol/dm^3 (Zn/N = 0.1). (1,1,0) corresponds to a complex [ZnL] and (1,2,0) corresponds to a complex of the type $[ZnL_2]$. From ref. [210].

These findings were also corroborated by computational studies on chitooligosaccharides (COS). Density functional theory calculations showed indeed an order of stability of the complexes depending on the metallic ions, being Cu > Ni > Zn [228, 229]. Molecular dynamics simulations between COS molecules and Mg^{2+}, Fe^{2+} or Zn^{2+} also suggest the formation of complexes composed of 2 trisaccharides of glucosamine residues for 1 divalent ion [230] (Figure 1.5-3).

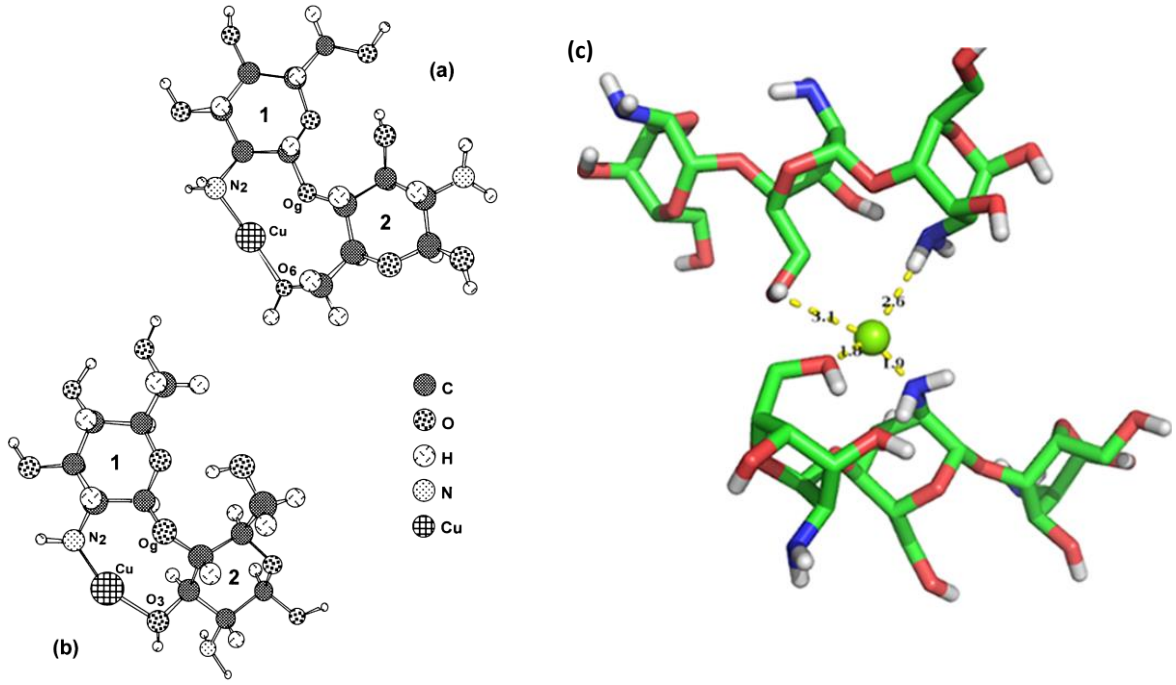

Figure 1.5-3. Simulated structures of the complexes formed between chitosan oligosaccharides and metals. a) and b) are the most stable structures obtained by DFT (density functional theory) calculations for chitosan-copper complexes from ref. [229]. c) Representative example of COS-Fe^{2+}/Zn^{2+}/Mg^{2+} complex obtained by Molecular Dynamics. The green ball represents the target Fe^{2+}/Zn^{2+}/Mg^{2+} ion, the red atoms oxygen atoms and blue ones, nitrogen. From ref. [230].

1.5.1.3. Parameters influencing the chelation

Various parameters have an effect on the chelation properties of chitosan. First of all, it is well established that the chelation properties of chitosan are before anything else, due to the presence of the amino group on the chitosan backbone. Indeed, it has been shown that the chelation is the most efficient with the deprotonation of the amines and the pH has therefore a major influence on the chitosan adsorption capacity [208, 211, 231–233]. The degree of acetylation has also an impact on the chitosan chelation behaviour, a 50% deacetylation degree being the threshold for a minimal relevant absorption of copper ions [234]. However, other studies suggest that a deacetylated amino group is not always necessary to observe a binding of metallic ions even though the chitin used was not characterized [221]. Additionally, the interaction is

shown much stronger from a deacetylated chitosan than from chitin when the two products are compared in the same conditions [235]. The affinity of deacetylated chitosan towards different individual divalent metallic ions has been established as Cu^{2+} >> Hg^{2+}> Zn^{2+}> Cd^{2+}> Ni^{2+}> Co^{2+} ~ Ca^{2+} and shown being not influenced by the physical form of chitosan (film, in solution or as powder) [211]. Moreover, this affinity was also visible in selectivity as Cu^{2+} is always bound selectively to chitosan in presence of other cations [231]. A recent study demonstrated the importance of the type of anion on the adsorption of heavy metal, the adsorption being significantly of higher extent for the metal cations of the sulfate salt [236]. Finally, it seems that a minimal length of 6 units for the chitosan chains is required in order to have an efficient binding of the chitosan towards copper [208].

1.5.2. Application of the chelating properties of chitosan

1.5.2.1. Chitosan for water treatment

Regarding its important chelating properties, chitosan has been extensively used as material for water treatment. Indeed, chitosan presents the most important chelating ability as compared to other common natural materials [237]. With this potential in mind, this capacity has been extensively developed by means of several modifications in order to increase the absorption capacity and selectivity. For instance, various composites have been developed based on chitosan or chitin as material for water treatment [238]. Under its native state, chitosan has shown great capacity to remove heavy metals like zinc, copper, cadmium, and lead from wastewaters [232, 233]. In the same manner, chitin has shown a small and lower affinity towards the chelation of a variety of metals [221].

This chelating property of chitosan toward heavy metals has also been hijacked in order to improve the binding affinity of chitosan to other compounds. For instance, microparticles of chitosan and zinc or chitosan and iron (III) have been successfully prepared and used to improve the adsorption capacity of chitosan for ciprofloxacin [239], making it a good candidate for the treatment of hospital wastewater.

This approach has also been adapted for the removal of phosphate ions. The low sorption capacity of phosphate ions from a formulation composed of bentonite clay and chitosan, could indeed be enhanced thanks to the introduction of metals (Fe, Ca or Zr) [240]. A chitosan-zinc complex has also shown great capacity in phosphate removal from aqueous solution, based on the mechanism proposed in Figure 1.5-4 [216]. Zinc ions chelated by free amines of the chitosan enable the complexation of phosphate ions in solution thanks to an electrostatic interaction

between the positive charge of the zinc ions and the negative one from the phosphate ions. This type of system could therefore be applied to the formation of complexes between the zinc chelated chitosan and the charged phosphate groups of nucleic acids.

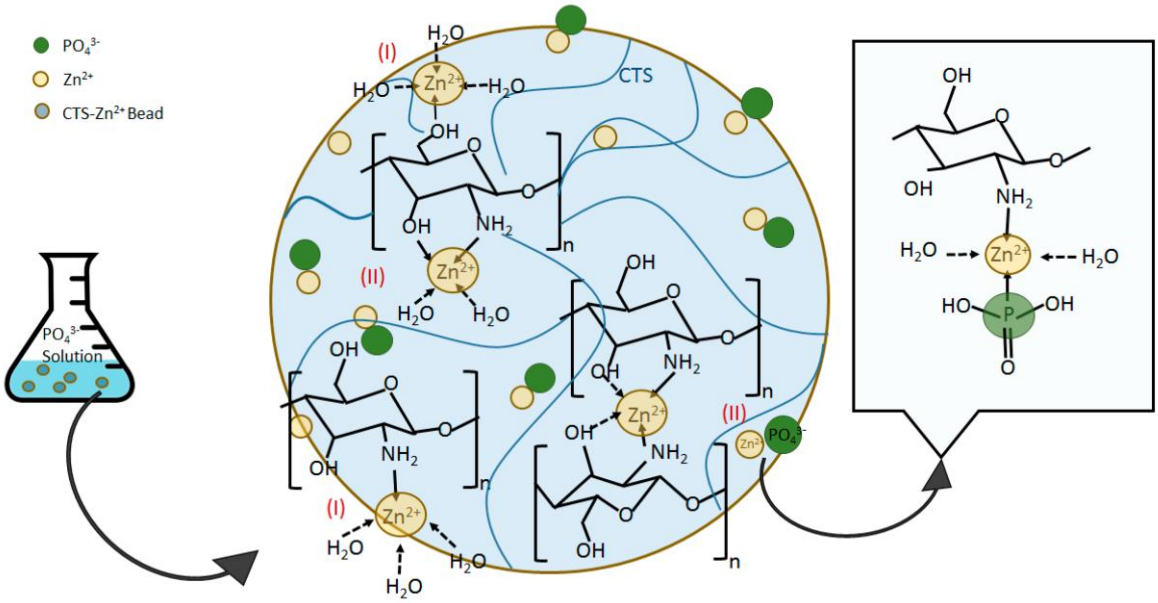

Figure 1.5-4. Chelation of Zn^{2+} by chitosan to enhance the phosphate uptake. From ref. [216].

1.5.2.2. The introduction of zinc to enhance the polycations biological properties

When applied to colloids and more specifically gene delivery, the use of metals has been considered to improve the stability and transfection efficiency of the complexes. For instance, the addition of zinc coordinating moieties on a branched PEI could effectively reduce the size of the complexes and improve the internalization of the complexes [241] (Figure 1.5-5). When applied to other polycations, the addition of zinc coordinating moieties could also improve the complexing properties of various polycations: decrease of the complex size, improved affinity towards nucleic acids and a greater cellular uptake efficacy [242]. Further studies on the introduction of zinc chelating moieties in a polycationic backbone showed also improved properties in gene transfection efficiency [243–245].

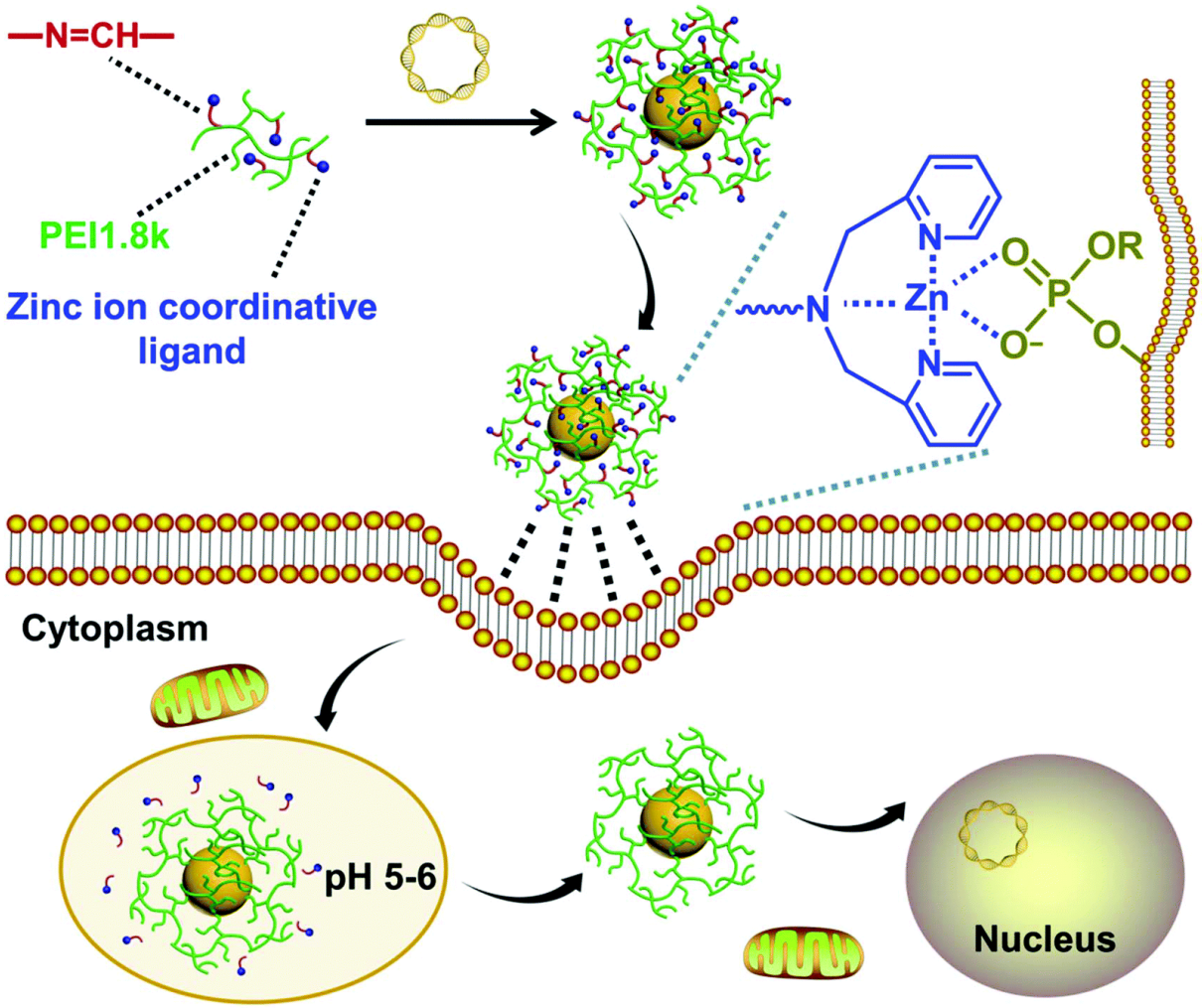

Figure 1.5-5. PEI-based zinc coordinating system for gene delivery. From ref. [241].

More generally, metals have been used to improve the chitosan properties for various biological applications. For instance, the use of a chitosan-zinc complex could greatly improve the antimicrobial properties of the native chitosan and offer a wider spectrum of antimicrobial properties. Indeed, the complex is 8 times more active than the chitosan alone against three bacteria [215]. In the field of colloids, the addition of zinc ions could greatly improve the stability of PECs based on chitosan and hyaluronan, up to 35 days in a phosphate buffered saline [246]. Additionally, this zinc-stabilized complex showed improved properties and great potential as anti-HIV therapeutic [247]. Finally, the incorporation of iron in chitosan-polyphosphate nanogels can greatly improve their properties in terms of stability and cellular uptake [219].

1.6. Nucleic acids interaction with metal ions

The behavior of nucleic acids in presence of transition metals has been studied for a long time, since it was discovered that strong coordinative bond could be formed between DNA and transition metals. From a fundamental point of view, the interest for this particular aspect grew in order to understand the mechanisms of interaction between metallic ions in solution and DNA. Another aspect was also the development of new applications based on this kind of interaction [248]. For instance, it was discovered that a complex of DNA involving Pt^{II} could become a strong antitumor agent now known as Cisplatin [249].

The interaction of nucleic acid with divalent metal ions has been largely studied as they are involved in the activity of enzymes with DNA and RNA, allowing rearrangements leading to various structures with specific activities [250–252]. A well-described phenomenon is the condensation of nucleic acid chains in presence of multivalent cations [253]. This phenomenon is mainly governed by electrostatic interactions with DNA. Indeed, it is stated that 90% of the DNA charge must be neutralized for the condensation to occur. However, the condensation does not induce conformational changes as shown by circular dichroism experiments. Pushed to further limits, this condensation observed with trivalent counterions has been called reentrant condensation and is characterized by an inversion of the global charge of the nucleic acids [254, 255].

In the literature, two types of interactions are discussed. Mainly, the electrostatic interaction referred as the ‘outer sphere’ binding, preferentially localized on the charged phosphate groups of the backbone and the coordinative bonding referred as the ‘inner sphere’ binding, localized on the nucleobases [256]. The latter might be preferred for transition metal ions but the behaviour of each cation is different with possible in-between behaviour and also a dependency on the sequence (some cations seem to be more sensitive to specific nucleobases-rich area) [256–258].

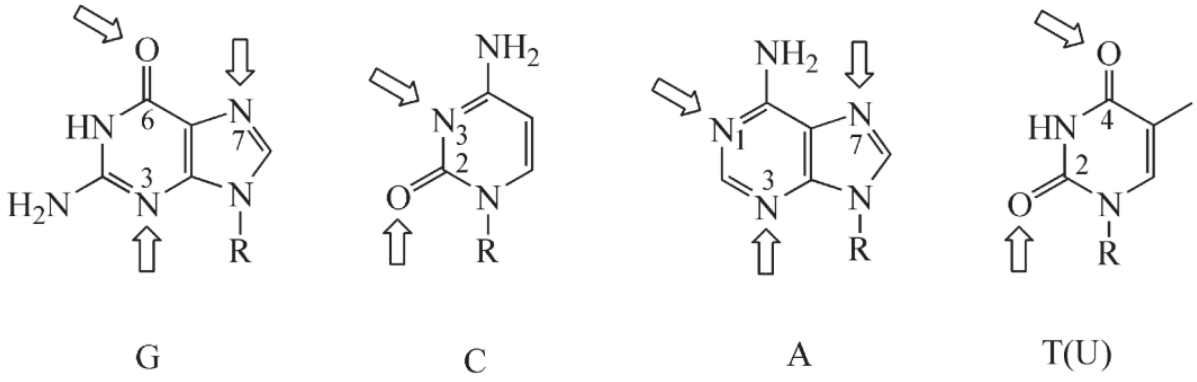

Figure 1.6-1. Metal binding sites of the nucleobases for coordinative bonding. From ref. [256].

These affinities have been particularly studied through thermal denaturation profiles: the increase or decrease of the melting temperature denotes the preferential site of binding and its nature (electrostatic *vs.* coordination) [259, 260]. It has been stated that the order of affinity towards the nucleobases would be Mg(II) < Co(II), Ni(II) < Mn(II) < Zn(II) < Cd(II) < Cu(II) < Ag(I) < Hg(II) based on melting temperature experiments [259].

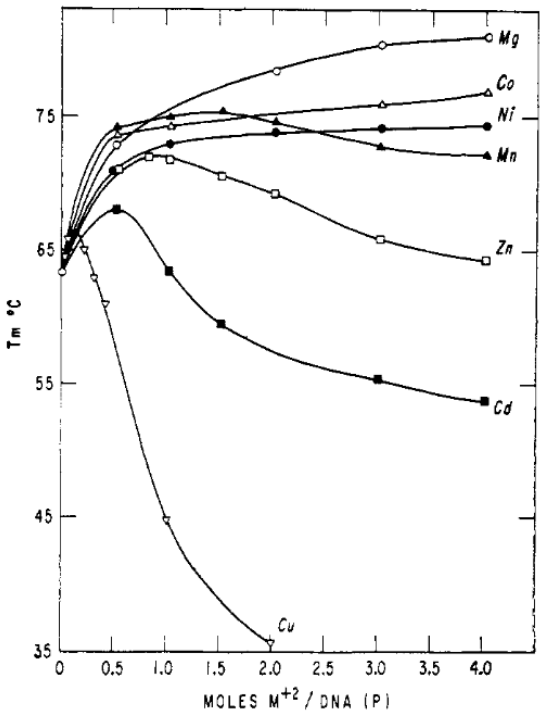

Figure 1.6-2. Variations of the melting temperature (T_m) of solutions of DNA as a function of metal ion and concentration. From ref. [259].

If the metal can interact with the phosphate groups through electrostatic interaction, the melting temperature increases due to the decrease of the electrostatic repulsion from the phosphate groups between the two strands (Figure 1.6-2). Thus, this can confirm an interaction towards

the phosphate groups rather than the nucleobases. Indeed, comparing the curves in Figure 1.6-2, it can be observed that the addition of copper will decrease the melting temperature of the paired strands, lowering it even more with further addition. This indicates a strong and almost exclusive affinity for the nucleobases. On the opposite, the addition of magnesium ions in DNA solution increases gradually the melting temperature of the latter. This behaviour suggests an exclusive affinity towards the phosphate groups of the DNA and hence, a pure electrostatic interaction [248]. Other divalent cations such as cadmium, manganese or zinc present an intermediate behaviour depending on the amount introduced. For instance, with zinc, it can first be seen that the melting temperature of the DNA increases, suggesting an affinity for the phosphate groups. However, further addition will decrease the melting temperature back to the initial one, suggesting an equilibrium between the electrostatic interaction with the phosphate groups stabilizing the structure and the coordinative bonding from the nucleobases [259].

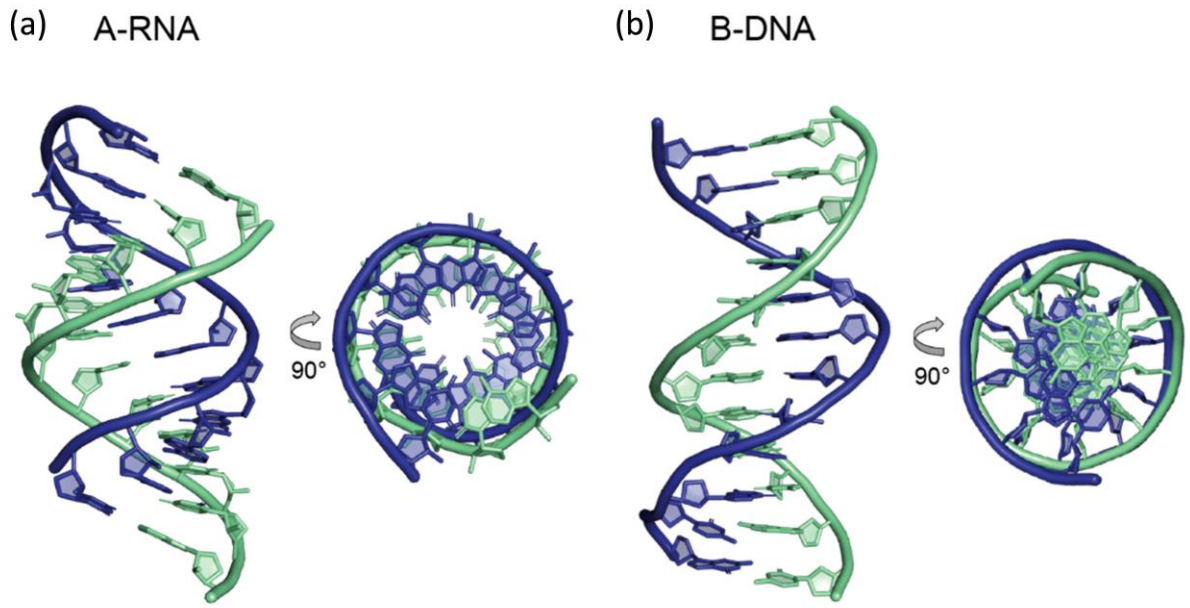

Figure 1.6-3. Double-helical forms of nucleic acids based on single-crystal X-ray diffraction analysis of dodecamers. a) Helical structure of the A-form in the case of a double stranded RNA. b) Helical structure of the B-form for the case of a double stranded DNA [261].

Despite the fact that monovalent cations such as Na^+ are known to stabilize duplexes thanks to electrostatic interaction with phosphate groups, the metallic ions may induce another behavior regarding their affinity with the bases. Indeed, depending on the metallic ion, conformational changes have been observed for DNA such as a transition from the B-form Figure 1.6-3 of the DNA to an "M-form" (metallic form) [260, 262–264]. The structure named M-DNA as 'metallic-DNA' present a very similar structure as the B-DNA but with enhanced stability (Figure 1.6-4.b). It has been found that Zn^{2+} were the most efficient ions to induce and stabilize the "M-form" of DNA [262]. However, the case which will be considered in this thesis is the use of siRNA presenting a helical structure of the "A-form" (Figure 1.6-3.a). The major

differences between the A and the B form rely on the number of bp per turn, being of 11 bp per turn in the case of the A-form with a length of 2.86 nm and 10 bp per turn for the B-form with a length of 3.4 nm. Moreover, the helix width of A-form is 2.3 nm whereas it is of 2 nm for the B-form [261].

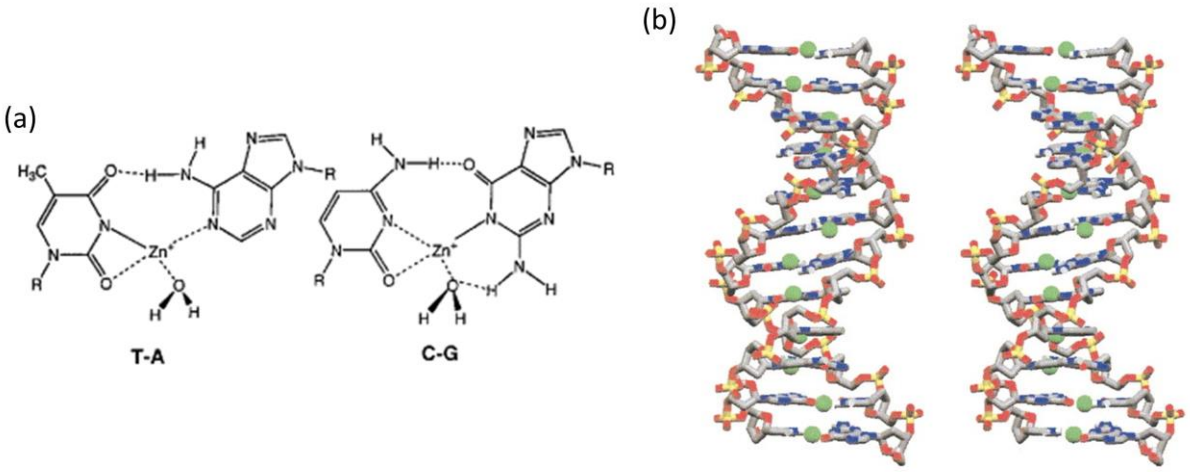

Figure 1.6-4. a) Base pairing in presence of zinc ions. b) Structure of the 'metallic' DNA (M-DNA) with zinc ions represented as the green spheres. From ref. [264].

A recent computational study using molecular dynamics provided a general overview regarding the type of metal and its affinity towards the nucleobases or the phosphate groups. Metal cations appear to preferentially bind to the DNA backbone following the direct Hofmeister series and the nucleobases following the reversed order. [265].

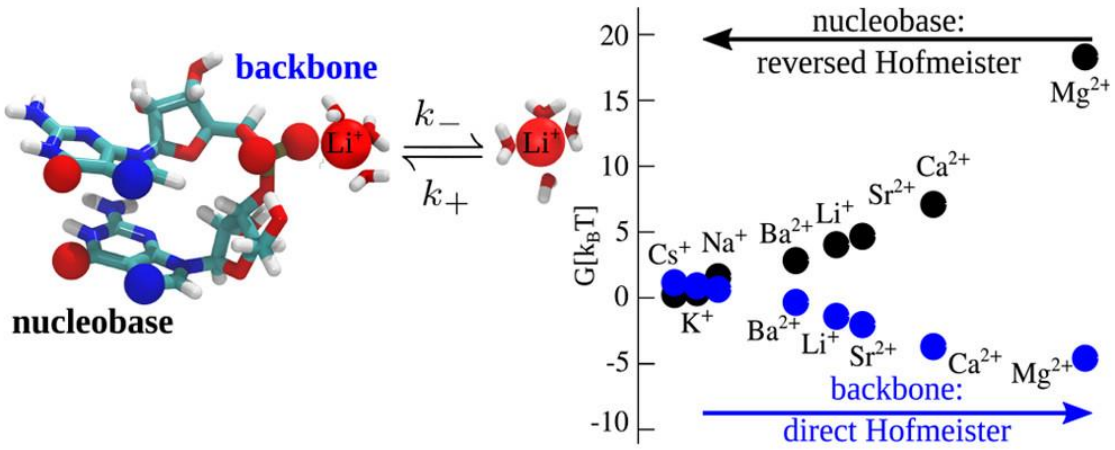

Figure 1.6-5. Binding free energy of the different cations as a function of their charge/diameter. From ref. [265].

1.7. Conclusion

This literature review has shown the great potential of siRNA for gene therapy but also the room for improvement in the design of polymeric carriers. Indeed, improvements are still needed to fulfil all the requirements in terms of efficiency of complexation and uptake of the nucleic acids, the stability of the complexes in physiological conditions, the release of the species, the targeting in a systemic administration, etc. Here, this review may have demonstrated that a new type of formulation can be considered with the use of metallic ions as intermediate between a polycation (such as chitosan) and the polyanionic siRNA to enhance the properties of the gene vectors. This review also showed that a variety of parameters can play a role in the final properties of the polyplexes, from the molecular characteristics of the polycation to the way of mixing the components. It seems then relevant to study these parameters separately and then combine them to design new siRNA vectors.

1.8. References

[1] Fire A, Xu S, Montgomery MK, Kostas SA, Driver SE, Mello CC (1998) Potent and specific genetic interference by double-stranded RNA in Caenorhabditis elegans. Nature 391:806–811. https://doi.org/10.1038/35888

[2] Elbashir SM, Harborth J, Lendeckel W, Yalcin A, Weber K, Tuschl T (2001) Duplexes of 21-nucleotide RNAs mediate RNA interference in cultured mammalian cells. Nature 411:494–498. https://doi.org/10.1038/35078107

[3] Davis ME, Zuckerman JE, Choi CHJ, Seligson D, Tolcher A, Alabi CA, Yen Y, Heidel JD, Ribas A (2010) Evidence of RNAi in humans from systemically administered siRNA via targeted nanoparticles. Nature 464:1067–1070. https://doi.org/10.1038/nature08956

[4] Adams D, Gonzalez-Duarte A, O'Riordan WD, et al (2018) Patisiran, an RNAi Therapeutic, for Hereditary Transthyretin Amyloidosis. N Engl J Med 379:11–21. https://doi.org/10.1056/NEJMoa1716153

[5] Scott LJ (2020) Givosiran: First Approval. Drugs 80:335–339. https://doi.org/10.1007/s40265-020-01269-0

[6] Liu F, Wang C, Gao Y, Li X, Tian F, Zhang Y, Fu M, Li P, Wang Y, Wang F (2018) Current Transport Systems and Clinical Applications for Small Interfering RNA (siRNA) Drugs. Mol Diagnosis Ther 22:551–569. https://doi.org/10.1007/s40291-018-0338-8

[7] Gantier MP, Williams BRG (2007) The response of mammalian cells to double-stranded RNA. Cytokine Growth Factor Rev 18:363–371. https://doi.org/10.1016/j.cytogfr.2007.06.016

[8] Agrawal N, Dasaradhi PVN, Mohmmed A, Malhotra P, Bhatnagar RK, Mukherjee SK (2003) RNA Interference: Biology, Mechanism, and Applications. Microbiol Mol Biol Rev 67:657–685. https://doi.org/10.1128/MMBR.67.4.657-685.2003

[9] Matranga C, Tomari Y, Shin C, Bartel DP, Zamore PD (2005) Passenger-Strand Cleavage Facilitates Assembly of siRNA into Ago2-Containing RNAi Enzyme Complexes. Cell 123:607–620. https://doi.org/10.1016/j.cell.2005.08.044

[10] Hutvagner G, Zamore PD (2002) A microRNA in a Multiple-Turnover RNAi Enzyme Complex. Science (80-) 297:2056–2060. https://doi.org/10.1126/science.1073827

[11] Manoharan M (2004) RNA interference and chemically modified small interfering RNAs. Curr Opin Chem Biol 8:570–579. https://doi.org/10.1016/j.cbpa.2004.10.007

[12] Caillaud M, El Madani M, Massaad-Massade L (2020) Small interfering RNA from the lab discovery to patients' recovery. J Control Release 321:616–628. https://doi.org/10.1016/j.jconrel.2020.02.032

[13] Turner JJ, Jones SW, Moschos SA, Lindsay MA, Gait MJ (2007) MALDI-TOF mass spectral analysis of siRNA degradation in serum confirms an RNAse A-like activity. Mol Biosyst 3:43–50. https://doi.org/10.1039/b611612d

[14] Fedorov Y, Anderson EM, Birmingham A, Reynolds A, Karpilow J, Robinson K, Leake D, Marshall WS, Khvorova A (2006) Off-target effects by siRNA can induce toxic phenotype. Rna 12:1188–1196. https://doi.org/10.1261/rna.28106

[15] Lam JKW, Chow MYT, Zhang Y, Leung SWS (2015) siRNA versus miRNA as therapeutics for gene silencing. Mol Ther - Nucleic Acids 4:e252. https://doi.org/10.1038/mtna.2015.23

[16] Jackson AL, Linsley PS (2010) Recognizing and avoiding siRNA off-target effects for target identification and therapeutic application. Nat Rev Drug Discov 9:57–67. https://doi.org/10.1038/nrd3010

[17] Khan AA, Betel D, Miller ML, Sander C, Leslie CS, Marks DS (2009) Transfection of small RNAs globally perturbs gene regulation by endogenous microRNAs. Nat Biotechnol 27:549–555. https://doi.org/10.1038/nbt.1543

[18] Houseley J, Tollervey D (2009) The Many Pathways of RNA Degradation. Cell 136:763–776. https://doi.org/10.1016/j.cell.2009.01.019

[19] Thomas MF, L'Etoile ND, Ansel KM (2014) Eri1: a conserved enzyme at the crossroads of multiple RNA-processing pathways. Trends Genet 30:298–307. https://doi.org/10.1016/j.tig.2014.05.003

[20] Chernikov I V., Vlassov V V., Chernolovskaya EL (2019) Current Development of siRNA Bioconjugates: From Research to the Clinic. Front Pharmacol 10:. https://doi.org/10.3389/fphar.2019.00444

[21] Johannes L, Lucchino M (2018) Current Challenges in Delivery and Cytosolic Translocation of Therapeutic RNAs. Nucleic Acid Ther 28:178–193. https://doi.org/10.1089/nat.2017.0716

[22] Hu B, Zhong L, Weng Y, Peng L, Huang Y, Zhao Y, Liang XJ (2020) Therapeutic siRNA: state of the art. Signal Transduct Target Ther 5:. https://doi.org/10.1038/s41392-020-0207-x

[23] Manoharan M (2002) Oligonucleotide Conjugates as Potential Antisense Drugs with Improved Uptake, Biodistribution, Targeted Delivery, and Mechanism of Action. Antisense Nucleic Acid Drug Dev 12:103–128. https://doi.org/10.1089/108729002760070849

[24] Ly S, Navaroli DM, Didiot MC, Cardia J, Pandarinathan L, Alterman JF, Fogarty K,

Standley C, Lifshitz LM, Bellve KD, Prot M, Echeverria D, Corvera S, Khvorova A (2017) Visualization of self-delivering hydrophobically modified siRNA cellular internalization. Nucleic Acids Res 45:15–25. https://doi.org/10.1093/nar/gkw1005

[25] Tai W, Gao X (2018) Noncovalent tagging of siRNA with steroids for transmembrane delivery. Biomaterials 178:720–727. https://doi.org/10.1016/j.biomaterials.2018.02.007

[26] Iversen F, Yang C, Dagnæs-Hansen F, Schaffert DH, Kjems J, Gao S (2013) Optimized siRNA-PEG conjugates for extended blood circulation and reduced urine excretion in mice. Theranostics 3:201–209. https://doi.org/10.7150/thno.5743

[27] Eisenstein M (2019) Pharma's roller-coaster relationship with RNA therapies. Nature 574:S4–S6. https://doi.org/10.1038/d41586-019-03069-3

[28] Heras-Palou C (2019) Patisiran's path to approval as an RNA therapy. Nature 574:S7–S7. https://doi.org/10.1038/d41586-019-03070-w

[29] Alnylam Pharmaceuticals Press Release | May 04, 2020 | Vir and Alnylam Identify RNAi Therapeutic Development Candidate, VIR-2703 (ALN-COV), Targeting SARS-CoV-2 for. https://investors.alnylam.com/press-release?id=24796. Accessed 14 Sep 2020

[30] Harries L (2019) It's time for scientists to shout about RNA therapies. Nature 574:S15–S15. https://doi.org/10.1038/d41586-019-03074-6

[31] Brüggenwirth IMA, Martins PN (2020) RNA interference therapeutics in organ transplantation: The dawn of a new era. Am J Transplant 20:931–941. https://doi.org/10.1111/ajt.15689

[32] Jain A, Hosseinkhani H, Domb AJ, Khan W (2015) Cationic Polymers for the Delivery of Therapeutic Nucleotides. In: Polysaccharides. Springer International Publishing, Cham, pp 1969–1990

[33] Zhang Q, Ichimaru N, Higuchi S, Cai S, Hou J, Fujino M, Nonomura N, Kobayashi M, Ando H, Uno A, Sakurai K, Mochizuki S, Adachi Y, Ohno N, Zou H, Xu J, Li XK, Takahara S (2015) Permanent acceptance of mouse cardiac allografts with CD40 siRNA to induce regulatory myeloid cells by use of a novel polysaccharide siRNA delivery system. Gene Ther 22:217–226. https://doi.org/10.1038/gt.2014.119

[34] Mangala LS, Han HD, Lopez-Berestein G, Sood AK (2009) Liposomal siRNA for Ovarian Cancer. In: Rondinone CM, Reidhaar-Olson JF (eds) Therapeutic Applications of RNAi: Methods and Protocols. Humana Press, Totowa, NJ, pp 29–42

[35] Christie RJ, Miyata K, Matsumoto Y, Nomoto T, Menasco D, Lai TC, Pennisi M, Osada K, Fukushima S, Nishiyama N, Yamasaki Y, Kataoka K (2011) Effect of Polymer Structure on Micelles Formed between siRNA and Cationic Block Copolymer Comprising Thiols and Amidines. Biomacromolecules 12:3174–3185. https://doi.org/10.1021/bm2006714

[36] DeRouchey J, Schmidt C, Walker GF, Koch C, Plank C, Wagner E, Rädler JO (2008) Monomolecular Assembly of siRNA and Poly(ethylene glycol)−Peptide Copolymers. Biomacromolecules 9:724–732. https://doi.org/10.1021/bm7011482

[37] Malcolm DW, Varghese JJ, Sorrells JE, Ovitt CE, Benoit DSW (2018) The Effects of Biological Fluids on Colloidal Stability and siRNA Delivery of a pH-Responsive Micellar Nanoparticle Delivery System. ACS Nano 12:187–197. https://doi.org/10.1021/acsnano.7b05528

[38] Di Silvio D, Martínez-Moro M, Salvador C, de los Angeles Ramirez M, Caceres-Velez

PR, Ortore MG, Dupin D, Andreozzi P, Moya SE (2019) Self-assembly of poly(allylamine)/siRNA nanoparticles, their intracellular fate and siRNA delivery. J Colloid Interface Sci 557:757–766. https://doi.org/10.1016/j.jcis.2019.09.082

[39] Serrano-Sevilla I, Artiga Á, Mitchell SG, De Matteis L, de la Fuente JM (2019) Natural Polysaccharides for siRNA Delivery: Nanocarriers Based on Chitosan, Hyaluronic Acid, and Their Derivatives. Molecules 24:2570. https://doi.org/10.3390/molecules24142570

[40] Hiemenz PC, Rajagopalan R (1997) Principles of Colloid and Surface Chemistry. CRC Press

[41] Hui SW, Langner M, Zhao YL, Ross P, Hurley E, Chan K (1996) The role of helper lipids in cationic liposome-mediated gene transfer. Biophys J 71:590–599. https://doi.org/10.1016/S0006-3495(96)79309-8

[42] Heyes J, Palmer L, Bremner K, MacLachlan I (2005) Cationic lipid saturation influences intracellular delivery of encapsulated nucleic acids. J Control Release 107:276–287. https://doi.org/10.1016/j.jconrel.2005.06.014

[43] Lee J, Ahn HJ (2018) PEGylated DC-Chol/DOPE cationic liposomes containing KSP siRNA as a systemic siRNA delivery Carrier for ovarian cancer therapy. Biochem Biophys Res Commun 503:1716–1722. https://doi.org/10.1016/j.bbrc.2018.07.104

[44] Walsh S, Kotz D (2018) FDA approves first-of-its kind targeted RNA-based therapy to treat a rare disease | FDA. https://www.fda.gov/news-events/press-announcements/fda-approves-first-its-kind-targeted-rna-based-therapy-treat-rare-disease. Accessed 2 Sep 2019

[45] Boussif O, LezoualC'H F, Zanta MA, Mergny MD, Scherman D, Demeneix B, Behr JP (1995) A versatile vector for gene and oligonucleotide transfer into cells in culture and in vivo: Polyethylenimine. Proc Natl Acad Sci U S A 92:7297–7301. https://doi.org/10.1073/pnas.92.16.7297

[46] Richards Grayson AC, Doody AM, Putnam D (2006) Biophysical and Structural Characterization of Polyethylenimine-Mediated siRNA Delivery in Vitro. Pharm Res 23:1868–1876. https://doi.org/10.1007/s11095-006-9009-2

[47] Fischer D, Li Y, Ahlemeyer B, Krieglstein J, Kissel T (2003) In vitro cytotoxicity testing of polycations: influence of polymer structure on cell viability and hemolysis. Biomaterials 24:1121–1131. https://doi.org/10.1016/S0142-9612(02)00445-3

[48] Kargaard A, Sluijter JPG, Klumperman B (2019) Polymeric siRNA gene delivery – transfection efficiency versus cytotoxicity. J Control Release 316:263–291. https://doi.org/10.1016/j.jconrel.2019.10.046

[49] Gosselin MA, Guo W, Lee RJ (2001) Efficient Gene Transfer Using Reversibly Cross-Linked Low Molecular Weight Polyethylenimine. Bioconjug Chem 12:989–994. https://doi.org/10.1021/bc0100455

[50] Matsumoto S, Christie RJ, Nishiyama N, Miyata K, Ishii A, Oba M, Koyama H, Yamasaki Y, Kataoka K (2009) Environment-Responsive Block Copolymer Micelles with a Disulfide Cross-Linked Core for Enhanced siRNA Delivery. Biomacromolecules 10:119–127. https://doi.org/10.1021/bm800985e

[51] Ulkoski D, Bak A, Wilson JT, Krishnamurthy VR (2019) Recent advances in polymeric materials for the delivery of RNA therapeutics. Expert Opin Drug Deliv 16:1149–1167. https://doi.org/10.1080/17425247.2019.1663822

[52] Chen B, Yu L, Li Z, Wu C (2018) Design of Free Triblock Polylysine- b -Polyleucine- b -Polylysine Chains for Gene Delivery. Biomacromolecules 19:1347–1357. https://doi.org/10.1021/acs.biomac.8b00287

[53] He C, Zhuang X, Tang Z, Tian H, Chen X (2012) Stimuli-Sensitive Synthetic Polypeptide-Based Materials for Drug and Gene Delivery. Adv Healthc Mater 1:48–78. https://doi.org/10.1002/adhm.201100008

[54] Dosta P, Ramos V, Borrós S (2018) Stable and efficient generation of poly(β-amino ester)s for RNAi delivery. Mol Syst Des Eng 3:677–689. https://doi.org/10.1039/C8ME00006A

[55] Parmar RG, Busuek M, Walsh ES, Leander KR, Howell BJ, Sepp-Lorenzino L, Kemp E, Crocker LS, Leone A, Kochansky CJ, Carr BA, Garbaccio RM, Colletti SL, Wang W (2013) Endosomolytic Bioreducible Poly(amido amine disulfide) Polymer Conjugates for the in Vivo Systemic Delivery of siRNA Therapeutics. Bioconjug Chem 24:640–647. https://doi.org/10.1021/bc300600a

[56] Troiber C, Edinger D, Kos P, Schreiner L, Kläger R, Herrmann A, Wagner E (2013) Stabilizing effect of tyrosine trimers on pDNA and siRNA polyplexes. Biomaterials 34:1624–1633. https://doi.org/10.1016/j.biomaterials.2012.11.021

[57] Reinhard S, Wagner E (2017) How to Tackle the Challenge of siRNA Delivery with Sequence-Defined Oligoamino Amides. Macromol Biosci 17:1600152. https://doi.org/10.1002/mabi.201600152

[58] He D, Müller K, Krhac Levacic A, Kos P, Lächelt U, Wagner E (2016) Combinatorial Optimization of Sequence-Defined Oligo(ethanamino)amides for Folate Receptor-Targeted pDNA and siRNA Delivery. Bioconjug Chem 27:647–659. https://doi.org/10.1021/acs.bioconjchem.5b00649

[59] Zhang X, Intra J, Salem AK (2007) Conjugation of Polyamidoamine Dendrimers on Biodegradable Microparticles for Nonviral Gene Delivery. Bioconjug Chem 18:2068–2076. https://doi.org/10.1021/bc070116l

[60] Suma T, Miyata K, Ishii T, Uchida S, Uchida H, Itaka K, Nishiyama N, Kataoka K (2012) Enhanced stability and gene silencing ability of siRNA-loaded polyion complexes formulated from polyaspartamide derivatives with a repetitive array of amino groups in the side chain. Biomaterials 33:2770–2779. https://doi.org/10.1016/j.biomaterials.2011.12.022

[61] Kim BS, Chuanoi S, Suma T, Anraku Y, Hayashi K, Naito M, Kim HJ, Kwon IC, Miyata K, Kishimura A, Kataoka K (2019) Self-Assembly of siRNA/PEG- b -Catiomer at Integer Molar Ratio into 100 nm-Sized Vesicular Polyion Complexes (siRNAsomes) for RNAi and Codelivery of Cargo Macromolecules. J Am Chem Soc 141:3699–3709. https://doi.org/10.1021/jacs.8b13641

[62] Chuanoi S, Kishimura A, Dong W-F, Anraku Y, Yamasaki Y, Kataoka K (2014) Structural factors directing nanosized polyion complex vesicles (Nano-PICsomes) to form a pair of block aniomer/homo catiomers: studies on the aniomer segment length and the catiomer side-chain structure. Polym J 46:130–135. https://doi.org/10.1038/pj.2013.82

[63] Schaffer D V., Fidelman NA, Dan N, Lauffenburger DA (2000) Vector unpacking as a potential barrier for receptor-mediated polyplex gene delivery. Biotechnol Bioeng 67:598–606. https://doi.org/10.1002/(SICI)1097-0290(20000305)67:5<598::AID-

BIT10>3.0.CO;2-G

[64] Greco CT, Epps TH, Sullivan MO (2016) Mechanistic Design of Polymer Nanocarriers to Spatiotemporally Control Gene Silencing. ACS Biomater Sci Eng 2:1582–1594. https://doi.org/10.1021/acsbiomaterials.6b00336

[65] Hwa Kim S, Hoon Jeong J, Chul Cho K, Wan Kim S, Gwan Park T (2005) Target-specific gene silencing by siRNA plasmid DNA complexed with folate-modified poly(ethylenimine). J Control Release 104:223–232. https://doi.org/10.1016/j.jconrel.2005.02.006

[66] Kunath K, von Harpe A, Petersen H, Fischer D, Voigt K, Kissel T, Bickel U (2002) The structure of PEG-modified poly(ethylene imines) influences biodistribution and pharmacokinetics of their complexes with NF-κB decoy in mice. Pharm Res 19:810–817. https://doi.org/10.1023/A:1016152831963

[67] Zhang W, Meng X, Liu H, Xie L, Liu J, Xu H (2017) Ratio of Polycation and Serum Is a Crucial Index for Determining the RNAi Efficiency of Polyplexes. ACS Appl Mater Interfaces 9:43529–43537. https://doi.org/10.1021/acsami.7b15797

[68] Raemdonck K, Van Thienen TG, Vandenbroucke RE, Sanders NN, Demeester J, De Smedt SC (2008) Dextran Microgels for Time-Controlled Delivery of siRNA. Adv Funct Mater 18:993–1001. https://doi.org/10.1002/adfm.200701039

[69] Zhang W, Liu J, Tabata Y, Meng J, Xu H (2014) The effect of serum in culture on RNAi efficacy through modulation ofpolyplexes size. Biomaterials 35:567–577. https://doi.org/10.1016/j.biomaterials.2013.09.102

[70] Hosseinkhani H, Azzam T, Tabata Y, Domb AJ (2004) Dextran-spermine polycation: An efficient nonviral vector for in vitro and in vivo gene transfection. Gene Ther 11:194–203. https://doi.org/10.1038/sj.gt.3302159

[71] Cohen JL, Schubert S, Wich PR, Cui L, Cohen JA, Mynar JL, Fréchet JMJ (2011) Acid-degradable cationic dextran particles for the delivery of siRNA therapeutics. Bioconjug Chem 22:1056–1065. https://doi.org/10.1021/bc100542r

[72] Wang JY, Casero RA (2006) Polyamine Cell Signaling. Humana Press, Totowa, NJ

[73] Chen C, Wang Z, Zhang J, Fan X, Xu L, Tang X (2019) Dextran-conjugated caged siRNA nanoparticles for photochemical regulation of RNAi-induced gene silencing in cells and mice. Bioconjug Chem 30:1459–1465. https://doi.org/10.1021/acs.bioconjchem.9b00204

[74] Yhee JY, Song S, Lee SJ, Park SG, Kim KS, Kim MG, Son S, Koo H, Kwon IC, Jeong JH, Jeong SY, Kim SH, Kim K (2015) Cancer-targeted MDR-1 siRNA delivery using self-cross-linked glycol chitosan nanoparticles to overcome drug resistance. J Control Release 198:1–9. https://doi.org/10.1016/j.jconrel.2014.11.019

[75] Vauthier C, Zandanel C, Ramon AL (2013) Chitosan-based nanoparticles for in vivo delivery of interfering agents including siRNA. Curr Opin Colloid Interface Sci 18:406–418. https://doi.org/10.1016/j.cocis.2013.06.005

[76] Lächelt U, Wagner E (2015) Nucleic Acid Therapeutics Using Polyplexes: A Journey of 50 Years (and Beyond). Chem Rev 115:11043–11078. https://doi.org/10.1021/cr5006793

[77] Wu D, Zhu L, Li Y, Zhang X, Xu S, Yang G, Delair T (2020) Chitosan-based Colloidal Polyelectrolyte Complexes for Drug Delivery: A Review. Carbohydr Polym

238:116126. https://doi.org/10.1016/j.carbpol.2020.116126

[78] Holzerny P, Ajdini B, Heusermann W, Bruno K, Schuleit M, Meinel L, Keller M (2012) Biophysical properties of chitosan/siRNA polyplexes: Profiling the polymer/siRNA interactions and bioactivity. J Control Release 157:297–304. https://doi.org/10.1016/j.jconrel.2011.08.023

[79] Mao S, Sun W, Kissel T (2010) Chitosan-based formulations for delivery of DNA and siRNA. Adv Drug Deliv Rev 62:12–27. https://doi.org/10.1016/j.addr.2009.08.004

[80] Rudzinski WE, Aminabhavi TM (2010) Chitosan as a carrier for targeted delivery of small interfering RNA. Int J Pharm 399:1–11. https://doi.org/10.1016/j.ijpharm.2010.08.022

[81] Debele TA, Mekuria SL, Tsai HC (2016) Polysaccharide based nanogels in the drug delivery system: Application as the carrier of pharmaceutical agents. Mater Sci Eng C 68:964–981. https://doi.org/10.1016/j.msec.2016.05.121

[82] Wang H, Qian J, Ding F (2017) Recent advances in engineered chitosan-based nanogels for biomedical applications. J Mater Chem B 5:6986–7007. https://doi.org/10.1039/c7tb01624g

[83] Katas H, Alpar HO (2006) Development and characterisation of chitosan nanoparticles for siRNA delivery. J Control Release 115:216–225. https://doi.org/10.1016/j.jconrel.2006.07.021

[84] Giacalone G, Bochot A, Fattal E, Hillaireau H (2013) Drug-Induced Nanocarrier Assembly as a Strategy for the Cellular Delivery of Nucleotides and Nucleotide Analogues. Biomacromolecules 14:737–742. https://doi.org/10.1021/bm301832v

[85] Huang Y, Lapitsky Y (2011) Monovalent Salt Enhances Colloidal Stability during the Formation of Chitosan/Tripolyphosphate Microgels. Langmuir 27:10392–10399. https://doi.org/10.1021/la201194a

[86] Villar-Alvarez E, Leal BH, Martínez-González R, Pardo A, Al-Qadi S, Juárez J, Váldez MA, Cambón A, Barbosa S, Taboada P (2019) siRNA Silencing by Chemically Modified Biopolymeric Nanovectors. ACS Omega 4:3904–3921. https://doi.org/10.1021/acsomega.8b02875

[87] Muzzarelli RAA (2009) Genipin-crosslinked chitosan hydrogels as biomedical and pharmaceutical aids. Carbohydr Polym 77:1–9. https://doi.org/10.1016/j.carbpol.2009.01.016

[88] Argüelles-Monal W, Goycoolea FM, Peniche C, Higuera-Ciapara I (1998) Rheological study of the chitosan/glutaraldehyde chemical gel system. Polym Gels Networks 6:429–440. https://doi.org/10.1016/S0966-7822(98)00032-X

[89] Coelho TC, Laus R, Mangrich AS, de Fávere VT, Laranjeira MCM (2007) Effect of heparin coating on epichlorohydrin cross-linked chitosan microspheres on the adsorption of copper (II) ions. React Funct Polym 67:468–475. https://doi.org/10.1016/j.reactfunctpolym.2007.02.009

[90] Amjad MW, Kesharwani P, Mohd Amin MCI, Iyer AK (2017) Recent advances in the design, development, and targeting mechanisms of polymeric micelles for delivery of siRNA in cancer therapy. Prog Polym Sci 64:154–181. https://doi.org/10.1016/j.progpolymsci.2016.09.008

[91] Marras AE, Vieregg JR, Ting JM, Rubien JD, Tirrell M V. (2019) Polyelectrolyte

complexation of oligonucleotides by charged hydrophobic-Neutral hydrophilic block copolymers. Polymers (Basel) 11:. https://doi.org/10.3390/polym11010083

[92] Butt AM, Amin MCIM, Katas H, Abdul Murad NA, Jamal R, Kesharwani P (2016) Doxorubicin and siRNA Codelivery via Chitosan-Coated pH-Responsive Mixed Micellar Polyplexes for Enhanced Cancer Therapy in Multidrug-Resistant Tumors. Mol Pharm 13:4179–4190. https://doi.org/10.1021/acs.molpharmaceut.6b00776

[93] Yin T, Wang L, Yin L, Zhou J, Huo M (2015) Co-delivery of hydrophobic paclitaxel and hydrophilic AURKA specific siRNA by redox-sensitive micelles for effective treatment of breast cancer. Biomaterials 61:10–25. https://doi.org/10.1016/j.biomaterials.2015.05.022

[94] Wang H, Ding S, Zhang Z, Wang L, You Y (2019) Cationic micelle: A promising nanocarrier for gene delivery with high transfection efficiency. J Gene Med 21:. https://doi.org/10.1002/jgm.3101

[95] Lebleu C, Rodrigues L, Guigner J-M, Brûlet A, Garanger E, Lecommandoux S (2019) Self-Assembly of PEG- b -PTMC Copolymers: Micelles and Polymersomes Size Control. Langmuir 35:13364–13374. https://doi.org/10.1021/acs.langmuir.9b02264

[96] Discher DE (2002) Polymer Vesicles. Science (80-) 297:967–973. https://doi.org/10.1126/science.1074972

[97] Kishimura A (2013) Development of polyion complex vesicles (PICsomes) from block copolymers for biomedical applications. Polym J 45:892–897. https://doi.org/10.1038/pj.2013.33

[98] Lee CC, MacKay JA, Fréchet JMJ, Szoka FC (2005) Designing dendrimers for biological applications. Nat Biotechnol 23:1517–1526. https://doi.org/10.1038/nbt1171

[99] Gorzkiewicz M, Kopeć O, Janaszewska A, Konopka M, Pędziwiatr-Werbicka E, Tarasenko II, Bezrodnyi V V., Neelov IM, Klajnert-Maculewicz B (2020) Poly(lysine) Dendrimers Form Complexes with siRNA and Provide Its Efficient Uptake by Myeloid Cells: Model Studies for Therapeutic Nucleic Acid Delivery. Int J Mol Sci 21:3138. https://doi.org/10.3390/ijms21093138

[100] BUHLEIER E, WEHNER W, VÖGTLE F (1978) "Cascade"- and "Nonskid-Chain-like" Syntheses of Molecular Cavity Topologies. Synthesis (Stuttg) 1978:155–158. https://doi.org/10.1055/s-1978-24702

[101] Jensen LB, Griger J, Naeye B, Varkouhi AK, Raemdonck K, Schiffelers R, Lammers T, Storm G, de Smedt SC, Sproat BS, Nielsen HM, Foged C (2012) Comparison of Polymeric siRNA Nanocarriers in a Murine LPS-Activated Macrophage Cell Line: Gene Silencing, Toxicity and Off-Target Gene Expression. Pharm Res 29:669–682. https://doi.org/10.1007/s11095-011-0589-0

[102] Bohr A, Tsapis N, Andreana I, Chamarat A, Foged C, Delomenie C, Noiray M, El Brahmi N, Majoral J-P, Mignani S, Fattal E (2017) Anti-Inflammatory Effect of Anti-TNF-α SiRNA Cationic Phosphorus Dendrimer Nanocomplexes Administered Intranasally in a Murine Acute Lung Injury Model. Biomacromolecules 18:2379–2388. https://doi.org/10.1021/acs.biomac.7b00572

[103] Watanabe S, Hayashi K, Toh K, et al (2019) In vivo rendezvous of small nucleic acid drugs with charge-matched block catiomers to target cancers. Nat Commun 10:. https://doi.org/10.1038/s41467-019-09856-w

[104] Yi Y, Kim HJ, Zheng M, Mi P, Naito M, Kim BS, Min HS, Hayashi K, Perche F, Toh

K, Liu X, Mochida Y, Kinoh H, Cabral H, Miyata K, Kataoka K (2019) Glucose-linked sub-50-nm unimer polyion complex-assembled gold nanoparticles for targeted siRNA delivery to glucose transporter 1-overexpressing breast cancer stem-like cells. J Control Release 295:268–277. https://doi.org/10.1016/j.jconrel.2019.01.006

[105] Dohmen C, Edinger D, Fröhlich T, Schreiner L, Lächelt U, Troiber C, Rädler J, Hadwiger P, Vornlocher H-P, Wagner E (2012) Nanosized Multifunctional Polyplexes for Receptor-Mediated SiRNA Delivery. ACS Nano 6:5198–5208. https://doi.org/10.1021/nn300960m

[106] Kabanov VA, Zezin AB (1984) Soluble interpolymeric complexes as a new class of synthetic polyelectrolytes. Pure Appl Chem 56:343–354. https://doi.org/10.1351/pac198456030343

[107] Philipp B, Dautzenberg H, Linow K-J, Kötz J, Dawydoff W (1989) Polyelectrolyte complexes — recent developments and open problems. Prog Polym Sci 14:91–172. https://doi.org/10.1016/0079-6700(89)90018-X

[108] Tsuchida E, Abe K (1982) Interactions between macromolecules in solution and intermacromolecular complexes. In: Tsuchida E, Abe K (eds) Interactions Between Macromolecules in Solution and Intermacromolecular Complexes. Springer-Verlag, Berlin/Heidelberg, pp 1–119

[109] Yan M, Liang M, Wen J, Liu Y, Lu Y, Chen ISY (2012) Single siRNA Nanocapsules for Enhanced RNAi Delivery. J Am Chem Soc 134:13542–13545. https://doi.org/10.1021/ja304649a

[110] Braconnot H (1811) Sur la nature des champignons. Ann Chim Phys 79:265–304

[111] Alabaraoye E, Achilonu M, Hester R (2018) Biopolymer (Chitin) from Various Marine Seashell Wastes: Isolation and Characterization. J Polym Environ 26:2207–2218. https://doi.org/10.1007/s10924-017-1118-y

[112] Gautier S (2009) Ultra-pure chitosan: Insight on new non-animal sources for use in advanced drug delivery & cell therapy. Drug Deliv Technol 9:20–22

[113] Lamarque G, Cretenet M, Viton C, Domard A (2005) New Route of Deacetylation of α- and β-Chitins by Means of Freeze−Pump Out−Thaw Cycles. Biomacromolecules 6:1380–1388. https://doi.org/10.1021/bm049322b

[114] Vachoud L, Zydowicz N, Domard A (1997) Formation and characterisation of a physical chitin gel. Carbohydr Res 302:169–177. https://doi.org/10.1016/S0008-6215(97)00126-2

[115] Aiba S ichi (1991) Studies on chitosan: 3. Evidence for the presence of random and block copolymer structures in partially N-acetylated chitosans. Int J Biol Macromol 13:40–44. https://doi.org/10.1016/0141-8130(91)90008-I

[116] Ottøy MH, Vårum KM, Smidsrød O (1996) Compositional heterogeneity of heterogeneously deacetylated chitosans. Carbohydr Polym 29:17–24. https://doi.org/10.1016/0144-8617(95)00154-9

[117] Aiba S ichi (1993) Studies on chitosan: 6. Relationship between N-acetyl group distribution pattern and chitinase digestibility of partially N-acetylated chitosans. Int J Biol Macromol 15:241–245. https://doi.org/10.1016/0141-8130(93)90044-M

[118] Cord-Landwehr S, Richter C, Wattjes J, Sreekumar S, Singh R, Basa S, El Gueddari NE, Moerschbacher BM (2020) Patterns matter part 2: Chitosan oligomers with defined

patterns of acetylation. React Funct Polym 151:104577. https://doi.org/10.1016/j.reactfunctpolym.2020.104577

[119] Vårum K, Ottøy MH, Smidsrød O (2001) Acid hydrolysis of chitosans. Carbohydr Polym 46:89–98. https://doi.org/10.1016/S0144-8617(00)00288-5

[120] Ilyina A., Tikhonov V., Albulov A., Varlamov V. (2000) Enzymic preparation of acid-free-water-soluble chitosan. Process Biochem 35:563–568. https://doi.org/10.1016/S0032-9592(99)00104-1

[121] Chapelle C, David G, Caillol S, Negrell C, Durand G, Desroches le Foll M, Trombotto S (2019) Water-Soluble 2,5-Anhydro-D-mannofuranose Chain End Chitosan Oligomers of a Very Low Molecular Weight: Synthesis and Characterization. Biomacromolecules 20:4353–4360. https://doi.org/10.1021/acs.biomac.9b01003

[122] Tømmeraas K, Vårum KM, Christensen BE, Smidsrød O (2001) Preparation and characterisation of oligosaccharides produced by nitrous acid depolymerisation of chitosans. Carbohydr Res 333:137–144. https://doi.org/10.1016/S0008-6215(01)00130-6

[123] Popa-Nita S, Lucas J-M, Ladavière C, David L, Domard A (2009) Mechanisms Involved During the Ultrasonically Induced Depolymerization of Chitosan: Characterization and Control. Biomacromolecules 10:1203–1211. https://doi.org/10.1021/bm8014472

[124] Trombotto S, Ladavière C, Delolme F, Domard A (2008) Chemical Preparation and Structural Characterization of a Homogeneous Series of Chitin/Chitosan Oligomers. Biomacromolecules 9:1731–1738. https://doi.org/10.1021/bm800157x

[125] Allan GG, Peyron M (1995) Molecular weight manipulation of chitosan I: kinetics of depolymerization by nitrous acid. Carbohydr Res 277:257–272. https://doi.org/10.1016/0008-6215(95)00207-A

[126] Strand SP, Danielsen S, Christensen BE, Vårum KM (2005) Influence of Chitosan Structure on the Formation and Stability of DNA−Chitosan Polyelectrolyte Complexes. Biomacromolecules 6:3357–3366. https://doi.org/10.1021/bm0503726

[127] Ma PL, Lavertu M, Winnik FM, Buschmann MD (2009) New Insights into Chitosan−DNA Interactions Using Isothermal Titration Microcalorimetry. Biomacromolecules 10:1490–1499. https://doi.org/10.1021/bm900097s

[128] Tsuchida E, Osada Y (1974) The rôle of the chain length in the stability of polyion complexes. Die Makromol Chemie 601:593–601. https://doi.org/10.1002/macp.1974.021750220

[129] Strand SP, Lelu S, Reitan NK, de Lange Davies C, Artursson P, Vårum KM (2010) Molecular design of chitosan gene delivery systems with an optimized balance between polyplex stability and polyplex unpacking. Biomaterials 31:975–987. https://doi.org/10.1016/j.biomaterials.2009.09.102

[130] Köping-Höggård M, Vårum KM, Issa M, Danielsen S, Christensen BE, Stokke BT, Artursson P (2004) Improved chitosan-mediated gene delivery based on easily dissociated chitosan polyplexes of highly defined chitosan oligomers. Gene Ther 11:1441–1452. https://doi.org/10.1038/sj.gt.3302312

[131] Alameh M, Lavertu M, Tran-Khanh N, Chang C-Y, Lesage F, Bail M, Darras V, Chevrier A, Buschmann MD (2018) siRNA Delivery with Chitosan: Influence of Chitosan Molecular Weight, Degree of Deacetylation, and Amine to Phosphate Ratio on in Vitro Silencing Efficiency, Hemocompatibility, Biodistribution, and in Vivo Efficacy.

Biomacromolecules 19:112–131. https://doi.org/10.1021/acs.biomac.7b01297

[132] Shi Q, Fernandes J, Winnik F, Benderdour M, Zhang, Qiu, Dai (2012) Low molecular weight chitosan conjugated with folate for siRNA delivery in vitro: optimization studies. Int J Nanomedicine 7:5833. https://doi.org/10.2147/IJN.S35567

[133] Schipper NGM, Vårum KM, Artursson P (1996) Chitosans as absorption enhancers for poorly absorbable drugs. 1: Influence of molecular weight and degree of acetylation on drug transport across human intestinal epithelial (Caco-2) cells. Pharm. Res. 13:1686–1692

[134] Huang M, Khor E, Lim L-Y (2004) Uptake and Cytotoxicity of Chitosan Molecules and Nanoparticles: Effects of Molecular Weight and Degree of Deacetylation. Pharm Res 21:344–353. https://doi.org/10.1023/B:PHAM.0000016249.52831.a5

[135] Lavertu M, Méthot S, Tran-Khanh N, Buschmann MD (2006) High efficiency gene transfer using chitosan/DNA nanoparticles with specific combinations of molecular weight and degree of deacetylation. Biomaterials 27:4815–4824. https://doi.org/10.1016/j.biomaterials.2006.04.029

[136] Brunel F, Véron L, Ladavière C, David L, Domard A, Delair T (2009) Synthesis and Structural Characterization of Chitosan Nanogels. Langmuir 25:8935–8943. https://doi.org/10.1021/la9002753

[137] Bravo-Anaya LM, Fernández-Solís KG, Rosselgong J, Nano-Rodríguez JLE, Carvajal F, Rinaudo M (2019) Chitosan-DNA polyelectrolyte complex: Influence of chitosan characteristics and mechanism of complex formation. Int J Biol Macromol 126:1037–1049. https://doi.org/10.1016/j.ijbiomac.2019.01.008

[138] Santos-Carballal B, Aaldering LJ, Ritzefeld M, Pereira S, Sewald N, Moerschbacher BM, Götte M, Goycoolea FM (2015) Physicochemical and biological characterization of chitosan-microRNA nanocomplexes for gene delivery to MCF-7 breast cancer cells. Sci Rep 5:1–15. https://doi.org/10.1038/srep13567

[139] Liu X, Howard KA, Dong M, Andersen MØ, Rahbek UL, Johnsen MG, Hansen OC, Besenbacher F, Kjems J (2007) The influence of polymeric properties on chitosan/siRNA nanoparticle formulation and gene silencing. Biomaterials 28:1280–1288. https://doi.org/10.1016/j.biomaterials.2006.11.004

[140] Sorlier P, Denuzière A, Viton C, Domard A (2001) Relation between the degree of acetylation and the electrostatic properties of chitin and chitosan. Biomacromolecules 2:765–772. https://doi.org/10.1021/bm015531+

[141] Schatz C, Pichot C, Delair T, Viton C, Domard A (2003) Static Light Scattering Studies on Chitosan Solutions: From Macromolecular Chains to Colloidal Dispersions. Langmuir 19:9896–9903. https://doi.org/10.1021/la034410n

[142] Rungsardthong U, Ehtezazi T, Bailey L, Armes SP, Garnett MC, Stolnik S (2003) Effect of polymer ionization on the interaction with DNA in nonviral gene delivery systems. Biomacromolecules 4:683–690. https://doi.org/10.1021/bm025736y

[143] de Britto D, Assis OBG (2007) A novel method for obtaining a quaternary salt of chitosan. Carbohydr Polym 69:305–310. https://doi.org/10.1016/j.carbpol.2006.10.007

[144] Mohamed RR, Abu Elella MH, Sabaa MW (2015) Synthesis, characterization and applications of N-quaternized chitosan/poly(vinyl alcohol) hydrogels. Int J Biol Macromol 80:149–161. https://doi.org/10.1016/j.ijbiomac.2015.06.041

[145] Hashemi V, Ahmadi A, Malakotikhah F, Chaleshtari MG, Baghi Moornani M, Masjedi A, Sojoodi M, Atyabi F, Nikkhoo A, Rostami N, Baradaran B, Azizi G, Yousefi B, Ghalamfarsa G, Jadidi-Niaragh F (2020) Silencing of p68 and STAT3 synergistically diminishes cancer progression. Life Sci 249:. https://doi.org/10.1016/j.lfs.2020.117499

[146] Dehousse V, Garbacki N, Jaspart S, Castagne D, Piel G, Colige A, Evrard B (2010) Comparison of chitosan/siRNA and trimethylchitosan/siRNA complexes behaviour in vitro. Int J Biol Macromol 46:342–349. https://doi.org/10.1016/j.ijbiomac.2010.01.010

[147] Kulkarni AD, Patel HM, Surana SJ, Vanjari YH, Belgamwar VS, Pardeshi C V. (2017) N,N,N-Trimethyl chitosan: An advanced polymer with myriad of opportunities in nanomedicine. Carbohydr Polym 157:875–902. https://doi.org/10.1016/j.carbpol.2016.10.041

[148] Shi B, Zhang H, Bi J, Dai S (2014) Endosomal pH responsive polymers for efficient cancer targeted gene therapy. Colloids Surfaces B Biointerfaces 119:55–65. https://doi.org/10.1016/j.colsurfb.2014.04.005

[149] Ghosn B, Singh A, Li M, Vlassov A V., Burnett C, Puri N, Roy K (2010) Efficient gene silencing in lungs and liver using imidazole-modified chitosan as a nanocarrier for small interfering RNA. Oligonucleotides 20:163–172. https://doi.org/10.1089/oli.2010.0235

[150] Roy K, Ghosn B, Kasturi S (2008) Enhancing Polysaccharide-Mediated Delivery of Nucleic Acids Through Functionalization with Secondary and Tertiary Amines. Curr Top Med Chem 8:331–340. https://doi.org/10.2174/156802608783790947

[151] Rudzinski WE, Palacios A, Ahmed A, Lane MA, Aminabhavi TM (2016) Targeted delivery of small interfering RNA to colon cancer cells using chitosan and PEGylated chitosan nanoparticles. Carbohydr Polym 147:323–332. https://doi.org/10.1016/j.carbpol.2016.04.041

[152] Guţoaia A, Schuster L, Margutti S, Laufer S, Schlosshauer B, Krastev R, Stoll D, Hartmann H (2016) Fine-tuned PEGylation of chitosan to maintain optimal siRNA-nanoplex bioactivity. Carbohydr Polym 143:25–34. https://doi.org/10.1016/j.carbpol.2016.01.010

[153] Vikøren Mo I, Feng Y, Øksnes Dalheim M, Solberg A, Aachmann FL, Schatz C, Christensen BE (2020) Activation of enzymatically produced chitooligosaccharides by dioxyamines and dihydrazides. Carbohydr Polym 232:115748. https://doi.org/10.1016/j.carbpol.2019.115748

[154] Pickenhahn VD, Grange M, De Crescenzo G, Lavertu M, Buschmann MD (2017) Regioselective chitosan end-group activation: the triskelion approach. RSC Adv 7:18628–18638. https://doi.org/10.1039/C7RA01348E

[155] Novoa-Carballal R, Müller AHE (2012) Synthesis of polysaccharide-b-PEG block copolymers by oxime click. Chem Commun 48:3781. https://doi.org/10.1039/c2cc30726j

[156] Mo IV, Dalheim MØ, Aachmann FL, Schatz C, Christensen BE (2020) 2,5-Anhydro-D-Mannose End-Functionalized Chitin Oligomers Activated by Dioxyamines or Dihydrazides as Precursors of Diblock Oligosaccharides. Biomacromolecules 21:2884–2895. https://doi.org/10.1021/acs.biomac.0c00620

[157] Ma PL, Lavertu M, Winnik FM, Buschmann MD (2009) New Insights into Chitosan−DNA Interactions Using Isothermal Titration Microcalorimetry. Biomacromolecules 10:1490–1499. https://doi.org/10.1021/bm900097s

[158] Dautzenberg H (1997) Polyelectrolyte complex formation in highly aggregating systems. 1. Effect of salt: Polyelectrolyte complex formation in the presence of NaCl. Macromolecules 30:7810–7815. https://doi.org/10.1021/ma970803f

[159] Thünemann AF, Müller M, Dautzenberg H, Joanny J-F, Löwen H (2004) Polyelectrolyte Complexes. In: Advance Polymer Science. pp 113–171

[160] Schatz C, Domard A, Viton C, Pichot C, Delair T (2004) Versatile and efficient formation of colloids of biopolymer-based polyelectrolyte complexes. Biomacromolecules 5:1882–1892. https://doi.org/10.1021/bm049786+

[161] Dubin P, Bock J, Davis R, Schulz DN, Thies C (1994) Macromolecular Complexes in Chemistry and Biology. Springer Berlin Heidelberg, Berlin, Heidelberg

[162] Müller M, Keßler B, Fröhlich J, Poeschla S, Torger B (2011) Polyelectrolyte Complex Nanoparticles of Poly(ethyleneimine) and Poly(acrylic acid): Preparation and Applications. Polymers (Basel) 3:762–778. https://doi.org/10.3390/polym3020762

[163] Mel'nikova YS, Lindman B (2000) pH-Controlled DNA Condensation in the Presence of Dodecyldimethylamine Oxide. Langmuir 16:5871–5878. https://doi.org/10.1021/la991382t

[164] Tavakoli Naeini A, Soliman OY, Alameh MG, Lavertu M, Buschmann MD (2017) Automated in-line mixing system for large scale production of chitosan-based polyplexes. J Colloid Interface Sci 500:253–263. https://doi.org/10.1016/j.jcis.2017.04.013

[165] Loy DM, Klein PM, Krzysztoń R, Lächelt U, Rädler JO, Wagner E (2019) A microfluidic approach for sequential assembly of siRNA polyplexes with a defined structure-activity relationship. PeerJ Mater Sci 1:e1. https://doi.org/10.7717/peerj-matsci.1

[166] André EM, Pensado A, Resnier P, Braz L, Rosa da Costa AM, Passirani C, Sanchez A, Montero-Menei CN (2016) Characterization and comparison of two novel nanosystems associated with siRNA for cellular therapy. Int J Pharm 497:255–267. https://doi.org/10.1016/j.ijpharm.2015.11.020

[167] Hussain Z, Katas H, Yan SL, Jamaludin D (2017) Efficient Colonic Delivery of DsiRNA by Pectin-Coated Polyelectrolyte Complex Nanoparticles: Preparation, Characterization and Improved Gastric Survivability. Curr Drug Deliv 14:1016–1027. https://doi.org/10.2174/1567201814666170224142446

[168] Sedlak M, Amis EJ, Konak C, Stepanek P (1991) Dynamic light scattering from strongly interacting multicomponent systems: salt-free polyelectrolyte solutions. In: Schmitz KS (ed). p 191

[169] Sedlák M (1997) Dynamic light scattering from binary mixtures of polyelectrolytes. I. Influence of mixing on the fast and slow polyelectrolyte mode behavior. J Chem Phys 107:10799–10804. https://doi.org/10.1063/1.474196

[170] Sedlák M (1999) What Can Be Seen by Static and Dynamic Light Scattering in Polyelectrolyte Solutions and Mixtures? †. Langmuir 15:4045–4051. https://doi.org/10.1021/la981189j

[171] Korchagina E V., Philippova OE (2010) Multichain Aggregates in Dilute Solutions of Associating Polyelectrolyte Keeping a Constant Size at the Increase in the Chain Length of Individual Macromolecules. Biomacromolecules 11:3457–3466. https://doi.org/10.1021/bm100990u

[172] Philippova OE, Volkov E V., Sitnikova NL, Khokhlov AR, Desbrieres J, Rinaudo M (2001) Two Types of Hydrophobic Aggregates in Aqueous Solutions of Chitosan and Its Hydrophobic Derivative. Biomacromolecules 2:483–490. https://doi.org/10.1021/bm005649a

[173] Anthonsen MW, Vårum KM, Hermansson AM, Smidsrød O, Brant DA (1994) Aggregates in acidic solutions of chitosans detected by static laser light scattering. Carbohydr Polym 25:13–23. https://doi.org/10.1016/0144-8617(94)90157-0

[174] Blagodatskikh I V, Bezrodnykh EA, Abramchuk SS, Muranov A V, Sinitsyna O V, Khokhlov AR, Tikhonov VE (2013) Short chain chitosan solutions: self-assembly and aggregates disruption effects. J Polym Res 20:. https://doi.org/10.1007/s10965-013-0073-0

[175] Troiber C, Kasper JC, Milani S, Scheible M, Martin I, Schaubhut F, Küchler S, Rädler J, Simmel FC, Friess W, Wagner E (2013) Comparison of four different particle sizing methods for siRNA polyplex characterization. Eur J Pharm Biopharm 84:255–264. https://doi.org/10.1016/j.ejpb.2012.08.014

[176] Patterson JP, Robin MP, Chassenieux C, Colombani O, O'Reilly RK (2014) The analysis of solution self-assembled polymeric nanomaterials. Chem Soc Rev 43:2412–2425. https://doi.org/10.1039/c3cs60454c

[177] Harada A, Kataoka K (1995) Formation of Polyion Complex Micelles in an Aqueous Milieu from a Pair of Oppositely-Charged Block Copolymers with Poly(ethylene glycol) Segments. Macromolecules 28:5294–5299. https://doi.org/10.1021/ma00119a019

[178] Stetefeld J, McKenna SA, Patel TR (2016) Dynamic light scattering: a practical guide and applications in biomedical sciences. Biophys Rev 8:409–427. https://doi.org/10.1007/s12551-016-0218-6

[179] Krichevsky O, Bonnet G (2002) Fluorescence correlation spectroscopy: the technique and its applications. Reports Prog Phys 65:251–297. https://doi.org/10.1088/0034-4885/65/2/203

[180] Pánek J, Loukotová L, Hrubý M, Štěpánek P (2018) Distribution of Diffusion Times Determined by Fluorescence (Lifetime) Correlation Spectroscopy. Macromolecules 51:2796–2804. https://doi.org/10.1021/acs.macromol.7b02158

[181] Reinhard S, Wagner E (2017) How to Tackle the Challenge of siRNA Delivery with Sequence-Defined Oligoamino Amides. Macromol Biosci 17:1600152. https://doi.org/10.1002/mabi.201600152

[182] Kean T, Thanou M (2010) Biodegradation, biodistribution and toxicity of chitosan. Adv Drug Deliv Rev 62:3–11. https://doi.org/10.1016/j.addr.2009.09.004

[183] Raja MAG, Katas H, Wen TJ (2015) Stability, intracellular delivery, and release of siRNA from chitosan nanoparticles using different cross-linkers. PLoS One 10:1–19. https://doi.org/10.1371/journal.pone.0128963

[184] Howard KA, Rahbek UL, Liu X, Damgaard CK, Glud SZ, Andersen M, Hovgaard MB, Schmitz A, Nyengaard JR, Besenbacher F, Kjems J (2006) RNA Interference in Vitro and in Vivo Using a Novel Chitosan/siRNA Nanoparticle System. Mol Ther 14:476–484. https://doi.org/10.1016/j.ymthe.2006.04.010

[185] Malmo J, Sørgård H, Vårum KM, Strand SP (2012) SiRNA delivery with chitosan nanoparticles: Molecular properties favoring efficient gene silencing. J Control Release 158:261–268. https://doi.org/10.1016/j.jconrel.2011.11.012

[186] Song Y, Tang C, Yin C (2018) Combination antitumor immunotherapy with VEGF and PIGF siRNA via systemic delivery of multi-functionalized nanoparticles to tumor-associated macrophages and breast cancer cells. Biomaterials 185:117–132. https://doi.org/10.1016/j.biomaterials.2018.09.017

[187] Vermeulen LMP, De Smedt SC, Remaut K, Braeckmans K (2018) The proton sponge hypothesis: Fable or fact? Eur J Pharm Biopharm 129:184–190. https://doi.org/10.1016/j.ejpb.2018.05.034

[188] Richard I, Thibault M, De Crescenzo G, Buschmann MD, Lavertu M (2013) Ionization behavior of chitosan and chitosan-DNA polyplexes indicate that chitosan has a similar capability to induce a proton-sponge effect as PEI. Biomacromolecules 14:1732–1740. https://doi.org/10.1021/bm4000713

[189] Thibault M, Lavertu M, Astolfi M, Buschmann MD (2016) Structure Dependence of Lysosomal Transit of Chitosan-Based Polyplexes for Gene Delivery. Mol Biotechnol 58:648–656. https://doi.org/10.1007/s12033-016-9964-8

[190] Ma Z, Yang C, Song W, Wang Q, Kjems J, Gao S (2014) Chitosan hydrogel as sirna vector for prolonged gene silencing. J Nanobiotechnology 12:1–9. https://doi.org/10.1186/1477-3155-12-23

[191] Lee J, Yun KS, Choi CS, Shin SH, Ban HS, Rhim T, Lee SK, Lee KY (2012) T cell-specific siRNA delivery using antibody-conjugated chitosan nanoparticles. Bioconjug Chem 23:1174–1180. https://doi.org/10.1021/bc2006219

[192] Zhang J, Tang C, Yin C (2013) Galactosylated trimethyl chitosan-cysteine nanoparticles loaded with Map4k4 siRNA for targeting activated macrophages. Biomaterials 34:3667–3677. https://doi.org/10.1016/j.biomaterials.2013.01.079

[193] Gao Y, Wang Z-Y, Zhang J, Zhang Y, Huo H, Wang T, Jiang T, Wang S (2014) RVG-Peptide-Linked Trimethylated Chitosan for Delivery of siRNA to the Brain. Biomacromolecules 15:1010–1018. https://doi.org/10.1021/bm401906p

[194] Lee SJ, Huh MS, Lee SY, Min S, Lee S, Koo H, Chu JU, Lee KE, Jeon H, Choi Y, Choi K, Byun Y, Jeong SY, Park K, Kim K, Kwon IC (2012) Tumor-homing poly-siRNA/glycol chitosan self-cross-linked nanoparticles for systemic siRNA delivery in cancer treatment. Angew Chemie - Int Ed 51:7203–7207. https://doi.org/10.1002/anie.201201390

[195] Sun P, Huang W, Jin M, Wang Q, Fan B, Kang L, Gao Z (2016) Chitosan-based nanoparticles for survivin targeted siRNA delivery in breast tumor therapy and preventing its metastasis. Int J Nanomedicine 11:4931–4945. https://doi.org/10.2147/IJN.S105427

[196] Chen J, Dou Y, Tang Y, Zhang X (2020) Folate receptor-targeted RNAi nanoparticles for silencing STAT3 in tumor-associated macrophages and tumor cells. Nanomedicine Nanotechnology, Biol Med 25:102173. https://doi.org/10.1016/j.nano.2020.102173

[197] Sava V, Fihurka O, Khvorova A, Sanchez-Ramos J (2020) Enriched chitosan nanoparticles loaded with siRNA are effective in lowering Huntington's disease gene expression following intranasal administration. Nanomedicine Nanotechnology, Biol Med 24:102119. https://doi.org/10.1016/j.nano.2019.102119

[198] He C, Yue H, Xu L, Liu Y, Song Y, Tang C, Yin C (2020) siRNA release kinetics from polymeric nanoparticles correlate with RNAi efficiency and inflammation therapy via oral delivery. Acta Biomater 103:213–222. https://doi.org/10.1016/j.actbio.2019.12.005

[199] Mi P, Cabral H, Kataoka K (2020) Ligand-Installed Nanocarriers toward Precision Therapy. Adv Mater 32:1902604. https://doi.org/10.1002/adma.201902604

[200] Chuan D, Jin T, Fan R, Zhou L, Guo G (2019) Chitosan for gene delivery: Methods for improvement and applications. Adv Colloid Interface Sci 268:25–38. https://doi.org/10.1016/j.cis.2019.03.007

[201] Gaspar VM, Costa EC, Queiroz JA, Pichon C, Sousa F, Correia IJ (2015) Folate-targeted multifunctional amino acid-chitosan nanoparticles for improved cancer therapy. Pharm Res 32:562–577. https://doi.org/10.1007/s11095-014-1486-0

[202] Zhang C, Zhu W, Liu Y, Yuan Z, Yang S, Chen W, Li J, Zhou X, Liu C, Zhang X (2016) Novel polymer micelle mediated co-delivery of doxorubicin and P-glycoprotein siRNA for reversal of multidrug resistance and synergistic tumor therapy. Sci Rep 6:23859. https://doi.org/10.1038/srep23859

[203] Yang S, Ren Z, Chen M, Wang Y, You B, Chen W, Qu C, Liu Y, Zhang X (2018) Nucleolin-Targeting AS1411-Aptamer-Modified Graft Polymeric Micelle with Dual pH/Redox Sensitivity Designed To Enhance Tumor Therapy through the Codelivery of Doxorubicin/TLR4 siRNA and Suppression of Invasion. Mol Pharm 15:314–325. https://doi.org/10.1021/acs.molpharmaceut.7b01093

[204] Zhu Q, Zhou Y, Guan M, Zhou X, Yang S, Liu Y, Chen W, Zhang C, Yuan Z, Liu C, Zhu A, Zhang X (2014) Low-density lipoprotein-coupled N-succinyl chitosan nanoparticles co-delivering siRNA and doxorubicin for hepatocyte-targeted therapy. Biomaterials 35:5965–5976. https://doi.org/10.1016/j.biomaterials.2014.03.088

[205] Muzzarelli RAA (1977) Chitin. Pergamon Press

[206] Park JW, Choi K-H, Park KK (1983) Acid-Base Equilibria and Related Properties of Chitosan.pdf. Bull Korean Chem Soc 4:68–72

[207] Domard A (1987) pH and c.d. measurements on a fully deacetylated chitosan: application to CuII—polymer interactions. Int J Biol Macromol 9:98–104. https://doi.org/10.1016/0141-8130(87)90033-X

[208] Rhazi M, Desbrières J, Tolaimate A, Rinaudo M, Vottero P, Alagui A (2002) Contribution to the study of the complexation of copper by chitosan and oligomers. Polymer (Guildf) 43:1267–1276. https://doi.org/10.1016/S0032-3861(01)00685-1

[209] Hernández RB, Franco AP, Yola OR, López-Delgado A, Felcman J, Recio MAL, Mercê ALR (2008) Coordination study of chitosan and Fe3+. J Mol Struct 877:89–99. https://doi.org/10.1016/j.molstruc.2007.07.024

[210] Bodek KH, Kufelnicki A (1995) Protolytic and complexing properties of microcrystalline chitosan with Co(II), Zn(II), and Cu(II) ions. J Appl Polym Sci 57:645–651. https://doi.org/10.1002/app.1995.070570515

[211] Rhazi M, Desbrières J, Tolaimate A, Rinaudo M, Vottero P, Alagui A, El Meray M (2002) Influence of the nature of the metal ions on the complexation with chitosan. Eur Polym J 38:1523–1530. https://doi.org/10.1016/S0014-3057(02)00026-5

[212] Shigemasa Y, Matsuura H, Sashiwa H, Saimoto H (1996) Evaluation of different absorbance ratios from infrared spectroscopy for analyzing the degree of deacetylation in chitin. Int J Biol Macromol 18:237–242. https://doi.org/10.1016/0141-8130(95)01079-3

[213] Brugnerotto J, Lizardi J, Goycoolea F., Argüelles-Monal W, Desbrières J, Rinaudo M

(2001) An infrared investigation in relation with chitin and chitosan characterization. Polymer (Guildf) 42:3569–3580. https://doi.org/10.1016/S0032-3861(00)00713-8

[214] Piron E, Domard A (1998) Interaction between chitosan and uranyl ions. Part 2. Mechanism of interaction. Int J Biol Macromol 22:33–40. https://doi.org/10.1016/S0141-8130(97)00083-4

[215] Wang X, Du Y, Liu H (2004) Preparation, characterization and antimicrobial activity of chitosan–Zn complex. Carbohydr Polym 56:21–26. https://doi.org/10.1016/j.carbpol.2003.11.007

[216] Yazdani M, Virolainen E, Conley K, Vahala R (2017) Chitosan–Zinc(II) Complexes as a Bio-Sorbent for the Adsorptive Abatement of Phosphate: Mechanism of Complexation and Assessment of Adsorption Performance. Polymers (Basel) 10:25. https://doi.org/10.3390/polym10010025

[217] Anandhavelu S, Thambidurai S (2011) Preparation of chitosan-zinc oxide complex during chitin deacetylation. Carbohydr Polym 83:1565–1569. https://doi.org/10.1016/j.carbpol.2010.10.006

[218] Tang L-G, Hon DNS (2001) Chelation of chitosan derivatives with zinc ions. II. Association complexes of Zn2+ onto O,N-carboxymethyl chitosan. J Appl Polym Sci 79:1476–1485. https://doi.org/10.1002/1097-4628(20010222)79:8<1476::AID-APP150>3.0.CO;2-A

[219] Giacalone G, Hillaireau H, Capiau P, Chacun H, Reynaud F, Fattal E (2014) Stabilization and cellular delivery of chitosan–polyphosphate nanoparticles by incorporation of iron. J Control Release 194:211–219. https://doi.org/10.1016/j.jconrel.2014.08.022

[220] Kim H-S (2004) Thermodynamic studies of interaction between chitosan and metal ions by isothermal titration calorimetry (I). J Ind Eng Chem 10:273–277

[221] Camci-Unal G, Pohl NLB (2010) Quantitative Determination of Heavy Metal Contaminant Complexation by the Carbohydrate Polymer Chitin. J Chem Eng Data 55:1117–1121. https://doi.org/10.1021/je900552w

[222] Feng F, Liu Y, Zhao B, Hu K (2012) Characterization of half N-acetylated chitosan powders and films. Procedia Eng 27:718–732. https://doi.org/10.1016/j.proeng.2011.12.511

[223] Pereira FS, Lanfredi S, González ERP, da Silva Agostini DL, Gomes HM, dos Santos Medeiros R (2017) Thermal and morphological study of chitosan metal complexes. J Therm Anal Calorim 129:291–301. https://doi.org/10.1007/s10973-017-6146-2

[224] Ogawa K, Oka K, Yui T (1993) X-ray study of chitosan-transition metal complexes. Chem Mater 5:726–728. https://doi.org/10.1021/cm00029a026

[225] Gregor HP, Luttinger LB, Loebl EM (1955) Metal–Polyelectrolyte Complexes. I. The Polyacrylic Acid–Copper Complex. J Phys Chem 59:34–39. https://doi.org/10.1021/j150523a011

[226] Irving HM, Rossotti HS (1954) The calculation of formation curves of metal complexes from pH titration curves in mixed solvents. J Chem Soc 2904. https://doi.org/10.1039/jr9540002904

[227] Hernández RB, Franco AP, Yola OR, López-Delgado A, Felcman J, Recio MAL, Mercê ALR (2008) Coordination study of chitosan and Fe3+. J Mol Struct 877:89–99. https://doi.org/10.1016/j.molstruc.2007.07.024

[228] Gomes JRB, Jorge M, Gomes P (2014) Interaction of chitosan and chitin with Ni, Cu and Zn ions: A computational study. J Chem Thermodyn 73:121–129. https://doi.org/10.1016/j.jct.2013.11.016

[229] Braier NC, Jishi RA (2000) Density functional studies of Cu 2+ and Ni 2+ binding to chitosan. J Mol Struct THEOCHEM 499:51–55. https://doi.org/10.1016/S0166-1280(99)00288-2

[230] Zhang B, Lv D, Fang C (2018) Chitooligosaccharide-metal ions complexes: insights from molecular dynamics simulations. Colloid Polym Sci 296:245–250. https://doi.org/10.1007/s00396-017-4239-x

[231] Vold IMN, Vårum KM, Guibal E, Smidsrød O (2003) Binding of ions to chitosan—selectivity studies. Carbohydr Polym 54:471–477. https://doi.org/10.1016/j.carbpol.2003.07.001

[232] BASSI R, PRASHER SO, SIMPSON BK (2000) Removal of Selected Metal Ions from Aqueous Solutions Using Chitosan Flakes. Sep Sci Technol 35:547–560. https://doi.org/10.1081/SS-100100175

[233] Benavente M (2008) Adsorption of Metallic ions onto chitosan: equilibrium and kinetic studies. Kemiteknik, Chemical and Engineering and Technology, Kungliga Tekniska högskolan

[234] Kurita K, Sannan T, Iwakura Y (1979) Studies on chitin. VI. Binding of metal cations. J Appl Polym Sci 23:511–515. https://doi.org/10.1002/app.1979.070230221

[235] Monteiro OAC, Airoldi C (1999) Some thermodynamic data on copper-chitin and copper-chitosan biopolymer interactions. J Colloid Interface Sci 212:212–219. https://doi.org/10.1006/jcis.1998.6063

[236] Weißpflog J, Gündel A, Vehlow D, Steinbach C, Müller M, Boldt R, Schwarz S, Schwarz D (2020) Solubility and Selectivity Effects of the Anion on the Adsorption of Different Heavy Metal Ions onto Chitosan. Molecules 25:2482. https://doi.org/10.3390/molecules25112482

[237] Varma AJ, Deshpande S V, Kennedy JF (2004) Metal complexation by chitosan and its derivatives: a review. Carbohydr Polym 55:77–93. https://doi.org/10.1016/j.carbpol.2003.08.005

[238] Ahmed MJ, Hameed BH, Hummadi EH (2020) Review on recent progress in chitosan/chitin-carbonaceous material composites for the adsorption of water pollutants. Carbohydr Polym 247:116690. https://doi.org/10.1016/j.carbpol.2020.116690

[239] Reynaud F, Tsapis N, Deyme M, Vasconcelos TG, Gueutin C, Guterres SS, Pohlmann AR, Fattal E (2011) Spray-dried chitosan-metal microparticles for ciprofloxacin adsorption: Kinetic and equilibrium studies. Soft Matter 7:7304. https://doi.org/10.1039/c1sm05509g

[240] Kumar IA, Viswanathan N (2017) Development of multivalent metal ions imprinted chitosan biocomposites for phosphate sorption. Int J Biol Macromol 104:1539–1547. https://doi.org/10.1016/j.ijbiomac.2017.02.100

[241] Fang H, Lin L, Chen J, Wu J, Tian H, Chen X (2019) Zinc ion coordination significantly improved the transfection efficiency of low molecular weight polyethylenimine. Biomater Sci 7:1716–1728. https://doi.org/10.1039/C9BM00039A

[242] Liu S, Jia H, Yang J, Pan J, Liang H, Zeng L, Zhou H, Chen J, Guo T (2018) Zinc

Coordinated Cationic Polymers Break Up the Paradox between Low Molecular Weight and High Transfection Efficacy. Biomacromolecules 19:4270–4276. https://doi.org/10.1021/acs.biomac.8b01140

[243] Huang X, Li Z, Wu J, Hang Y, Wang H, Yuan L, Chen H (2019) Small addition of Zn 2+ in Ca 2+ @DNA results in elevated gene transfection by aminated PGMA-modified silicon nanowire arrays. J Mater Chem B 7:566–575. https://doi.org/10.1039/c8tb03045f

[244] Asayama S, Nishinohara S, Kawakami H (2011) Zinc-chelated imidazole groups for DNA polyion complex formation. Metallomics 3:680. https://doi.org/10.1039/c1mt00019e

[245] Yu QY, Guo Y, Zhang J, Huang Z, Yu XQ (2019) Zn(ii) coordination to cyclen-based polycations for enhanced gene delivery. J Mater Chem B 7:451–459. https://doi.org/10.1039/c8tb02414f

[246] Wu D, Delair T (2015) Stabilization of chitosan/hyaluronan colloidal polyelectrolyte complexes in physiological conditions. Carbohydr Polym 119:149–158. https://doi.org/10.1016/j.carbpol.2014.11.042

[247] Wu D, Ensinas A, Verrier B, Primard C, Cuvillier A, Champier G, Paul S, Delair T (2016) Zinc-stabilized colloidal polyelectrolyte complexes of chitosan/hyaluronan: a tool for the inhibition of HIV-1 infection. J Mater Chem B 4:5455–5463. https://doi.org/10.1039/C6TB00898D

[248] Hadjiliadis N, Sletten E (2009) Metal Complex–DNA Interactions. John Wiley & Sons, Ltd, Chichester, UK

[249] Lippert B (1999) Cisplatin. Wiley

[250] DeRose VJ (2009) Chapter 5. Characterization of Nucleic Acid-Metal Ion Binding by Spectroscopic Techniques. In: Nucleic Acid-Metal Ion Interactions. Royal Society of Chemistry, Cambridge, pp 154–179

[251] Mitra S, Brenowitz M (2009) Chapter 7. Metal Ions and RNA Folding Kinetics. In: Nucleic Acid-Metal Ion Interactions. Royal Society of Chemistry, Cambridge, pp 221–259

[252] Giedroc DP, Grossoehme NE (2008) Chapter 6. Metal Ions and the Thermodynamics of RNA Folding

[253] Bloomfield VA (1997) DNA condensation by multivalent cations. Biopolymers 44:269–282. https://doi.org/10.1002/(SICI)1097-0282(1997)44:3<269::AID-BIP6>3.0.CO;2-T

[254] Zhou J, Ke F, Liang D (2010) Kinetic Study on the Reentrant Condensation of Oligonucleotide in Trivalent Salt Solution. J Phys Chem B 114:13675–13680. https://doi.org/10.1021/jp1074187

[255] Nguyen TT, Rouzina I, Shklovskii BI (2000) Reentrant condensation of DNA induced by multivalent counterions. J Chem Phys 112:2562–2568. https://doi.org/10.1063/1.480819

[256] Lippert B (2009) Chapter 2. Coordinative Bond Formation Between Metal Ions and Nucleic Acid Bases. In: Nucleic Acid-Metal Ion Interactions. Royal Society of Chemistry, Cambridge, pp 39–74

[257] goleman, daniel; boyatzis, Richard; Mckee A (1995) Bioinorganic Chemistry. Springer Netherlands, Dordrecht

[258] Hud N V, Engelhart AE (2009) Sequence-specific DNA – Metal Ion Interactions

[259] Eichhorn GL, Shin YA (1968) Interaction of metal ions with polynucleotides and related compounds. XII. The relative effect of various metal ions on DNA helicity. J Am Chem Soc 90:7323–7328. https://doi.org/10.1021/ja01028a024

[260] Lee JS, Latimer LJP, Reid RS (1993) A cooperative conformational change in duplex DNA induced by Zn 2+ and other divalent metal ions. Biochem Cell Biol 71:162–168. https://doi.org/10.1139/o93-026

[261] Heinemann U, Roske Y (2020) Symmetry in Nucleic-Acid Double Helices. Symmetry (Basel) 12:737. https://doi.org/10.3390/sym12050737

[262] Sorokin VA, Valeev VA, Usenko EL, Rakovsky YP, Andrushchenko V V. (2013) Specific features of Zn2+, Co2+ and Ni2+ ion binding to DNA in alkaline solutions. Int J Biol Macromol 55:137–141. https://doi.org/10.1016/j.ijbiomac.2013.01.001

[263] Wood DO (2002) M-DNA is stabilised in G*C tracts or by incorporation of 5-fluorouracil. Nucleic Acids Res 30:2244–2250. https://doi.org/10.1093/nar/30.10.2244

[264] Aich P, Labiuk SL, Tari LW, Delbaere LJT, Roesler WJ, Falk KJ, Steer RP, Lee JS (1999) M-DNA: a complex between divalent metal ions and DNA which behaves as a molecular wire. J Mol Biol 294:477–485. https://doi.org/10.1006/jmbi.1999.3234

[265] Cruz-León S, Schwierz N (2020) Hofmeister Series for Metal-Cation–RNA Interactions: The Interplay of Binding Affinity and Exchange Kinetics. Langmuir 36:5979–5989. https://doi.org/10.1021/acs.langmuir.0c00851

Chapter 2: Effects of chain length of chitosan oligosaccharides on solution properties and complexation with siRNA

*Chapter published as an article in *Polymers*: Delas, Mock-Joubert, Faivre, Hofmaier, Sandre, Dole, Chapel, Crépet, Trombotto, Delair, Schatz (2019) Effects of Chain Length of Chitosan Oligosaccharides on Solution Properties and Complexation with siRNA. Polymers (Basel) 11:1236.

2.1. Abstract

In the context of gene delivery, chitosan has been widely used as a safe and effective polycation to complex DNA, RNA and more recently, siRNA. However, much less attention has been paid to chitosan oligosaccharides (COS) despite their biological properties. This study proposed to carry out a physicochemical study of COS varying in degree of polymerization (DP) from 5 to 50, both from the point of view of the solution properties and the complexing behavior with siRNA. The main parameters studied as a function of DP were the apparent pKa, the solubility versus pH, the binding affinity with siRNA and the colloidal properties of complexes. Some parameters, like the pKa or the binding enthalpy with siRNA, showed a marked transition from DP 5 to DP 13, suggesting that electrostatic properties of COS vary considerably in this range of DP. The colloidal properties of siRNA/COS complexes were affected in a different way by the COS chain length. In particular, COS of relatively high DP (≥ 50) were required to form small complex particles with good stability.

2.2. Introduction

Chitosan, the chitin partially deacetylated derivative composed of β-(1→4)-linked D-glucosamine (GlcN) and N-acetyl-D-glucosamine (GlcNAc) groups, is a biopolymer of major importance with applications spanning water treatment, agriculture, cosmetics, the food industry and biopharmaceutics [1]. Among these, chitosan is well-known for its potential in biomedical applications owing to its biocompatibility, biodegradability and bioactivity including bacteriostatic, healing, immunologic and antitumoral activities [2]. In particular, chitosan has been used as a polycation for the design of non-viral systems for DNA delivery and more recently, for small-interfering RNA (siRNA) [3–8]. These systems rely on the electrostatic complexation of the phosphate groups of nucleic acids with the protonated amine functions of chitosan under mild acid conditions. Unlike most polyamine systems used in gene delivery like polyethyleneimine or polylysine, chitosan has a low toxicity in relation to its low cationicity at physiological pH [9]. Several parameters related to the formation of chitosan/DNA (siRNA) polyplexes have been studied with the aim of increasing the stability of complexes toward dissociation, the resistance to serum proteases, the escape from the immune system, cell targeting, cell internalization and the endosome escape. The main parameters include: The degree of protonation of chitosan related to the pH of the medium; the amine to phosphate molar ratio (N:P); the degree of N-acetylation of chitosan (DA); and the molar mass of chitosan [6, 7, 10–12]. The precise control of these four parameters enables:

The size and surface charge of polyplexes to be adjusted; the binding affinity with nucleic acids; and the resulting stability of complexes. In the case of siRNA delivery, the size of polyplexes is primarly determined by the chitosan chain length; low molar mass chitosan usually give rise to small-sized complexes [13, 14]. However, different studies have demonstrated that chitosans of low molar mass (<10 kDa) have difficulty in forming stable complexes, especially in the presence of serum, where destabilization through competitive plasma protein displacement may occur [11, 13, 14]. For chitosans of higher molar mass (>10 kDa), the chain length has little effect on the polyplexes stability, the cell uptake and the gene knockdown [14]. The latter is primarily determined by the surface charge of the polyplexes which is related to the degree of acetylation and pH. A knockdown efficiency higher than 70% was reported with an almost fully N-deacetylated chitosan (DA of 2%) [14]. However, no significant effect of the (N:P) ratio above 5 was evidenced on the size, colloidal stability and gene knockdown [14].

This work investigated the role of the chitosan chain length on the complexing properties with siRNA and attempts were made to correlate it with the solution behaviour of chitosan chains alone. For this purpose, this study used chitosan oligosaccharides (COS) of low DA (<1%) with degrees of polymerization (DPs) comprised between 5 and 50. Even though low molar mass chitosans are not best suited for siRNA delivery, it is important to understand, at least from a fundamental point of view, the role of the DP on the affinity with siRNA and the resulting stability of complexes. In this study, the physicochemical properties of COS were studied by potentiometric titration and dynamic light scattering (DLS). Then, the properties of COS-siRNA complexes were assessed by DLS, siRNA assay and isothermal titration calorimetry. The COS were always used in their fully protonated state to study complexation with siRNA under the best conditions. An important aspect of this work is to determine whether an oligomer-to-polymer transition can be evidenced in the cooperative binding of chitosan with siRNA, as already demonstrated with DNA [15].

2.3. Materials and methods

siRNA. The siRNA duplex was provided by Kaneka Eurogentec S.A. (Seraing, Belgium) and received as lyophilisate after purification by reverse phase HPLC. The sense sequence was 5’-[Phos]GUCUCAGCCUCUUCUCAUUCCUG[dC][dT]-3’ (M = 7807.6 g/mol) and the antisense was 5’-AGCAGGAA[mU]G[mA]G[mA]A[mG]A[mG]G[mC]U[mG]A[mG]A [mC][mA][mU][dT][dT] (M = 8999.6 g/mol). The molar masses were determined by MALDI-TOF analysis. The annealing step was performed by Eurogentec according to standard procedures.

Chitosan oligosaccharides (COS). N-deacetylated chitosan (DA < 1%) with Mn ~ 90,000 g/mol and Đ = 2.1 (Figure appendix 1) was provided from Mahtani Chitosan (batch 20140503). A nitrous acid depolymerization was performed according to the method proposed by Allan and Peyron [16, 17]. Chitosan was dissolved at 3 wt % in water in the presence of a stoichiometric amount of HCl relative to amine functions. After 3 days of vigorous stirring, sodium nitrite was added to the chitosan solution at various nitrite/GlcN molar ratios depending on the targeted DP. The reaction proceeded under magnetic stirring in a closed reaction vessel for 24 h at room temperature. After filtration on a 1.0 µm pore size glass fiber membrane (Pall), the solution was lyophilized and the lyophilisate was dissolved in a minimum volume of ultrapure water. The COS were precipitated in ethanol:acetone (1:1 v:v) mixture and the precipitate was washed three times with the same solvent mixture and centrifuged. The swollen oligomers were then repeatedly (3×) dissolved in ultrapure water and lyophilized. The final mass yield of purified COS under their hydrochloride salt form was above 70%.

COS characterization by ^{1}H NMR and SEC-MALLS. The chemical structure of COS was determined at 298 K from proton nuclear magnetic resonance (^{1}H-NMR) spectroscopy on a Bruker AVANCE III HD 400 MHz spectrometer using a 5 mm Bruker multinuclear z-gradient direct probe. The ^{1}H NMR spectra were calibrated from the signal of HOD at 4.79 ppm [18]. The degree of polymerization (DP) of COS which corresponds to the number of glucosamine (GlcN) units within the COS chain was obtained from the integral ratio of the H-2 protons of GlcN units at 3.20 ppm and the H-1 or H-3 protons of the terminal 2,5-anhydro-D-mannose (M-unit) located at 5.11 and 4.46 ppm, respectively [19]. Note that in the ^{1}H-NMR analysis conditions used here, the aldehyde group of the M-units does not exist in its free (–CHO) form but exclusively in its hydrated (–CH(OH)$_2$) form [20]. The mass-average molar mass (M_w), the number-average molar mass (M_n) and the dispersity (Đ) of COS were determined by high-performance size exclusion chromatography (SEC) (UltiMate 3000 HPLC, Thermofisher, Waltham, MA, USA) with a multiangle laser light scattering detection (MALLS) (Dawn Heleos, Wyatt, Santa Barbara, CA, USA) operating at λ_0 = 658 nm and a differential refractive index detector (Optilab rEX, Wyatt) operating at the same wavelength. The COS samples were separated on two serially connected columns (Tosoh TSK gel columns, G4000PWXL & G3000PWXL, Tokyo, Japan). A degassed 0.3 M acetic acid/0.2 M sodium acetate buffer (pH 4.5) was used as eluent after filtration on a 0.22 µm pore size membrane (Millipore). The flow rate was maintained at 0.6 mL/min, and the amount of sample injected was 100 µL at a concentration of 5 mg/mL. The values of the refractive index increment (dn/dc) were independently determined from a range of five chitosan concentrations for each DP with the Optilab reX refractive index detector using same conditions for SEC-MALLS analysis but without degassing the buffer. The values of the

number-average degree of polymerization (DP_n) of COS were derived from SEC-MALLS analysis by using the following relation: $DP_n = (M_n - M_{M\text{-}unit})/M_{GlcN}$ where MM-unit is the molar mass of the terminal 2,5-anhydro-D-mannose unit and M_{GlcN} is the molar mass of the glucosamine unit.

Thermogravimetric Analysis. The thermogravimetric analyses were performed using a Q50 device (TA instruments, New Castle, DE, USA) in order to determine the water content of chitosan samples. It was operated from 25 to 150 °C at a ramp temperature of 2 ◦C/min under a flow of nitrogen. The values of water content were taken into account in the preparation of the COS solution.

Potentiometric Titration. The potentiometric titrations of COS varying in DP were performed using an automatic pH titrator (TitroLine 7800, SI Analytics, Mainz, Germany) equipped with a microelectrode. The COS solutions were prepared at 1 g/L in water and the pH was adjusted to 3.0 with a known amount of HCl 0.1M to ensure the full protonation of glucosamine residues. The titrations were performed with 10 mL of COS solution using 0.1 M NaOH (NIST Standard Concentrate, for Volumetric Analysis, Fisher Chemical, Pittsburgh, PA, USA). The volume of each injection of NaOH was set to 10 µL at a rate of 5 mL/min and the time between each injection was set to 60 s. The apparent values of pK_a were derived from the Henderson-Hasselbalch equation:

$$pK_a = pH + \log\frac{1-\alpha}{\alpha} \quad (1)$$

where α is the degree of dissociation of the ammonium groups defined as:

$$\alpha = \frac{[ChitNH_2]}{[ChitNH_3^+] + [ChitNH_2]} \quad (2)$$

and according to the requirement of the electroneutrality:

$$[ChitNH_3^+] = [Cl^-] + [OH^-] - [Na^+] - [H_3O^+] \quad (3)$$

Note that Cl^- ions come from both the added HCl and the glucosamine hydrochloride residues. All concentrations were corrected by the dilution factor related to the titration. In addition to the degree of dissociation, the values of the degree of protonation (γ) of the COS were also determined from the titration data:

$$\gamma = \frac{[ChitNH_3^+]}{[ChitNH_3^+] + [ChitNH_2]} \quad (4)$$

Solubility of COS as function of pH. The COS solutions were prepared at 1 g/L in deionized water and filtered on 0.22 µm cellulose acetate filter. The pH of the COS solutions increased

by adding 0.1 M NaOH, and aliquots were taken at various pHs. The scattered intensity (kilo counts per second, Kcps) of the COS solutions was determined at 25 °C using a ZetaSizer Nano ZS (Malvern Panalytical Ltd., Malvern, UK) working at λ = 632.8 nm with a back scattering angle detection (173°).

Preparation of COS/siRNA complexes. The complexes between siRNA and chitosan were formed by mixing 50 µL of COS solution with 50 µL of siRNA solution, both prepared in RNase free water. The concentration of the siRNA solution was set at 0.1 g/L (0.294 mM in phosphate groups), while the COS concentration in protonated glucosamine residues was varied according to the targeted nitrogen to phosphate (N:P) ratio. The COS solution was filtered on 0.22 µm cellulose acetate membrane prior to use. The complexation was carried out by a one shot addition with a micropipette of the COS solution to the siRNA solution for N:P < 1. The opposite order of addition was used for N:P > 1. By doing so the component in default was always added to the one in excess. Hence the system avoided the experience of the neutral state at charge stoichiometry [21, 22]. The fast mixing conditions were obtained by achieving the complexation reaction in a 1.5 mL plastic microtube placed in a VXR basic Vibrax (IKA) set at 1000 rpm. The particles of complexes were analyzed by dynamic light scattering using a ZetaSizer Nano ZS (see above) at 25 °C. Further, three to five measurements were performed for each condition of complexation. The particle size distribution was determined using a non-negative least squares (NNLS) algorithm with a quadratic weighting scheme, which places more emphasis on fitting the earlier channels where the signal intensity is the greatest.

siRNA assay with toluidine blue (TB). The amount of complexed siRNA was assayed with toluidine blue O (Sigma Aldrich) according to a depletion protocol. The dispersions of complexes prepared at various N:P ratios were incubated (30 min) in 1.4 mL of 0.1 M acetate buffer pH 4.0 containing an excess of TB. After centrifugation (20 min at 14000 rpm), free TB was titrated in 200 µL of supernatant by absorbance measurements at λ = 585 nm using a microplate reader (SpectraMax M2, Molecular Devices, San Jose, CA, USA). The free siRNA concentration in the complexes was determined via calibration curves established in similar conditions (Figure appendix 8). The amount of complexed siRNA was then deduced by a simple difference between the initial and final siRNA concentrations in the complex dispersions. All experiments were performed in triplicate.

Isothermal Titration Calorimetry. The binding studies were performed using a Microcal iTC200 (Malvern Panalytical Ltd., Malvern, UK). All titrations were performed at 25 °C in 10 mM acetate buffer at pH = 4.5. Further, 16 consecutive injections of 2 µL (0.4 µL for the first injection) of COS solution at a concentration of 10 mM in GlcN units were performed in 200 µL of siRNA solution at a concentration of 0.7 mM in the phosphate groups. The

injections were made at intervals of 180 s. All solutions were degassed before use. The COS solutions were also injected into the buffer as blank titrations. All experiments were carried out in duplicate. The thermograms were analyzed using a modified multiple non-interacting sites (MNIS) model (see details in Chapter 2 supporting information) [23].

2.4. Results

2.4.1. Solution properties of chitosan oligosaccharides

Preparation of a library of COS. Chitosan oligosaccharides were prepared by depolymerization of an almost fully N-deacetylated chitosan (DA < 1%) of 9×10^4 g/mol with nitrous acid (Figure appendix 1). In this reaction, the number of broken glycosidic linkages is approximately stoichiometric to the amount of nitrous acid used. After several purification steps, the COS were obtained under the water-soluble hydrochloride salt form. All chemical shifts could be assigned on ^{1}H NMR spectra performed in D_2O (Figure appendix 2). In particular, the signal at 5.11 ppm was assigned to the gem diol group of the terminal 2,5-anhydro-D-mannose (M-unit) [19]. Importantly, no trace of hydroxymethylfurfural (HMF), the main degradation product of the M-unit, was evidenced by the absence of the characteristic peaks of HMF at 9.52, 7.52, 6.66 and 4.68 ppm [19]. The COS were used without reducing the M-unit with sodium borohydride ($NaBH_4$) or sodium cyanoborohydride ($NaBH_3CN$) as it has been recently shown that the reduction step could significantly increase the COS molar mass through side-branching reactions involving the aldehyde group of the M-unit and amino groups of the COS chain [24]. The average values of the molar mass, the degree of polymerization and dispersity obtained through SEC-MALLS and ^{1}H NMR are given in Table 2.4.1. The mass recoveries derived from the mass injected and the dn/dc values of COS were always higher than 80%, thus emphasizing the absence of strong enthalpic interactions between the macromolecules and the column packing. Similar values of DP were obtained by SEC and NMR, with the exception of the largest COS where NMR provided a higher DP value. This may be due to the uncertainties associated with the baseline determination and integral limits by NMR, particularly when the signal of the terminal M-unit is of low intensity.

Table 2.4.1. Chitosan oligosaccharides (COS) characterization by SEC-MALLS and nuclear magnetic resonance (NMR) analysis.

	SEC-MALLS					***^{1}H NMR***
COS	M_n (g/mol)	M_w (g/mol)	Đ	dn/dc (mL/g)	DP_n[1]	DP_n[1]
COS-5	1030	1240	1.20	0.1660	5.4	4.5
COS-13	2290	2900	1.26	0.1752	13.2	12.2
COS-16	2710	3630	1.34	0.1860	15.8	20.2
COS-27	4560	6420	1.41	0.1863	27.3	33.0
COS-50	8190	11970	1.46	0.1801	49.8	69.7

[1] number-average degree of polymerization of the chitosan without the M-unit.

2.4.1.1. Potentiometric titration of COS

The pK_a values of COS were determined as a function of the dissociation degree of protonated glucosamine units (α) (Figure 2.4-1.a) by applying the Henderson Hasselbalch equation (Equation (1)). For polyelectrolytes, only apparent pK_a values are obtained as the dissociation is influenced by the presence of existing charges on the chain. In the case of a polybase like chitosan, the expression of the apparent pK_a is [25]:

$$pK_{app} = pK_0 - \frac{0.4343}{RT}\left(\frac{\delta G_{el}}{\delta \alpha}\right) \quad (5)$$

where pK_0, the intrinsic dissociation constant of an isolated protonated glucosamine group, is determined by extrapolating pK_{app} to $\alpha = 1$, and $\frac{\delta G_{el}}{\delta \alpha}$ is the electrostatic Gibbs free energy per unit of α. The latter term is related to the surface potential of the polyion, ψ_0, through $\frac{\delta G_{el}}{\delta \alpha} = eN_a\psi_0(\alpha)$ where e is the elemental electric charge and N_a the Avogadro's number.

By combining these two equations:

$$pK_{app} = pK_0 - \frac{0.4343}{kT}e\psi_0(\alpha) \quad (6)$$

Four main results can be drawn from the Figure 2.4-1.a. First, the increase of pK_{app} with α emphasizes a polyelectrolyte behavior in contrast to D-glucosamine characterized by a single pK_a value of 7.55 [26]. The origin of this behavior originates from the electrostatic repulsion among neighboring charges which makes the energy cost of protonation higher at low degrees

of dissociation. A similar trend has been reported for chitosan [9, 27–29], chitosan oligomers [26, 30] and other polyamines [31]. Second, the $pK_{app}(\alpha)$ variations are linear which suggests that COS chains do not undergo significant conformational change during titration. However, it was observed that the pK_{app} variation tends to flatten at high values of α due to the polymer precipitation. In such cases, the values of pK_{app} were extrapolated to α =1 from the linear part of the plots. Third, the decrease in pK_{app} values with the DP, already observed for chitosan oligomers [26, 32], means that increasing the COS chain length has same effect on the electrostatic potential of the COS chains as decreasing α, that is, favoring the proton dissociation by electrostatic repulsion between charged units. Finally, COS-5 has distinct behavior from COS-13-16-27-50 as shown by the much higher pK_{app} values across the range of α, suggesting that a marked transition occurred between these two regimes of DP in relation with the increase of the electrostatic potential of the chains.

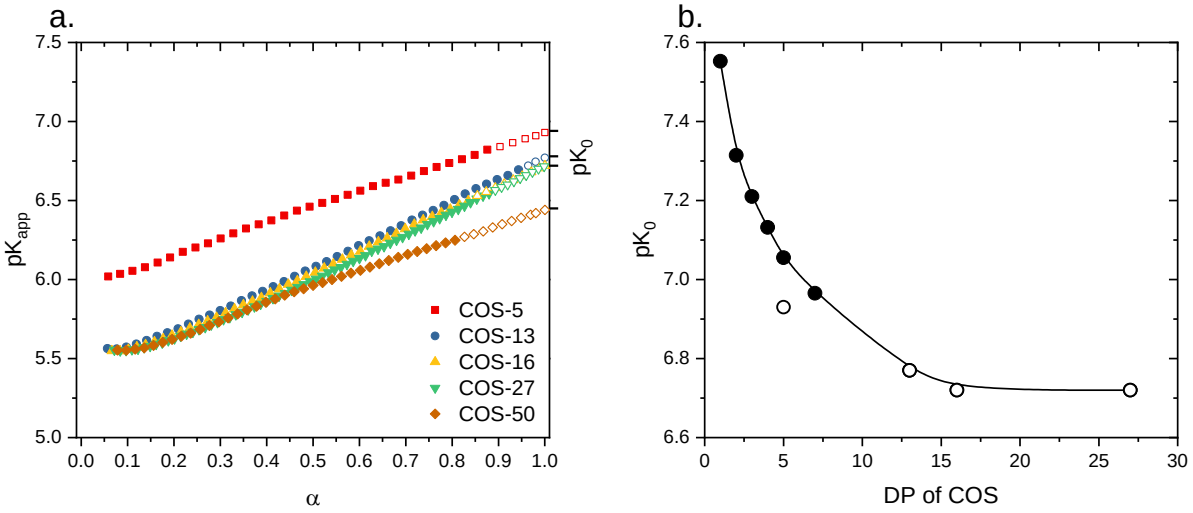

Figure 2.4-1. The variation of the apparent pK_a of COS as a function of the degree of dissociation (α). The open symbols correspond to extrapolated values. The concentration of COS is 1 g/L. (b) The variation of the intrinsic dissociation constant (pK_0) as a function of the degree of polymerization (DP) (open symbols). The data are plotted together with those in Ref. [26] obtained on isomolecular COS fractions of DP 1 to DP 7 (closed symbols). The line was added to guide the eye.

Regarding the pK_0 values, COS-5 had a pK_0 of 6.93, while pK_0 values of 6.77 to 6.72 were found for COS-13-16-27 (Table 2.4.2). For COS-50, the pK_0 of 6.44 was probably underestimated because the pK_{app} variation strongly deviated from the linearity around α = 0.5 (i.e pH = 6.0) due to decreased solubility of COS [29]. The pK_0 values were plotted together with those found by Tsukada and Inoue on pure COS fractions ranging from DP 1 to DP 7 (Figure 2.4-1.b) [26]. The authors have interpreted the progressive decrease of pK_0 with DP as a chain-end effect, since the intrinsic dissociation constant of the internal residues of the COS chain was lower than the terminal residues. The values of 6.74 and 7.62 were

respectively derived for the internal and terminal residues [26]. The value of 6.74 agrees well with the pK_0 found for COS-16 and COS-27 where chain end effects can be neglected. From Figure 2.4-1.b, it appears that increasing the chain length above DP 10 does not significantly modify the values of pK_0.

Table 2.4.2. The values of pK_0, $pK_{1/2}$ and n of COS varying in DP (see text).

DP_n	pK_0	$pK_{1/2}$	n
5	6.93	6.46	1.53
13	6.77	6.08	1.74
16	6.72	6.04	1.73
27	6.72	6.00	1.73
50	6.44	5.95	1.56

The titration data were also fitted with the extended Henderson-Hasselbalch equation introduced by Katchalsky and Spitnik [33]:

$$pH = pK_{1/2} + n \log \frac{\alpha}{1-\alpha} \quad (7)$$

where $pK_{1/2}$ is the pKa at $\alpha = 0.5$ and n an empirical parameter related to intramolecular interaction in chitosan chains [34]. For monomeric acids or bases, n is equal to 1. The values of n higher than 1 reflect electrostatic interactions between neighboring charged groups. For the COS-5, n = 1.53, while n~1.73 for the COS-13-16-27 (Table 2.4.2, Figure appendix 3) which is again consistent with the existence of two distinct regimes of DP. A similar trend was observed for the variation of $pK_{1/2}$. From these results, it can be concluded that the gradual increase of the electrostatic free energy of COS with the chain length results in anti-cooperative proton binding to COS due to the increased repulsions between charged units. The range of the electrostatic interactions in solution can be evaluated though the Debye length (λ_D) defined by:

$$\lambda_D = (8\pi l_B I)^{-1/2} \quad (8)$$

with l_B, the Bjerrum length and I the ionic strength ($I = \frac{1}{2}\sum_i c_i z_i^2$). In the conditions of concentration used for the titration of COS, λ_D = 3.5 nm which corresponds to a segment of 7 units of COS regularly aligned, considering a length per unit of chitosan of 0.51 nm [35]. As

the decrease in pK_a was most significant between DP1 and DP7 (Figure 2.4-1), the proton binding to COS chains must be mainly governed by the extent of electrostatic interaction evaluated by λ_D. In the presence of added salt, the Debye length is decreased which results in a dramatic increase of the apparent pK_a in the whole range of α values [9].

Eventually, the degree of protonation (γ) of COS as a function of pH was also derived from potentiometry data (Figure 2.4-2). All COS samples were fully protonated at pH 4, while less than 20% of the glucosamine units were still charged at pH 7.4, suggesting low solubility of COS under such conditions (see below).

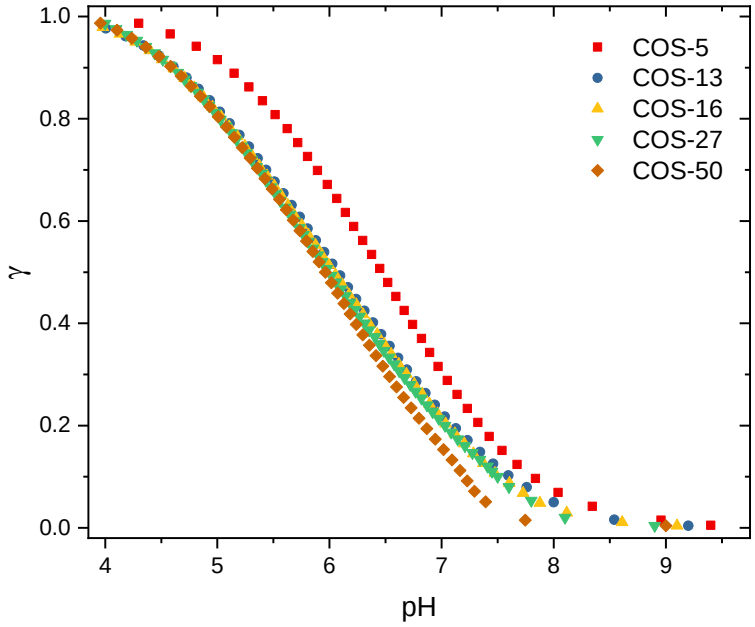

Figure 2.4-2. The degree of protonation (γ) as function of the pH for COS varying in DP. The concentration of COS is 1 g/L.

2.4.1.2. Solubility behavior of COS

The hydrochloride form of COS is completely soluble in water, giving a pH of 4 for solutions prepared in dilute conditions. The solubility of COS as a function of pH was determined by light scattering (Figure 2.4-3.a). Light scattering is a more sensitive technique than transmittance to detect aggregation and precipitation phenomena owing to the sixth power dependence of the particle radius to the scattered intensity (Rayleigh scattering). Three main results can be drawn from the Figure 2.4-3: (i) The onset of chitosan precipitation is observed within a narrow range of pH values in agreement with previous studies (Figure 2.4-3.a) [36, 37]; (ii) the corresponding critical pH values are lowered when the DP is increased and becomes constant from DP 27 (Figure 2.4-3.b); (iii) the degree of protonation (γ) at the critical

pH follows the opposite trend, namely γ increases with the DP and becomes constant from DP 27. The differences observed in the pH solubility profiles are in agreement with the respective pK_a values of COS, that is, the higher the pK_a, the higher the solubility. The increase with DP of the degree of protonation at the critical pH may emphasize a stronger involvement of cooperative hydrogen bonding in the precipitation of chitosan, associated with a less unfavorable mixing entropy.

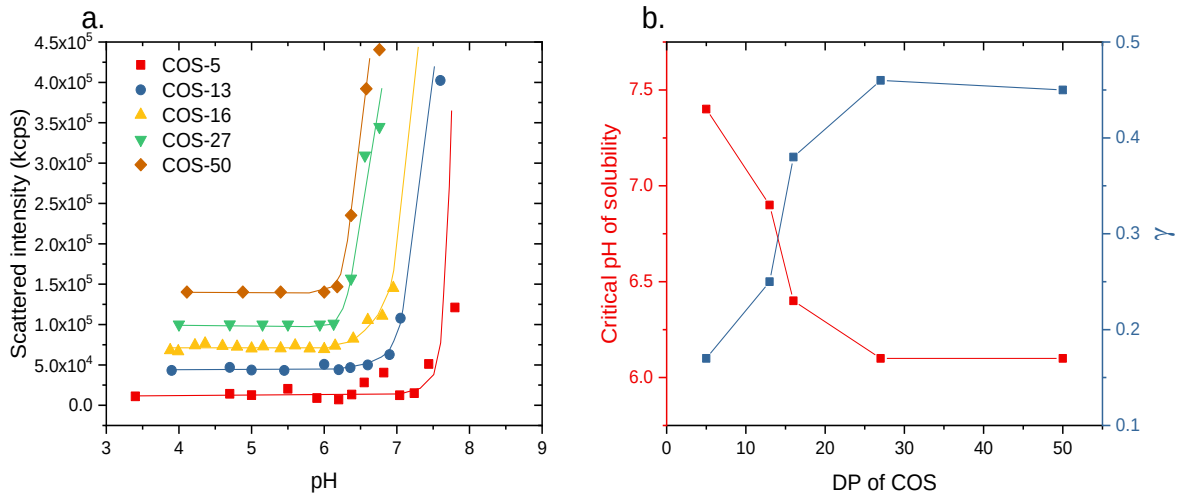

Figure 2.4-3. (a) The variation of the scattered light intensity (in kcps, kilo count-per-second) of COS solutions at 1 g/L as a function of the pH. The plots are shifted along the y-axis for better visibility; (b) the variation of the pH at the onset of the COS precipitation as a function of the DP. The corresponding values of degrees of protonation (γ) at the critical pH are also plotted (see Figure 2.4-2). The lines were added to guide the eye.

2.4.2. Complexation of COS with siRNA

The complexation of COS under their hydrochloride form with siRNA was performed at various N:P ratios in water without added salt in order to maximize the formation of salt bonds between the two polyions. The complexes obtained from siRNA and chitosan can be classified as strong in the sense of the ion pairing between opposite charges is strong enough to hydrophobize the complexed polymer segments and promote their segregation into dense particles. As such, the complexes differ from coacervate systems where the ion pairing is less strong, resulting in more liquid-like structures [38]. The strong character of the complexation was well evidenced by the formation of a solid precipitate close to charge neutrality, i.e., at N:P = 1 (result not shown). In the presence of an excess of chitosan (N:P >1) or siRNA (N:P < 1), the complexes can be stabilized by unpaired segments of excess polyion forming a stabilizing shell around the particles [22].

It was noticed that the particle size distributions (PSDs) of complexes determined by DLS were dependent on the conditions of mixing of polyions, which suggests that complexes do not form equilibrium structures. As a consequence, much attention was paid to ensure the reproducible mixing conditions of COS and siRNA solutions. In addition, the COS solution was systematically added to the siRNA for N:P < 1, while the opposite mixing order was chosen for N:P > 1, so that the polyion in default was always added to that in excess. This mixing order prevents the system reaching the charge neutrality (N:P = 1) thus limiting aggregation [21, 22]. The influence of the addition rate of the titrant on the scattered intensity and PSD of complexes was studied using the COS-50 at two N:P ratios (0.5 and 10) and two siRNA concentrations (0.1 and 1 g/L). The titrant was either added in a dropwise manner (slow addition) or by a one-shot injection with the micropipette (fast addition). As shown in Figure 2.4-4.a, the fast addition always promoted the formation of complexes of smaller sizes and of lower scattered intensities compared to the slow addition. The polyelectrolyte complexation is a fast process with typical reaction times less than a millisecond [39, 40]. Thus, in the case of a slow addition, the complexation medium was not homogeneized before the complexation started. The local over-concentrations of titrant could then result in the formation of larger and probably denser complexes, as shown by the higher scattered intensity values (Figure 2.4-4.b). Conversely, a fast addition favoured the rapid homogeneization of the medium and the formation of less aggregated complexes. In this respect, the use of micromixers as those found in microfluidic chips should form complexes of the lowest achievable size [41–43].

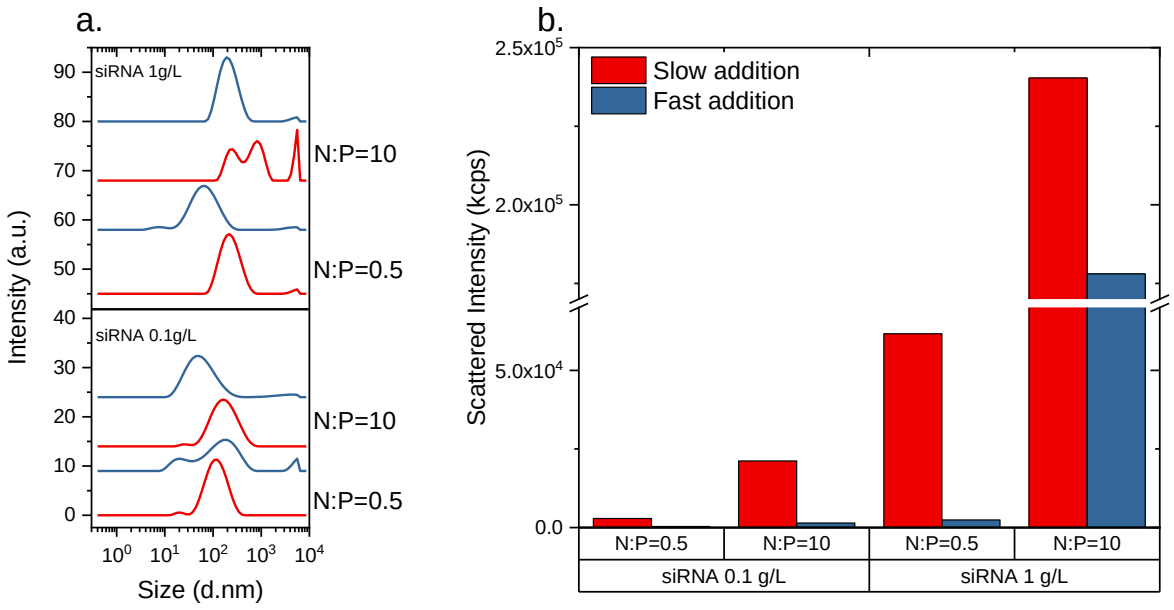

Figure 2.4-4. A dynamic light scattering (DLS) analysis of COS-50/siRNA complexes prepared by the dropwise addition (red) or one-shot injection (blue) of the component in default. The intensity-

average size distributions of complexes (a) and the corresponding scattered intensities at 173◦ detection angle (b). The complexation was studied at two siRNA concentrations (0.1 g/L and 1 g/L) in RNase-free water and two N:P ratios (0.5 and 10).

2.4.2.1. Size distribution of complexes by dynamic light scattering

The intensity-average particle size distributions (PSDs) of COS/siRNA complexes were determined for four COS and parent chitosan (90×10^3 g/mol) at various N:P ratios, from 0.5 to 20 (Figure appendix 4). The complexes were always prepared by a fast addition of the component in default. Typical examples of PSDs obtained with the COS-50/siRNA at various N:P ratios are represented in Figure 2.4-5.a together with the COS-50 and siRNA alone. For the latter, a hydrodynamic diameter of 5 nm could be determined in agreement with a previous study reporting a value of 4.2 nm for a duplex oligonucleotide of 20 base pairs [44]. The aggregates could also be detected, but they represented a negligible amount as shown by the absence of the aggregation peak in the number-average size distribution (Figure appendix 5). A similar aggregation phenomenon was observed in 10 mM MES buffer at pH 6.2 (result not shown). For the COS-50, the peak detected at 15 nm must correspond to the COS chains (Figure 2.4-5.a). Another peak was detected at 0.8 nm which was really small regarding the size of a saccharidic unit (0.51 nm) [35]. This peak was probably related to a fast diffusion mode where the motion of the polyion was coupled with the dynamics of small and much faster counterions [45]. In the presence of increasing amounts of salt, the fast mode progressively disappeared (Figure appendix 6). Notably, the fast mode was not observed with siRNA, probably because of traces of salt in the sample. Despite the filtration of COS solutions, the PSD of COS-50 also showed an aggregation peak that was not detected in the number-average size distribution (Figure appendix 5). Chitosan is known to have a strong tendency towards self-aggregation but this behaviour has been mostly documented for chitosans of relatively high MW and/or DA [46, 47]. However, a few studies have reported the formation of weak aggregates in aqueous solutions of COS of low DA [32]. Specifically, Blagodatskikh et al. showed that COS of low MW (<12 kDa) and low DA (<3%) formed aggregates of constant sizes below the pK_a of chitosan. The aggregates that can be visualized by electron microscopy are weakly bound as evidenced by their disruption under moderate shear stress [48] or in the presence of added salt (Figure appendix 6). Here, the long-range electrostatic interaction with oppositely charged siRNA polyions is also expected to result in the aggregate disruption.

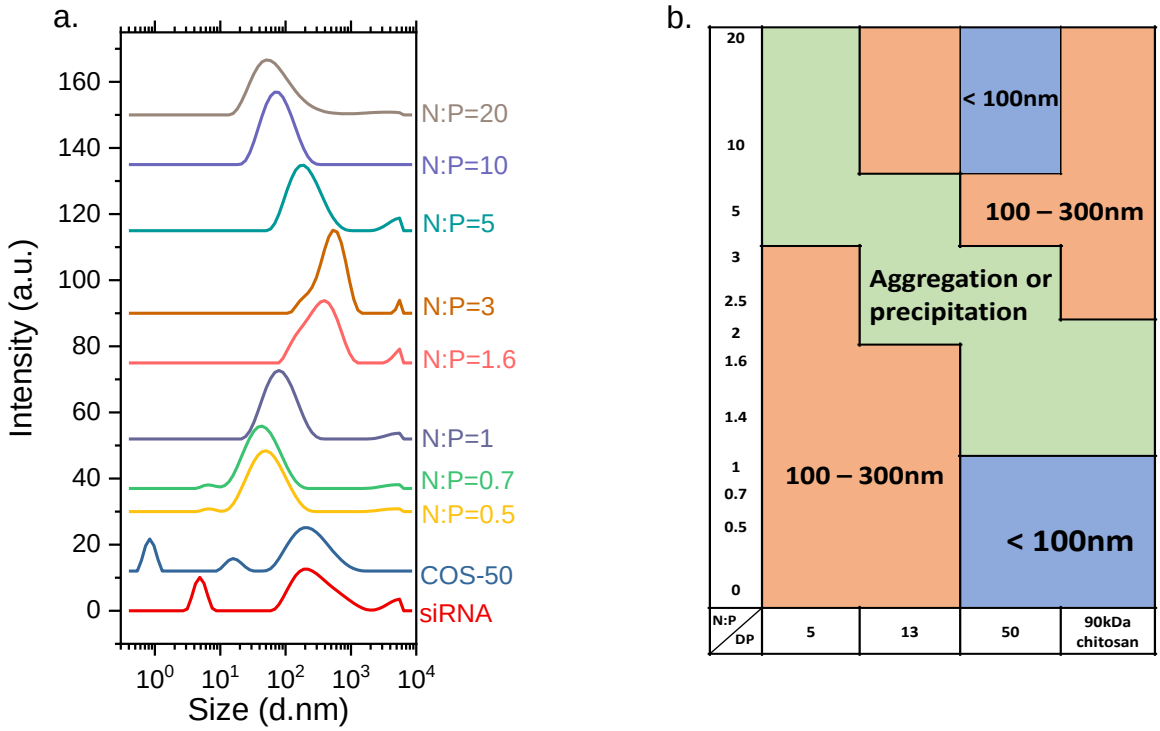

Figure 2.4-5. (a) The intensity-average particle size distributions of COS-50/siRNA complexes in RNase-free water by DLS with a 173◦ angle detection at various N:P ratios using a siRNA concentration of 0.1 g/L. (b) The particle size map representing the typical values of hydrodynamic diameter (D_H) of complexes obtained at various N:P ratios with COS varying in DP and parent chitosan (90 kDa).

The PSDs of the complexes obtained with the COS-50 at various N:P ratios can be classified into three broad categories depending on the typical particle size found (Figure 2.4-5.a). For N:P ≤ 1, small particles of the complex below 100 nm in diameter were detected. For 1 < N:P ≤ 3, the formation of some precipitates was observed highlighting the instability of the system near the charge neutrality. For N:P > 3, stable complexes of relatively small sizes were obtained. The evolution of the PSD with the N:P ratio was in agreement with a stabilization mechanism where the excess polyion, respectively the siRNA at N:P ≤ 1 and the COS-50 at N:P > 3, was located at the particle surface thereby preventing the aggregation of particles [49, 50]. In most studies, N:P ratios ranging from 4 to 30 were used regardless the molar mass and DA of chitosan, thus emphasizing the limited stabilizing capacity of chitosan [3, 14, 51, 52]. The PSDs were determined in a similar manner for COS varying in DP and parent chitosan at various N:P ratios (Figure appendix 4). The role of the COS chain length on the complex formation is twofold: (i) It impacts the strength of the ion pairing with siRNA through a cooperative effect; (ii) it determines the stability of the complexes through the formation of a stabilizing shell around particles when COS is in excess. A map illustrating the correlation between the COS chain length and the complex size is represented in Figure

2.4-5.b. For N:P ≤ 1 (excess siRNA), the size of the complex particles varied between 100 and 300 nm with COS-5 and COS-13, while smaller sizes (<100 nm) were obtained with COS-50 and the parent chitosan of 90 kDa. This can be interpreted by considering the affinity of COS with siRNA increases with the DP of COS as expected for a cooperative binding. As a result, the complexes obtained with larger COS may have a denser structure giving smaller sizes than those obtained with shorter COS. For N:P > 2, some aggregation was observed with COS-5-13, whereas the complexes formed with COS-50 and the parent chitosan were more stable, probably due to the more efficient electrosteric stabilization of long COS in excess. The most interesting system was obtained with the COS-50 at N:P 10 or N:P 20 where complexes of approximately 80 and 65 nm in diameter could be formed, respectively. The longer chitosan of 90 kDa did not form particles below 100 nm even at high N:P, which suggests that a compromise must be found regarding the optimal chain length of chitosan to achieve the stabilization of the complexes.

2.4.2.2. Efficiency of the complexation

The binding affinity of polyion to siRNA was determined by a direct titration of free siRNA in the complexation medium at various N:P ratios. This approach has been preferred to indirect methods, like the dye exclusion assay with ethidium bromide (EtBr), since the exclusion mechanism of the intercalated dye from siRNA (or DNA) is not completely known. In particular, it cannot be assumed that the dye displacement is stoichiometric with respect to the added amine groups. Nowadays, the RiboGreen RNA quantification kit is very popular to directly quantify siRNA via a calibration procedure. However, it was shown that reliable quantification of siRNA with RiboGreen could only be achieved under specific conditions of pH and ionic strength, particularly in Tris-EDTA buffer 1X at pH 8.0 where the mean fluorescence varied almost linearly with the siRNA concentration between 10 and 1000 ng/mL (Figure appendix 7). In RNase-free water, used here as complexation medium, a strong curvature of the mean fluorescence as function of the siRNA concentration was obtained (Figure appendix 7). In the acetate buffer pH 4.0, which is a suitable medium for complexation because COS are fully protonated at this pH, fluorescence was hardly detectable (Figure appendix 7). In such conditions, the toluidine blue (TB), a conventional indicator in colloidal titration [53], was investigated to directly quantify siRNA in various solvent conditions [54–56]. The TB is a positively charged dye that can interact with phosphate groups of siRNA through electrostatic interaction [57]. A depletion approach was used in which the dispersions of complexes were first incubated with an excess of TB. After centrifugation, unreacted TB was titrated by absorbance measurements in the supernatants. As shown in Figure appendix 8, a linear calibration curve of siRNA could be obtained in 0.1 M acetate buffer pH 4.0.

COS-13-16-27-50 have high affinity with siRNA, as evidenced by the Langmuir-like shape of the binding plots in Figure 2.4-6. The stoichiometry of complexation which refers to the number of formed salt bonds could be determined from the initial slope. Note that the stoichiometry of complexation differs from the composition of complexes where an excess of COS can be found for N:P > 1 (Figure 2.4-5). The initial slope is close to the unity for COS-13-16-27-50, indicating that the complexation stoichiometry is 1:1 (GlcN:phosphate) which is consistent with the full protonation of the COS at pH 4.0 (Figure 2.4-2). It confirms that the complexation is mainly of electrostatic origin, even though secondary interactions probably take place as well. Under such conditions, COS should be almost totally complexed for N:P < 1. No difference in affinity was detected with this method between COS-13-16-27-50. On the other hand, the binding of the COS-5 with siRNA is of much lower affinity as shown by the shape of the plot in Figure 2.4-6. A complexation stoichiometry of 5:1 (GlcN:phosphate) could be determined for this COS. These results are consistent with a cooperative binding mechanism of COS with siRNA, that is, the higher the DP the stronger the binding. A minimum of 13 units of COS is required here to achieve a stoichiometric complexation with siRNA. By using a larger library of COS samples, the critical DP could be determined more precisely, with the actual value probably between 5 and 13.

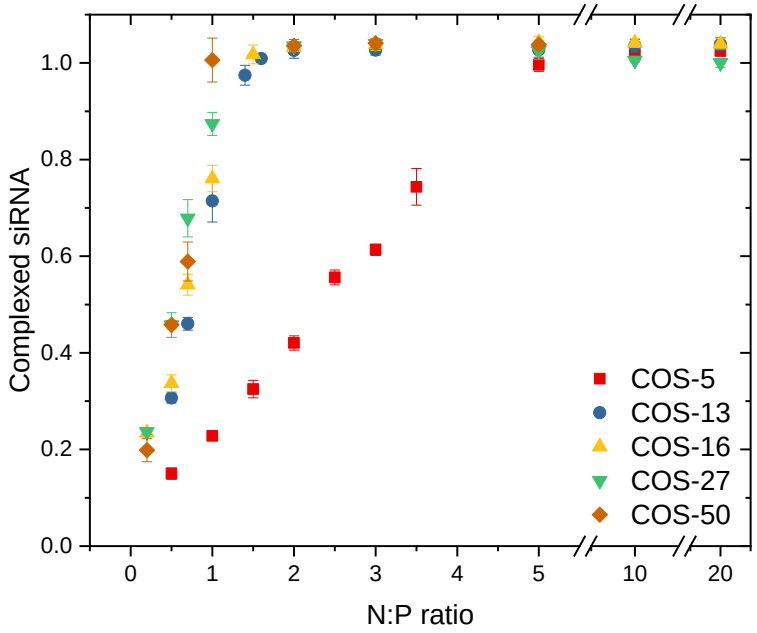

Figure 2.4-6. The fraction of complexed siRNA (ratio of the concentration of complexed siRNA to the total siRNA concentration) as function of the N:P ratio, determined by titration of free siRNA with toluidine blue in 0.1 M acetate buffer pH 4.0.

2.4.2.3. Thermodynamics of complexation

Isothermal titration calorimetry (ITC) was used to study the thermodynamics of complexation of siRNA with COS varying in DP. All experiments were performed in 10 mM acetate buffer at pH 4.5 which has a low ionization enthalpy [58] to prevent heat effects associated with proton exchange during the complexation. The experimental data represented in Figure 2.4-7 indicate that the complexation was always exothermic which is in agreement with the data of the literature [6, 59]. However, non-sigmoidal shapes of titration curves were observed with the exception of chitosan of higher molar mass. Under such conditions, the data could not be properly fitted with a single set or two sets of identical sites model. However, a close inspection of the ITC thermograms of COS of low DP reveals that the initial peaks consisted of a narrow and negative component followed by another one, broad and positive (inserts in Figure 2.4-7). The first component (exothermic) was attributed to the electrostatic ion pairing of protonated glucosamine units with phosphate groups. The different possibilities were considered for the second one (endothermic). First, the blank titration, i.e., the injection of COS in the acetate buffer was endothermic because the hydrochloride form of the COS slightly deprotonated upon dilution in the buffer at pH 4.5 (Figure appendix 9) [59]. However, this effect should be negligible as the heat of dilution was subtracted from the integrated peak area. In addition, the dilution peaks are rather narrow (Figure appendix 9) compared to the broad endothermic peaks observed in Figure 2.4-7. Second, the pK_a of chitosan is expected to increase upon complexation with siRNA for the same reason that the pK_a increases with α (Figure 2.4-1.a) [60]. However, this effect should give negative peaks as the protonation of chitosan is exothermic [59]. In addition, since COS were almost completely protonated in the acetate buffer, such effects must be negligible. Third, the broad shape of the endothermic peaks could be the signature of an aggregation process through hydrophobic interaction for which the unfavorable enthalpy arises from the energy associated with the disruption of structured water molecules. Due to its position away from stoichiometry, the aggregation peak differs from the coacervation or precipitation peak that can be observed for synthetic polyelectrolyte systems at neutrality [23, 61, 62]. It also differs from the so-called condensation peak (endothermic) attributed to the collapse of DNA chains after neutralization of phosphate groups by cationic ligands [63, 64]. Here, the aggregation was stronger for smaller COS as seen by the more pronounced V shape on the thermograms of COS 13 and COS 16. It suggests that the complexes obtained from shorter COS were not stable at low N:P which is in agreement with previous observations by DLS (Figure 2.4-5.b). In addition, the fact that the COS solution was slowly added to the siRNA in the ITC cell must also favor the aggregation of the complexes as discussed previously (Figure 2.4-4). For the chitosan of 90 kDa, for which no aggregation was observed at N:P < 1 (Figure 2.4-5.b), the titration curve

exhibited a sigmoid shape as typically found for high molar mass chitosans [3, 59]. For the COS-5, the injection peaks were barely detected but the V shape was detected at the beginning of the titration, thus indicating that complexation occurred with a concomitant aggregation process (Figure 2.4-7).

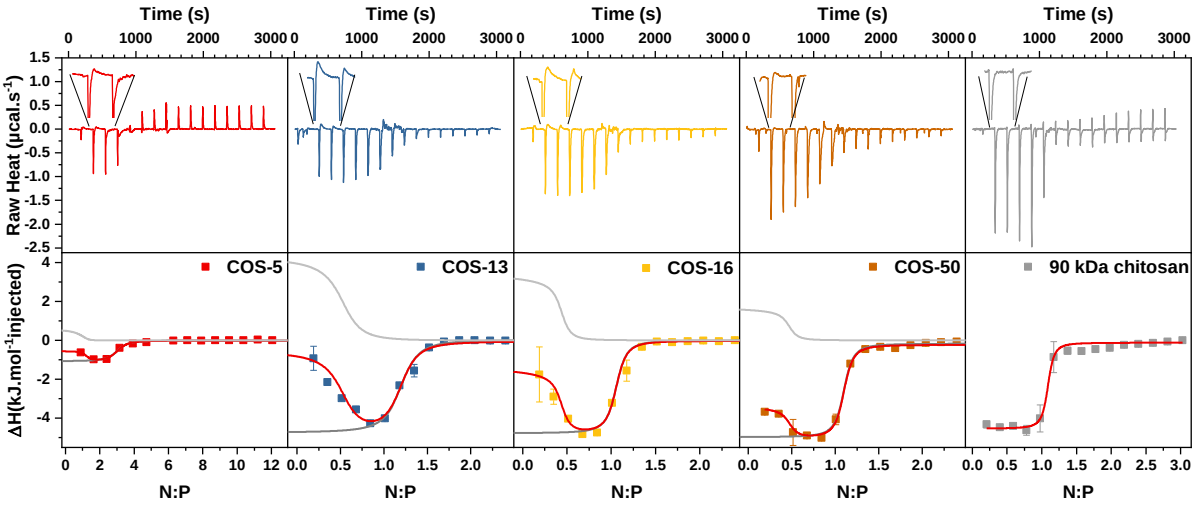

Figure 2.4-7. (Upper panel) The heat flow per injection versus time for the isothermal titration of siRNA (0.7 mM) by COS varying in DP (10 mM). The first injection peaks are magnified to illustrate the presence of an endothermic component superimposed on the main exothermic one. (Lower panel) The integrated heats of binding versus the N:P ratio. The continuous red lines represent the overall fit to the experimental data. The dark grey and light grey lines represent the ion-pairing and the aggregation contributions to the overall process, respectively. All titrations were performed at 25 °C in 10 mM acetate buffer at pH 4.5.

The thermograms were analyzed using a modified version of the multiple non-interacting sites (MNIS) model. This model has been applied previously to the two-step complexation of a polyelectrolyte system in which small particles of the complex formed before reorganizing into a dense coacervate phase at neutrality [23]. For COS 5-13-16-50, ITC data were adjusted with the MNIS model by considering two independent contributions, the exothermic electrostatic ion pairing that can be observed throughout the titration, and superimposed by an endothermic aggregation step detected only at low N:P. Both contributions rely on a set of independent adjustable parameters, including the binding constant (K_b), the enthalpy change per mole of injectant (ΔH) and the reaction stoichiometry (n) (see Supporting Information). The binding constant allows the determination of the free energy change, $\Delta G = -RT \ln(K_b)$ and the entropic contribution, $T\Delta S = \Delta H - \Delta G$. For the parent chitosan, only the exothermic ion pairing was considered since no aggregation could be detected at the beginning of the titration. The thermodynamic parameters obtained through this procedure are presented in

Table 2.4.3. The ion pairing was exothermic as expected for a strongly interacting system giving a solid precipitate at neutrality in contrast to more weakly interacting systems like coacervates. These were often found to be endothermic in relation with their highly hydrated state that opposes ion pairing [38, 61, 65]. The enthalpy change associated with the ion pairing (ΔH) showed a marked increase (in absolute value) from COS-5 to COS-13 and then remained constant for longer COS. Similarly, the stoichiometry decreased from 3 to 1 and remained constant for higher DPs. The entropic contribution associated with the ion pairing ($T\Delta S$) was systematically higher than ΔH and regularly increased with DP. Consequently, the binding constant (K_b) also increased with DP. The entropy change related to the ion pairing could be considered as the sum of the unfavorable entropy change caused by the fixation of the polymer chains (ΔS_p) and the favourable entropy changes related both to the release of counter-ions ($\Delta S_i > 0$) and the hydrophobic interactions ($\Delta S_h > 0$) [66]. Further, ΔS_p should decrease with the DP because of the less significant loss of configurational entropy when the chain length increased. Whereas, ΔS_h which was related to the release of structured water molecules upon hydrophobic interactions of the complexed segments, should increase with the DP. As such, the hydrophobic interactions represent another level of cooperativity [66]. However, ΔS_i could be considered the main component of the entropy change due to the high degree of charging of COS and siRNA at pH 4.5. It can be, however, assumed that ΔS_i is independent of the chain length. Thus, the observed increase in total entropy change with DP was mainly due to the decrease of ΔS_p and the increase of ΔS_h.

Table 2.4.3. Thermodynamic parameters of the siRNA/COS complexation evaluated by isothermal titration calorimetry (ITC) at T = 298 K with a multiple non-interacting sites (MNIS) model by considering two contributions, the ion pairing throughout the titration and the aggregation at initial N:P ratios. Note that the aggregation step was observed with COS 5-13-16-50 but not with the parent chitosan of 90 kDa. ΔH ($kJ \cdot mol^{-1}$), $T\Delta S$ ($kJ \cdot mol^{-1}$), ΔG ($kJ \cdot mol^{-1}$), K_b ($L \cdot mol^{-1}$) and n denote the enthalpy change, the entropic contribution to the free energy, the free energy change, the binding constant and reaction stoichiometry (the mole refers to monomer units of COS).

	Ion pairing					**Aggregation**			
	ΔH	$T\Delta S$	ΔG	K_b	n	ΔH	$T\Delta S$	ΔG	K_b
COS-5	-1.1	23.5	-24.5	2.0×10^4	3.0	0.7	28.8	-28.1	8.5×10^4
COS-13	-5.1	24	-29.1	1.3×10^5	1.1	4.4	32.7	-28.4	9.4×10^4
COS-16	-4.8	24.9	-29.7	1.6×10^5	1.0	3.4	34.4	-30.9	2.6×10^5
COS-50	-5.2	26.8	-31.9	4.0×10^5	1.0	1.9	32.8	-30.9	2.6×10^5
Parent chitosan	-4.3	29.8	-34	9.6×10^5	1.0				

Regarding the secondary process at play, the values of enthalpy change are good indicators of the propensity of aggregation obtained during the initial stages of the titration. Accordingly, the aggregation was maximal with COS-13 and COS-16 and minimal for COS-5 and COS-50 (Table 2.4.3). The differences in the aggregation level can be explained from arguments based on the respective chain lengths and flexibilities of siRNA and COS. Considering that the siRNA is a rigid rod of 8 nm long [4], the COS-13 and COS-16 with a contour length of 6.5 nm and 8 nm and higher flexibility than siRNA as shown by their respective persistence length [67, 68], can achieve an almost complete ion pairing with siRNA leading to quasi-neutral complexes without enough unpaired phosphate groups to stabilize the particles [22]. In contrast, by increasing the DP of COS to 50 and above, COS chains could bind to several siRNA chains, increasing the probability of having multiple unpaired phosphate groups that can participate in the colloidal stabilization at N:P < 1. For the COS-5, its lower affinity with siRNA must lead to incomplete ion pairing at low N:P and thus less aggregation.

2.5. Discussion

The interaction between complementary macromolecules, as oppositely charged polyelectrolytes (PEs), is a cooperative process, often explained as an entropy effect—when one of the active sites interacts with a complementary one, the neighboring sites have a more favorable entropy of binding resulting from the reduced loss of configurational entropy. Therefore, the reaction of complexation proceeds according to a zipping mechanism [66, 69, 70]. The stable complexes can be formed when the free energy change of the complexation exceeds the kinetic energies of the starting polymers [69]. For a cooperative process, the binding constant (K_b) is defined as: $K_b = K_n^1$ where K_1 is the complexation constant of a monomer unit and n is the DP of the oligomer. It follows that K_b must depend strongly on the length of the oligomer [69, 71]. Specifically, it has shown that the dependence of complex stability on the chain length of PE has a threshold character, that is, the complexation equilibrium is displaced abruptly towards the formation of the complexes when a certain critical DP is reached [69, 71]. The experimental K_b values obtained for the ion pairing step did not completely support this prediction as K_b linearly increased with the DP rather than exponentially (Figure appendix 10). This may suggest that the complexation process was not fully cooperative within the definition given above, i.e., multiple ionic pairing reactions, each characterized by its own equilibrium constant. The reason could be that the interaction between COS and siRNA was very strong, as shown by the exothermicity of the ion pairing. Therefore, the complexation reaction was likely under kinetic rather than thermodynamic control. However, the existence of a critical DP could be still evidenced in the binding

isotherm where a dramatic increase in chitosan affinity for siRNA was observed when the DP increased from 5 to 13 (Figure 2.4-6). Also, the enthalpy of the ion pairing which is directly equal to the difference in Coulomb energy before and after complexation strongly increased (in absolute value) in the same range of DP (Table 2.4.3). These results agree with the work of Strand et al. where authors showed that a minimum of 6–9 protonated chitosan units were needed to provide interaction strength with DNA comparable to that of chitosan polymer [15]. It can be thus assumed that DNA and siRNA exhibit similar complexation behavior with chitosan. Interestingly, similar critical DPs have been reported for various polyelectrolyte systems: For peptides, a sequence of 6–8 cationic amino acids was required to allow strong binding with siRNA [72]; for synthetic polyelectrolytes, critical DPs between 4 and 6 were found for the system oligoethyleneimine-poly(methacrylic acid) depending on the hydrophobicity of oligoethyleneimine [73]; a critical DP of 7 was found for the complexation of poly(dimethylaminoethyl methacrylate) with oligophosphates [74].

The effect of the COS chain length on binding properties with siRNA must correlate with the solution properties of the COS alone since the variation of the pK_a with the DP showed the existence of a similar critical DP of approximately 10 (Figure 2.4-1 and Table 2.4.2). Therefore, the chain length influences the electrostatic properties of COS in a similar way at the intermolecular level (binding with siRNA) and intramolecular level (pK_a). The dependence of the electrostatic properties of COS to the DP can be evaluated through the Debye screening length (λ_D) which defines the characteristic range of electrostatic interaction in solution. In the conditions of ionic strength used, the Debye length was estimated to $\lambda_D \sim 3.5$ nm, which corresponds to the size of a COS segment of 7 units regularly aligned. The assumption of a rod-like conformation is compatible with the persistence length of 5 nm for chitosan [68]. Thus, the intensity of intramolecular electrostatic repulsions between neighboring charges increased between DP 1 and DP 7 resulting in a significant decrease in pK_a in this range of DP. Similarly, the complexation of a COS segment of 7 units with siRNA or other polyanions must considerably reduce the Coulomb energy of the system as shown by the significant decrease in the enthalpy change associated with the ion pairing step between COS 5 and COS 13 (Table 2.4.3). No significant difference in enthalpy change per mole of COS unit was detected for larger DPs, although the binding constant increased continuously with the DP, but mainly for entropy reasons as described previously. A good way to verify the dependence of the critical DP on the Debye length would be to add salt to decrease λ_D and see if the critical DP increases. These experiments have not been performed here. However, a similar situation can be found in the case of H-bonding complexes where the critical DP is approximately 40 as hydrogen bonds are weaker than electrostatic interactions [75]. Finally, while the requirement of having COS chains containing approximately 10 units to form stable complexes is important at the molecular level, however, this is not sufficient to achieve the

colloidal stability of the complexes in solution. Specifically, it was shown that only COS of DP 50 or higher and used in excess (N:P > 5) formed small and stable colloidal complexes (Figure 2.4-5). Under such conditions, the particles are stabilized by a shell of COS chains with sufficient unpaired protonated glucosamine groups that provide electrosteric stabilization.

2.6. Conclusion

In this work, the electrostatic complexation of N-deacetylated chitosan oligosaccharides (COS) with siRNAs was studied under conditions of full protonation of COS and correlated with the properties of COS in solution. The behavior of COS, alone or in the presence of siRNA, is governed by the length of the chain. This has been varied here between DP5 and DP50. In particular, it was shown that, on the one hand, the binding affinity of COS for siRNA increased sharply between DP5 and DP13 and that, on the other hand, the pK_a of COS decreased just as abruptly between the same DP values. This highlights the existence of a critical DP from which the electrostatic interactions become particularly high, resulting in both significant repulsions between neighboring charge residues on COS chains and strong attraction with polymers of opposite charge like siRNA. Similar critical values of DP have been reported in the context of polyelectrolyte complexation which suggests that this behavior is universal. With regard to the colloidal properties of the complexes, and beyond the efficiency of the complexation, a rather high DP (~50) is necessary to provide a good stability to the complex particles through an electrosteric mechanism. These findings could apply in the context of gene delivery where both in vivo complex stability and the complex dissociation at targeted sites are needed. However, the limited solubility of N-deacetylated chitosan at pH 7.4, even for low DPs, remains for the moment a major difficulty in biological applications. New approaches to address this issue without altering the structure of chitosan are still relevant.

2.7. References

[1] Zargar V, Asghari M, Dashti A (2015) A Review on Chitin and Chitosan Polymers: Structure, Chemistry, Solubility, Derivatives, and Applications. ChemBioEng Rev 2:204–226 . https://doi.org/10.1002/cben.201400025

[2] Shariatinia Z (2019) Pharmaceutical applications of chitosan. Adv Colloid Interface Sci 263:131–194 . https://doi.org/10.1016/j.cis.2018.11.008

[3] Holzerny P, Ajdini B, Heusermann W, Bruno K, Schuleit M, Meinel L, Keller M (2012) Biophysical properties of chitosan/siRNA polyplexes: Profiling the

polymer/siRNA interactions and bioactivity. J Control Release 157:297–304 . https://doi.org/10.1016/j.jconrel.2011.08.023

[4] Ragelle H, Riva R, Vandermeulen G, Naeye B, Pourcelle V, Le Duff CS, D'Haese C, Nysten B, Braeckmans K, De Smedt SC, Jérôme C, Préat V (2014) Chitosan nanoparticles for siRNA delivery: Optimizing formulation to increase stability and efficiency. J Control Release 176:54–63 . https://doi.org/10.1016/j.jconrel.2013.12.026

[5] Vauthier C, Zandanel C, Ramon AL (2013) Chitosan-based nanoparticles for in vivo delivery of interfering agents including siRNA. Curr Opin Colloid Interface Sci 18:406–418 . https://doi.org/10.1016/j.cocis.2013.06.005

[6] Buschmann MD, Merzouki A, Lavertu M, Thibault M, Jean M, Darras V (2013) Chitosans for delivery of nucleic acids. Adv Drug Deliv Rev 65:1234–1270 . https://doi.org/10.1016/j.addr.2013.07.005

[7] Lavertu M, Méthot S, Tran-Khanh N, Buschmann MD (2006) High efficiency gene transfer using chitosan/DNA nanoparticles with specific combinations of molecular weight and degree of deacetylation. Biomaterials 27:4815–4824 . https://doi.org/10.1016/j.biomaterials.2006.04.029

[8] Esmaeilzadeh Gharehdaghi E, Amani A, Khoshayand MR, Banan M, Esmaeilzadeh Gharehdaghi E, Amini MA, Faramarzi MA (2014) Chitosan Nanoparticles for siRNA Delivery: Optimization of Processing/Formulation Parameters. Nucleic Acid Ther 24:420–427 . https://doi.org/10.1089/nat.2014.0484

[9] Sorlier P, Denuzière A, Viton C, Domard A (2001) Relation between the degree of acetylation and the electrostatic properties of chitin and chitosan. Biomacromolecules 2:765–772 . https://doi.org/10.1021/bm015531+

[10] Huang M, Fong C-W, Khor E, Lim L-Y (2005) Transfection efficiency of chitosan vectors: Effect of polymer molecular weight and degree of deacetylation. J Control Release 106:391–406 . https://doi.org/10.1016/j.jconrel.2005.05.004

[11] Liu X, Howard KA, Dong M, Andersen MØ, Rahbek UL, Johnsen MG, Hansen OC, Besenbacher F, Kjems J (2007) The influence of polymeric properties on chitosan/siRNA nanoparticle formulation and gene silencing. Biomaterials 28:1280–1288 . https://doi.org/10.1016/j.biomaterials.2006.11.004

[12] Malmo J, Sørgård H, Vårum KM, Strand SP (2012) SiRNA delivery with chitosan nanoparticles: Molecular properties favoring efficient gene silencing. J Control Release 158:261–268 . https://doi.org/10.1016/j.jconrel.2011.11.012

[13] Shi Q, Fernandes J, Winnik F, Benderdour M, Zhang, Qiu, Dai (2012) Low molecular weight chitosan conjugated with folate for siRNA delivery in vitro: optimization studies. Int J Nanomedicine 7:5833 . https://doi.org/10.2147/IJN.S35567

[14] Alameh M, Lavertu M, Tran-Khanh N, Chang C-Y, Lesage F, Bail M, Darras V, Chevrier A, Buschmann MD (2018) siRNA Delivery with Chitosan: Influence of Chitosan Molecular Weight, Degree of Deacetylation, and Amine to Phosphate Ratio on in Vitro Silencing Efficiency, Hemocompatibility, Biodistribution, and in Vivo Efficacy. Biomacromolecules 19:112–131 . https://doi.org/10.1021/acs.biomac.7b01297

[15] Strand SP, Danielsen S, Christensen BE, Vårum KM (2005) Influence of Chitosan Structure on the Formation and Stability of DNA−Chitosan Polyelectrolyte Complexes. Biomacromolecules 6:3357–3366 . https://doi.org/10.1021/bm0503726

[16] Allan GG, Peyron M (1995) Molecular weight manipulation of chitosan I: kinetics of depolymerization by nitrous acid. Carbohydr Res 277:257–272 . https://doi.org/10.1016/0008-6215(95)00207-A

[17] Allan GG, Peyron M (1995) Molecular weight manipulation of chitosan II: prediction and control of extent of depolymerization by nitrous acid. Carbohydr Res 277:273–282 . https://doi.org/10.1016/0008-6215(95)00208-B

[18] Fulmer GR, Miller AJM, Sherden NH, Gottlieb HE, Nudelman A, Stoltz BM, Bercaw JE, Goldberg KI (2010) NMR Chemical Shifts of Trace Impurities: Common Laboratory Solvents, Organics, and Gases in Deuterated Solvents Relevant to the Organometallic Chemist. Organometallics 29:2176–2179 . https://doi.org/10.1021/om100106e

[19] Tømmeraas K, Vårum KM, Christensen BE, Smidsrød O (2001) Preparation and characterisation of oligosaccharides produced by nitrous acid depolymerisation of chitosans. Carbohydr Res 333:137–144 . https://doi.org/10.1016/S0008-6215(01)00130-6

[20] Salim E, Ailincai D, Trombotto S (2014) Chitooligosaccharide-2,5-anhydro-D-mannonic Acid. Molbank 2014:M832 . https://doi.org/10.3390/M832

[21] Müller M, Keßler B, Fröhlich J, Poeschla S, Torger B (2011) Polyelectrolyte Complex Nanoparticles of Poly(ethyleneimine) and Poly(acrylic acid): Preparation and Applications. Polymers (Basel) 3:762–778 . https://doi.org/10.3390/polym3020762

[22] Schatz C, Domard A, Viton C, Pichot C, Delair T (2004) Versatile and efficient formation of colloids of biopolymer-based polyelectrolyte complexes. Biomacromolecules 5:1882–1892 . https://doi.org/10.1021/bm049786+

[23] Vitorazi L, Ould-Moussa N, Sekar S, Fresnais J, Loh W, Chapel J-P, Berret J-F (2014) Evidence of a two-step process and pathway dependency in the thermodynamics of poly(diallyldimethylammonium chloride)/poly(sodium acrylate) complexation. Soft Matter 10:9496–9505 . https://doi.org/10.1039/C4SM01461H

[24] Bezrodnykh EA, Blagodatskikh I V., Kulikov SN, Zelenikhin P V., Yamskov IA, Tikhonov VE (2018) Consequences of chitosan decomposition by nitrous acid: Approach to non-branched oligochitosan oxime. Carbohydr Polym 195:551–557 . https://doi.org/10.1016/j.carbpol.2018.05.007

[25] Katchalsky A, Shavit N, Eisenberg H (1954) Dissociation of weak polymeric acids and bases. J Polym Sci 13:69–84 . https://doi.org/10.1002/pol.1954.120136806

[26] Tsukada S, Inoue Y (1981) Conformational properties of chito-oligosaccharides: titration, optical rotation, and carbon-13 N.M.R. studies of chito-oligosaccharides. Carbohydr Res 88:19–38 . https://doi.org/10.1016/S0008-6215(00)84598-X

[27] Zentz F, Bédouet L, Almeida MJ, Milet C, Lopez E, Giraud M (2001) Characterization and Quantification of Chitosan Extracted from Nacre of the Abalone Haliotis tuberculata and the Oyster Pinctada maxima. Mar Biotechnol 3:36–44 . https://doi.org/10.1007/s101260000042

[28] Filion D, Lavertu M, Buschmann MD (2007) Ionization and Solubility of Chitosan Solutions Related to Thermosensitive Chitosan/Glycerol-Phosphate Systems. Biomacromolecules 8:3224–3234 . https://doi.org/10.1021/bm700520m

[29] Domard A (1987) pH and c.d. measurements on a fully deacetylated chitosan: application to CuII—polymer interactions. Int J Biol Macromol 9:98–104 . https://doi.org/10.1016/0141-8130(87)90033-X

[30] Domard A, Gey C, Taravel F (1991) Glucosamine oligomers: 2. N.m.r. studies on a DP3. Int J Biol Macromol 13:105–109 . https://doi.org/10.1016/0141-8130(91)90057-2

[31] Kodama H, Miyajima T, Mori M, Takahashi M, Nishimura H, Ishiguro S (1997) A unified analytical treatment of the acid-dissociation equilibria of weakly acidic linear polyelectrolytes and the conjugate acids of weakly basic linear polyelectrolytes. Colloid Polym Sci 275:938–945 . https://doi.org/10.1007/s003960050169

[32] Kulikov S, Tikhonov V, Blagodatskikh I, Bezrodnykh E, Lopatin S, Khairullin R, Philippova Y, Abramchuk S (2012) Molecular weight and pH aspects of the efficacy of oligochitosan against methicillin-resistant Staphylococcus aureus (MRSA). Carbohydr Polym 87:545–550 . https://doi.org/10.1016/j.carbpol.2011.08.017

[33] Katchalsky A, Spitnik P (1947) Potentiometric titrations of polymethacrylic acid. J Polym Sci 2:487–487 . https://doi.org/10.1002/pol.1947.120020504

[34] Tsuchida E, Osada Y, Abe K (1974) Formation of polyion complexes between polycarboxylic acids and polycations carrying charges in the chain backbone. Die Makromol Chemie 175:583–592 . https://doi.org/10.1002/macp.1974.021750219

[35] Rinaudo M, Milas M, Dung P Le (1993) Characterization of chitosan. Influence of ionic strength and degree of acetylation on chain expansion. Int J Biol Macromol 15:281–285 . https://doi.org/10.1016/0141-8130(93)90027-J

[36] QIN C, LI H, XIAO Q, LIU Y, ZHU J, DU Y (2006) Water-solubility of chitosan and its antimicrobial activity. Carbohydr Polym 63:367–374 . https://doi.org/10.1016/j.carbpol.2005.09.023

[37] Vårum KM, Ottøy MH, Smidsrød O (1994) Water-solubility of partially N-acetylated chitosans as a function of pH: effect of chemical composition and depolymerisation. Carbohydr Polym 25:65–70 . https://doi.org/10.1016/0144-8617(94)90140-6

[38] Liu X, Chapel J-P, Schatz C (2017) Structure, thermodynamic and kinetic signatures of a synthetic polyelectrolyte coacervating system. Adv Colloid Interface Sci 239:178–186 . https://doi.org/10.1016/j.cis.2016.10.004

[39] Bakeev KN, Izumrudov VA, Kuchanov SI, Zezin AB, Kabanov VA (1992) Kinetics and mechanism of interpolyelectrolyte exchange and addition reactions. Macromolecules 25:4249–4254 . https://doi.org/10.1021/ma00043a003

[40] Kabanov VA (1994) Basic Properties of Soluble Interpolyelectrolyte Complexes Applied to Bioengineering and Cell Transformations. In: Macromolecular Complexes in Chemistry and Biology. Springer Berlin Heidelberg, Berlin, Heidelberg, pp 151–174

[41] Majedi FS, Hasani-Sadrabadi MM, Hojjati Emami S, Shokrgozar MA, VanDersarl JJ,

Dashtimoghadam E, Bertsch A, Renaud P (2013) Microfluidic assisted self-assembly of chitosan based nanoparticles as drug delivery agents. Lab Chip 13:204–207 . https://doi.org/10.1039/C2LC41045A

[42] Debus H, Beck-Broichsitter M, Kissel T (2012) Optimized preparation of pDNA/poly(ethylene imine) polyplexes using a microfluidic system. Lab Chip 12:2498 . https://doi.org/10.1039/c2lc40176b

[43] Iliescu C, Tresset G (2015) Microfluidics-Driven Strategy for Size-Controlled DNA Compaction by Slow Diffusion through Water Stream. Chem Mater 27:8193–8197 . https://doi.org/10.1021/acs.chemmater.5b04129

[44] Eimer W, Pecora R (1991) Rotational and translational diffusion of short rodlike molecules in solution: Oligonucleotides. J Chem Phys 94:2324–2329 . https://doi.org/10.1063/1.459904

[45] Sedlák M (1999) What Can Be Seen by Static and Dynamic Light Scattering in Polyelectrolyte Solutions and Mixtures? †. Langmuir 15:4045–4051 . https://doi.org/10.1021/la981189j

[46] Philippova OE, Volkov E V., Sitnikova NL, Khokhlov AR, Desbrieres J, Rinaudo M (2001) Two Types of Hydrophobic Aggregates in Aqueous Solutions of Chitosan and Its Hydrophobic Derivative. Biomacromolecules 2:483–490 . https://doi.org/10.1021/bm005649a

[47] Korchagina E V., Philippova OE (2010) Multichain Aggregates in Dilute Solutions of Associating Polyelectrolyte Keeping a Constant Size at the Increase in the Chain Length of Individual Macromolecules. Biomacromolecules 11:3457–3466 . https://doi.org/10.1021/bm100990u

[48] Blagodatskikh I V, Bezrodnykh EA, Abramchuk SS, Muranov A V, Sinitsyna O V, Khokhlov AR, Tikhonov VE (2013) Short chain chitosan solutions: self-assembly and aggregates disruption effects. J Polym Res 20: . https://doi.org/10.1007/s10965-013-0073-0

[49] Mende M, Schwarz S, Zschoche S, Petzold G, Janke A (2011) Influence of the Hydrophobicity of Polyelectrolytes on Polyelectrolyte Complex Formation and Complex Particle Structure and Shape. Polymers (Basel) 3:1363–1376 . https://doi.org/10.3390/polym3031363

[50] Cousin F, Gummel J, Ung D, Boué F (2005) Polyelectrolyte−Protein Complexes: Structure and Conformation of Each Specie Revealed by SANS. Langmuir 21:9675–9688 . https://doi.org/10.1021/la0510174

[51] Alatorre-Meda M, Taboada P, Hartl F, Wagner T, Freis M, Rodríguez JR (2011) The influence of chitosan valence on the complexation and transfection of DNA: The weaker the DNA–chitosan binding the higher the transfection efficiency. Colloids Surfaces B Biointerfaces 82:54–62 . https://doi.org/10.1016/j.colsurfb.2010.08.013

[52] Richards Grayson AC, Doody AM, Putnam D (2006) Biophysical and Structural Characterization of Polyethylenimine-Mediated siRNA Delivery in Vitro. Pharm Res 23:1868–1876 . https://doi.org/10.1007/s11095-006-9009-2

[53] Terayama H (1952) Method of colloid titration (a new titration between polymer ions). J Polym Sci 8:243–253 . https://doi.org/10.1002/pol.1952.120080209

[54] Schatz C, Lucas J-M, Viton C, Domard A, Pichot C, Delair T (2004) Formation and Properties of Positively Charged Colloids Based on Polyelectrolyte Complexes of Biopolymers. Langmuir 20:7766–7778 . https://doi.org/10.1021/la049460m

[55] Drogoz A, David L, Rochas C, Domard A, Delair T (2007) Polyelectrolyte Complexes from Polysaccharides: Formation and Stoichiometry Monitoring. Langmuir 23:10950–10958 . https://doi.org/10.1021/la7008545

[56] Vleugels LFW, Ricois S, Voets IK, Tuinier R (2017) Reversal of metachromasy revisited; displacement of Toluidine-blue from alginate by surfactants. Colloids Surfaces A Physicochem Eng Asp 529:454–461 . https://doi.org/10.1016/j.colsurfa.2017.06.027

[57] Sato S, Matsumoto S, Freivalds T, Erenpreisa J (2010) Consideration on the Metachromatic Spectra of Toluidine Blue Dimers Formed on DNA Oligomers. Bull Chem Soc Jpn 83:1216–1222 . https://doi.org/10.1246/bcsj.20100032

[58] Fukada H, Takahashi K (1998) Enthalpy and heat capacity changes for the proton dissociation of various buffer components in 0.1 M potassium chloride. Proteins Struct Funct Genet 33:159–166 . https://doi.org/10.1002/(SICI)1097-0134(19981101)33:2<159::AID-PROT2>3.0.CO;2-E

[59] Ma PL, Lavertu M, Winnik FM, Buschmann MD (2009) New Insights into Chitosan−DNA Interactions Using Isothermal Titration Microcalorimetry. Biomacromolecules 10:1490–1499 . https://doi.org/10.1021/bm900097s

[60] Petrov AI, Antipov AA, Sukhorukov GB (2003) Base−Acid Equilibria in Polyelectrolyte Systems: From Weak Polyelectrolytes to Interpolyelectrolyte Complexes and Multilayered Polyelectrolyte Shells. Macromolecules 36:10079–10086 . https://doi.org/10.1021/ma034516p

[61] Priftis D, Megley K, Laugel N, Tirrell M (2013) Complex coacervation of poly(ethylene-imine)/polypeptide aqueous solutions: Thermodynamic and rheological characterization. J Colloid Interface Sci 398:39–50 . https://doi.org/10.1016/j.jcis.2013.01.055

[62] Feng X, Leduc M, Pelton R (2008) Polyelectrolyte complex characterization with isothermal titration calorimetry and colloid titration. Colloids Surfaces A Physicochem Eng Asp 317:535–542 . https://doi.org/10.1016/j.colsurfa.2007.11.053

[63] Kim W, Yamasaki Y, Kataoka K (2006) Development of a Fitting Model Suitable for the Isothermal Titration Calorimetric Curve of DNA with Cationic Ligands. J Phys Chem B 110:10919–10925 . https://doi.org/10.1021/jp057554e

[64] Utsuno K, Uludağ H (2010) Thermodynamics of Polyethylenimine-DNA Binding and DNA Condensation. Biophys J 99:201–207 . https://doi.org/10.1016/j.bpj.2010.04.016

[65] Alonso T, Irigoyen J, Iturri JJ, Larena IL, Moya SE (2013) Study of the multilayer assembly and complex formation of poly(diallyldimethylammonium chloride) (PDADMAC) and poly(acrylic acid) (PAA) as a function of pH. Soft Matter 9:1920–1928 . https://doi.org/10.1039/C2SM26884A

[66] Kabanov VA, Papisov IM (1979) Formation of complexes between complementary synthetic polymers and oligomers in dilute solution review. Polym Sci USSR 21:261–307 . https://doi.org/10.1016/0032-3950(79)90245-4

[67] Pärnaste L, Arukuusk P, Langel K, Tenson T, Langel Ü (2017) The Formation of Nanoparticles between Small Interfering RNA and Amphipathic Cell-Penetrating Peptides. Mol Ther - Nucleic Acids 7:1–10 . https://doi.org/10.1016/j.omtn.2017.02.003

[68] Schatz C, Viton C, Delair T, Pichot C, Domard A (2003) Typical Physicochemical Behaviors of Chitosan in Aqueous Solution. Biomacromolecules 4:641–648 . https://doi.org/10.1021/bm025724c

[69] Tsuchida E, Abe K (1982) Interactions between macromolecules in solution and intermacromolecular complexes. In: Tsuchida E, Abe K (eds) Interactions Between Macromolecules in Solution and Intermacromolecular Complexes. Springer-Verlag, Berlin/Heidelberg, pp 1–119

[70] KABANOV VA (1973) THE COOPERATIVE INTERACTIONS OF COMPLEMENTARY SYNTHETIC MACROMOLECULES IN SOLUTIONS. In: Macromolecular Chemistry–8. Elsevier, pp 121–145

[71] Papisov IM, Litmanovich AA (1977) Specificity of cooperative interactions between simple synthetic macromolecules and its connection with chain length. Polym Sci USSR 19:830–837 . https://doi.org/10.1016/0032-3950(77)90236-2

[72] Plank C, Tang MX, Wolfe AR, Szoka FC (1999) Branched Cationic Peptides for Gene Delivery: Role of Type and Number of Cationic Residues in Formation and in Vitro Activity of DNA Polyplexes. Hum Gene Ther 10:319–332 . https://doi.org/10.1089/10430349950019101

[73] Tsuchida E, Osada Y (1974) The rôle of the chain length in the stability of polyion complexes. Die Makromol Chemie 601:593–601 . https://doi.org/10.1002/macp.1974.021750220

[74] Kharenko AV, Starikova YA, Lutsenko VV, Zezin AB (1976) Study of cooperative reactions of oligo- and polyphosphates with polybases. Polym Sci USSR 18:1837–1843 . https://doi.org/10.1016/0032-3950(76)90316-6

[75] Ikawa T, Abe K, Honda K, Tsuchida E (1975) Interpolymer complex between poly(ethylene oxide) and poly(carboxylic acid). J Polym Sci Polym Chem Ed 13:1505–1514 . https://doi.org/10.1002/pol.1975.170130703

Chapter 3: Interaction of metallic ions with small interfering RNA at molecular and colloidal level

3.1. Introduction

Today, the design of non-viral gene vectors is a very active area of research, particularly in the context of siRNA delivery. It has recently been proposed to make use of metal ions in the formulation of polymer-based systems to improve the affinity between the polymers and the nucleic acids, the stability of the vectors as well as the transfection efficacy.[1–8] However, the effect of these ions on the siRNA structure, morphology and cytotoxicity is not yet well documented. In fact, the interaction of metallic ions with DNA was extensively studied from the 1950s to the 1990s, but the same research effort was not carried out with siRNA. The metallic ions are well known to stabilise or oppositely, destabilise the structure of nucleic acids depending on their affinity with the phosphate groups of the backbone and the nucleobases [9–11]. The respective affinities have been particularly studied by thermal denaturation profiles: the increase or decrease of the melting temperature denotes the preferential site of binding and its nature [9, 11]. Despite the fact that monovalent cations such as Na^+ are known to stabilise duplexes thanks to electrostatic interactions with phosphate groups, the metallic ions may induce the formation of various adducts according to their affinity with the nucleobases. Indeed, depending on the metallic ion considered, a transition from the regular B-form of the DNA to a so-called “M-form” (metallic form) was previously reported [11–13]. For siRNAs which are known to have a structure of A-form, the transition to the M-form has not been reported to our knowledge. Moreover, the formation of clusters made of siRNA or DNA formed in presence of zinc showed transfection abilities [7].

This study investigated the effect of four metallic ions (Mg^{2+}, Zn^{2+}, Fe^{2+} and Fe^{3+}) on the siRNA structure both at the local and colloidal scale. A better understanding of the interaction of these metallic ions with siRNA should also help to better design future polymeric carriers.

3.2. Material and methods

3.2.1. Materials

siRNA. The siRNA was provided as duplex by Kaneka Eurogentec S.A. (Seraing, Belgium) and received as lyophilisate after purification by reverse phase HPLC. The sense sequence was 5’-[Phos]GUCUCAGCCUCUUCUCAUUCCUG[dC][dT]-3’(M = 7807.6 g/mol) and the antisense was 5’-AGCAGGAA[mU]G[mA]G[mA]A[mG]A[mG]G[mC]U[mG]A[mG]A [mC][mA][mU][dT][dT] (M = 8999.6 g/mol). The molar masses were determined by

MALDI-TOF analysis. The annealing step was performed by Eurogentec according to standard procedures in a buffer 50 mM TRIS-HCl, 100 mM NaCl, pH 7.6.

Chemicals. $ZnCl_2$ was provided by abcr GmbH Germany, $MgCl_2$ by Sigma Aldrich, $FeCl_2.4H_2O$ and $FeNO_3.6H_2O$ by Alfa Aesar and ethidium bromide by Fischer Scientific. All components are of chemical grade.

3.2.2. Methods

Thermal denaturation profiles. Thermal melting profiles were recorded on a Cary 100 UV-visible spectrophotometer (Agilent technologies, CA, USA) in an 80 µL cuvette. The absorbance was measured at 260 nm from 20 °C to 90 °C at 1 °C/min. The solutions were prepared to reach a final concentration of 2 µM in siRNA with various concentrations of metal salts to investigate M:P (metal:phosphate) ratios of 0.5, 1, 2, 5 and 10. The blanks were recorded over the same temperature range from solutions of metal salts at same concentrations without siRNA.

Zeta-potential measurements. Zeta potential measurements were performed on a ZetasizerUltra (Malvern Panalytical Ltd., Malvern, UK) using the diffusive barrier technique. The capillary cell was filled with a 20 mM NaCl solution filtered on 0.2 µm cellulose acetate membrane and 100 µL of the sample was introduced at the bottom of the cell. The samples were made of 1g/L of siRNA (60 µM) containing various concentrations of metal to reach the M:P ratios of 0, 1, 2, 5, 10, and 30. The measurements were done in triplicate (mean value and standard deviations calculated).

Dynamic Light Scattering (DLS) measurements. The size and scattered intensity of the solutions containing the siRNA and metal were determined on the same apparatus as for the zeta-potential measurements. Three measurements were done at 25 °C before and after the zeta-potential measurements to verify the stability of the complexes. The light source was a 10 mW laser operating at λ = 632.8 nm. The size distribution of the objects in solution was given by fitting the correlation data with a non-negative least square algorithm. The solutions of ions metal were systematically filtered on cellulose acetate membrane of 0.22 µm porosity prior to use.

Circular Dichroism. CD spectra were recorded on a Jasco J-815 between λ = 200 and λ = 400 nm at a scan speed of 100 nm/min with 3 accumulations. Solutions of 10µM of siRNA with various concentrations of metal to cover M:P ratios of 1, 5, 10 and 30 were analysed at 37°C. The blanks were recorded from solutions of metal salts at same concentrations without siRNA.

Ethidium Bromide displacement. A 1 µM solution of siRNA containing ethidium bromide (EtBr) at a concentration of 0.677 µg/mL was prepared in RNAse free water. Various volumes of concentrated solutions of metal ions were then successively added to the siRNA solution to obtain M:P values of 1, 6, 16, 36 and 66. Fluorescence measurements were performed at each M:P ratio after 2 min of incubation at 37 °C [14]. The fluorescence spectra were recorded on a Jasco FP-8500 spectrophotometer between λ = 550 nm and λ = 700 nm with the excitation set at λ = 519 nm. Blank measurements with same solutions without siRNA were performed as well in similar conditions. Fluorescence data were corrected by the blank and by taking into account the dilution factor corresponding to the successive addition of the metal ion solution.

Agarose gel electrophoresis. Solutions of siRNA at a concentration of 15 µM were prepared in RNase-free water. Various volumes of concentrated solutions of metal ions were added to obtain M:P ratios of 1, 5, 10 and 30. Aliquots containing 1 µg of siRNA were loaded in a 3% agarose gel prepared in 40 mM Tris-HCl buffer (pH = 8.4) and run at 50 V for 1h30. The migration was performed a second time in the same conditions in the presence of 370 mM of NaCl. For this purpose, a low volume of a concentrated NaCl solution was introduced in the mixture of siRNA and metal to reach a final concentration of 370 mM and incubated 30 minutes. Note that salt has not been added to the buffer because at this concentration the high conductivity would cause strong heating and melting of the gel.

FTIR. Infrared spectra of complexes of metal ions with siRNA were recorded on a VERTEX 70 spectrometer from Bruker, equipped with a diamond crystal (GladiATR PIKE technologies) for attenuated total reflection (ATR) mode and a heating module. The spectra were acquired from 4000 to 400 cm^{-1} (64 scans, resolution of 4 cm^{-1}). 20 µL of a 0.5 g/L siRNA solution (30 µM) containing the metal ions at M:P ratios of 1, 5, 10, 30 were deposited on the crystal at 40°C to favor the drying of the solution while keeping the temperature below the melting temperature of the double stranded oligonucleotides. The solutions were dried under air flow before analysis. The siRNA samples containing the annealing buffer, it was necessary to analyse the Tris-HCl buffer as a reference. 20 µL of a Tris-HCl solution at the concentration estimated in the complexes was deposited and dried as described previously.

Atomic Force Microscopy (AFM). For the AFM analysis, the complexes were prepared at a siRNA concentration of 1 mg/mL and then diluted 10 times. A droplet of 4µl of solution was deposited onto freshly cleaved mica and allowed to dry at RT overnight. AFM measurements were performed at room temperature using a Nanoscope IIIa microscope (Veeco Instruments Inc.). Both topographic and phase images of individual particles were obtained in Tapping Mode ™ using rectangular silicon cantilever (AC 160-TS, Atomic Force,

Germany) with a spring constant of 42 $N.m^{-1}$, a resonance frequency lying in the 270-320 kHz range and a radius of curvature of less than 10 nm.

Cell culture. The cell culture tests were conducted on a cell line of Macrophage Murin RAW 264.7 acquired from American Type Culture Collection (USA). The cells were cultured in a Dulbeco's Modified Eagle's Medium (DMEM), supplemented with 10% fetal bovine serum, penicillin G (10 000 units/mL) and streptomycin (10 mg/mL). The cells were maintained in a humidified incubator at 37 °C in an atmosphere of 5% CO_2.

Cell viability. The effect of the formulations on the cell viability has been determined on the cell line RAW 264.7 with the colorimetric MTT assay (3-(4,5-dimethylthiazol-2-Yl)-2,5-diphenyltetrazolium bromide) [15]. For this test, the cells were seeded in 96 well plates at a density of 8.10^3 cells per well and incubated 24h until 80% of confluence was reached. The formulations (siRNA, siRNA-Mg^{2+}, siRNA-Zn^{2+}, siRNA-Fe^{2+} and siRNA-Fe^{3+} as well as the metal ions at different concentrations) were added at the corresponding concentrations. For all the formulations of complexes, the final siRNA concentration was fixed at 100 nM.

After 24h and 48h of incubation, 20µL of MTT solution at 5 mg/mL were added in each well and incubated 1h until the formation of the violet formazan crystals. The crystal formation is the result of the MTT reduction by the metabolically active cells. The cell culture medium was then replaced by 200 µL of DMSO to dissolve the formazan crystals. The absorbance was then measured at a wavelength of 570 nm. The percentage of the cells still viable has been calculated as the ratio of absorbance between the treated and untreated cells (control) (Equation 1).

$$\%\, cell\ \ viability\ = \frac{abs\ (cell +\ \ treat.) - abs\ (treat. + DMEM)}{abs\ cell\ non\ treat.\ (control) - abs\ (DMEM)}\ x\ 100 \qquad (1)$$

With $abs\ (cell + treat.)$ the absorbance of the cell suspensions exposed to the formulations, $abs\ (treat. + DMEM)$ the absorbance of the medium with the formulations, $abs\ cell\ non\ treat.\ (control)$ the absorbance of the cell suspension without the formulation, the control and $abs\ (DMEM)$ the absorbance of the culture media.

The half-maximal inhibitory concentration (IC_{50}) was determined based on the dose–response curve using a non-linear regression and estimated from the fitted line.

3.3. Results

3.3.1. Colloidal properties of siRNA-metal ion complexes

DLS and zeta measurements can provide information on the aggregation state of siRNA molecules in presence of various metal ions. Here, DLS evidenced the formation of colloidal structures of various sizes depending on the type of ion and the M:P ratio, i.e. the ratio of moles of metal ions introduced to those of phosphate groups of siRNA. The initial size distribution of siRNA obtained by DLS without added metal ion is quite complex as shown by the presence of three distinct size populations which can be attributed to the siRNA molecules, electrostatic aggregates (slow relaxation mode) and very large structures, the latter may be an artifact of the analysis (Figure 3.3-1). As the distributions are weighted by the intensity of the scattering objects, the two largest populations represent a little fraction of the total sample as shown by the size distribution in number (data not shown) and therefore the amount of large aggregates must be low. The addition of Mg^{2+} has little impact on the colloidal behaviour of siRNA even at high M:P ratios meaning that there is no strong interaction and the effect of ionic strength (μ = 0.264 M) is not high enough to drastically modify the hydrodynamic behaviour of the siRNA (Figure 3.3-1.a). This is also well confirmed by the low levels of scattering intensities whatever the M:P ratio values (Figure 3.3-2.a). The behaviour of siRNA in the presence of Zn^{2+}, Fe^{2+} and Fe^{3+} is markedly different from that with Mg^{2+}. Clearly these ions induce important aggregation effects of siRNA as shown by the evolution of size distributions and scattered intensities when M:P increases. This highlights the presence of strong interactions, probably by a mechanism of electrostatic complexation of phosphate groups of siRNA by metal cations. From the DLS analysis, the following order of interaction strength can be established: $Fe^{3+} > Fe^{2+} >> Zn^{2+} >> Mg^{2+}$. It is worth to mention that Zn^{2+} is best suited to control the aggregation level of siRNA by varying the M:P ratio. In contract, high levels of aggregation are already obtained with Fe^{2+} and Fe^{3+} at low M:P ratios (Figure 3.3-1.b and Figure 3.3-2.a).

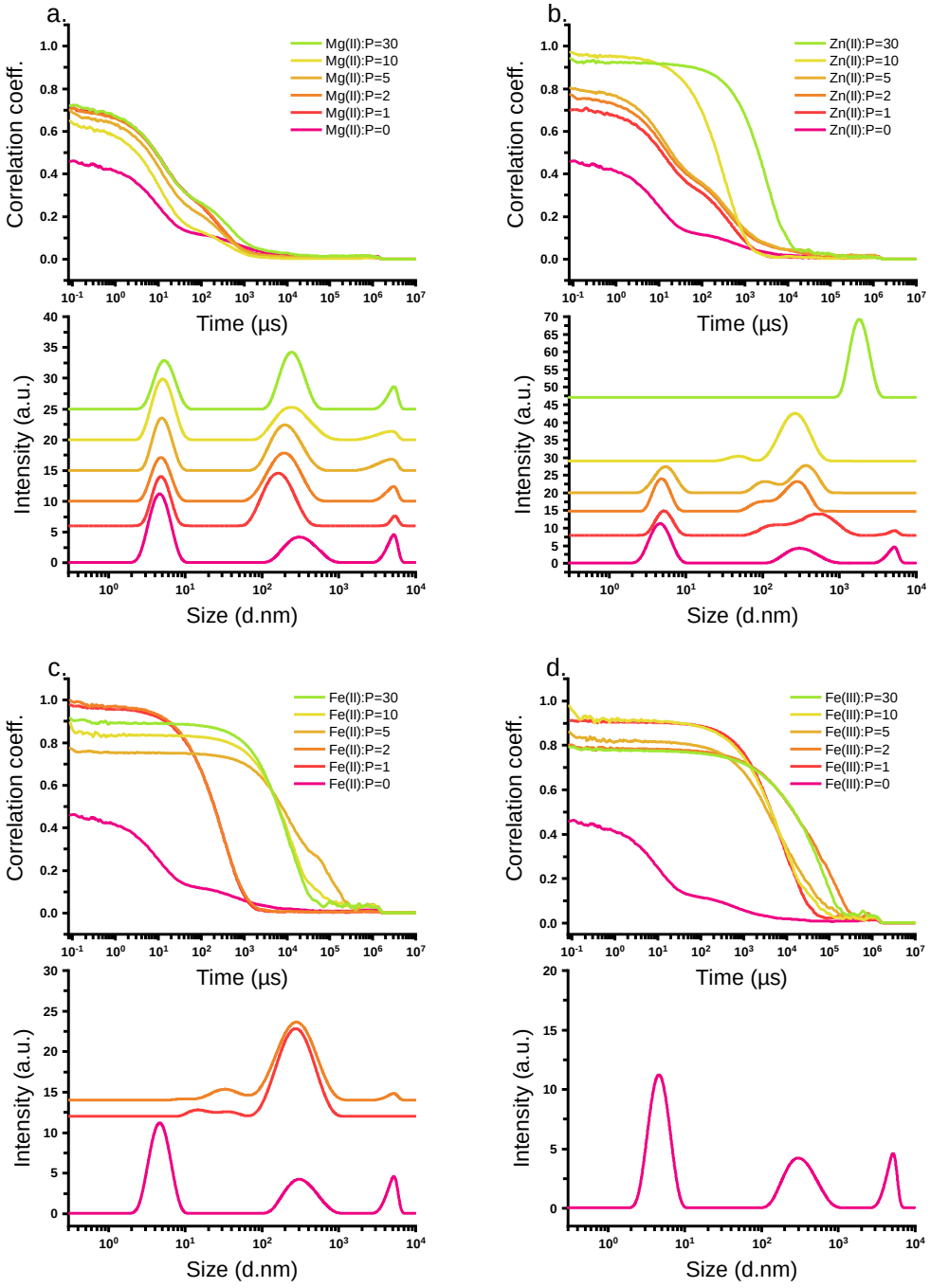

Figure 3.3-1. DLS analysis of 60 µM siRNA solutions in RNase-free water in presence of metal ions at different M:P ratios. The autocorrelation functions and the intensity-weighted size distributions (diameter in nm) are plotted for a) Mg^{2+} b) Zn^{2+} c) Fe^{2+} d) Fe^{3+}. Note that the sizes of the aggregates are out of range for M:P > 2 with Fe^{2+} and for all M:P ratios with Fe^{3+}.

Regarding the zeta-potential (ZP) of the structures formed in solution, the same trend was obtained for Mg^{2+}, Zn^{2+} and Fe^{2+}, i.e. the ZP increases with the M:P ratio without reaching positive values even with a large excess of metal ion (Figure 3.3-2.b). The behaviour of siRNA in presence of Fe^{3+} is clearly different since positive ZP values are obtained for all M:P ratios greater than or equal to 1. Such a charge inversion behaviour is reminiscent of the

phenomenon of reentrant condensation which is generally observed with polyanions such as DNA in presence of trivalent cations [16–18]. Charge inversion is here concomitant with the formation of the largest colloidal structures as shown by DLS (Figure 3.3-1.d). Therefore, both size and ZP measurements demonstrate that the strongest interaction of siRNA with metal ion is obtained with Fe^{3+}.

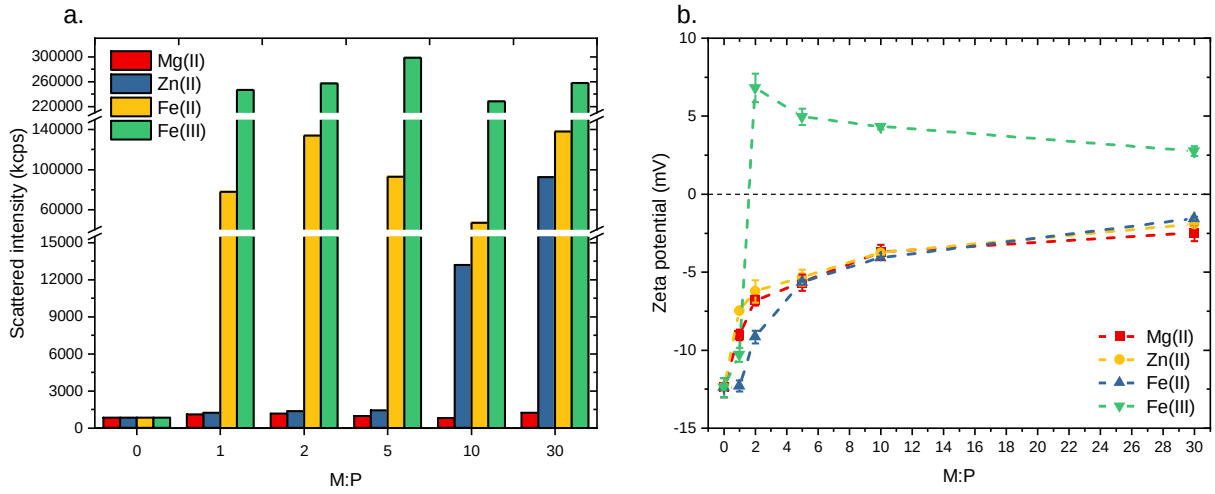

Figure 3.3-2. a) Scattered intensities of siRNA solutions in RNase-free water in presence of metal ions at various M:P ratios. b) Zeta potential values of same solutions.

The structures detected by DLS and zeta potential measurements were further characterised by AFM for two mixture compositions (Zn^{2+}:P = 10 and Fe^{2+}:P = 1) (Figure 3.3-3). Plain and round particles of about 200 nm in size with a high size-dispersity were evidenced, in agreement with the DLS analysis (Figure 3.3-1).

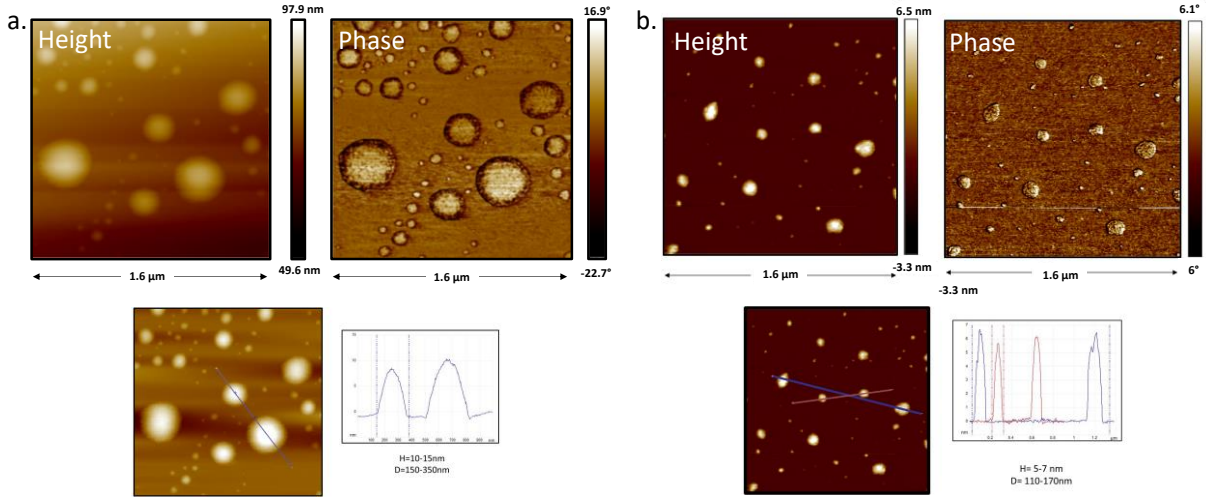

Figure 3.3-3. AFM analysis of the aggregates formed by complexation of siRNA with Zn^{2+} and Fe^{2+}. The height and phase analysis are provided for mixtures prepared at Zn^{2+}:P = 10 (a) and Fe^{2+}:P = 1 (b). The topographic profiles of selected aggregates are given as well below.

3.3.2. Thermal denaturation

The melting temperature (T_m) of the siRNA in presence of the various metallic ions was determined through absorbance measurements at λ = 260 nm as a function of the amount of metal introduced (M:P ratio). By this mean, it is possible to visualize the effect of the ions on the duplex stability. Indeed, it is has been shown on DNA that some ions stabilise the duplex structure (increase of T_m) by electrostatically interacting with the phosphate groups and thus decreasing the repulsive interactions between anionic charges while other ions can destabilise the duplex (decrease of T_m) through direct interaction with the bases [9]. From the Figure 3.3-4, it is observed that Fe^{2+} and Mg^{2+} have a stabilising effect on the siRNA duplex illustrated with the increase of the T_m value in the conditions studied. The Zn^{2+} ions present a different behaviour with a first increase in the T_m value followed by its decrease with the increase in Zn(II) content. This can be attributed to a predominant binding of zinc ions to the bases of the oligonucleotides rather than to the phosphate groups when the M:P ratio is equal or higher to 1 [9, 11]. In the specific case of Fe(III), the T_m of the siRNA could not be determined as the absorbance of the solution was too high due to the high molar extinction coefficient of the Fe^{3+} ions in these conditions [Figure 2 of ref [19]].

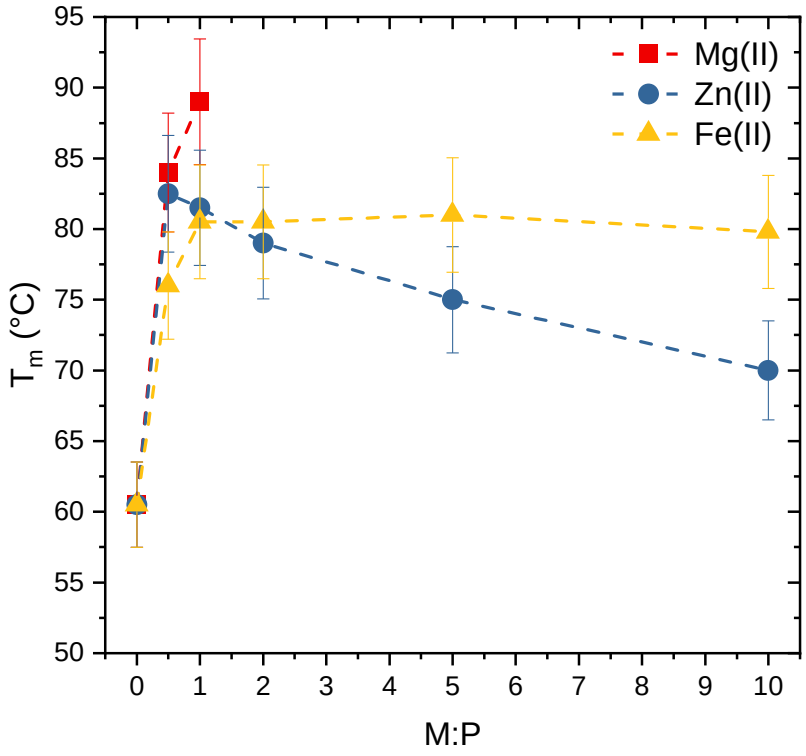

Figure 3.3-4. Melting temperature of siRNA in solution at a concentration of 2 µM in RNase-free water in presence of various metal ions (M:P ratios).

3.3.3. Circular Dichroism

siRNA, a small duplex of RNA presents a structure of "A-type" helix geometry which has a specific signature in circular dichroism with a positive and intense band around 260 nm and a negative band at 210 nm [20–23]. The band at 260 nm originates from the stacking geometry of the bases whereas the band at 210 nm is attributed to the helicity of the double stranded oligonucleotide [24]. On the other hand, the B-form of an helix presents a spectrum with a positive peak around 275 nm and a negative one at 245 nm, both of equal intensities [25]. Circular dichroism measurements of siRNA in presence of various amount of metals (Figure 3.3-5) showed that no change in the helical form of the duplex was observed in presence of Mg(II) and Zn(II), preserving its A-form. The increase in intensity of the peak at 260 nm in presence of Mg(II) has been attributed in the literature to a change in the average glycosidic angle due to the interaction of the ions with the negatively charged phosphate groups, which can be also interpreted as an increase in the flexibility of the strand [26]. Even though Zn(II) can interact with the bases according to T_m measurements, the interaction strength is not high enough to destabilise the "A-type" structure of siRNA. However, a first increase of the absorbance at 210 nm followed by a decrease with further addition of Zn(II) suggests small changes in the helicity of the siRNA [24]. In presence of Fe(II), no significant change of the

CD spectra was observed at low M:P ratios lower or equal to 10. Only small changes in the helicity and flexibility were observed through an increase of the peak absorbance at 210 and 260 nm. The decrease in absorbance at M:P = 30 was likely due to the massive precipitation of siRNA (Figure 3.3-1). In the case of Fe(III), the CD signals of siRNA solutions were saturated due to the strong absorbance of Fe(III).

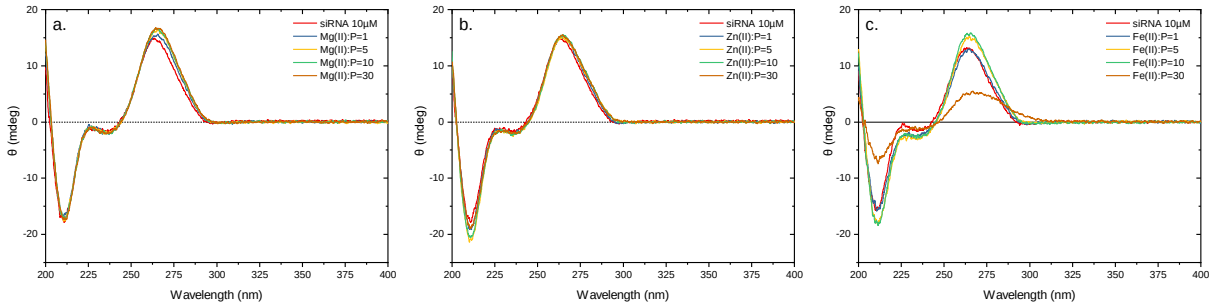

Figure 3.3-5. Circular dichroism spectra of siRNA at 10 µM in RNase-free water in presence of a) Mg^{2+}, b) Zn^{2+} and c) Fe^{2+}.

3.3.4. Fluorescence study with ethidium bromide

Ethidium Bromide (EtBr) emits fluorescence when it intercalates between the bases of nucleic acids in their native form [7, 27, 28]. Therefore, the fluorescence of siRNA in presence of EtBr must be sensitive to changes in the duplex structure. For instance, the intensity of the fluorescent signal is much stronger for a dsDNA than a ssDNA when the two are compared in the same conditions of concentration [29]. In the same manner, the fluorescent signal will be of higher intensity for a triplex compared to a duplex of DNA [30]. Ethidium Bromide was also used to attest the conformation change from a B to Z transition [31]. Importantly, EtBr can also interact with the phosphate groups of the nucleic acids through its positive charge but it has been shown that this interaction does not result in a fluorescent signal [29, 32, 33]. The EtBr displacement technique typically consists in analysing the fluorescence decay of nucleic acids in the presence of molecules having more affinity with bases than EtBr. This technique is therefore well suited to the analysis of metal ion interaction with siRNA bases. From the Figure 3.3-6, Mg(II) has a lower affinity with the bases compared to the other metals. It was found that the affinity order of metal ions with bases was the following: Mg(II) < Zn(II) < Fe(II) < Fe(III), which is in agreement with the measurements of melting temperatures.

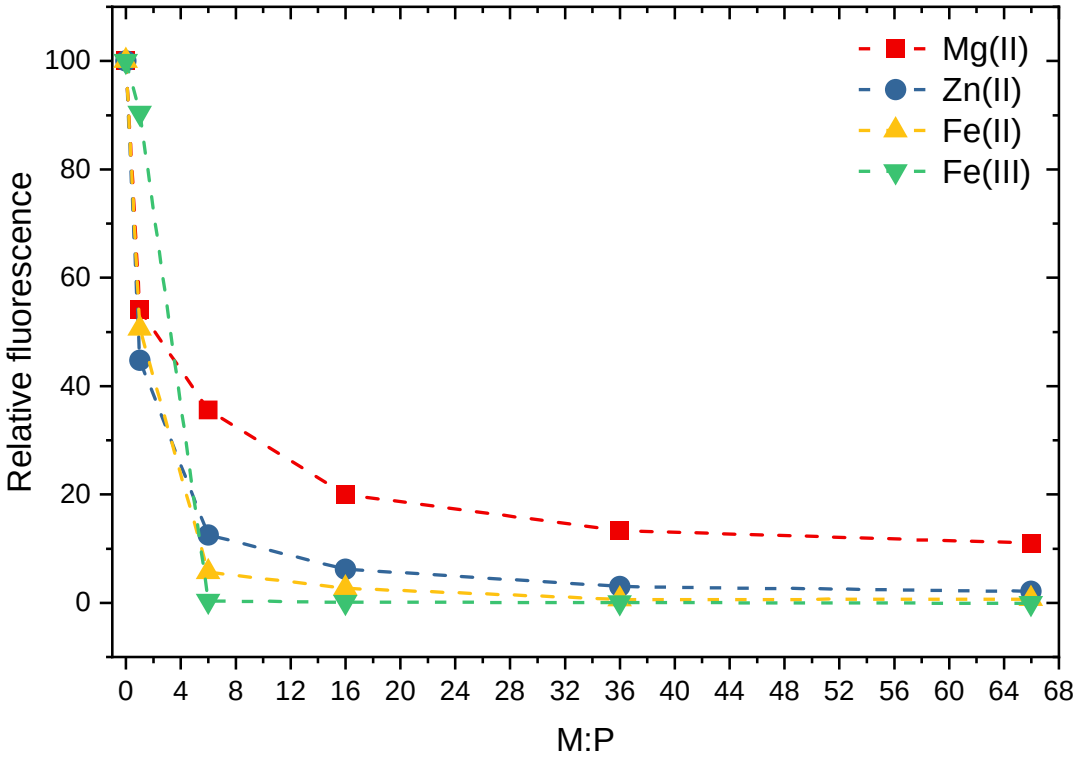

Figure 3.3-6. Fluorescence (measured at λ = 585 nm) of EtBr in siRNA solutions at 1 µM in RNase-free water in presence of various amounts of metal salts of Mg(II), Zn(II), Fe(II) and Fe(III).

3.3.5. Fourier transform infrared spectroscopy

FTIR spectroscopy was also used to characterise the interactions between siRNA and metal at the molecular level. The peaks of interest of the siRNA were attributed according to the literature on nucleic acids [10, 34–37]. Namely, three signals were considered: the signal at 858 cm^{-1} attributed to the vibration of the furanose-phosphodiester bond, the peak at 1238 cm^{-1} corresponding to the asymmetric stretching mode of PO_2^- and the signal at 1706 cm^{-1} assigned to uracil bases (C2=O2) and guanine bases (C6=O6). The other signals of nucleic acids were difficult to attribute due to the presence of traces of Tris-HCl that was used as annealing buffer by Eurogentec. Nevertheless, shifts of the aforementioned signals could give information on the interaction of the metals to the bases or the phosphate groups of the siRNA. Indeed, a shift of the band at 858 cm^{-1} towards higher wavenumbers was systematically observed with all metal cations, increasing with the amount of cation introduced (Figure 3.3-7). This signal is a marker of the A-form of a double stranded oligonucleotide. A shift of this peak can be interpreted as a binding of the cations to the phosphate groups of the siRNA [35]. Regarding the peak at 1238 cm^{-1} attributed to phosphate groups, the interpretation is more straightforward: a major shift was only observed in the presence of magnesium (Figure 3.3-7.a.). Therefore, one can assume that Zn^{2+}, Fe^{2+} and Fe^{3+} mainly interact with the bases of the

nucleic acids and poorly but non insignificantly with the phosphate groups. Concerning the signal at 1706 cm^{-1}, a displacement is also observed for every cation studied which can highlight an interaction with the bases of the siRNA. Indeed, studies have demonstrated that depending on the amount of metallic ion introduced, Mg^{2+} will almost exclusively bind the phosphate groups of nucleic acids at a low concentration (Mg^{2+}:P < 1) or bind to the bases at higher concentration of Mg(II) [35]. Clearly, with the conditions investigated here, Mg^{2+} can interact both with the phosphate groups and the bases of the siRNA. Nonetheless, for the ratio Mg^{2+}:P = 1, considered in the literature as the binding threshold of the ions to the bases, one can only see a shift of the signal corresponding to the phosphate groups (1238 cm^{-1}) and not for the bases (Figure 3.3-7.a, yellow) [35]. The case of Fe(II) and Fe(III) was also described in the literature by two different situations depending on the amount of cation introduced. In any case, Fe(II) has been shown to bind with both the phosphate groups and the bases of nucleic acids, namely with the phosphate groups at low Fe(III) concentrations and with the guanine bases at higher Fe(III) concentrations [38].

Regarding the increase of the signal in the region 1600-1700 cm^{-1}, this might be attributed to the bending vibration of water molecules, revealing the hydration state of the film [39–41]. This signal increases with increasing amounts of Mg(II), Zn(II) and Fe(II) but not with Fe(III). Indeed, water molecules might still be present in the film coming from the hydration shell of the cations even though the number of water molecules fixed per one metal ion must be reduced after coordination of the latter by the bases. The increase of the band in the 1400-1300 cm^{-1} region of the spectrum with Fe(III) is attributed to the increasing amount of NO_3^- species in the starting Fe(III) salt [42]. The correlation between the FTIR analysis and the EB displacement will be discussed in the last part.

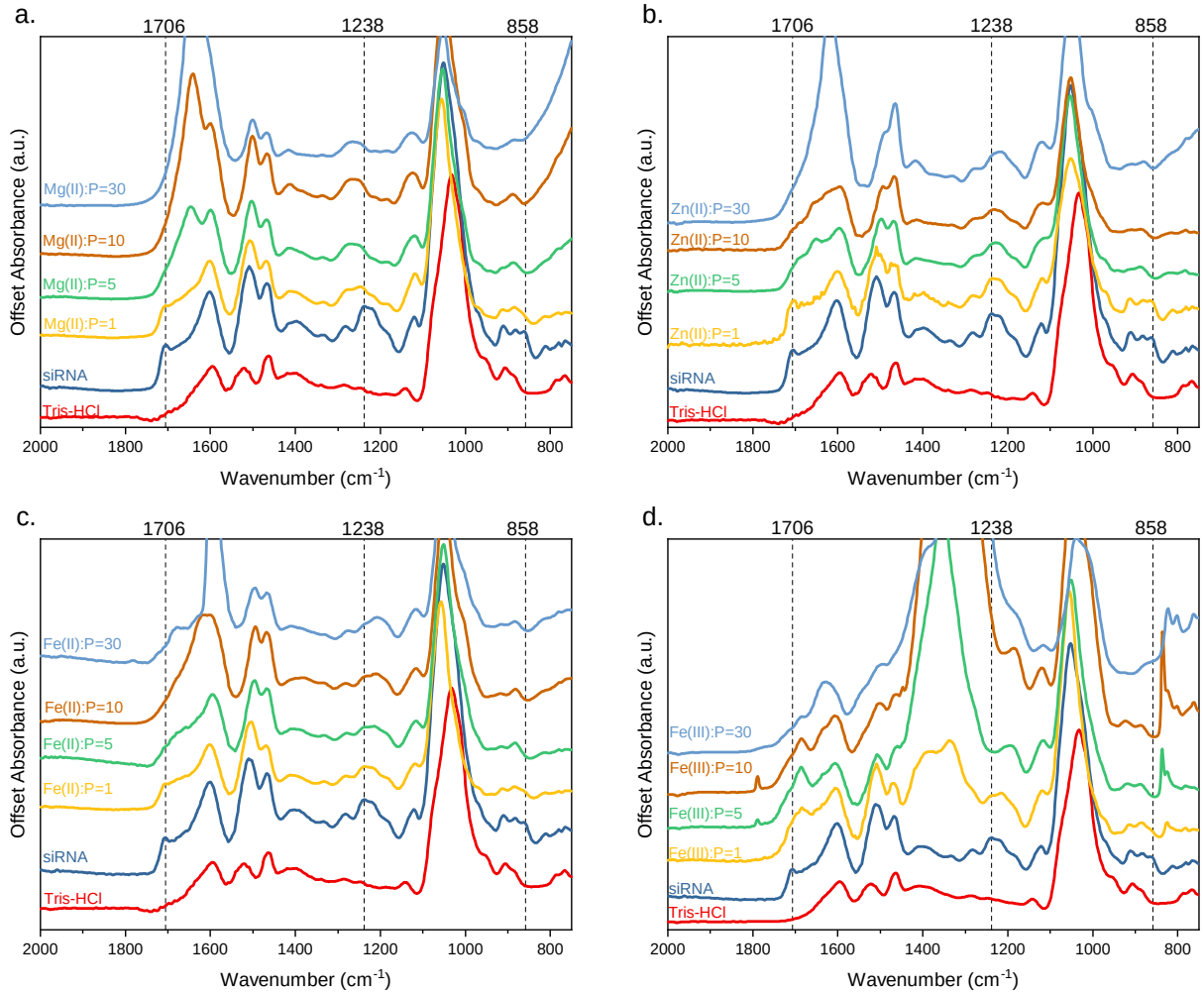

Figure 3.3-7. FTIR analysis of siRNA with metals ions at various ratio M:P ratios. a) Mg(II), b) Zn(II), c) Fe(II), d) Fe(III).

3.3.6. Agarose gel electrophoresis

In addition to DLS and zeta potential analysis, the colloidal state of siRNA-metal assemblies was assessed by agarose gel electrophoresis, which is a technique sensitive to both the size and charge of macromolecules. The presence of metal cations must reduce the net total charge of the siRNA, whether the interaction is with the bases or the phosphate groups. For example, in presence of Mg(II), the migration of siRNA is delayed which emphasizes a screening of the negative charges of siRNA (Figure 3.3-8.a). A similar behaviour was observed with Zn(II) except at M:P = 30 where a band broadening was observed, probably due to the aggregation of siRNA, as shown by DLS previously (Figure 3.3-1.b). With Fe(II) and Fe(III), no bands were visible at M:P ≥ 10 and only a band of very low intensity could be seen at M:P = 5 with Fe(III) which confirms the formation of large particles under these conditions, as suspected by DLS analysis. The migration pattern in presence of a large excess of NaCl suggests that

for both Fe(II) or Fe(III) considered, the interaction was partly of electrostatic origin. Indeed, for the samples prepared with 370mM of NaCl, the siRNA could partially migrate for the ratios Fe^{2+}:P = 10 and Fe^{3+}:P = 5 and 10, suggesting that the increase of the ionic strength reduced the electrostatic interaction between the metallic ions and the siRNA (Figure 3.3-8.b). Additionally, the electrophoretic pattern obtained in these conditions for a ratio Zn^{2+}:P = 30 was very similar to that obtained without addition of salt as it migrated much less than for other ratios and siRNA alone. It supports the hypothesis of a non-electrostatic interaction between Zn^{2+} and siRNA.

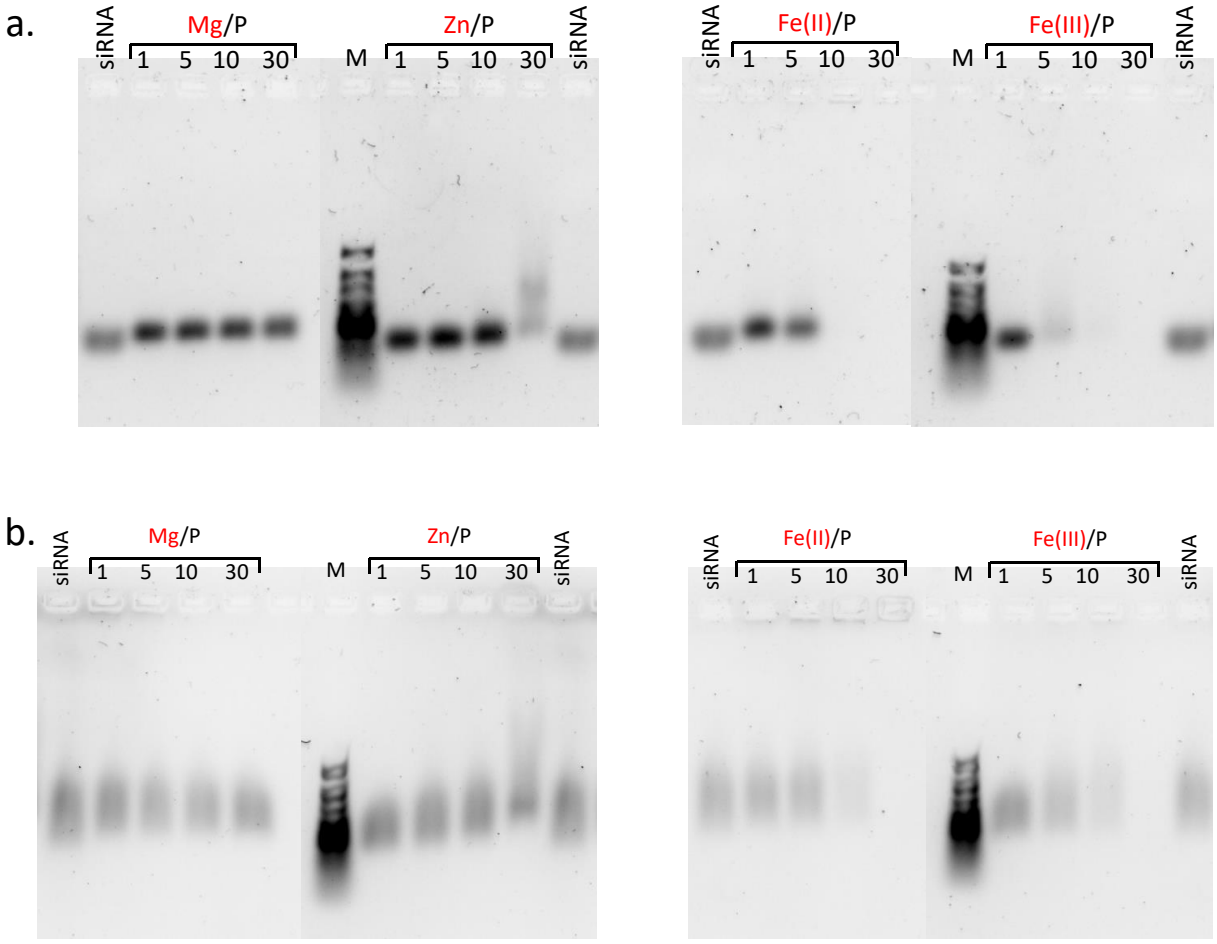

Figure 3.3-8. Electrophoresis gel assay of siRNA with metal ions at various M:P ratios. (a) no salt addition, (b) addition of NaCl (370mM) in the solutions before migration. Note that the introduction of an important amount of salt in the samples can induce artefacts in the gel: it screens the charge of the siRNA, inducing the formation of broad bands.

3.3.7. In vitro behaviour of siRNA in presence of metals

The cell viability evaluated by the MTT assay on RAW 264.7 macrophages showed that the siRNA alone is tolerated by the cells in a large range of concentrations (from 0.9 nM to 240 nM) (Figure 3.3-9.a). Metals alone did not show significant cytotoxicity up to 2000 µM except for Zn(II) where a dramatic drop in cell viability was observed at concentrations higher than 1000 µM as shown by IC_{50} values (Figure 3.3-9.a and Table 3.3.1). These values are in accordance with the literature where a maximal concentration of 10 mM in Mg^{2+} was considered safe for various cell lines [43]. An EC_{50} of 0.185 mM was found for Zn^{2+} on PC12 cells [44]. Importantly, the cytotoxicity of metals was increased in presence of siRNA. This is particularly well evidenced with Mg(II) and Zn(II) for which a strong decrease of IC_{50} values was observed in presence of siRNA (Table 3.3.1). The mixtures of siRNA and Fe(II) (or Fe(III)) are much less cytotoxic, probably due to the intrinsic lower toxicity of iron ions.

Table 3.3.1. Half maximal inhibitory concentration (IC_{50}) of metal ions and siRNA-metal mixtures on RAW 264.7 macrophages.

	Metal alone	Metal-siRNA complexes*	
Metal	**IC_{50} (µM)**	**IC_{50} (µM)**	**M:P ratio at IC_{50}**
Mg(II)	3800	77.6	15.84
Zn(II)	738.3	46.4	9.47
Fe(II)	> 1960	> 1960	> 400
Fe(III)	1784	704.1	143.70

*at a concentration of siRNA of 100 nM.

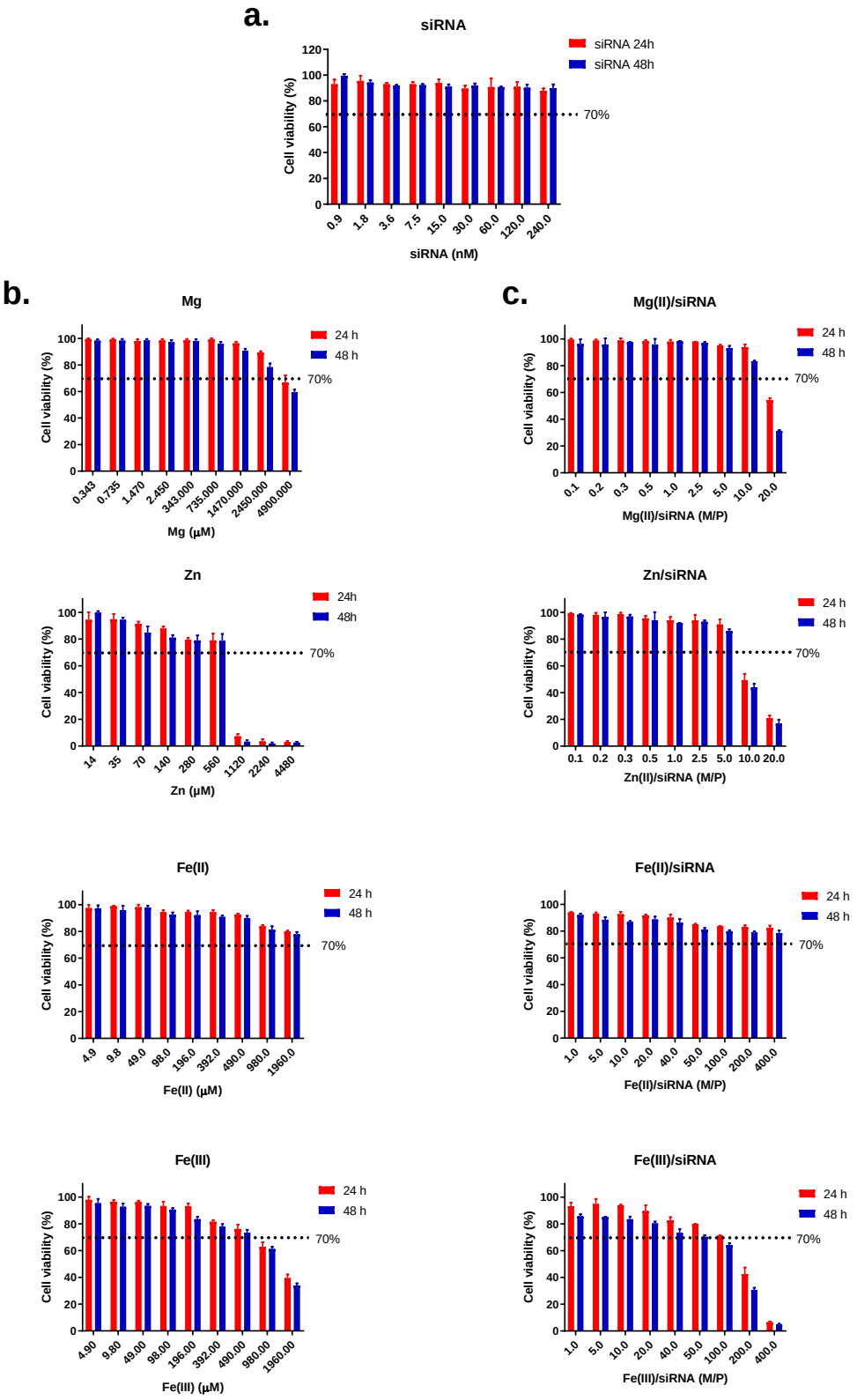

Figure 3.3-9. Cell viability of RAW 264.7 cells in presence of a) siRNA, b) metal ions alone and c) siRNA-metal ions mixtures at various M:P ratios (concentration of siRNA of 100 nM) at 24h (red) and 48h (blue) after incubation. Data points represent mean values ± SD ($n \geq 2$).

3.4. Discussion and conclusion

The interaction between nucleic acids and metallic ions has been greatly studied with DNA. It was shown that various sites and types of binding exist according to the nature of the ion [9, 11]. Evidence was made in the case of zinc that a metallic form of the DNA ("M-form") could be obtained [11, 12]. Despite these evidences, no correlation has been established between the interaction of metallic ions with nucleic acids and the colloidal behaviour of the latter. Here we studied the interaction of siRNA with metal ions. Magnesium showed a preferentially binding with the phosphate groups of the siRNA through electrostatic interactions as evidenced by the increased thermal stability and confirmed by infrared spectroscopy (Figure 3.3-7.a.). However, electrostatic interactions are not strong enough with Mg(II) to aggregate the siRNA molecules. EB displacement (Figure 3.3-6) on the other hand, suggests a weak interaction of Mg(II) with the bases (also supported by the infrared spectrum) which has been also reported for DNA [35]. The case of zinc is of particular interest as it was shown previously that it can form clusters of siRNA chains capable of transfection [7]. The clusters were well evidenced by DLS. They are formed mainly through interactions between zinc ions and nucleic acid bases, as shown previously on DNA [9, 11] and confirmed here through experiments of EB displacement (Figure 3.3-6). In addition, no displacement of the phosphate band was observed in the infrared spectrum (Figure 3.3-7.b.). The evolution of the melting temperature as a function of the amount of zinc also shows an interaction of Zn(II) with bases, as found with DNA. [9, 11]. On the other hand, the circular dichroism spectrum showed that the helical structure of the siRNA of "A-type" is kept constant on the whole range of zinc concentration suggesting a "M-form" of the siRNA as for DNA. Finally, Fe(II) and Fe(III) lead both to colloidal changes with the formation of large and dense structures evidenced by the scattered intensity from the DLS measurements (Figure 3.3-2.a). The aggregates were well imaged by AFM as solid and round nanoparticles. At the molecular level, EB displacement and infrared spectroscopy showed that the interaction between the two types of iron ions and siRNA takes place on the bases as seen by the drop in fluorescence intensity in presence of iron (II) or (III) (Figure 3.3-6). Besides, no shift of the asymmetric stretching mode of PO_2^- (Figure 3.3-7.c and d) were detected by IR spectroscopy, even though Fe^{3+} ions were reported to interact with the phosphate groups of DNA [10]. However, Fe^{2+} ions did not cause same changes on the melting temperature as the zinc ions (Figure 3.3-4): iron ions at low concentration increased the T_m during, but no additional variation is detected at higher concentrations. This might be explained by the nature of the interaction between Fe^{2+} ions and the nucleic acids which is astride between the electrostatic interaction with the phosphate groups and the coordination with the bases: the two interactions compensate each

other, hence the stable value of the T_m. There is no evidence that structural changes occur in presence of Fe^{2+} since the helical structure of "A-type" is retained.

Regarding the toxicity of the structures formed, one explanation may rely on the size of the structures. In the case of magnesium and zinc, the aggregation of siRNAs is relatively low but the anionic charge is considerably attenuated, which must somehow favour the crossing of the cell membrane. Thus, siRNAs would allow the cell-internalization of Mg(II) and Zn(II) ions in significant quantities causing cell death. On the other hand, the large objects formed in presence of iron prevent the internalization of the objects, and hence, no toxicity is observed.

3.5. References

[1] Gujjari A, Rodriguez B V., Pescador J, Maeder C, Beall GW, Lewis LK (2018) Factors affecting the association of single- and double-stranded RNAs with montmorillonite nanoclays. Int J Biol Macromol 109:551–559 . https://doi.org/10.1016/j.ijbiomac.2017.12.124

[2] Liu S, Jia H, Yang J, Pan J, Liang H, Zeng L, Zhou H, Chen J, Guo T (2018) Zinc Coordinated Cationic Polymers Break Up the Paradox between Low Molecular Weight and High Transfection Efficacy. Biomacromolecules 19:4270–4276 . https://doi.org/10.1021/acs.biomac.8b01140

[3] Liu G, Choi KY, Bhirde A, Swierczewska M, Yin J, Lee SW, Park JH, Hong JI, Xie J, Niu G, Kiesewetter DO, Lee S, Chen X (2012) Sticky Nanoparticles: A Platform for siRNA Delivery by a Bis(zinc(II) dipicolylamine)-Functionalized, Self-Assembled Nanoconjugate. Angew Chemie Int Ed 51:445–449 . https://doi.org/10.1002/anie.201105565

[4] Yu QY, Guo Y, Zhang J, Huang Z, Yu XQ (2019) Zn(ii) coordination to cyclen-based polycations for enhanced gene delivery. J Mater Chem B 7:451–459 . https://doi.org/10.1039/c8tb02414f

[5] He C, Liu D, Lin W (2015) Biomaterials Self-assembled nanoscale coordination polymers carrying siRNAs and cisplatin for effective treatment of resistant ovarian cancer. Biomaterials 36:124–133 . https://doi.org/10.1016/j.biomaterials.2014.09.017

[6] Fang H, Lin L, Chen J, Wu J, Tian H, Chen X (2019) Zinc ion coordination significantly improved the transfection efficiency of low molecular weight polyethylenimine. Biomater Sci 7:1716–1728 . https://doi.org/10.1039/C9BM00039A

[7] Lim KS, Lee DY, Valencia GM, Won Y-W, Bull DA (2015) Nano-Self-Assembly of Nucleic Acids Capable of Transfection without a Gene Carrier. Adv Funct Mater 25:5445–5451 . https://doi.org/10.1002/adfm.201502067

[8] Zhu J, Chu C, Li D, Pang X, Zheng H, Wang J, Shi Y, Zhang Y, Cheng Y, Ren E, Cheng J, Chen X, Liu G (2019) Fe(III)-Porphyrin Sonotheranostics: A Green Triple-Regulated ROS Generation Nanoplatform for Enhanced Cancer Imaging and Therapy. Adv Funct Mater 29:1–10 . https://doi.org/10.1002/adfm.201904056

[9] Eichhorn GL, Shin YA (1968) Interaction of metal ions with polynucleotides and

related compounds. XII. The relative effect of various metal ions on DNA helicity. J Am Chem Soc 90:7323–7328 . https://doi.org/10.1021/ja01028a024

[10] Zhizhina GP, Oleinik EF (1972) Infrared Spectroscopy of Nucleic Acids. Russ Chem Rev 41:258–280 . https://doi.org/10.1070/rc1972v041n03abeh002043

[11] Lee JS, Latimer LJP, Reid RS (1993) A cooperative conformational change in duplex DNA induced by Zn 2+ and other divalent metal ions. Biochem Cell Biol 71:162–168 . https://doi.org/10.1139/o93-026

[12] Sorokin VA, Valeev VA, Usenko EL, Rakovsky YP, Andrushchenko V V. (2013) Specific features of Zn2+, Co2+ and Ni2+ ion binding to DNA in alkaline solutions. Int J Biol Macromol 55:137–141 . https://doi.org/10.1016/j.ijbiomac.2013.01.001

[13] Hadjiliadis N, Sletten E (2009) Metal Complex–DNA Interactions. John Wiley & Sons, Ltd, Chichester, UK

[14] Messai I, Delair T (2006) Cationic biodegradable particles: Comparison of one or two step processes. Colloids Surfaces A Physicochem Eng Asp 278:188–196 . https://doi.org/10.1016/j.colsurfa.2005.12.018

[15] Mosmann T (1983) Rapid colorimetric assay for cellular growth and survival: Application to proliferation and cytotoxicity assays. J Immunol Methods 65:55–63 . https://doi.org/10.1016/0022-1759(83)90303-4

[16] Nguyen TT, Rouzina I, Shklovskii BI (2000) Reentrant condensation of DNA induced by multivalent counterions. J Chem Phys 112:2562–2568 . https://doi.org/10.1063/1.480819

[17] Shklovskii BI (1999) Screening of a macroion by multivalent ions: Correlation-induced inversion of charge. Phys Rev E - Stat Physics, Plasmas, Fluids, Relat Interdiscip Top 60:5802–5811 . https://doi.org/10.1103/PhysRevE.60.5802

[18] Luo Z, Wang Y, Li S, Yang G (2018) DNA phase transition in charge neutralization and comformation induced by trivalent-hydrolysed metal ions. Polymers (Basel) 10: . https://doi.org/10.3390/polym10040394

[19] Loures C, Alcântara M, Filho H (2013) Advanced Oxidative Degradation Processes: Fundamentals and Applications. Int Rev Chem Eng 5:102–120

[20] Kypr J, Kejnovská I, Bednářová K, Vorlíčková M (2012) Circular Dichroism Spectroscopy of Nucleic Acids. In: Comprehensive Chiroptical Spectroscopy. John Wiley & Sons, Inc., Hoboken, NJ, USA, pp 575–586

[21] Baranowski DS, Kotkowiak W, Kierzek R, Pasternak A (2015) Hybridization properties of RNA containing 8-methoxyguanosine and 8-benzyloxyguanosine. PLoS One 10:1–9 . https://doi.org/10.1371/journal.pone.0137674

[22] Andrzejewska W, Wilkowska M, Peplińska B, Skrzypczak A, Kozak M (2019) Structural characterization of transfection nanosystems based on tricationic surfactants and short double stranded oligonucleotides. Biochem Biophys Res Commun 518:706–711 . https://doi.org/10.1016/j.bbrc.2019.08.114

[23] Sipa K, Sochacka E, Kazmierczak-Baranska J, Maszewska M, Janicka M, Nowak G, Nawrot B (2007) Effect of base modifications on structure, thermodynamic stability, and gene silencing activity of short interfering RNA. Rna 13:1301–1316 . https://doi.org/10.1261/rna.538907

[24] Pawlowska R, Janicka M, Jedrzejczyk D, Chworos A (2016) RNA fragments mimicking tRNA analogs interact with cytochrome c. Mol Biol Rep 43:295–304 . https://doi.org/10.1007/s11033-016-3954-6

[25] Bloomfield VA, Crothers DM, Tinoco I, Hearst JE, Wemmer DE, Killman PA, Turner DH (2000) Nucleic acids: structures, properties and functions. University Science Books

[26] Formoso C (1972) Circular dichroism study of the effects of magnesium perchlorate and temperature on the solution conformation of uridine 5'-monophosphate, uridine 3'-monophosphate, urdine, and uridylyl-(3' →5')-uridine. Biochemistry 11:4031–4036 . https://doi.org/10.1021/bi00772a004

[27] Veron L, Ganée A, Charreyre MT, Pichot C, Delair T (2004) New hydrolyzable pH-responsive cationic polymers for gene delivery: A preliminary study. Macromol Biosci 4:431–444 . https://doi.org/10.1002/mabi.200300064

[28] Waring MJ (1965) Complex formation between ethidium bromide and nucleic acids. J Mol Biol 13:269–282 . https://doi.org/10.1016/S0022-2836(65)80096-1

[29] Vardevanyan PO, Antonyan AP, Parsadanyan MA, Davtyan HG, Karapetyan AT (2003) The binding of ethidium bromide with DNA: interaction with single- and double-stranded structures. Exp Mol Med 35:527–533 . https://doi.org/10.1038/emm.2003.68

[30] Scaria P V., Shafer RH (1991) Binding of ethidium bromide to a DNA triple helix. Evidence for intercalation. J Biol Chem 266:5417–5423 . https://doi.org/10.1016/S0021-9258(19)67611-8

[31] Bhanjadeo MM, Subudhi U (2019) Praseodymium promotes B–Z transition in self-assembled DNA nanostructures. RSC Adv 9:4616–4620 . https://doi.org/10.1039/C8RA10164G

[32] Domard M, Rinaudo M, Rinaldi R (1973) Étude de l'interaction électrostatique entre l'ion. Ethidium et les polyanions à densité de charge variable. J Chim Phys 70:1410–1416 . https://doi.org/10.1051/jcp/1973701410

[33] Lepecq JB, Paoletti C (1967) A fluorescent complex between ethidium bromide and nucleic acids. Physical-Chemical characterization. J Mol Biol 27:87–106 . https://doi.org/10.1016/0022-2836(67)90353-1

[34] Banyay M, Sarkar M, Gräslund A (2003) A library of IR bands of nucleic acids in solution. Biophys Chem 104:477–488 . https://doi.org/10.1016/S0301-4622(03)00035-8

[35] Serec K, Babić SD, Podgornik R, Tomić S (2016) Effect of magnesium ions on the structure of DNA thin films: an infrared spectroscopy study. Nucleic Acids Res 44:8456–8464 . https://doi.org/10.1093/nar/gkw696

[36] Dovbeshko GI, Gridina NY, Kruglova EB, Pashchuk OP (2000) FTIR spectroscopy studies of nucleic acid damage. Talanta 53:233–246 . https://doi.org/10.1016/S0039-9140(00)00462-8

[37] Mello MLS, Vidal BC (2012) Changes in the Infrared Microspectroscopic Characteristics of DNA Caused by Cationic Elements, Different Base Richness and Single-Stranded Form. PLoS One 7:e43169 . https://doi.org/10.1371/journal.pone.0043169

[38] Ouameur AA, Arakawa H, Ahmad R, Naoui M, Tajmir-Riahi HA (2005) A Comparative Study of Fe(II) and Fe(III) Interactions with DNA Duplex: Major and Minor Grooves Bindings. DNA Cell Biol 24:394–401 . https://doi.org/10.1089/dna.2005.24.394

[39] Cai Y, Xue J, Polya DA (2007) A Fourier transform infrared spectroscopic study of

Mg-rich, Mg-poor and acid leached palygorskites. Spectrochim Acta Part A Mol Biomol Spectrosc 66:282–288 . https://doi.org/10.1016/j.saa.2006.02.053

[40] Kunimatsu K, Bae B, Miyatake K, Uchida H, Watanabe M (2011) ATR-FTIR Study of Water in Nafion Membrane Combined with Proton Conductivity Measurements during Hydration/Dehydration Cycle. J Phys Chem B 115:4315–4321 . https://doi.org/10.1021/jp112300c

[41] Falk M, Hartman KA, Lord RC (1963) Hydration of Deoxyribonucleic Acid. II. An Infrared Study. J Am Chem Soc 85:387–391 . https://doi.org/10.1021/ja00887a004

[42] Hemery G, Garanger E, Lecommandoux S, Wong AD, Gillies ER, Pedrono B, Bayle T, Jacob D, Sandre O (2015) Thermosensitive polymer-grafted iron oxide nanoparticles studied by in situ dynamic light backscattering under magnetic hyperthermia. J Phys D Appl Phys 48:494001 . https://doi.org/10.1088/0022-3727/48/49/494001

[43] Wang J, Witte F, Xi T, Zheng Y, Yang K, Yang Y, Zhao D, Meng J, Li Y, Li W, Chan K, Qin L (2015) Recommendation for modifying current cytotoxicity testing standards for biodegradable magnesium-based materials. Acta Biomater 21:237–249 . https://doi.org/10.1016/j.actbio.2015.04.011

[44] Pavlica S, Gaunitz F, Gebhardt R (2009) Comparative in vitro toxicity of seven zinc-salts towards neuronal PC12 cells. Toxicol Vitr 23:653–659 . https://doi.org/10.1016/j.tiv.2009.03.003

Chapter 4: Study of the interaction of zinc with chitosan. Towards an improved stabilization of the chitosan-siRNA PECs

4.1. Introduction

Chitosan is a polymer extracted from natural resources that is known to be the only polysaccharide to carry positive charges. Thanks to its cationic behaviour, it has been largely used to formulate particles under the form of polyelectrolyte complexes (PECs) [1]. More recently, and thanks to the discovery of the tremendous potential of siRNA, chitosan has been studied as candidate for non-viral siRNA delivery [2]. Before that, it has also been extensively used for the delivery of plasmid DNA [3]. An excess of chitosan is generally used to complex and protect nucleic acids, regardless of the type of nucleic acid used. Different parameters can have an influence on the efficiency and stoichiometry of the complexation and the stability of complexes. The length of the chitosan chain plays a critical role to form nanosized particles under acidic conditions. Another parameter of importance is the degree of acetylation of chitosan which will be investigated in this chapter.

One of the main problems in the formulation of chitosan-based colloids for biological applications is the low protonation degree of chitosan at physiological pH (pH=7.4). Under such pH conditions, chitosan is no longer soluble and cannot stabilize PECs, resulting in their aggregation or dissociation. Many routes have been investigated to solve this problem, particularly the chemical modification of chitosan. A well-known chemical route is the quaternization of the amines of chitosan to make the chitosan protonated whatever the pH conditions [4, 5]. However, the quaternization is a covalent, i.e irreversible, modification that contributes to increase the toxicity of chitosan. Another approach consists in finding a way to increase the cationicity of chitosan at physiological pH by means of reversible bonds like coordination bonds. A coordinate bond (or dative bond) is a covalent bond in the sense of it involves a shared pair of electrons but both electrons come from the same atom. Coordinate bonds are less energetic than simple covalent bonds and therefore reversible under defined conditions. Here, the study focuses on the formation of coordinate bonds (chelates) of metallic ions (electron acceptor) with deprotonated amine groups (electron donor) of chitosan at pHs above the pKa. This approach, already proposed in previous studies [6, 7] should substantially improve the stability of polyelectrolyte complexes at pH 7.4. It also presents the advantage of keeping chitosan under its native form, without compromising its biocompatibility with chemical modifications. Different aspects have to be taken into account in this new way of formulating chitosan with nucleic acids, from the individual interaction of metallic ions with the components, to the optimal amount of ions required to achieve the stability of particles under various pH conditions.

In this chapter, we studied how to improve the pH stability of chitosan/siRNA complexes. Two main studies will be presented. First, the interaction between zinc and chitosan will be presented. Then, the effect of zinc ions on the stability of the chitosan-siRNA complexes will be discussed.

4.2. Interactions between zinc and chitosan

4.2.1. Introduction

The study of the interaction between chitosan and metals goes back to the seventies [8] when the interest was mostly motivated by the treatment of water for metal removal. Indeed, chitosan has the ability to chelate metals, mostly thanks to its amino groups. The mechanism of chelation can be described through the Lewis acid-base theory. A metal can be considered as an acid, that is, an acceptor of a pair of electrons while an amine is a donor of electrons. The specific interaction between metals and amine groups of chitosan has been shown to be strongly dependant on the pH of the solution. For instance, the highest adsorption of zinc ions onto chitosan particles is obtained for a pH value of 6 [9]. Two coordination modes have been proposed in order to describe the structure obtained from the chelation of metallic ions by the nitrogen atoms of chitosan: the “bridge model” [10] (Figure 4.2-1.b) and the “pendant model” [11] (Figure 4.2-1.a); they have been under debate for a few years. The first coordination mode which was described for the complexation of chitosan with copper suggests a planar geometry involving four nitrogen ligands coordinating a metal ion (CuN_4 form); it was established by electron spin resonance (ESR). (Figure 4.2-1.b). The second one, resolved by X-ray suggests that only one amino group chelates a metallic ion, hence the pendant term used. The complexes were also identified with more straightforward and simple techniques such as potentiometry and were found of the ML_1 or ML_2 form, M being the metal and L the ligand, which supports the pendant model with either one or two amino groups involved (Figure 4.2-1.a).

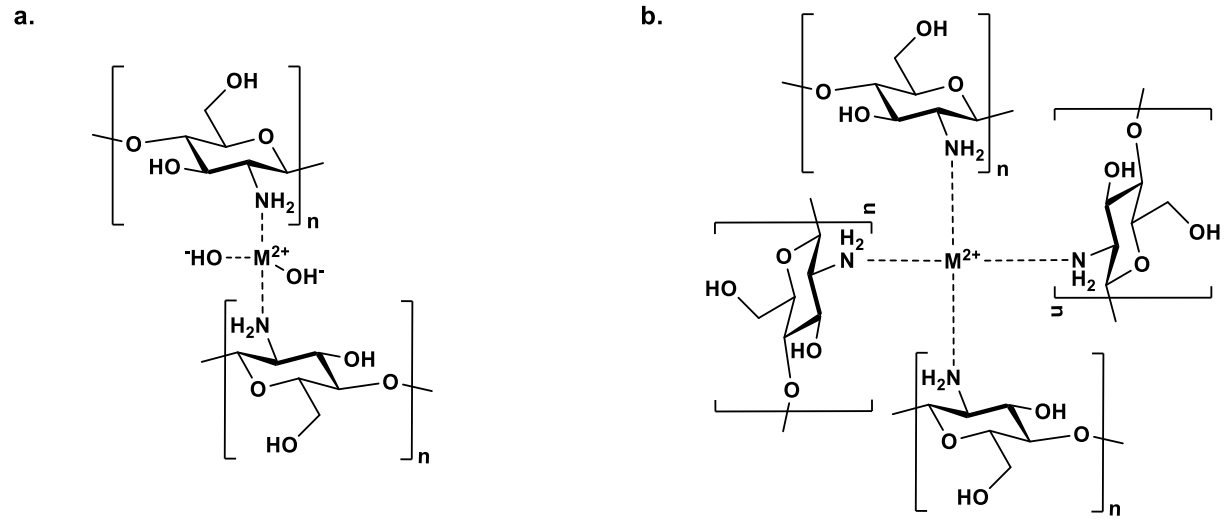

Figure 4.2-1. The two coordination modes of chitosan in presence of metallic ions. a) pendant model and b) bridge model.

In this part, the interaction between zinc and chitosan will be highlighted thanks to various techniques such as Fourier Transform Infrared Spectroscopy, potentiometry and zeta potential measurements.

4.2.2. Materials and methods

Chitosan. Three different chitosans varying in molecular weight and degrees of acetylation (DA) were used and denoted according to their composition using the nomenclature [DA-M_n] with M_n the number-average molar mass in kg/mol. A first chitosan [0-8], a chitosan oligosaccharide (COS), was obtained from the depolymerization of a N-deacetylated chitosan (DA < 1%) of M_n ~ 90 000 g/mol according to the protocol proposed by Allan and Peyron [12]. Briefly, chitosan was dissolved in water at 3 wt % with a stoichiometric amount of HCl relative to amine functions. After 3 days of vigorous stirring, sodium nitrite was added to the chitosan solution at a ratio nitrite/GlcN = 28 to target a DP of 50. The reaction proceeded under magnetic stirring in a closed reaction vessel for 24 h at room temperature. After filtration on a 1.0 µm pore size glass fiber membrane (Pall), the solution was lyophilized and the lyophilisate was dissolved in a minimum volume of ultrapure water. The chitosan was precipitated in ethanol:acetone (1:1 v:v) mixture and the precipitate was washed three times with the same solvent mixture and centrifuged. The swollen chitosan was then repeatedly (3×) dissolved in ultrapure water and lyophilized. The final mass yield of purified COS under its hydrochloride salt form was above 70%.

A chitosan [12-23] (DA = 12% according to the NMR Figure 4.2-3) was provided by our partner at the Laboratoire Ingénierie des Matériaux Polymères (IMP) in Lyon. A third chitosan sample [24-55] (DA = 24% according to the NMR Figure 4.2-3) was obtained from the acetylation and depolymerization of a commercial chitosan (DA = 8% and M_n ~ 550 kDa) according to the N-acetylation protocol adapted from Vachoud, L. and al. [13–15]. A last chitosan sample [32-57] (DA = 32% according to the NMR Figure 4.2-3) was obtained from the reacetylation of [24-55] following the same protocol. Briefly, the N-acetylation of chitosan was performed with acetic anhydride in a water/alcohol medium. First, 10 mL of solution of chitosan at 1% containing 0.5 % of acetic acid was mixed with 8 mL of methanol. Then, the acetylating medium, composed of a freshly prepared mixture of 2 mL of methanol with a variable volume of acetic anhydride, was added slowly to the above solution and stirred for 12 h. The amount of acetic anhydride was chosen according to an experimental equation obtained previously in the case of DA = 0% [16]: DA = 66.77 R_A + 12.23 (R_A being the molar ratio acetic anhydride/glucosamine residues). This equation was adapted such as: $DA_{targ.} - DA_{start.} = 66.77\ R_A + 12.23$ with $DA_{targ.}$ the targeted DA and $DA_{start.}$ the DA of the starting chitosan. The reaction is described in Figure 4.2-2. After reaction, the product was precipitated by addition of a mixture of ammonia and methanol (50/50) and washed several times by dispersion/centrifugation with deionized water until the pH reach neutrality.

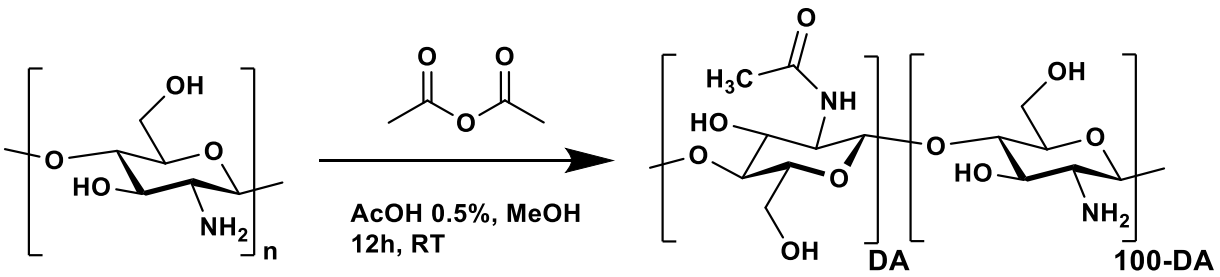

Figure 4.2-2. Acetylation of chitosan with acetic anhydride.

Chitosan characterization by ^{1}H NMR and SEC-MALLS. The structure of chitosan was determined at 298 K by proton nuclear magnetic resonance (^{1}H-NMR) spectroscopy on a Bruker AVANCE III HD 400 MHz spectrometer using a 5 mm Bruker multinuclear z-gradient direct probe (Figure 4.2-3). The ^{1}H NMR spectra were calibrated from the signal of HOD at 4.79 ppm [17]. The degree of polymerization (DP) of the chitosan oligosaccharide [0-8] which corresponds to the number of glucosamine (GlcN) units within the COS chain was obtained from the integral ratio of the H-2 protons of GlcN units at 3.20 ppm and the H-1 or H-3 protons of the terminal 2,5-anhydro-D-mannofuranose (M-unit) located at 5.11 and 4.46 ppm, respectively [18] (Figure 4.2-3). Note that in the ^{1}H-NMR analysis conditions used here, the aldehyde group of the M-units does not exist in its free (–CHO) form but exclusively

in its hydrated ($–CH(OH)_2$) form [19]. The degree of acetylation of was obtained from the equation established by Hasako Hirai and al. [20]:

$$DA = \frac{\frac{1}{3}(HAc)}{\frac{1}{6}(H2-6)} \times 100 \qquad 4.1$$

(H2-6) corresponds to the integral of the protons between 3 and 4 ppm and (HAc) to the integral of the three protons of the acetyl group at 2.07 ppm.

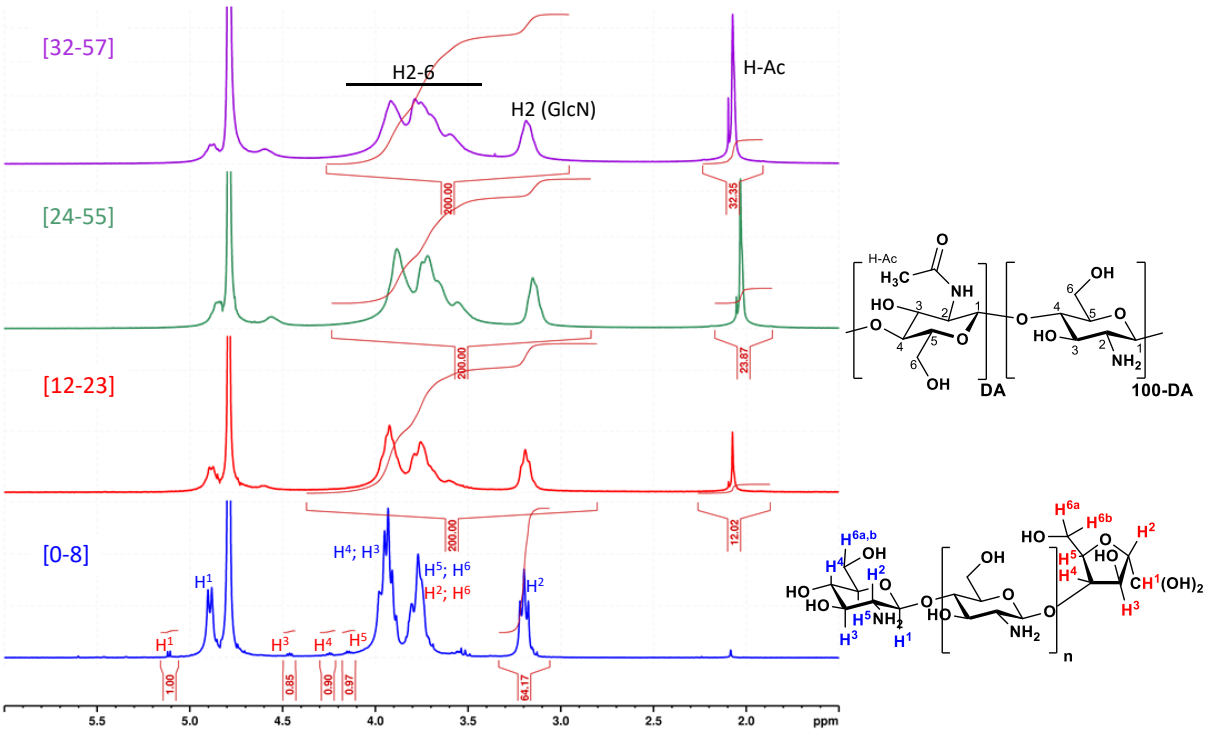

Figure 4.2-3. H^1 NMR spectra of the chitosans used in the study. [0-8] (blue) with a DA < 1%, [12-23] (red), [24-55] (green) and [32-57] (purple).

The mass-average molar mass (M_w), the number-average molar mass (M_n) and the dispersity (Đ) of the COS and chitosans were determined by high-performance size exclusion chromatography (SEC) (UltiMate 3000 HPLC, Thermofisher, Waltham, MA, USA) with a multiangle laser light scattering detection (MALLS) (Dawn Heleos, Wyatt, Santa Barbara, CA, USA) operating at λ_0 = 658 nm and a differential refractive index detector (Optilab rEX, Wyatt) operating at the same wavelength. The four chitosans, the chitosan [0-8] and the longer chitosans, [12-23], [24-55] and [32-57] were separated on two serially connected columns (Tosoh TSK gel columns, G5000PWXL & G4000PWXL, Tokyo, Japan) (Figure 4.2-4). A

degassed 0.3 M acetic acid/0.2 M sodium acetate buffer (pH 4.5) was used as eluent after filtration on a 0.22 µm pore size membrane (Millipore). The flow rate was maintained at 0.6 mL/min, and the amount of sample injected was 100 µL at a concentration of 5 mg/mL. The value of the average degree of polymerization of the chitosan samples could be determined using the following equation:

$$DP_n = {M_n}/{[(100 - DA)/100 \times M_{GlcN} + DA/100 \times M_{GlcNAc}]}$$

with M_{GlcN} the molar mass of the glucosamine unit and M_{GlcNAc} the molar mass of a N-acetyl glucosamine unit.

Table 4.2.1. Characterization of chitosan by SEC-MALLS.

Chitosan	DA (%)	M_n (g/mol)	M_w (g/mol)	Đ	DP_n
[0-8][1]	0	8 190	11 970	1.46	49.8[2]
[12-23][3]	12	23 610	34 220	1.45	142
[24-55][3]	24	55 250	95 420	1.73	323
[32-57][3]	32	57 520	101 700	1.77	329

[1]dn/dc value measured previously (0.1801 mL/g)
[2]Corresponds to the number of GlcN units exclusively
[3]dn/dc values based on ref. [13, 21]

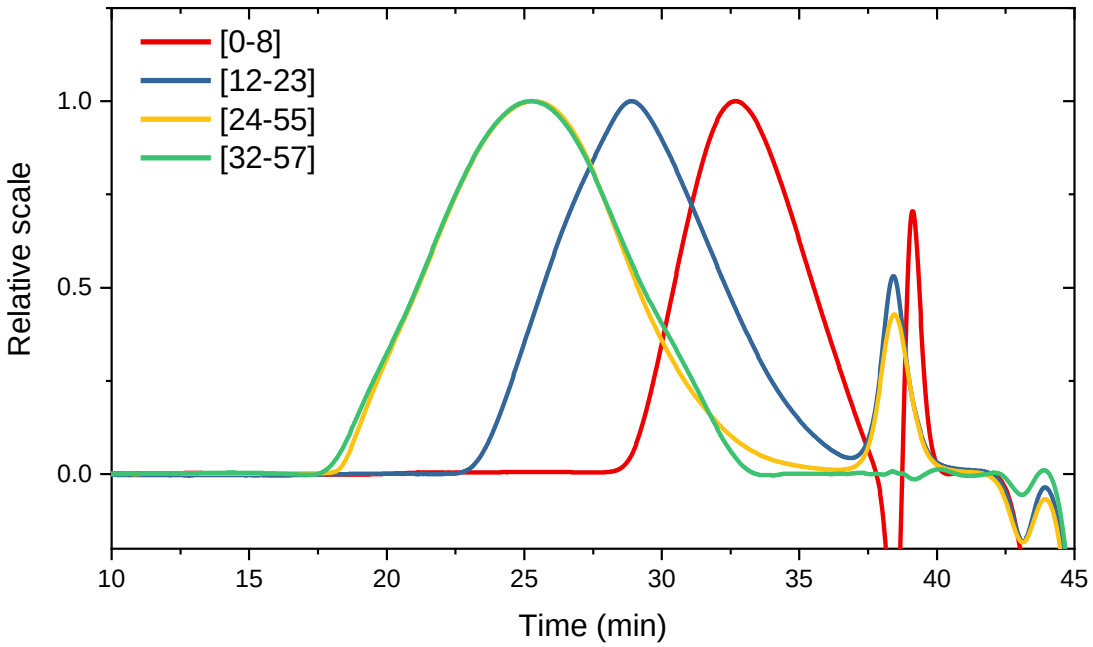

Figure 4.2-4. SEC traces of chitosans [0-8] (red) with a DA < 1%, [12-23] (blue), [24-55] (yellow) and [32-57] (green), the differential refractive index signal is represented.

Potentiometry. The potentiometric titrations of the chitosan samples varying in DP and DA were performed using an automatic pH titrator (TitroLine 7800, SI Analytics, Mainz, Germany) equipped with a microelectrode. The chitosan solutions were prepared at 1 g/L in water with or without added $ZnCl_2$ and the pH was adjusted to 3.0 with HCl 0.1 M to ensure the full protonation of glucosamine residues and introduce an excess of acid in the solution. The titrations were performed with 10 mL of chitosan solution using standard 0.1 M NaOH solution (NIST Standard Concentrate, for Volumetric Analysis, Fisher Chemical, Pittsburgh, PA, USA). The volume of each injection of NaOH was set to 10 µL at a rate of 5 mL/min and the time between each injection was set to 60 s. The apparent values of pK_a were derived from the Henderson-Hasselbalch equation:

$$pK_a = pH + \log\frac{1-\alpha}{\alpha} \quad 4.2$$

With α the degree of dissociation of protonated amines defined as:

$$\alpha = \frac{[-NH_2]}{[-NH_3^+] + [-NH_2]} \quad 4.3$$

$[-NH_3^+]$ can be calculated all along the titration according to the requirement of the electroneutrality in solution:

$$[-NH_3^+] = [Cl^-] + [OH^-] - [Na^+] - [H_3O^+] \quad 4.4$$

Fourier-Transform Infrared Spectroscopy. Infrared spectra were recorded on a Bruker VERTEX 70 spectrometer, equipped with a diamond crystal (GladiATR PIKE technologies) for attenuated total reflection mode (ATR). The spectra were acquired from 4000 to 400 cm^{-1}. 64 scans were acquired for the background and for the sample with a resolution of 4 cm^{-1}. The samples to be analyzed were prepared from a 2.7 g/L chitosan solution [0-8] containing a stoichiometric amount of HCl. 15 mM of $ZnCl_2$ were added in a portion of the solution. The pH was then adjusted between 4 and 6.5 in steps of 0.5 in each solution. After one night under stirring, the solutions were freeze-dried and the powder analyzed by FTIR.

Zeta potential and Dynamic Light Scattering. Zeta potential and DLS measurements were performed at 25 °C with a ZetasizerUltra (Malvern Panalytical Ltd., Malvern, UK) operating at λ = 632.8 nm and a detection angle of 173°. The measurements carried at different pHs were performed with the automatic titrator MPT-2 (Malvern) coupled to the zetasizer.

4.2.3. Results and discussion

4.2.3.1. Chitosan properties

4.2.3.1.1 Electrostatic properties

The electrostatic properties of chitosan were assayed by potentiometric titration. From the titrations it is possible to determine the variation of the pK_a with the dissociation degree (α) as well as the corresponding intrinsic pK_a (pK_0) of chitosan by extrapolating pK_a to α = 1. The protonation rate of the chitosan can also be calculated at each pH value.

Figure 4.2-5.a represents the variation of the apparent pK_a as a function of the degree of dissociation from which we can deduce the values of pK_0 of the chitosans by extrapolating the value of pK_a at α = 1. The values found for the different chitosans are summarized in

Table 4.2.2. It is possible to determine the surface potential of the chitosan, from the variation of the pK_a as a function of α (Equation 4.2) [22]:

$$pH = pK_0 - \log\frac{1-\alpha}{\alpha} + \frac{0.4343}{RT}\left(\frac{\delta G_{el}}{\delta \alpha}\right) \quad 4.5$$

Where pK_0 is the extrapolated pK_a at α = 1, and $\frac{\delta G_{el}}{\delta \alpha}$ is the electrostatic Gibbs free energy change per unit of dissociation degree α. The latter is related to the surface potential ψ_0 by $\frac{\delta G_{el}}{\delta \alpha} = -eN_a\psi_0(\alpha)$ where e is the elemental electric charge and N_a the Avogadro's number.

With the combination of the expressions 4.2 and 4.5, the variation of the surface potential of chitosan as a function of its dissociation degree can be described such as [23]:

$$\psi_0 = \frac{(pK_0 - pK_a)k_BT}{0.4343e} \quad 4.6$$

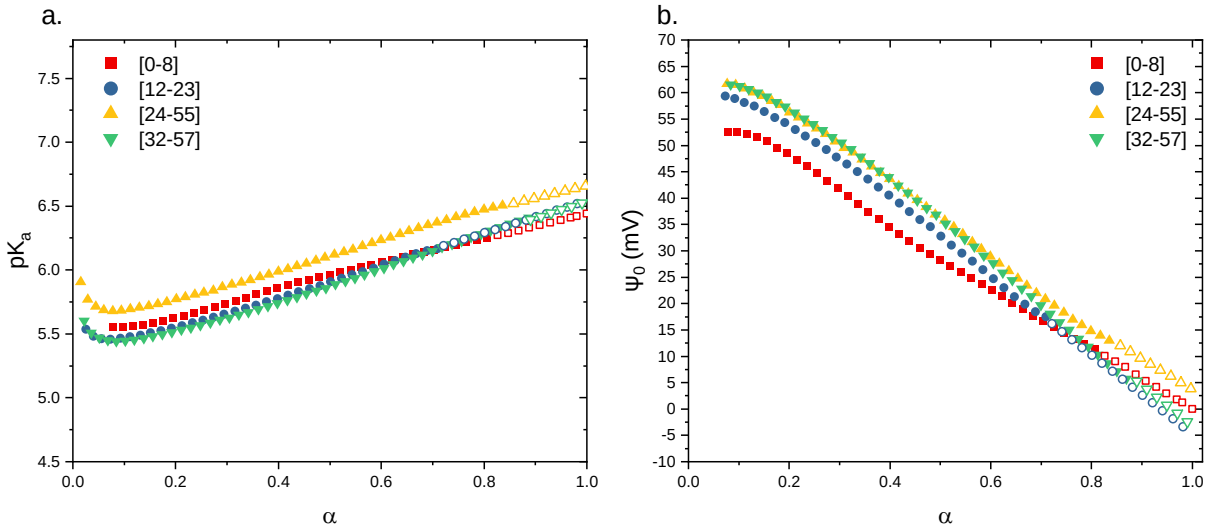

Figure 4.2-5. Variation of the apparent pK_a (a) and surface potentials of chitosan (b) as a function of the degree of dissociation α. The extrapolation at α = 1 gives the pK_0 value of chitosan.

This increase in the pK_a values with the dissociation degree is consistent with the literature and confirms the polyelectrolyte nature of the four chitosans. The increase in pK_a is linear which emphasizes the absence of conformational transition in the course of the titration. However, the precipitation of the polymer at α > 0.6-0.7 did not allow to accurately determine the pK_a at high dissociation degrees. Hence, it was necessary to extrapolate those values for values of α approaching 1 based on the linear part of the curve. Unfortunately, the evolution of the pK_0 found as a function of the acetylation degree was not entirely consistent with previous findings [15, 24] as it usually increases with the DA, due to a decrease of the charge density along the chains. For instance, the chitosan [24-55] has a relatively high pK_0 compared to the others. This result can be explained by the chitosans of different origin used in this study and also the variety of molar mass and DA.

It can also be noted that the surface potential of chitosan decreased with the deprotonation of the amino groups (Figure 4.2-5.b) as expected for a polybase. This potential is also sensitive to the acetylation degree of the chitosan, an acetylated chitosan presenting a higher surface potential at early stage of the titration.

Table 4.2.2. pK_0 of chitosans from potentiometric titrations.

Chitosan	DA (%)	M_n (g/mol)	pK_0
[0-8]	0	8 190	6.44
[12-23]	12	23 610	6.5
[24-55]	24	55 250	6.65
[32-57]	32	57 520	6.56

From the titration data, the value of the protonation rate (γ) can be calculated all along the titration such as:

$$\gamma = \frac{[-NH_3^+]}{[-NH_3^+] + [-NH_2]} \quad 4.7$$

Figure 4.2-6 shows the variations of γ as a function of the pH. Both the Figure 4.2-5.a and Figure 4.2-6 showed the effect of DA on the electrostatic properties of chitosan. Indeed, the increase of the DA induced a higher cationicity as seen by the increase of the pK_0 values for acetylated chitosans as compared to the fully deacetylated [0-8]. This might be explained by the decrease of the charge density on the chitosan chains with the increase of the DA in combination with an increase of its hydrophobic character. However, it was demonstrated in the chapter 2 that the chain length also plays an important role on the protonation rate of chitosan, namely that the protonation decreased with the increase of the chain length [25]. Since the effect of DA and molar mass on the protonation state of chitosan varies in opposite directions, it is difficult to predict the acid-base behaviour of the polymer for a series of chitosan where these two parameters evolve.

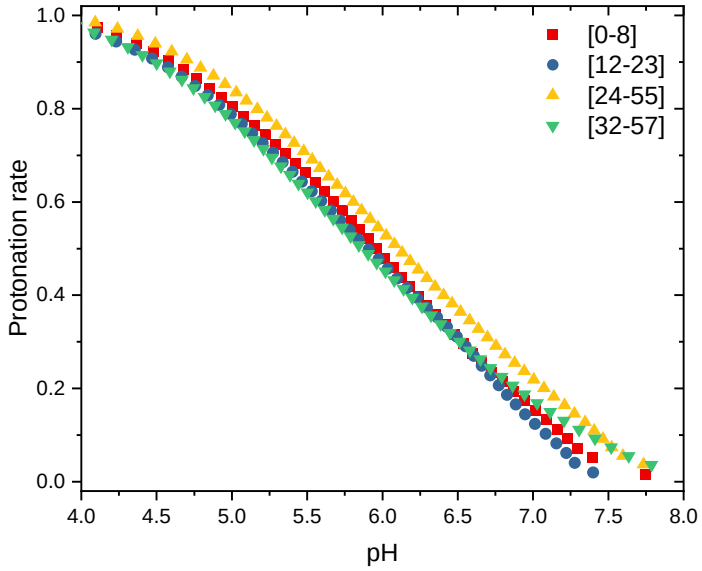

Figure 4.2-6. Protonation rate of chitosan as function of the pH.

4.2.3.1.2 Solubility behaviour

The solubility of the chitosans as a function of the pH was evaluated by light scattering. As seen previously, light scattering is a very sensitive technique to characterize the solubility state of a polymer in comparison to transmittance. Figure 4.2-7 indicates that the higher the DA of the chitosan, the larger the pH solubility as confirmed from previous studies [24].

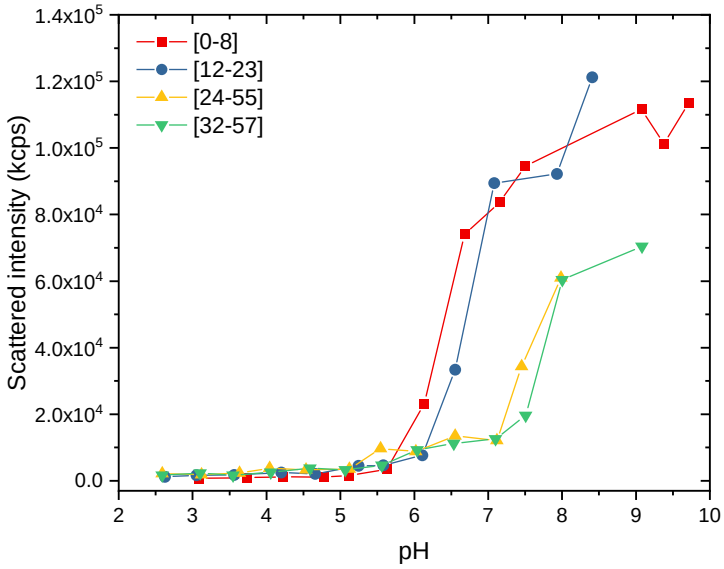

Figure 4.2-7. Scattered intensity of chitosan solutions at 1 g/L as a function of pH.

The apparent solubility of chitosan is also dependant of the chain length, especially for chitosan oligosaccharides [26]. Then, with four chitosan samples varying both in chain length and DA, no specific trend can be really drawn.

4.2.3.2. Interaction with zinc

4.2.3.2.1 Potentiometric titrations

Based on the work of M. Rhazi et al. [27], we tried to evidence the interaction between zinc ions and the glucosamine residues of the chitosans by means of potentiometric titrations. The formation of a complex between chitosan and zinc ions can be described as an interaction between a Lewis base (chitosan), giving a pair of electrons to the Lewis acid (Zn^{2+}). More specifically, it is assumed that only the free amino groups on the glucosamine units can form a complex with the metallic ions.

The reaction between chitosan and zinc ions can be simply expressed as:

$$-NH_2 + Zn^{2+} \rightarrow (complex)^{2+} \quad 4.8$$

Considering also the acid-base equilibrium of chitosan in water:

$$-NH_3^+ + H_2O \rightleftharpoons \ -NH_2 + H_3O^+ \quad 4.9$$

And by combining equations 4.8 and 4.9, the reaction between the amino groups of chitosan and zinc ions is:

$$-NH_3^+ + Zn^{2+} + \ H_2O \ \rightarrow (complex)^{2+} + H_3O^+ \quad 4.10$$

Then, it might be expected that protons are released upon the formation of the complex. Figure 4.2-8, representing the titration curves of the chitosan [0-8] alone or in the presence of zinc (Zn:N = 0.5) shows indeed a lower pH in presence of zinc for the same amount of NaOH introduced, suggesting the formation of the complexes with the release of protons.

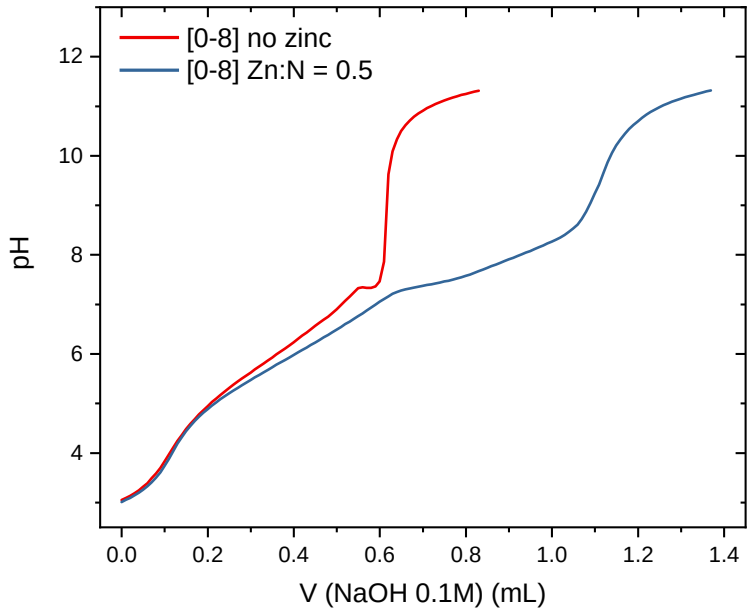

Figure 4.2-8. Titration curve of a chitosan [0-8] solution at 1 g/L by 0.1 M NaOH with (blue) and without (red) addition of $ZnCl_2$.

Based on previous works [27–30], the complexation can be described as follow:

$$M + L \rightleftharpoons ML \tag{4.11}$$

And in a more general way for a complex involving more ligands:

$$ML_{n-1} + L \rightleftharpoons ML_n \tag{4.12}$$

With M the metal (Zn) and L the ligand ($-NH_2$). Hence the complexation constant K_n is expressed as:

$$K_n = {[ML_n]}/{[ML_{n-1}][L]} \tag{4.13}$$

And

$$\log K_n = -\log[L] + \log\left({[ML_n]}/{[ML_{n-1}]}\right) \tag{4.14}$$

In the literature, -log[L] is also written as pL. The final expression is then:

$$pL = \log K_n + \log([ML_{n-1}]/[ML_n]) \tag{4.15}$$

Moreover, it is possible to evaluate $\bar{n}$, the average number of ligands per metal atom:

$$\bar{n} = \frac{Total\ concentration\ of\ ligand\ bound\ to\ metal}{Total\ concentration\ of\ metal} \tag{4.16}$$

Which can be expressed:

$$\bar{n} = ([L]_t - [L] - [LH^+])/[M]_t \quad 4.17$$

With $[L]_t$ the total concentration of ligand in the system, [L] the concentration of free ligand and $[LH^+]$ the concentration of free ligand under its protonated form.

More precisely, the equation 4.17 can be written for the chitosan-Zn^{2+} system as:

$$\bar{n} = \frac{([-NH_2]_t - [-NH_2] - [-NH_3^+])}{[Zn^{2+}]_t} \quad 4.18$$

With $[\text{-}NH_2]_t$ the total concentration of amine groups and $[\text{-}NH_3^+]$, $[\text{-}NH_2]$, $[Zn^{2+}]_t$ the concentration of protonated and deprotonated amines and the total concentration of zinc ions.

The total concentration of amine groups can be known from the weighted amount of chitosan in solution while the concentration of protonated amine groups can be deduced from the conservation of the electroneutrality in solution by considering the concentration of each ions in solution all along the titration (NH_3^+, H^+, OH^-, Cl^-, Na^+ and Zn^{2+}). Finally, $[\text{-}NH_2]$ can be calculated from the pK_a of the chitosan. For the purpose of this method, an important approximation is made, namely we consider that the pKa in equation 4.19 is equal to the pK_0 of chitosan, that is, the dissociation constant of an isolated glucosamine residue [27]. Hence:

$$[-NH_2] = \frac{K_a[-NH_3^+]}{[H_3O^+]} \quad 4.19$$

With $K_a = 10^{-pK_a}$ and $[H_3O^+] = 10^{-pH}$.

Therefore, the total concentration of ligand bound to metal in the expression of $\bar{n}$ corresponds to the amount of ligand that is not directly titrated but involved in the complexation of Zn^{2+}.

It is possible then to obtain, as referred in the literature, the 'formation curve' of the complexes as a function of pL or the pH (Figure 4.2-9). The stability constant of the complexes can be extrapolated graphically using a method described by H. Irving and H. Rossoti [31] (Figure appendix 11). Note that the curves deviate from their regular shape for pH values near 6. An early study demonstrated that an excess of ligand compared to zinc could form a complex of the form ZnL_2 for a ratio Zn:N = 0.1 [28]. The variation of this ratio was not investigated here. Instead, a ratio Zn:N of 0.5 was chosen for three reasons:

- A larger amount of zinc would impose the introduction of an important volume of NaOH for the neutralisation of the solution and involve an important dilution of the system

- Variations in the neutralisation curves with smaller amount of zinc would have been difficult to observe and analyse
- Such ratio is within the range of ratios investigated in the next part of the study dedicated to improving the complex stability

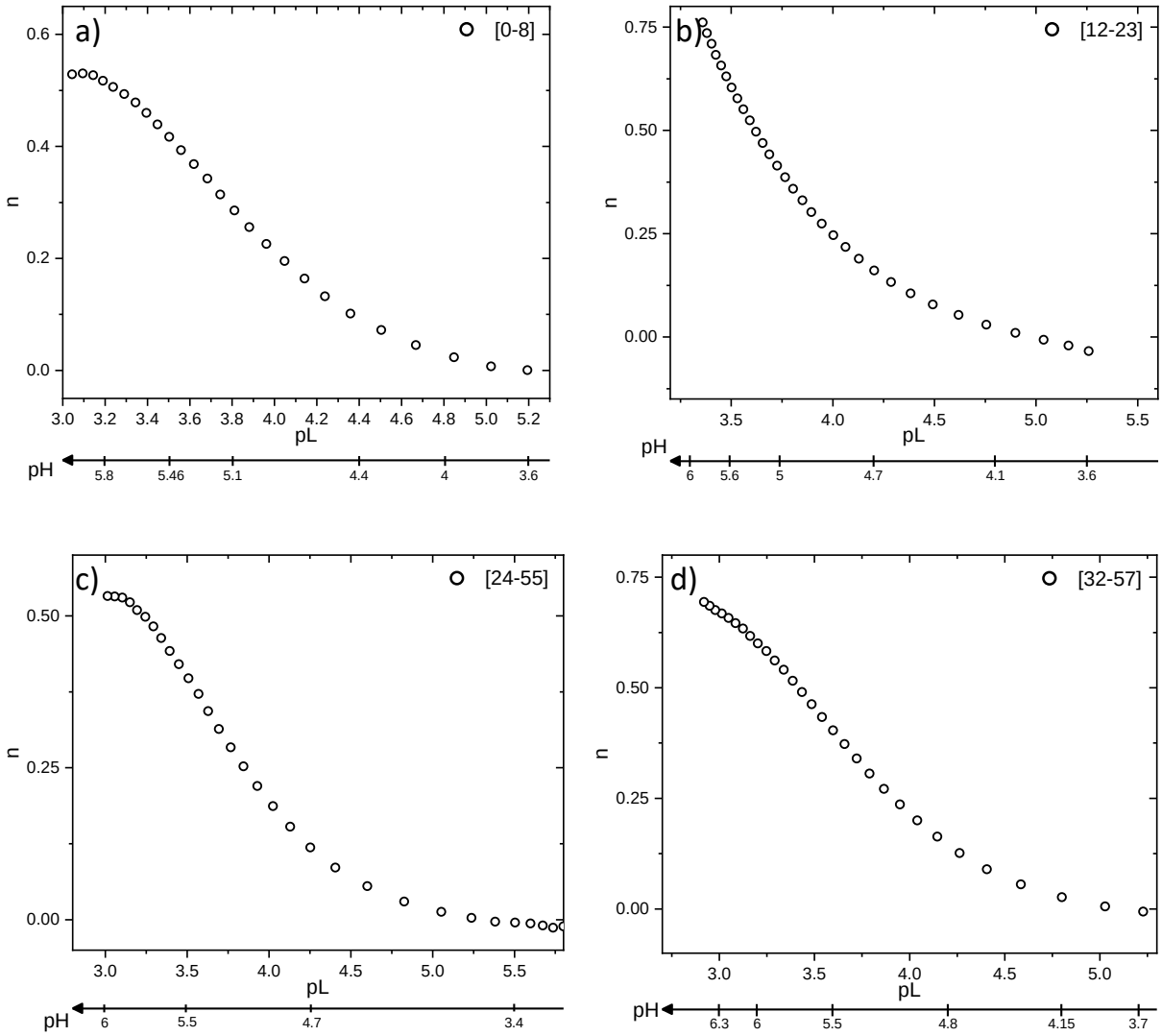

Figure 4.2-9. Variation of n̄ as function of pL from the titration of chitosan with Zn:N = 0.5 : a) [0-8], b) [12-23], c) [24-55], d) [32-57].

All the chitosans studied show an affinity towards zinc with the formations of complexes of the type $[Zn(\text{-}NH_2)]^{2+}$ with a maximum of amino groups involved at a pH around 6, consistent with the literature [28]. Note that $\bar{n}$ only denotes an average number of ligands complexing a metallic atom. Here, $\bar{n}$ tends toward 1 which means that the complex involves one Zn^{2+} ion per amino group. This type of complexes can only be described with the pendant model, as seen in Figure 4.2-10 with zinc adopting a tetrahedral conformation.

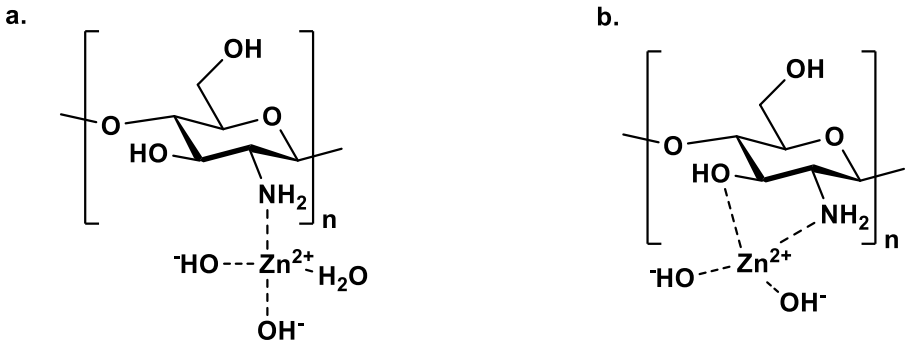

Figure 4.2-10. Structure of the complex chitosan-Zn^{2+} described by the pendant model involving a) a water molecule b) the closest oxygen atom.

The complexation constants between glucosamine residues and zinc ions are reported in the Table 4.2.3. They were determined from the following equation, based on the graphical interpolation of pL at half $\bar{n}$ values [31] (Figure appendix 11):

$$\log K_n = pL_{n-\frac{1}{2}} \qquad 4.20$$

Table 4.2.3. Complexation constants determined graphically from the formation curves of the zinc-chitosan system (Zn:N = 0.5).

Chitosan	K_1 (M^{-1})
[0-8]	**1.8×10^3**
[12-23]	**4×10^3**
[24-55]	**1.8×10^3**
[32-57]	**2.5×10^3**

The constant of complexation is not influenced by the DA since all the K_1 values found are in the same order of magnitude. Moreover, in this study, we considered only a ratio Zn:N = 0.5. As mentioned previously, the introduction of a larger amount of ligand can favour the formation of a complex involving 2 ligands for one Zn^{2+}. However, it was demonstrated that the constants of complexation for the formation of the complex $[Zn(-NH_2)]^{2+}$ were almost not dependent on the amount of ligand introduced [28].

Potentiometric titrations can be also used to estimate the constants of complexation but some approximations were necessary for the treatment of the experimental data such as the need to set the apparent pK_a to a constant value for the formation of the chitosan-Zn^{2+} complex.

4.2.3.2.2 Fourier-Transform Infrared spectroscopy

FT-IR spectroscopy is an appropriate technique to study the interaction between the amino groups of chitosan and zinc ions. Here, the chitosan [0-8] was chosen because it gives a simple IR spectrum thanks to the absence of acetylated units (DA < 1%). The interaction between zinc ions and chitosan was studied at different pHs. For this purpose, 5 solutions of the chitosan [0-8] were prepared at 2.7 g/L. Each of these solutions was adjusted to a different pH: 4, 5, 5.5, 6 and 6.5 and freeze dried after one night under stirring. The same solutions were prepared with 15 mM of Zn^{2+}, corresponding to a ratio Zn:N = 10.

The peak at 1070 cm^{-1} was chosen as reference peak since it corresponds to the C-O stretching of the glucosamine ring which must remain unchanged whatever the DA and the conditions. First it was seen on the IR spectrum of the chitosan alone that the absorbance of the $-NH_2$ band at 1502 cm^{-1} decreases when the pH increases [32]. It is contradictory with the previous observations of J. Brugnerotto et al. [33] who stated the invariance of this band according to the degree of protonation of the sample (Figure 4.2-11). This band is attributed to the Amide II band usually observed at 1590 cm^{-1} of a common chitosan spectra. A fully deacetylated chitosan shouldn't present an amide I band, corresponding to the C=O function carried by an acetylated unit. However, the chitosan [0-8] analysed here, present a peak at 1605 cm^{-1} which can be attributed to the C=O bond of the aldehyde on the 2,5-anhydro-D-mannofuranose terminal unit, specific of a chitosan oligosaccharide. The attribution of these peaks is reported in Table 4.2.4.

Table 4.2.4. Peak positions and assignment of main absorption bands of chitosan [0-8] by FTIR.

Origin	Wavenumber (cm^{-1})	Assignment
C-O stretching	1070	C_6-OH of the glucosamine ring
C-O-C stretching	1153	Glycosidic linkage
C-N stretching	1250	C-N bond of the glucosamine residues
C-H rocking	1380	
NH_2 bending	1502	Primary amine of the glucosamine residues
C=O stretching	1605	Aldehyde of the terminal AMF unit (non-hydrated form after freeze-drying)

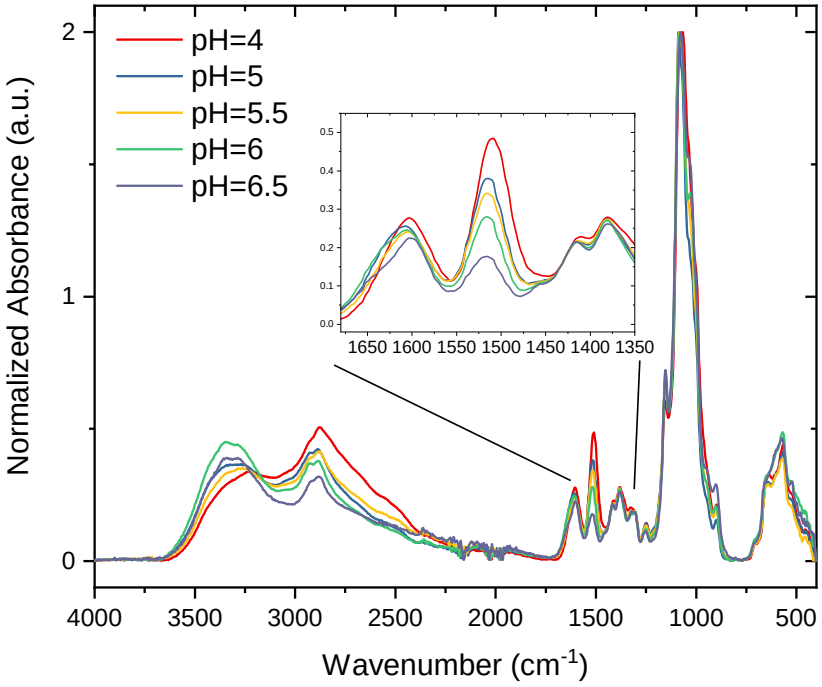

Figure 4.2-11. FTIR analysis of the freeze-dried chitosan [0-8] at various pHs.

This evidences the correspondence of this peak to the -NH_2 groups. Moreover, it is affected by the protonation state of the chitosan and is therefore expected to be modified after the

chelation with Zn^{2+} ions. Indeed, the chitosan [0-8] which has been freeze-dried at different pHs in presence of an excess of zinc (Zn:N = 10) showed an interesting infrared spectrum.

First, the spectra of the chitosan [0-8] in presence of zinc demonstrates the same sensitivity upon deprotonation, illustrated by the decrease in intensity of the band corresponding to the - NH_2 groups (Figure 4.2-12).

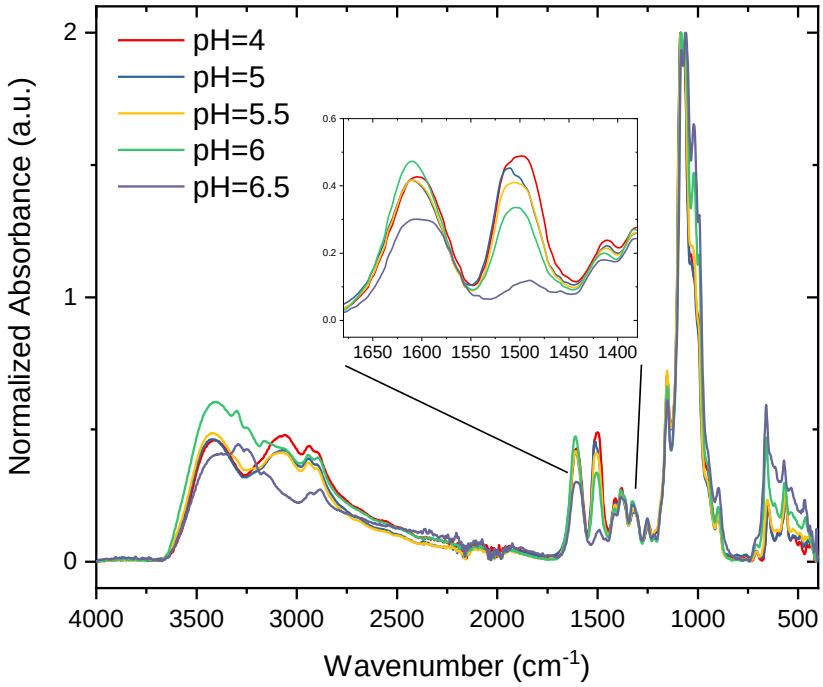

Figure 4.2-12. FTIR analysis of the freeze-dried chitosan [0-8] at various pHs at Zn:N = 10.

Moreover, if we compare at a same pH, the spectrum of chitosan [0-8] with and without zinc, a shift of the band sensitive to the deprotonation state can be observed. Indeed, this band at 1502 cm^{-1} attributed to the -NH_2 bending of the glucosamine units not only decreases in intensity with the increase of the pH but also shifts gradually towards lower wavenumbers with the modification of the pH in the presence of zinc (Figure 4.2-13). This can be interpreted as a clear evidence of the zinc chelation by the -NH_2 groups of the chitosan [0-8] upon deprotonation.

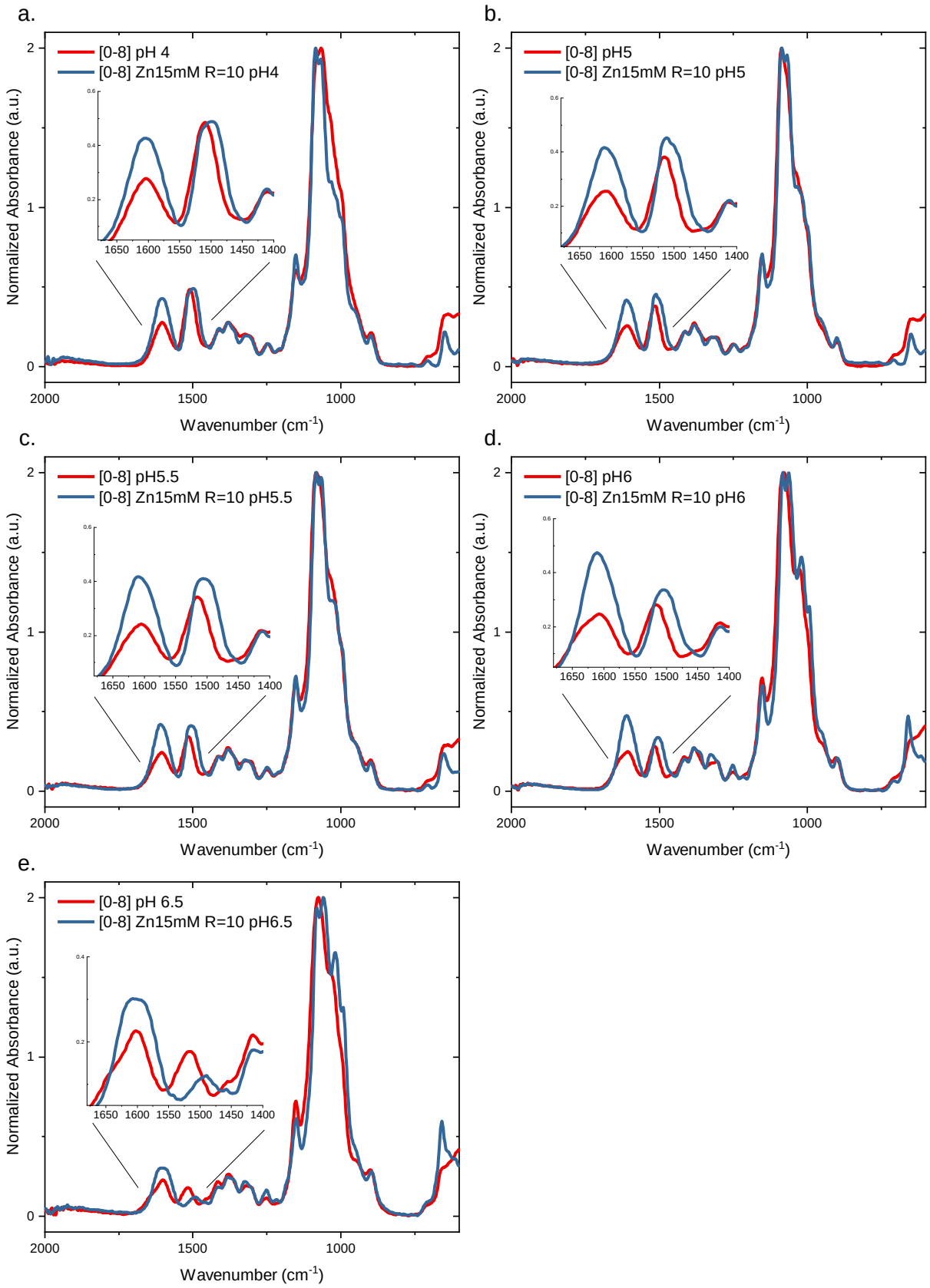

Figure 4.2-13. Infrared spectra of chitosan [0-8] solutions freeze dried at various pH in the presence (blue) or absence (red) of zinc. a) initial pH=4, b) pH=5, c) pH=5.5, d) pH=6 and e) pH=6.5.

4.2.3.2.3 Solubility behaviour of chitosan in presence of zinc

The solubility of chitosans was assayed in presence of zinc at various pHs. We expect that thanks to the chelation of zinc, the cationic state of chitosan could persist on a larger range of pH and hence allowing an apparent solubility at physiological pH. The solubility assay was performed in similar conditions than as the potentiometric titrations. The solutions of chitosan were prepared at 1 g/L with the right amount of zinc to reach a Zn:N ratio of 0.5 taking into account the acetylation degree of chitosan determined by H^1 NMR. The solutions were then adjusted at various pH thanks to the automatic titrator coupled with the DLS instrument.

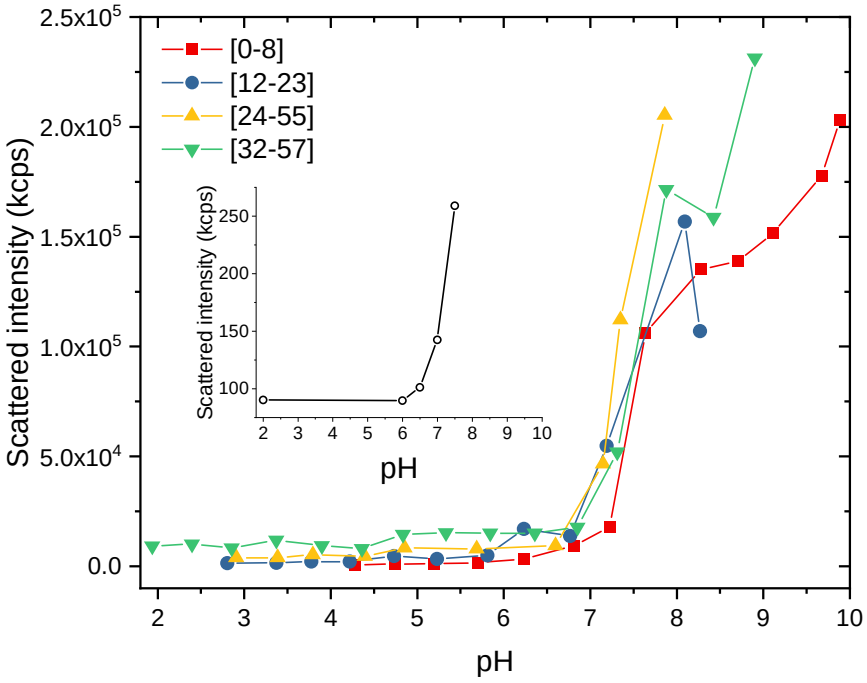

Figure 4.2-14. Scattered intensity of chitosan solutions in presence of zinc (Zn:N=0.5) at various pHs. Inset: scattered intensity of a 6 mM $ZnCl_2$ solution at various pHs.

Figure 4.2-14 represents the scattered intensity of chitosan solutions as function of pH. No clear trend can be extracted: it seems that all solutions present a similar critical pH of solubility around 7. However, compared to the chitosans alone in solution (Figure 4.2-7), we can notice that the apparent solubility of chitosans [0-8] and [12-23] is enhanced in presence of zinc whereas the solubility of chitosans [24-55] and [32-57] is not modified. However, we have to take into account the fact that zinc ions themselves present a critical pH of solubility around pH = 7 due to the formation of hydroxides, even at low concentrations (inset Figure 4.2-14). One can suppose that the presence of zinc enhances the solubility of chitosan as seen for [0-8] and [12-23] but the precipitation of Zn^{2+} at higher pHs masks the beaviour of

chitosans [24-55] and [32-57]. Thus, one cannot fully conclude on the role of Zn^{2+} on the solubility of chitosan at high pHs.

4.2.3.2.4 Zeta potential of chitosan

With the goal to determine if chitosan could keep a certain cationicity at high pHs thanks to the addition of zinc, zeta potential measurements of chitosan solutions with or without added $ZnCl_2$ were performed. The zeta-potential of chitosan is expected to decrease upon deprotonation in the same manner as the surface potential seen earlier (Figure 4.2-5.b) [34]. From Figure 4.2-15, we can observe for low DAs ([0-8] and [12-23]) a clear effect of the addition of zinc on the zeta potential. Indeed, compared to the measurements done without zinc, much higher values of zeta potential were found for chitosan solutions in presence of zinc at pH > 7.

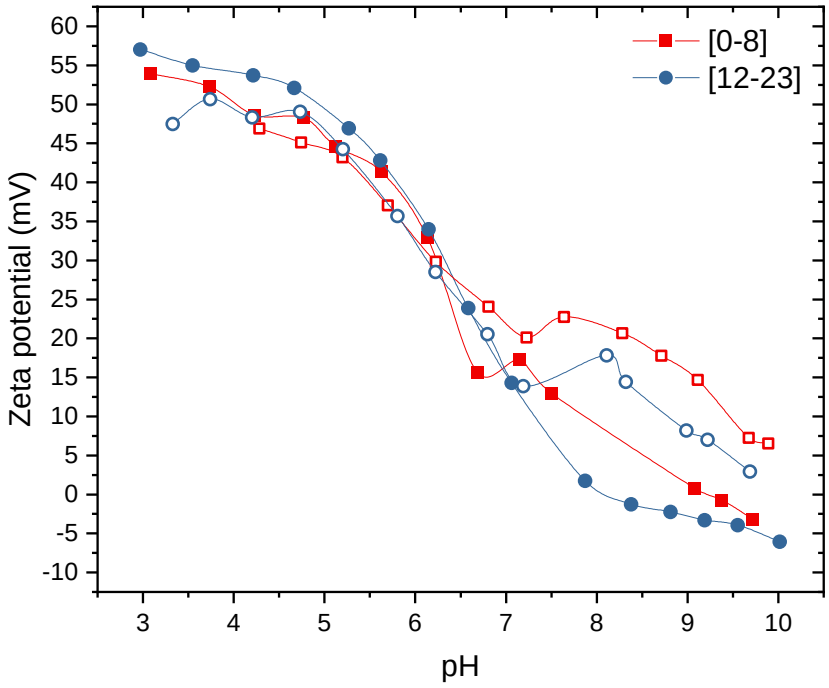

Figure 4.2-15. Zeta-potential measurements of chitosans [0-8] and [12-23] solutions at 1 g/L at various pHs (closed symbols) and with addition of $ZnCl_2$ (Zn:N = 0.5) (open symbols).

However, the effect of Zn^{2+} was less pronounced for chitosans of higher DAs (Figure 4.2-16) where a similar decrease of the zeta-potential was observed with and without added $ZnCl_2$. This might simply be explained by the decrease in the density of amino groups along the chitosan chain when he DA increases.

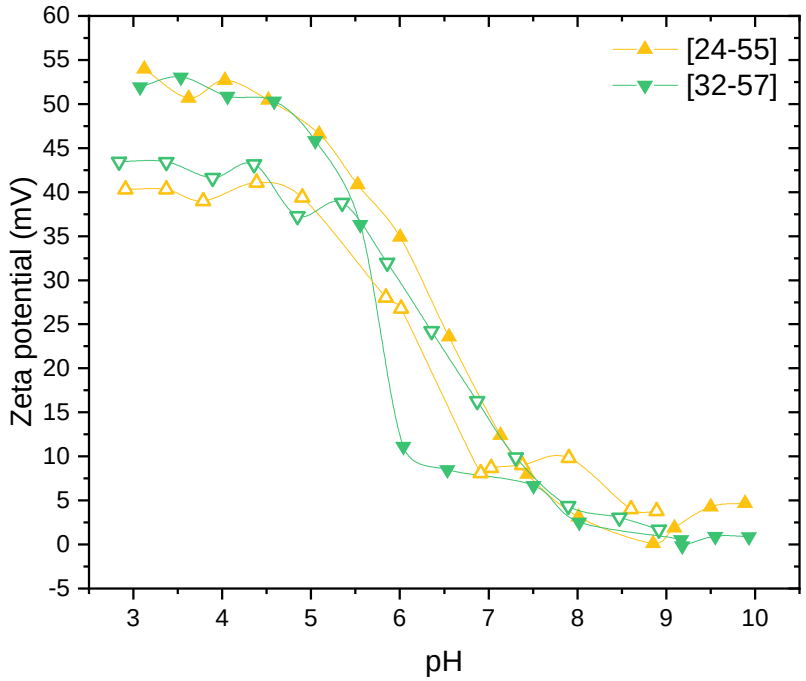

Figure 4.2-16. Zeta-potential measurements of chitosans [24-55] and [32-57] solutions at 1 g/L at various pHs (closed symbols) and with addition of $ZnCl_2$ (Zn:N = 0.5) (open symbols).

4.2.4. Conclusion

The interaction between chitosan and metallic ions has been studied for many decades. However, the interaction has been mainly studied in the case of transition metals considered to be pollutants in water such as copper, manganese, iron, etc. Here, the interaction with zinc was considered. Zinc is not always considered as a transition metal according to the IUPAC definition [35]. Indeed, in contrast to transition metals, it possesses a complete *d* sub-shell and only forms cations by involving its *s* sub-shell electrons. It was found by potentiometric titration that ZnL-type complexes were formed between amino groups and Zn^{2+} at Zn:N = 0.5. The interaction was also evidenced by Fourier-transform infrared spectroscopy as well as dynamic light scattering and zeta-potential measurements to a certain extent. It was indeed possible to observe the effect of the introduction of zinc ions on the solubility behaviour of chitosan, especially for the chitosans of low DA. This effect was also detected by zeta-potential measurements in presence of zinc where the conservation of a cationicity at increasing pH was observed for chitosans of low DA.

4.3. Towards an improved stability of the chitosan-siRNA complexes

4.3.1. Introduction

Sometimes eluded in the literature but usually evidenced, the lack of stability of chitosan-siRNA complexes in physiological conditions is a major drawback. This lack of stability is mostly explained by the cationic nature of chitosan, decreasing with the increase of the pH to the physiological pH near 7.4. This decrease in cationicity lowers the affinity between chitosan and siRNA, leading to an eventual complex dissociation. In addition, the colloidal stability of the complexes, which depends on the excess of charges on their surface, is strongly influenced by the ionic strength of the biological media (= 154 mM), which can therefore also lead to the aggregation and precipitation of the complexes. From the quaternization of amino groups to the PEGylation of chitosan, several routes were investigated to increase the stability of the complexes. Here, the introduction of metallic ions has been considered and more precisely the focus has been made on the role of zinc ions to improve the stability of complexes in physiological conditions.

First, the lack of stability of chitosan-siRNA complexes will be emphasised. Then, the improved stability of the complexes in physiological conditions thanks to the increase of the DA or the introduction of zinc ions will be considered.

4.3.2. Materials and methods

Dynamic Light Scattering and zeta potential. Dynamic Light Scattering measurements were performed with a Malvern ZetasizerUltra (Malvern Panalytical Ltd., Malvern, UK) operating with a laser operating at a wavelength λ = 632.8 nm and the detector at an angle of 173°. The measurements were done on 50 µL of solution in a quartz cuvette. Five measurements at 25 °C were made on each sample. The Z-average hydrodynamic diameters (Z-avg) and polydispersity indexes (PdI) were determined using the cumulant method to analyse the correlation function (g^1). The Z-avg is calculated from the first cumulant (a_1) and the PdI from the second (a_2) such as $PdI = \frac{2a_2}{a_1^2}$. The size distributions were obtained using a non-negative least squares (NNLS) fit, more relevant for polydisperse samples.

Zeta-potential measurements were performed on the same apparatus using the diffusion barrier technique, a convenient technique where only 100 µL of sample are needed. The

capillary cell was filled with the buffer, a 20 mM NaCl solution in order to obtain a minimal conductivity for a reliable measurement and will be considered as the zeta potential measured in water. The 100 µL of sample are introduced with a gel loading tip at the bottom of the cell.

Agarose gel electrophoresis. Agarose gels formed at 3% (w/w) were run at 30 V for 2h in a Tris-HCl buffer (40 mM, pH = 8.4). The buffer was prepared without EDTA in order to avoid the chelation of the zinc introduced in the complexes. 25 µL of the complexes formed with the chitosans [0-8], [12-23], [24-55] and [32-57] and siRNA were mixed with 3 µL of the home-made loading buffer (60% glycerol and Tris-HCl 20mM). 20 µL of the mixture was deposited in the wells such as the final amount of siRNA loaded was 1 µg. The SybrSafe dye was introduced during the preparation of the gel to reveal the presence of siRNA after the run. siRNA alone and complexes formulated with Mg^{2+} instead of Zn^{2+} were used as controls.

Formation of the complexes. In the absence of zinc, the complexes between siRNA and chitosans were formed by adding 50 µL of siRNA at a concentration of 0.1 g/L (6 µM, 0.294 mM in phosphate groups) in 50 µL of the chitosan solution. Chitosan was solubilised in RNase free water with a stoichiometric amount of HCl to ensure the full protonation of the glucosamine residues. The concentration of the chitosan solution was adjusted according to the targeted N:P ratio (N:P = 10) corresponding to the number of amine groups brought by the chitosan varying in DA over the number of phosphate groups. This ratio of N:P = 10 was chosen as it was optimal to form well-defined polyplexes with the chitosan [0-8] (chitosan COS50) as seen in Chapter 2. However, well-defined polyplexes could be obtained at lower ratios (N:P = 3 and N:P = 5) with the longer acetylated chitosans but this won't be discussed (Figure appendix 12). Chitosan solutions were filtered on 0.22 µm mixed cellulose membrane. Since complexes were formed at a ratio N:P > 1, the solution of siRNA was added in one shot with a micropipette in the chitosan solution, so that the component in default is added under stirring to the component in excess avoiding the neutral state at charge stoichiometry. Fast mixing conditions were obtained with a 1.5 mL plastic microtube placed in a VXR basic Vibrax (IKA) set at 1000 rpm.

The formation of complexes in presence of zinc was performed in similar conditions. For a given Zn:P ratio, half of the Zn^{2+} are introduced into the chitosan solution and the other half into the siRNA solution.

The freshly formed complexes were diluted in water (1:1) to use as reference or their stability was checked by diluting one volume of complexes with one volume of salt solution or buffer (Table 4.3.1). The incubation was done under stirring in a 1.5 mL plastic microtube placed in a VXR basic Vibrax (IKA) set at 1000 rpm for at least 30 minutes if not specified longer.

Table 4.3.1. Characteristics of the solutions used for stability tests.

Incubating solution	Concentration before incubation	Final concentration	Ionic strength, pH
NaCl	1.8 % (v/v), 308 mM	0.9% (v/v), 154 mM	154 mM
HEPES pH = 7.4	200 mM	100 mM	50 mM, pH = 7.4
PBS	2X	1X	154 mM, pH = 7.4

Inductively Coupled Plasma / Optical Emission Spectrometry (ICP/OES). ICP/OES analysis of the complexes formulated with zinc was performed on a Varian 720-ES (Agilent, CA, USA) at the Institut de Chimie de la Matière Condensée de Bordeaux (ICMCB). 3 mL of the polyplexes sample was diluted with mQ water into a volume of 25 mL. Calibration curves were obtained from diluted standard solutions of zinc or phosphorous (Initial concentration of 1000 mg/L) with zinc concentrations between 1 mg/L and 15 mg/L and phosphorous concentrations between 0.1 and 1.5 mg/L.

Atomic Force Microscopy. AFM measurements were performed at room temperature in a dry state using a Nanoscope IIIa microscope (Veeco Instruments Inc.). Both topographic and phase images of individual particles were obtained in Tapping Mode™ using rectangular silicon cantilever (AC 160-TS, Atomic Force, Germany) with a spring constant of 42 $N.m^{-1}$, a resonance frequency lying in the 270-320 kHz range and a radius of curvature of less than 10 nm. Samples were prepared by solvent casting at ambient temperature from water solution. A drop (4 µl) of solution was deposited onto freshly cleaved mica and allowed to dry at RT overnight. The complexes were prepared at a siRNA concentration of 0.1 mg/mL and diluted 10 times.

Cell culture. The cell culture tests were conducted on a cell line of Macrophage Murin RAW 264.7 acquired from American Type Culture Collection (USA). The cells were cultured in a Dulbeco's Modified Eagle's Medium (DMEM), supplemented with 10% fetal bovine serum, penicillin G (10 000 units/mL) and streptomycin (10 mg/mL). The cells were maintained in a humidified incubator at 37 °C in an atmosphere of 5% CO_2.

Cell viability. The effect of the formulations on the cell viability has been determined on the cell line RAW 264.7 with the colorimetric MTT assay (3-(4,5-dimethylthiazol-2-Yl)-2,5-diphenyltetrazolium bromide) [36]. For this test, the cells were seeded in 96 well plates at a density of 8.10^3 cells per well and incubated 24h until 80% of confluence was reached. The viability of the cells was assayed with zinc alone and the formulations (siRNA-Zn^{2+} and

chitosan [0-8]-Zn^{2+}). For the formulation siRNA-zinc, the final siRNA concentration was fixed at 100 nM.

After 24h and 48h of incubation, 20µL of MTT solution at 5 mg/mL was added in each well and incubated 1h until the formation of the violet formazan crystals. The crystal formation is the result of the MTT reduction by the metabolically active cells. The cell culture medium was then replaced by 200 µL of DMSO to dissolve the formazan crystals. The absorbance was then measured at a wavelength of 570 nm. The percentage of the cells still viable was calculated as the ratio of absorbance between the treated and untreated cells (control) (Equation 4.19).

$$\%\, cel.viability = \frac{abs\,(cel + treat.) - abs\,(treat. + DMEM)}{abs\ cel\ non\ treat.(control) - abs\,(DMEM)}\ x\ 100 \qquad 4.21$$

4.3.3. Chitosan-siRNA complexes: a lack of stability…

Well-defined complexes of chitosan and siRNA prepared in RNase-free water loss their stability once diluted in HEPES (50 mM; pH = 7.4) or PBS buffer, as shown by the increase of the sizes and count rates in these in comparison to the dilution in water (Table 4.3.2 and Figure 4.3-1).

Table 4.3.2. Characteristics of complexes of siRNA and chitosans [0-8] or [12-23] at N:P = 10 diluted in RNase-free water, in HEPES (50 mM) or PBS 2X (1:1 v:v).

Chitosan	Dispersant for dilution	Z-average (nm)	PdI	Scattered Intensity (kcps)
[0-8]	Water	43.9	0.26	1726
	HEPES 50 mM	2530	0.39	62890
	PBS 2X	2270	0.51	53230
[12-23]	Water	68.6	0.27	2468
	HEPES 50 mM	138.8	0.22	44120
	PBS 2X	99.3	0.07	16660

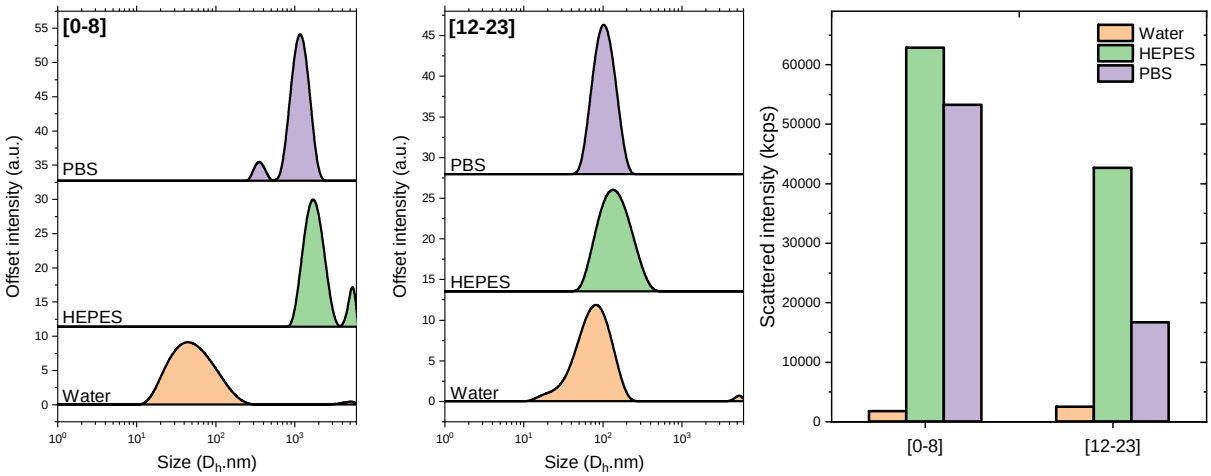

Figure 4.3-1. Particle size distribution and scattered intensities of polyplexes from siRNA and chitosan at N:P = 10: dilution in water (2x), dilution in HEPES buffer (50 mM; pH = 7.4) (2x), dilution in PBS buffer (2x) using chitosans [0-8] and [12-23].

The aggregation of complexes could be due to the high ionic strength of buffers which can screen the stabilizing charges at complex surface. It could be also due simply to a loss of solubility of chitosan at pH 7.4. The fact that a similar aggregation was obtained in both buffers despite their difference of ionic strength (12.5 mM for HEPES and 154 mM for PBS) rather supports a pH-induced aggregation mechanism. In addition, the level of aggregation is much less pronounced for the chitosan [12-23] in relation with the higher pH-solubility of chitosan when the DA increases.

In the following we will examine the effect of the acetylation degree and the introduction of zinc ions on the stability of complexes.

4.3.4. Improved stability under physiological salt conditions, the effect of the acetylation degree

The increase of the acetylation degree of chitosan can enhance the stability of the complexes. However, a lower charge density can also be expected at the surface of complexes as well as a lower affinity with siRNA. We could observe that the increase of the DA results in the increase of the size of the complexes. PECs with a size below 100 nm were obtained with a full deacetylated chitosan whereas PEC with sizes between 100-200 nm were obtained at higher DA (Figure 4.3-2). Broader particle size distributions were also obtained for the acetylated chitosans [12-23] and [24-55]. Besides, the Figure 4.3-2 shows an important effect of the acetylation degree on the stability of the complexes in NaCl 0.9%, i.e., the physiological salt concentration. The size distributions in water and NaCl solutions were very similar in the

case of acetylated chitosans, thus demonstrating a clear effect of the DA on the stability of complexes in physiological conditions. Moreover, the scattered intensities of the PECs with and without added salt become closer when the acetylation degree is increased (Figure 4.3-2.e). The dramatic decrease in the scattered intensity for the chitosan [0-8] (Figure 4.3-2.e) in 0.9% NaCl was due to the precipitation of the complexes. The high salt concentration screens the charges of the stabilizing shell of the complexes.

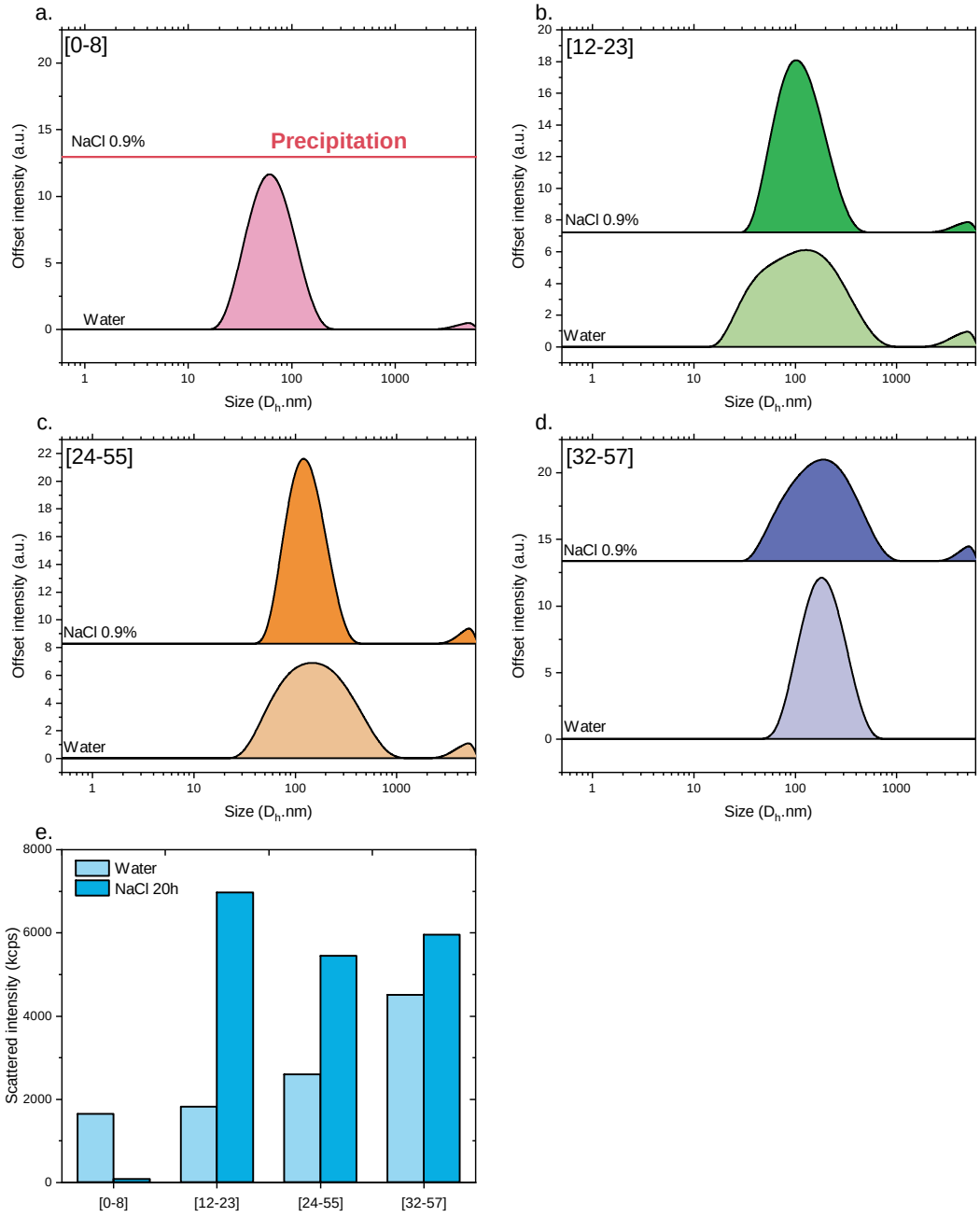

Figure 4.3-2. Particle size distribution (a, b, c, d) and scattered intensities (e) of complexes from siRNA and chitosan at N:P =10. Dilution of the complexes in water (2x) (bottom) or in NaCl 1.8% (2x) (top) for various chitosans a) [0-8], b) [12-23], c) [24-55] and d) [32-57]. Note that the precipitation of the complexes after dilution in NaCl was observed in a).

The stability over the time was also assayed in physiological conditions. More precisely, the complexes were incubated up to 20h in a NaCl (1.8% w/w) solution to reach a final concentration of 0.9%. Three DLS measurements were then performed, after 2h, 3h and 20h (Figure 4.3-3).

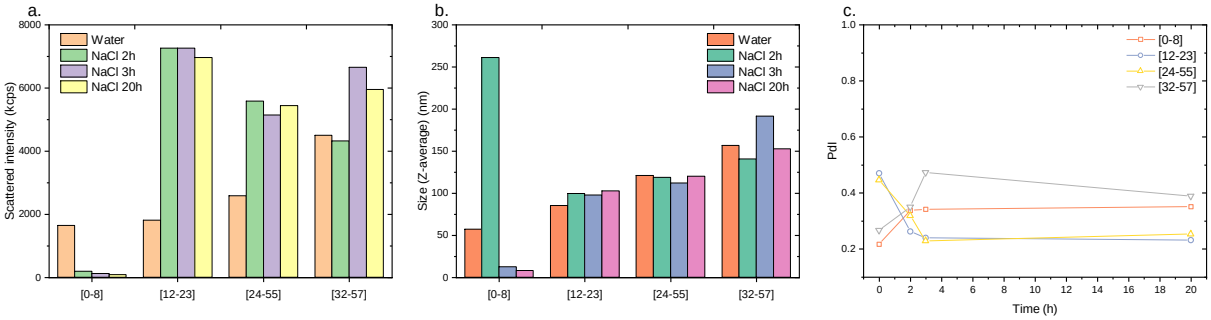

Figure 4.3-3. Assessment of the stability of the siRNA-chitosan complexes (N:P = 10) in physiological salt conditions over 20 hours. a) Scattered intensity of the complexes diluted in water (t_0) and after 2h, 3h and 20h of incubation in a NaCl solution. b) Evolution of the Z-average (in nm) of the polyplexes before incubation in a NaCl solution (diluted in water) and after 2h, 3h and 20h of incubation. c) Evolution of the PdI of the polyplexes with the incubation time in a NaCl solution.

The decrease of the scattered intensity over time for the complexes formed with chitosan [0-8] demonstrates an important lack of stability leading to the aggregation of the complexes. This aggregation induces a decrease in the number of scatterers dispersed in solution hence a lower scattered intensity. For the chitosan [12-23], the complex size slightly increased upon incubation in NaCl, probably due to a slight aggregation of the complexes. The strong increase in scattering intensity observed cannot be explained by the small increase in size but rather by an increase of the osmotic compressibility of the solution due to the charge screening within the complex and at particle surface (Figure 4.3-3.a) [37]. The same tendency was observed for the chitosan [24-55] and [32-57]. The important result is that the complexes based on chitosan having a DA > 10 % were stable in solution at a physiological salt concentration. The Figure 4.3-4 presents the zeta-potential values of the complexes in water. A decrease of the zeta-potential with the increase of the acetylation degree was observed, in relation with the decrease in charge density when the DA increased.

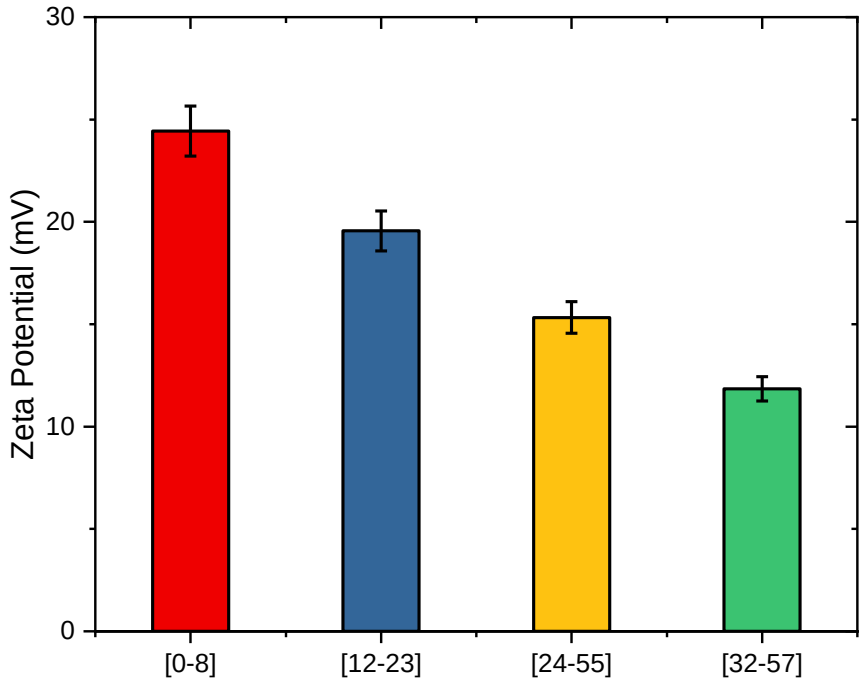

Figure 4.3-4. Zeta-potential of the siRNA-chitosan complexes (N:P = 10) obtained with different chitosan samples using the diffusion barrier method where the cell was filled with a 20 mM NaCl solution and 100 µL of complexes were introduced at the bottom of the cell.

The increase of the stability of complexes in physiological conditions is an important parameter and a great improvement. However, another critical parameter, namely the pH, cannot be settled only with the increase of the DA as seen previously in Figure 4.3-1. Another approach must be considered.

4.3.5. Enhancement of the stability of complexes at physiological pH with zinc ions

It has been shown previously that Zn^{2+} ions can interact both with siRNA and with the amino groups of chitosan upon deprotonation. From these observations, the idea emerged to use zinc ions as an intermediate in the interaction between siRNA and the chitosan's amino groups. This intermediate would allow to preserve the link between chitosan and siRNA at higher pH values. Moreover, the chelation of zinc by the chitosan would eventually also permit to preserve the positive surface charge at physiological pH and therefore enhance the stability of complexes.

4.3.5.1. Influence of the zinc concentration

The concentration of zinc to introduce in the formulation is a crucial factor. A sufficient amount of zinc is necessary to obtain the desired effect on the stability of the complexes but the introduction of an excess could become a problem due to its cytotoxicity. In addition, zinc can start to precipitate at pH = 7 to form zinc hydroxide ($Zn(OH)_2$) [38]. A study on the cytotoxicity of zinc and its association with siRNA and chitosan [0-8] was the starting point to determine the amount of zinc that can be used in the formulations. From this experiment (Figure 4.3-5.b), a cytotoxicity was observed and characterized by a Zn:P ratio (zinc:phosphate groups) larger than 10 for a fixed concentration of siRNA of 100 nM. The cytotoxicity was also found to be related to the concentration of chitosan (Figure 4.3-5.c). It seemed that a maximum concentration of 14.7 mM in amines (N) can be used for a ratio Zn:N = 11.3.

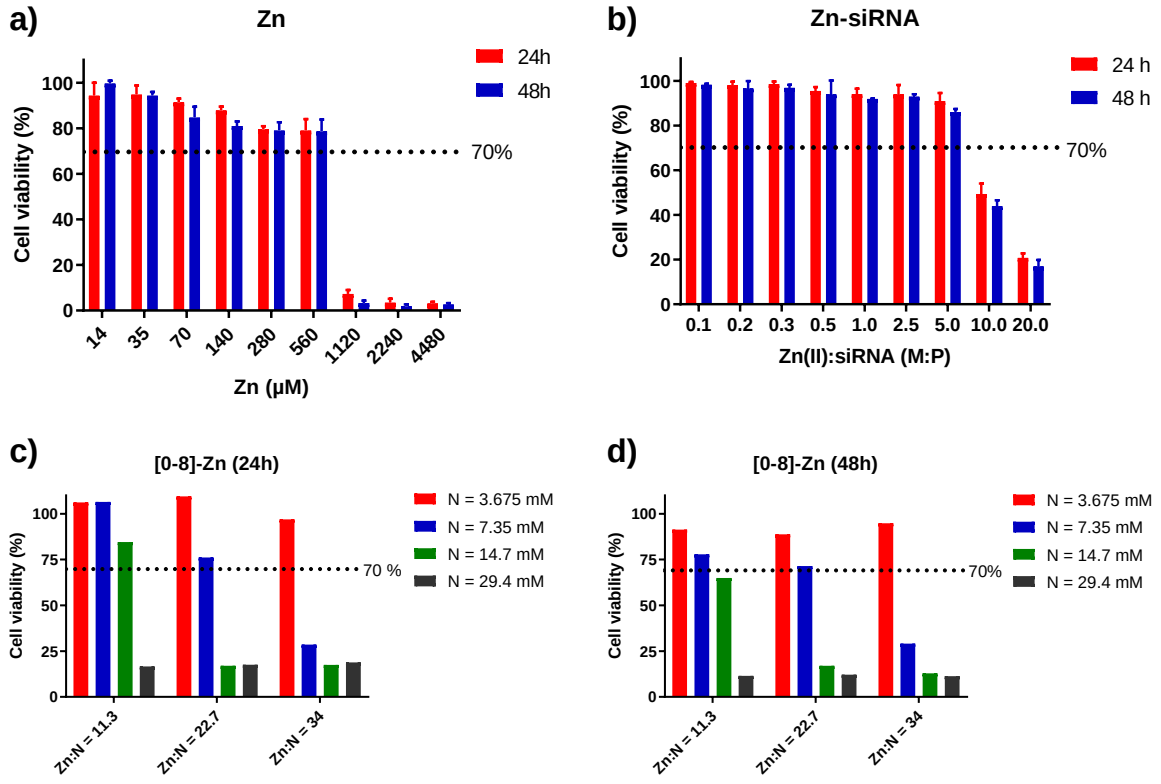

Figure 4.3-5. Cell viability of RAW 264.7 cells in presence of (a) zinc alone after 24h and 48h (n=3) (b) siRNA-Zn^{2+} mixture after 24h and 48h of incubation (n=3) with a siRNA concentration of 100 nM and Zn:P ratios varying from 0.1 to 20, (c,d) mixture of chitosan [0-8] and zinc with concentrations in chitosan amino groups varying from 3.75 mM to 29.4 mM (N:P = 10 and Zn:N = 11.3, 22.7 and 34) after c) 24h of incubation (n=1) and d) 48h of incubation.

The formation of complexes was studied with two zinc concentrations. No noticeable effect of Zn^{2+} ions was detected on the particle size distribution and scattering intensities of the complexes (Figure 4.3-6). Only a slight increase in size and intensity could be seen for the highest zinc concentration (Zn:P = 20) for both chitosans [0-8] and [12-23] (Table 4.3.3).

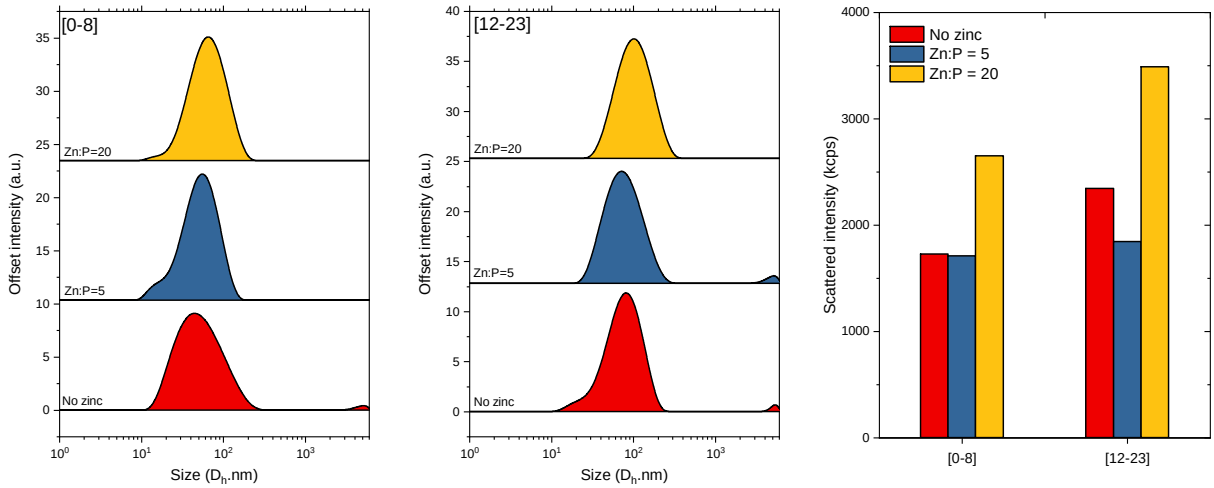

Figure 4.3-6. Particle size distribution and scattered intensities of complexes from siRNA and chitosan at N:P = 10 without zinc (red) and at Zn:P = 5 (blue) and Zn:P = 20 (yellow), using the chitosans [0-8] and [12-23]. The initial preparations were diluted in water (2x).

Table 4.3.3. Characteristics of the complexes (N:P = 10) formed with and without zinc using chitosans [0-8] and [12-23], obtained from the cumulant analysis of the correlation data (Z-average and PdI). The complexes were diluted in water (1:1) before analysis.

Chitosan	**Z-average (nm)**			**PdI**		
	No zinc	Zn:P = 5	Zn:P = 20	No zinc	Zn:P = 5	Zn:P = 20
[0-8]	43.9	43.9	56.7	0.26	0.20	0.20
[12-23]	68.6	66.3	88.5	0.27	0.27	0.25

The stability of complexes in presence of zinc was assayed at physiological pH in order to estimate the minimal amount of zinc to obtain a significant effect on stability. From the Figure 4.3-7, we can evaluate the apparent stability of the complexes once incubated at pH = 7.4 in a HEPES buffer at 50 mM (C_{fin}=25 mM, I = 12.5 mM). The conservation of an apparent stability for the chitosan [0-8], illustrated by a similar PSD after incubation in the buffer could only be achieved with the highest zinc concentration, Zn:P = 20 (Figure 4.3-7.a). In the case of the chitosan [12-23], similar PSD were obtained for the two zinc concentrations with only a minor shift in the distribution of sizes (Figure 4.3-7.c). We therefore concluded that the

combination of the DA and the introduction of zinc led to stable complexes in HEPES buffer at pH = 7.4. A ratio Zn:P = 5 was not enough to obtain the targeted stability whereas a ratio Zn:P = 20 seemed to confer this apparent stability. However, it cannot be excluded that free zinc ions were in solution at this ratio of 20 and that the optimal amount of zinc was in reality between a ratio of 5 and 20.

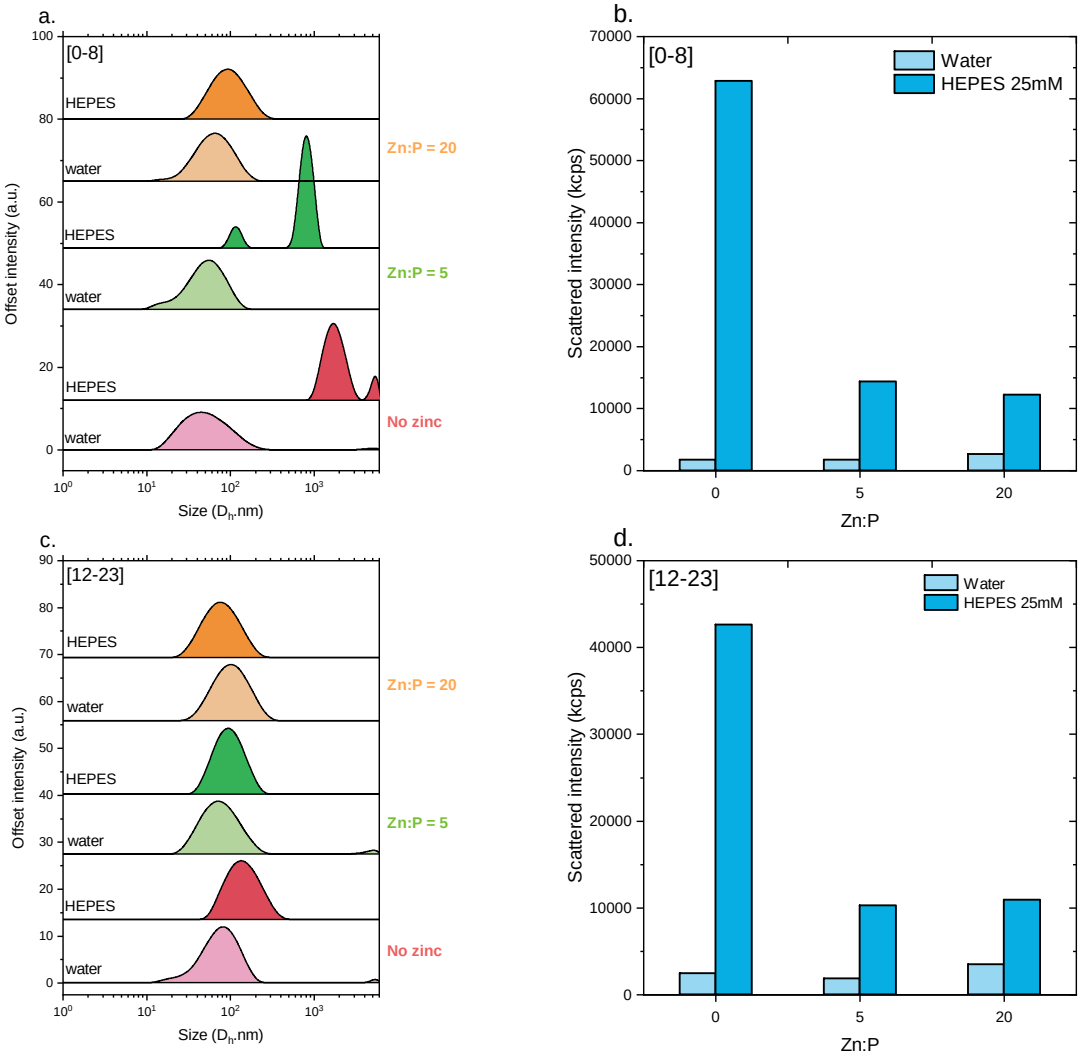

Figure 4.3-7. Particle size distribution (a,c) and scattering intensities (b,d) of polyplexes from siRNA and chitosans [0-8] and [12-23] prepared at N:P = 10 and at two zinc concentrations (Zn:P = 5 in green and Zn:P = 20 in orange). The light colour corresponds to the PSD of the complexes diluted in water (1:1) and the darker one to the complexes diluted in a 50 mM HEPES buffer (pH = 7.4) (1:1).

The Zn^{2+} ions being a potential source of cytotoxicity, a new formulation pathway was set up in order to optimize the concentration of Zn^{2+} ions in the complexes and to remove the excess for the formulation at Zn:P = 20.

4.3.5.2. Optimizing the zinc concentration in complexes

It was demonstrated that the maximum of amino groups involved in the chelation of zinc was found at pH = 6 (Section 4.2.3.2). From this finding, it was decided to form the complexes at a ratio Zn:P = 20 and dialyse them against water adjusted at pH = 6. By doing so, the chelation of zinc with chitosan must be maximized while the excess of zinc ions can be removed Moreover, the dialysis step should allow rearrangements, if any, in the polyplexes structure.

The complexes were formed with the four available chitosans with and without zinc and dialysed. The dialysis step allowed the conservation of a good particle size distribution as represented on Figure 4.3-8 and Table 4.3.4. One can notice that the polydispersity was a bit high for complexes dialyzed at pH = 6 without zinc. This might be explained by a lowering of the affinity between the siRNA and chitosan with the increase of the pH to 6. On the other hand, the low PdI values of the complexes containing zinc after dialysis were a good sign regarding the incorporation of zinc in the complexes.

The zeta-potential of the complexes was also measured before and after the dialysis step (Figure 4.3-8.e and f). Before the dialysis, higher values of potential zeta were obtained in the formulations containing zinc. Moreover, the effect of the DA was still noticeable in presence of zinc as seen by the decrease of the zeta-potential with the increase of the DA (Figure 4.3-8.e). After dialysis at pH = 6 (Figure 4.3-8.f) the decrease of the protonation rate of chitosan in the absence of zinc led to an almost neutral zeta-potential. On the other hand, a positive zeta potential was preserved at pH = 6 thanks to the introduction of zinc ions. However, this was not the case for the complexes formed with the fully deacetylated chitosan, chitosan [0-8] for which the zeta-potential was negative or slightly positive with or without zinc. This may indicate a particular role of the acetylated units in the complexation mechanism of the Zn^{2+} involving the oxygen atom of the amide group [39] which is unexpected regarding the literature [40, 41]. The conservation of a positive zeta-potential is a good sign for further *in vitro* experiments, where the interaction with negatively charged cell membranes could be favoured.

Table 4.3.4. Characteristics of the complexes (N:P = 10) after dialysis (3x) against water at pH 6.

Chitosan	Z-average (nm)		PdI	
	No zinc	Zn:P = 20	No zinc	Zn:P = 20
[0-8]	57.2	97.5	0.22	0.22
[12-23]	85.1	68.6	0.47	0.25
[24-55]	121.1	111.1	0.45	0.28
[32-57]	156.7	222.6	0.27	0.29

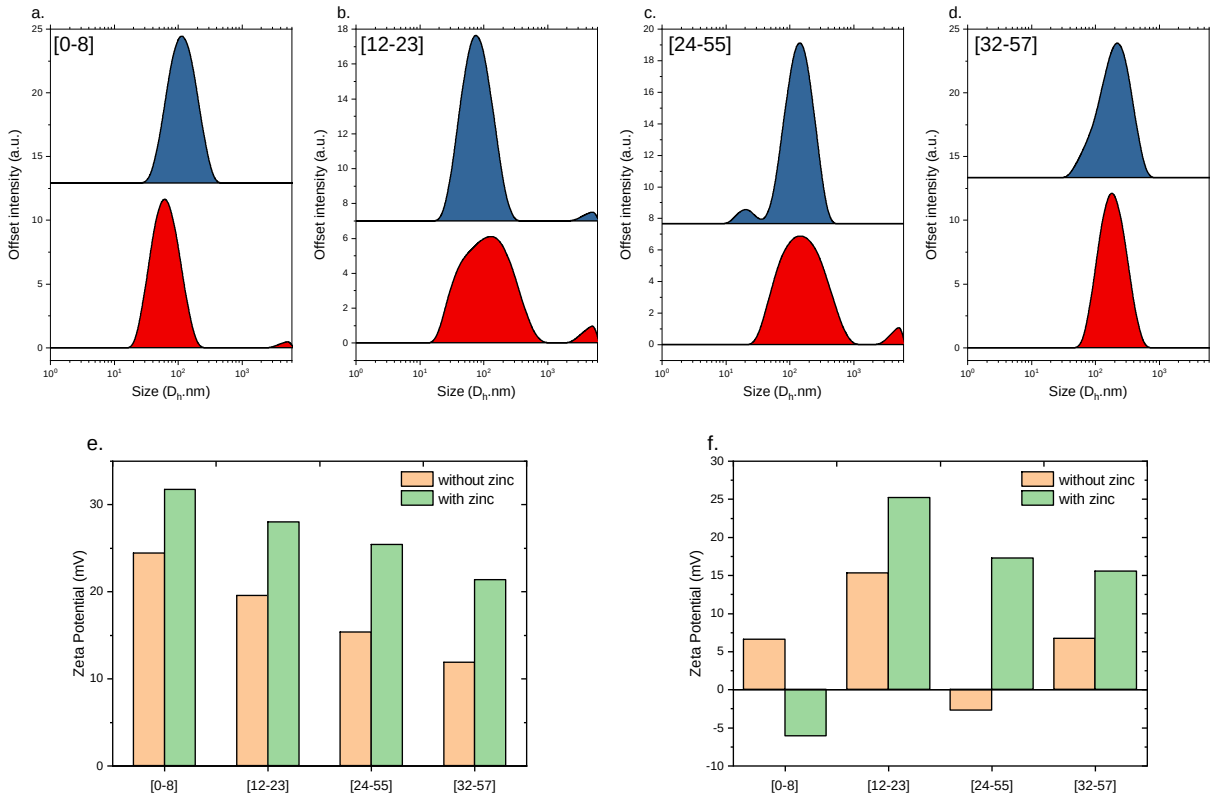

Figure 4.3-8. Particle size distribution of the complexes from siRNA and chitosan prepared at N:P = 10 without zinc (red) or with zinc (blue) at Zn:P = 20 with a) [0-8], b) [12-23], c) [24-55] and d) [32-57] and dialysed three times against water adjusted at pH = 6. Zeta-potential measured with the diffusion barrier technique of the polyplexes formed without zinc (orange) or with zinc (green) e) before dialysis and f) after dialysis at pH = 6.

After dialysis, a first trial was performed to titrate the remaining zinc in the complexes with a colorimetric assay based on the use of 1-(2-pyridylazo)-2-naphthol in a carbonate buffer adapted from references [42, 43]. A linear calibration could be obtained within the range of

zinc concentrations investigated (Figure appendix 13). However, this technique seemed to be dependent on the incubation time and hardly reliable in our conditions; the zinc concentrations found were for some reasons too high.

The amount of zinc remaining in the complexes was titrated by inductively coupled plasma (ICP). After dialysis, the volume of the suspension of complexes was changed. The dilution can induce an important error in the determination of the amount of Zn^{2+} ions in in the complexes. Therefore, the amount of phosphorous – coming exclusively from the siRNA – was also titrated as an internal reference. Calibrations were performed in the range of the expected concentrations of zinc and phosphorous found in the complexes. They both gave a linear curve for each wavelength tested allowing a robustness in the results (Figure appendix 14).

Table 4.3.5. Concentrations of zinc and phosphorous measured by ICP after dialysis of the complexes (N:P = 10) at pH 6 (3x).

Chitosan	Concentration of zinc titrated (mg/L)	Concentration of phosphorous titrated (mg/L)	Zn:P ratio	Zn:N[a]
[0-8]	9.84	0.27	17.2	1.72
[12-23]	10.103	0.35	13.67	1.367
[24-55]	9.64	0.34	13.39	1.339

[a] assuming N:P = 10.

The zinc ions were well incorporated in the polyplexes as demonstrated by the amount titrated thanks to ICP (Table 4.3.5). Moreover, the titration of the zinc present in the polyplexes solution combined with the titration of phosphorous allowed to determine the Zn:P ratio in the complexes after dialysis.

The Zn:P ratios were found between 5 and 20, as hypothesised earlier. The dialysis ensured a maximal insertion of zinc in the polyplexes and the removal of the excess. Moreover, the amount of zinc incorporated in the polyplexes was not the same whether chitosan is acetylated or not. The complexes formed with a fully deacetylated chitosan seemed to chelate more zinc ions than an acetylated one. This might be explained by the nature of the interaction between zinc and chitosan originating almost exclusively from the deprotonated amino groups. Based on the literature, chitosan-zinc complexes were also found to be of the form ZnL_2 when chitosan is present in a large excess (N:Zn = 10) [28].

4.3.5.3. Effect of the zinc on the morphology of complexes

The complexes prepared with or without zinc and dialyzed at pH 6 as described before were characterized by AFM (Figure 4.3-9). The images obtained by AFM showed the presence of nanosized complexes, with mean sizes and PdI in the expected range (Figure 4.3-8). No clear difference in morphology could be observed between the complexes formed with and without zinc, except that the complex particles obtained in presence of zinc appeared to be slightly denser.

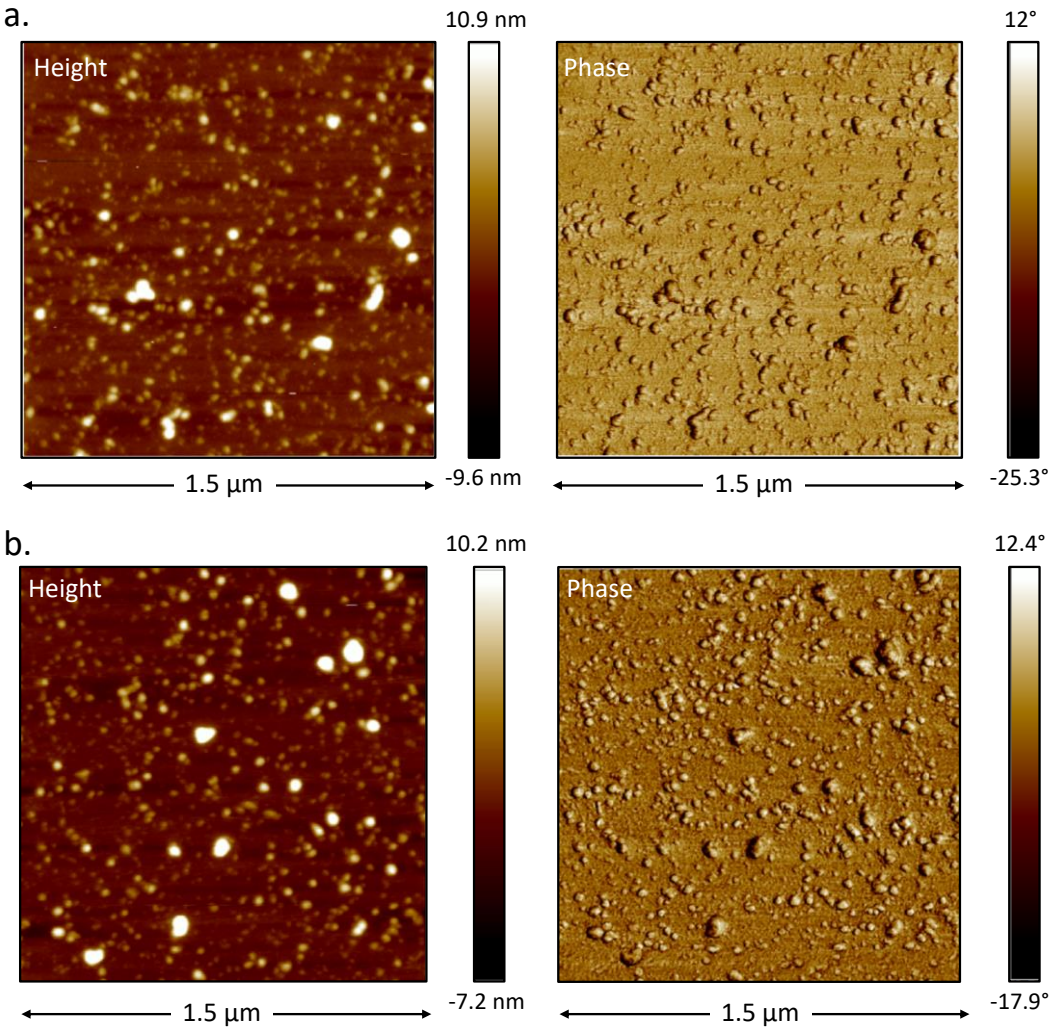

Figure 4.3-9. AFM images of the complexes formed between siRNA and the chitosan [24-55] at N:P = 10. (a) Complexes formed without zinc and dialysed at pH 6, (b) Complexes formed in presence of zinc (initial Zn:P = 10) and dialysed.

4.3.5.4. Stability of complexes with the optimal amount of zinc

The stability of the new formulations developed with Zn^{2+} ions was investigated in physiological conditions. In particular, the stability of the complexes formulated with the four chitosans at N:P = 10 and Zn:P = 20 after dialysis was evaluated at high pH by means of gel electrophoresis at pH = 8.6 or after incubation in HEPES buffer at pH = 7.4 by DLS. In addition, the stability at physiological salt conditions was verified. These formulations were compared to the complexes formulated without zinc.

4.3.5.4.1 Electrophoresis on agarose gels

Gel electrophoresis experiments were conducted to investigate the improvements in the complex stability at physiological pH thanks to the introduction of zinc. The complexes prepared with or without zinc (Zn:P = 20 and N:P = 10) after dialysis were run on a 3% agarose gel in a Tris-HCl buffer at pH = 8.6 (without EDTA). From Figure 4.3-10.a, a clear difference was observed between the electrophoretic pattern of the polyplexes formed with or without zinc. Without zinc, the polyplexes were indeed clearly unstable in this buffer as expected and the siRNA completely released from the complexes, giving the same electrophoretic pattern than siRNA alone. It is interesting to note that under these pH conditions, chitosan precipitates, but this does not prevent the release of siRNA and its migration into the gel. In presence of zinc, a totally different pattern was observed: a long trail appeared which can be interpreted as an uncomplete release of the siRNA from the polyplexes. However, to make sure that this long trail is not an artefact coming from electrostatic interactions, a control experiment was performed in same conditions by replacing zinc with magnesium. The complexes formed in presence of magnesium (Mg:P = 20) and in presence of zinc were electrophoresed on the same gel (Figure 4.3-10.b). In this case, the electrophoretic pattern of complexes in presence of magnesium was similar to that of siRNA alone whereas the same trail is observed in the case of the complexes formed with zinc. This suggests that the incorporation of zinc in the formulation increases the stability of the complexes with only a partial release of the entrapped siRNA. Moreover, the same behaviour was observed for the three chitosans used here ([0-8], [12-23] and [24-55]), indicating that the presence of zinc improves greatly the stability of complexes whatever the chitosan composition (Figure 4.3-10 and Figure 4.3-11). It confirms that the stability of the polyplexes at high pH comes exclusively from the association of the three species: siRNA, zinc and chitosan.

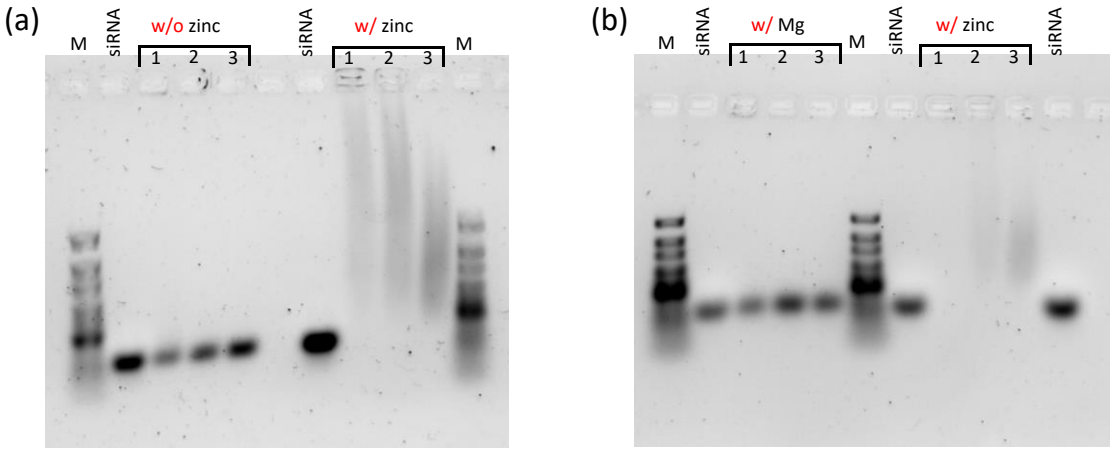

Figure 4.3-10. Electrophoretic pattern on an agarose gel of siRNA stained with SybrSafe. The numbers 1, 2 and 3 correspond respectively to the complexes formed with [0-8], [12-23] and [24-55] at N:P = 10. a) Complexes prepared with and without zinc (Zn:P = 20, dialysis pH 6), (b) Complexes prepared with magnesium (Mg:P = 20, dialysis pH 6) or with zinc (Zn:P = 20, dialysis pH 6). M denotes the size marker, ultra-low range.

The electrophoretic patterns obtained from agarose gels emphasized the increase in stability of the polyplexes thanks to the introduction of zinc. However, it is interesting to remark that the interaction of siRNA with chitosan in presence of zinc ions is somewhat labile as shown by the partial release of siRNA under the electric field (see the tails in the electrophoretic pattern).

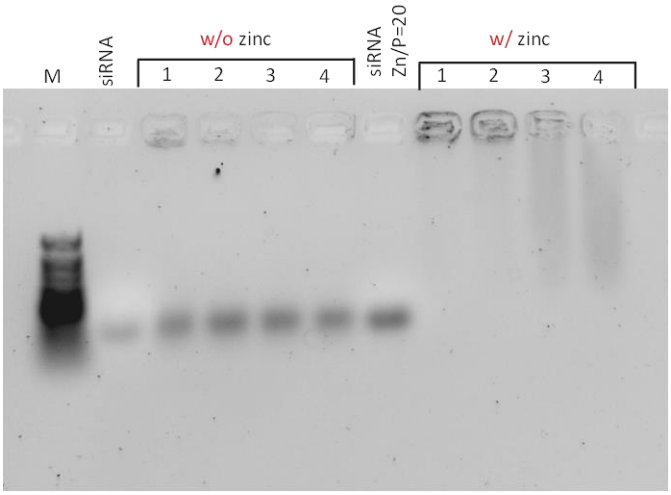

Figure 4.3-11. Electrophoretic pattern of siRNA-chitosan complexes (N:P = 10) without zinc (left) and with zinc (right, Zn:P = 20, dialysis pH 6). Various chitosans were tested: [0-8] (1), [12-23] (2), [24-55] (3) and [32-57]. siRNA alone and siRNA with zinc (Zn:P = 20) were electrophoresed as references. M denotes the size marker, ultra-low range.

4.3.5.4.2 Stability of complexes at physiological pH followed by DLS

The stability of complexes at physiological pH was also investigated by DLS. The formulations in presence of zinc were compared to those formulated without zinc. The complexes were diluted in a 200 mM HEPES buffer at pH = 7.4 (see Table 4.3.1) to assay their stability at high pH. The size distributions after 1 h and 16 h of incubation in buffer were compared to the formulations diluted in water.

The Figure 4.3-12 summarizing the results indicated a lack of stability in HEPES buffer of complexes prepared without zinc with the chitosans [0-8] and [12-23] (Figure 4.3-12.a and c). Indeed, the PSD showed the disappearance of the population corresponding to the complexes when they were incubated in HEPES buffer. Moreover, the drastic increase of the scattered intensity and the mean size (Z-average) of the complexes after one hour of incubation is a clear indication of their aggregation in the buffer (Figure 4.3-12.i and j). The addition of zinc in the formulations with these two chitosans ([0-8] and [12-23]) showed a great improvement of the complex stability, as seen from the PSD in HEPES buffer at pH = 7.4. This was especially the case for the formulation with the chitosan [12-23] for which the PSD after 1h or 16h of incubation in buffer was very similar to the PSD of complexes in water. In more details, despite an increase in the scattered intensity upon incubation in the buffer (Figure 4.3-12.i), the introduction of zinc allowed to preserve the mean size of complexes below 200 nm with only a slight increase in size after 16 h of incubation. Moreover, a good PdI with a value under 0.2 was obtained after 16 h of incubation. This can be attributed to the aggregation of the smallest complex particles with the largest, thus contributing to the increase in size and intensity concomitantly to a decrease in the PdI.

The case of the chitosans [24-55] and [32-57] was much less straightforward. Indeed, no particular difference was observed between the complexes prepared with or without zinc, based on the comparison of the PSD of complexes in water and after incubation in HEPES (Figure 4.3-12.e, f, g and h). However, if the bar charts are watched closely (Figure 4.3-12.i, j and k), some differences revealed some improvements in stability when zinc was added.

- For the chitosan [24-55], almost no change in size (Z-average) was observed when incubating zinc-containing complexes in HEPES buffer; the complex size remained below 100 nm, in contrast to the zinc-free formulation where an increase in the Z-average was observed (Figure 4.3-12.j). The PdI of the complexes decreased after incubation in presence of zinc, reaching a stable value below 0.2 while in the absence of zinc, the PdI decreased after 1h of incubation before rising to a high value (Figure 4.3-12.k). The scattering intensity of complexes in HEPES was also lower for zinc-containing formulations in comparison to zinc-free formulations (Figure 4.3-12.i)

These data associated with the electrophoretic patterns (Figure 4.3-10 and Figure 4.3-11) of the complexes made with chitosan [24-55], clearly indicated an increase in the stability of the complexes thanks to the introduction of zinc.

- For the chitosan [32-57], the zinc-based formulations showed an important increase in intensity after incubation in the HEPES buffer that was not observed with zinc-free formulations. However, none of these formulations precipitated after 16h of incubation in buffer. In fact, the sizes obtained in water and after incubation in buffer were very similar, between 200 nm and 150 nm (Figure 4.3-12.j). One can only notice that the correlation data are slightly better in the case of the formulation with zinc (Figure appendix 15). No significant change can be observed from the variation of the PdI for the formulations of complexes with and without zinc when incubated in HEPES buffer.

The introduction of zinc in the formulations improved the stability of complexes at physiological pH. However, the addition of zinc is especially relevant for chitosans of DA 12% and 24%. For the chitosan of DA 32% such an effect has not been observed which suggests that zinc would be especially useful to stabilize complexes obtained from low acetylated chitosan.

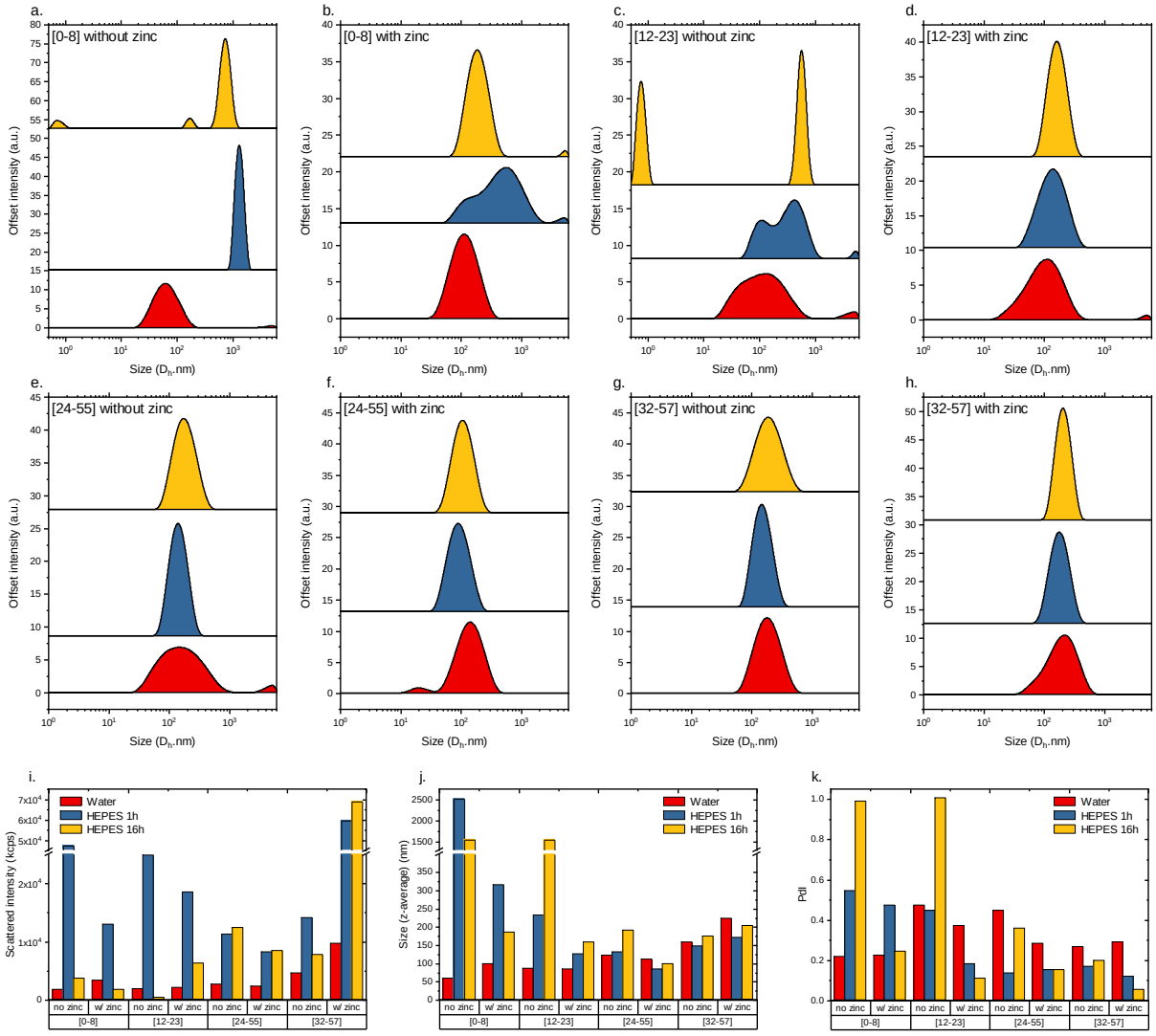

Figure 4.3-12. Particles size distribution of the siRNA-chitosan complexes (N:P = 10) formulated with or without zinc, dialysed three times against water at pH = 6 and diluted in water (1:1 in red), incubated 1 h in a HEPES buffer (1:1 in blue) or incubated 16 h in a HEPES buffer (1:1 in yellow). Various chitosan samples were complexed with siRNA: [0-8] (a,b), [12-23] (c,d), [24-55] (e,f) and [32-57] (g,h). (i) Scattered intensities of the complexes w/ or w/o zinc upon dilution in water (red) or incubation in a HEPES buffer 1h (blue) and 16h (yellow). (j) Z-average and (k) PdI.

4.3.5.4.3 Stability of complexes at physiological ionic strength followed by DLS

Despite the improved stability at physiological pH of complexes formed in presence of zinc, one can wonder if the effect of the DA on the complex stability at physiological ionic strength is preserved. Figure 4.3-13 presents the PSD of the complexes prepared with zinc that have been diluted in either water or NaCl 1.8% (final concentration of 0.9%, i.e the physiological salt concentration). As indicated previously (see Figure 4.3-2), a lack of stability was observed

in the case of chitosan [0-8], which precipitated in the NaCl solution (Figure 4.3-13.a). For the other chitosans, the PSD are very similar when diluted in water or after 20h of incubation in the NaCl solution (Figure 4.3-13.b, c and d). The incubation at high salt concentration led to a densification of the structure as seen by the increase in the scattered intensity.

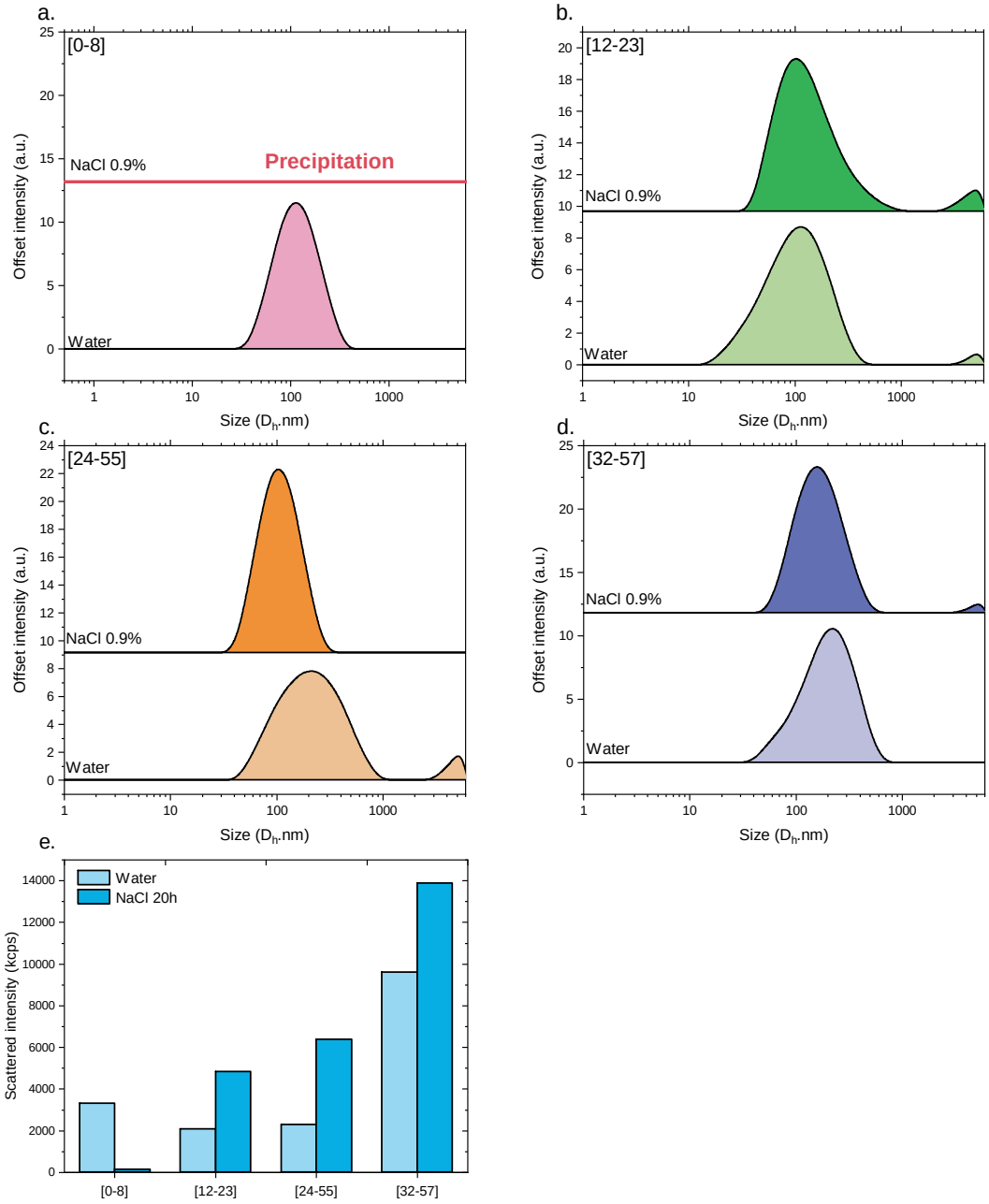

Figure 4.3-13. PSD and scattering intensities of complexes from siRNA and chitosan at N:P = 10, formulated with zinc (Zn:P = 20) and dialysed against water at pH 6 (3x): complexes diluted in water (2x), diluted in NaCl 1.8% (2x) using chitosans a) [0-8], b) [12-23], c) [24-55] and d) [32-57].

In the same manner as for the complexes prepared without zinc (Figure 4.3-3), the scattered intensity, the Z-average and PdI of complexes prepared with zinc (Zn:P = 20, dialysis pH 6)

were measured after 2h, 3h and 20h of incubation in a NaCl solution (0.9% final concentration) (Figure 4.3-14). The data were very similar to those obtained without zinc. Mainly, the complexes formed with chitosan [0-8] were not stable and precipitated. In the case of the chitosan [12-23], an increase in the scattered intensity can be seen while the size of the complexes remained around 100 nm, with a slight increase with the incubation time whereas the PdI values decreased below 0.3 after 3h of incubation. The formulation with chitosan [24-55] presents an increase of the scattered intensity. However, the mean size of the complexes seemed to decrease upon incubation in NaCl, going from below 200 nm to below 100 nm which was associated with a decrease of the PdI to values close to 0.2. The case of chitosan [32-57] was of particular interest: a stable scattered intensity was maintained after incubation at the same level than the complexes diluted in water. The size of the complexes decreased after incubation to 150 nm with PdI values below 0.25. Finally, the effect of the DA on complex size, previously commented (see 4.3.4), can be also observed for the formulation with zinc as seen by the increase of the polyplexes sizes in water with the increase of the DA.

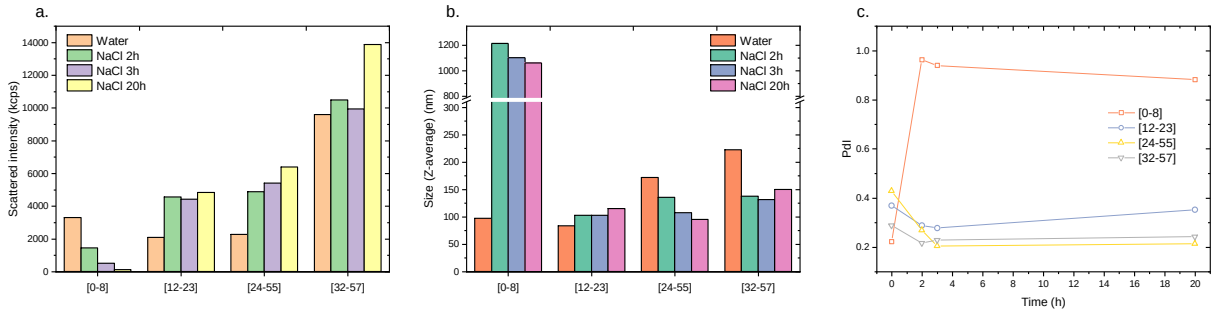

Figure 4.3-14. Colloidal characteristics of siRNA-chitosan complexes (N:P = 10, Zn:P = 20, dialysis against water pH 6 (3x)) in water and after various times of incubation in NaCl (0.9% final concentration). a) Scattered intensity b) Z-average (in nm) c) PdI.

Except for the formulation with chitosan [0-8], the incubation of the complexes at physiological salt concentration did not aggregate the system. On the contrary, the addition of salt seemed to induce rearrangements within the complexes leading to smaller complexes and smaller PdI values. This might be attributed to the role of the acetylated units in the stability of the complexes, allowing a better steric stabilisation despite the decrease in the thickness of the stabilizing shell of the positively charged chitosan at complex surface.

4.3.5.4.4 Stability of complexes in PBS

Thanks to the improved stability of complexes at physiological ionic strength on one side and physiological pH on the other side, the Holy Grail of stability in a PBS buffer seemed within reach.

In the same manner as for previous stability investigations, the complexes formulated in presence of zinc were incubated in a PBS buffer during one hour. Figure 4.3-15 shows the correlation data for complexes diluted in water (1:1) in red and those diluted in PBS buffer (1:1) in blue. The correlation data for the three chitosans clearly indicated an important aggregation of the PECs after one hour of incubation in the PBS buffer, illustrated by the increase of the decay times. Moreover, the huge increase in scattered intensity of the complexes diluted in PBS compared to those diluted in water left no doubt regarding their lack of stability in PBS (Figure 4.3-15.d). These results are similar to those obtained without zinc, suggesting that the addition of zinc may not be the key to stabilize the complexes in a physiological medium such as a PBS buffer.

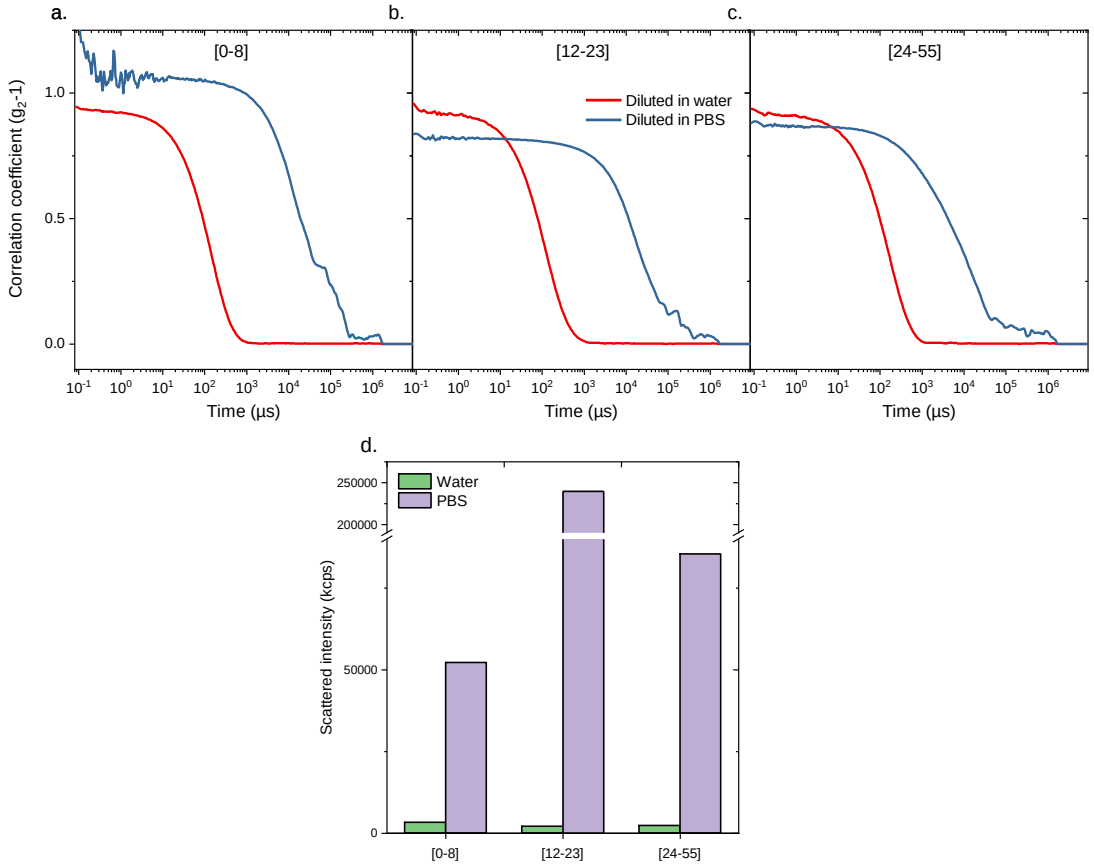

Figure 4.3-15. Correlation functions of the scattered light of the siRNA-chitosan complexes (N:P =10, Zn:P = 20, dialysis pH 6) for various chitosans: (a) [0-8], (b) [12-23] and (c) [24-55]. The complexes were diluted in water (red) or incubated one hour in PBS buffer at 25°C (blue). (d) Scattered intensity of the complexes diluted in water (green) or incubated in the PBS buffer (purple).

Following this result, the kinetics of aggregation of complexes in PBS was studied. First, 50 µL of the dialyzed complexes (chitosan [32-57], N:P = 10, Zn:P = 20) were introduced in a quartz cell. Then, 50 µL of PBS 2X were introduced inside the cell just before starting the measurement. DLS measurements were then performed on the suspension of complexes at

various time intervals during 1h. Note that for this experiment, no stirring could be applied. An increase of the scattered intensity over the time can be clearly observed, especially for the formulation containing zinc (Figure 4.3-16.a). This increase was accompanied with an increase of the size for the two formulations. The incubation of the complexes led to a decrease of the PdI as observed for the formulation of polyplexes containing zinc down to a moderate polydispersity index of 0.3 which was not the case for the zinc-free formulation (Figure 4.3-16.c). The low increase of the scattered intensity for the zinc-free formulation over the time suggests a decomplexation and maybe the formation of chitosan nanogels as stable aggregates. This formation is due to the predominance of hydrophobic interactions and hydrogen bonding with the almost full disappearance of the chitosan cationic character [24]. Finally, the size and PdI after 1h for the formulation containing zinc are really close to the ones obtained after incubation in a HEPES buffer (Figure 4.3-12) or in a NaCl solution (Figure 4.3-14).

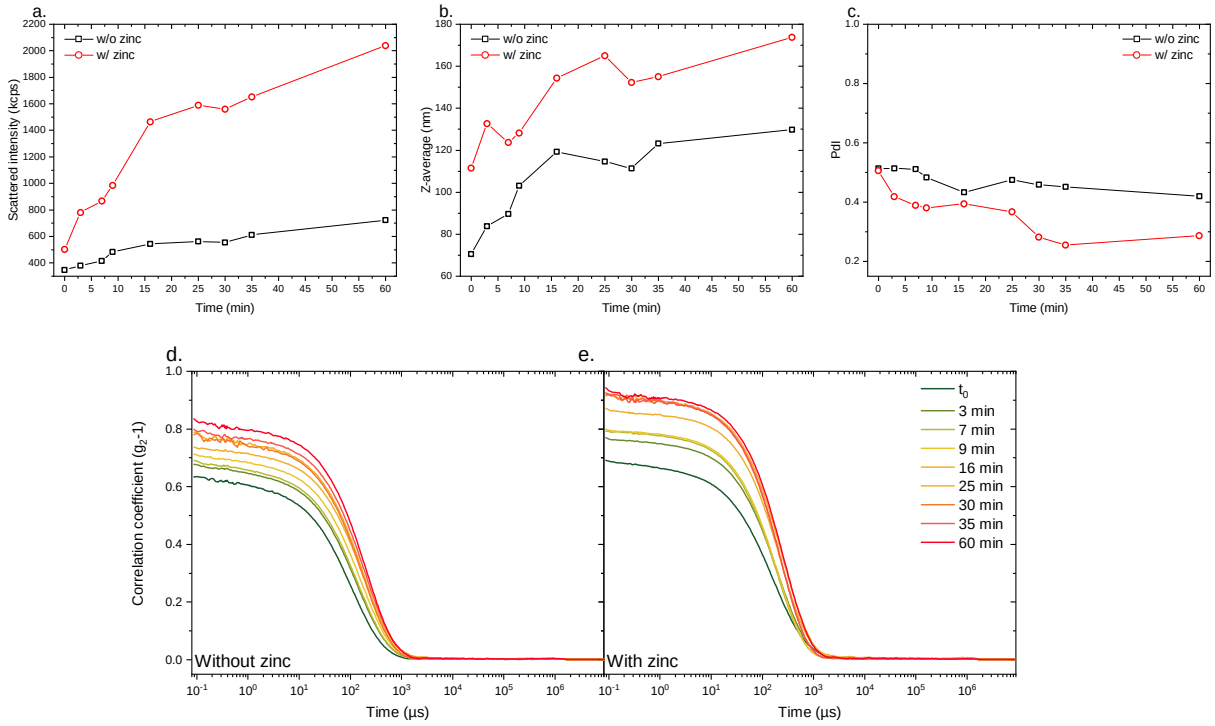

Figure 4.3-16. Aggregation kinetics of siRNA-chitosan complexes (chitosan [32-57], N:P = 10, monitored by DLS. Complexes are prepared with or without zinc (Zn:P = 20, dialysis pH 6). a,b) autocorrelation functions b) scattering intensity, c) Z-avg (d, nm), e) PdI. t_0 corresponds to the first measurement after addition of the PBS.

4.4. Conclusion

The interaction between chitosan and zinc was studied in the first part of this chapter. It has been shown to be dependent of the pH of the chitosan solution, with an optimal pH of interaction around pH = 6. The complexes formed under the conditions used were of the ZnL form with one zinc ion being coordinated by a single nitrogen atom (L) of chitosan. The formation of these complexes allowed to preserve the cationic character for chitosans with a low DA ([0-8] and [12-23]) at high pHs compared to the chitosan on its native form. However, the chelation of zinc by chitosans of higher DA didn't allow to preserve the cationic character at high pHs as seen by zeta-potential measurements.

In the second part of this chapter, efforts were made to improve the colloidal stability of siRNA-chitosan complexes (N:P) under physiological pH and ionic strength. The experiments led to the observation that the stability could be indeed improved in 0.9% NaCl thanks to the increase of the chitosan's DA. However, the main issue regarding the stability of polyplexes formulated with chitosan is their stability at pH 7.4. This challenge was tackled by the introduction of divalent zinc ions in the formulation. The chelation of the Zn^{2+} ions by chitosan on the one hand and the interaction of the ions with siRNA on the other hand have made it possible to preserve the structure of the complexes. Zinc can interact with siRNA through electrostatic interaction with phosphate groups or by forming coordinating bonds with the nucleobases. The introduction of zinc ions improved the stability of complexes in HEPES buffer at pH 7.4 and preserved their positive zeta-potential.

However, the combination of high DA and the addition of Zn^{2+} was not sufficient to allow the stability of the complexes in the PBS buffer.

4.5. References

[1] Wu D, Zhu L, Li Y, Zhang X, Xu S, Yang G, Delair T (2020) Chitosan-based Colloidal Polyelectrolyte Complexes for Drug Delivery: A Review. Carbohydr Polym 238:116126 . https://doi.org/10.1016/j.carbpol.2020.116126

[2] Serrano-Sevilla I, Artiga Á, Mitchell SG, De Matteis L, de la Fuente JM (2019) Natural Polysaccharides for siRNA Delivery: Nanocarriers Based on Chitosan, Hyaluronic Acid, and Their Derivatives. Molecules 24:2570 . https://doi.org/10.3390/molecules24142570

[3] Shi Q, J. M, Zhang X, Dai K, Benderdour M, C. J (2011) Chitosan-DNA/siRNA Nanoparticles for Gene Therapy. In: Non-Viral Gene Therapy. InTech

[4] Mohamed RR, Abu Elella MH, Sabaa MW (2015) Synthesis, characterization and applications of N-quaternized chitosan/poly(vinyl alcohol) hydrogels. Int J Biol

Macromol 80:149–161 . https://doi.org/10.1016/j.ijbiomac.2015.06.041

[5] de Britto D, Assis OBG (2007) A novel method for obtaining a quaternary salt of chitosan. Carbohydr Polym 69:305–310 . https://doi.org/10.1016/j.carbpol.2006.10.007

[6] Wu D, Delair T (2015) Stabilization of chitosan/hyaluronan colloidal polyelectrolyte complexes in physiological conditions. Carbohydr Polym 119:149–158 . https://doi.org/10.1016/j.carbpol.2014.11.042

[7] Giacalone G, Hillaireau H, Capiau P, Chacun H, Reynaud F, Fattal E (2014) Stabilization and cellular delivery of chitosan–polyphosphate nanoparticles by incorporation of iron. J Control Release 194:211–219 . https://doi.org/10.1016/j.jconrel.2014.08.022

[8] Muzzarelli RAA (1977) Chitin. Pergamon Press

[9] Benavente M, Moreno L, Martinez J (2011) Sorption of heavy metals from gold mining wastewater using chitosan. J Taiwan Inst Chem Eng 42:976–988 . https://doi.org/10.1016/j.jtice.2011.05.003

[10] Schlick S (1986) Binding sites of copper 2+ in chitin and chitosan. An electron spin resonance study. Macromolecules 19:192–195 . https://doi.org/10.1021/ma00155a030

[11] Ogawa K, Oka K, Yui T (1993) X-ray study of chitosan-transition metal complexes. Chem Mater 5:726–728 . https://doi.org/10.1021/cm00029a026

[12] Allan GG, Peyron M (1995) Molecular weight manipulation of chitosan I: kinetics of depolymerization by nitrous acid. Carbohydr Res 277:257–272 . https://doi.org/10.1016/0008-6215(95)00207-A

[13] Brugnerotto J, Desbrières J, Roberts G, Rinaudo M (2001) Characterization of chitosan by steric exclusion chromatography. Polymer (Guildf) 42:09921–09927 . https://doi.org/10.1016/S0032-3861(01)00557-2

[14] Vachoud L, Zydowicz N, Domard A (1997) Formation and characterisation of a physical chitin gel. Carbohydr Res 302:169–177 . https://doi.org/10.1016/S0008-6215(97)00126-2

[15] Sorlier P, Denuzière A, Viton C, Domard A (2001) Relation between the degree of acetylation and the electrostatic properties of chitin and chitosan. Biomacromolecules 2:765–772 . https://doi.org/10.1021/bm015531+

[16] Berto P (2014) Synthèse d'une bibliothèque de dérivés hydrophobes du chitosane : caractérisation et étude de l'auto-assemblage en solution

[17] Fulmer GR, Miller AJM, Sherden NH, Gottlieb HE, Nudelman A, Stoltz BM, Bercaw JE, Goldberg KI (2010) NMR Chemical Shifts of Trace Impurities: Common Laboratory Solvents, Organics, and Gases in Deuterated Solvents Relevant to the Organometallic Chemist. Organometallics 29:2176–2179 . https://doi.org/10.1021/om100106e

[18] Tømmeraas K, Vårum KM, Christensen BE, Smidsrød O (2001) Preparation and characterisation of oligosaccharides produced by nitrous acid depolymerisation of chitosans. Carbohydr Res 333:137–144 . https://doi.org/10.1016/S0008-6215(01)00130-6

[19] Salim E, Ailincai D, Trombotto S (2014) Chitooligosaccharide-2,5-anhydro-D-mannonic Acid. Molbank 2014:M832 . https://doi.org/10.3390/M832

[20] Hirai A, Odani H, Nakajima A (1991) Determination of degree of deacetylation of chitosan by 1H NMR spectroscopy. Polym Bull 26:87–94 . https://doi.org/10.1007/BF00299352

[21] Nguyen S, Winnik FM, Buschmann MD (2009) Improved reproducibility in the determination of the molecular weight of chitosan by analytical size exclusion chromatography. Carbohydr Polym 75:528–533 . https://doi.org/10.1016/j.carbpol.2008.08.013

[22] Katchalsky A, Shavit N, Eisenberg H (1954) Dissociation of weak polymeric acids and bases. J Polym Sci 13:69–84 . https://doi.org/10.1002/pol.1954.120136806

[23] Zhang H, Dubin PL, Kaplan J, Moorefield CN, Newkome GR (1997) Dissociation of Carboxyl-Terminated Cascade Polymers: Comparison with Theory. J Phys Chem B 101:3494–3497 . https://doi.org/10.1021/jp962962r

[24] Schatz C, Pichot C, Delair T, Viton C, Domard A (2003) Static Light Scattering Studies on Chitosan Solutions: From Macromolecular Chains to Colloidal Dispersions. Langmuir 19:9896–9903 . https://doi.org/10.1021/la034410n

[25] Delas, Mock-Joubert, Faivre, Hofmaier, Sandre, Dole, Chapel, Crépet, Trombotto, Delair, Schatz (2019) Effects of Chain Length of Chitosan Oligosaccharides on Solution Properties and Complexation with siRNA. Polymers (Basel) 11:1236 . https://doi.org/10.3390/polym11081236

[26] Delas T, Mock-Joubert M, Faivre J, Hofmaier M, Sandre O, Dole F, Chapel JP, Crépet A, Trombotto S, Delair T, Schatz C (2019) Effects of chain length of chitosan oligosaccharides on solution properties and complexation with siRNA. Polymers (Basel) 11: . https://doi.org/10.3390/polym11081236

[27] Rhazi M, Desbrières J, Tolaimate A, Rinaudo M, Vottero P, Alagui A (2002) Contribution to the study of the complexation of copper by chitosan and oligomers. Polymer (Guildf) 43:1267–1276 . https://doi.org/10.1016/S0032-3861(01)00685-1

[28] Bodek KH, Kufelnicki A (1995) Protolytic and complexing properties of microcrystalline chitosan with Co(II), Zn(II), and Cu(II) ions. J Appl Polym Sci 57:645–651 . https://doi.org/10.1002/app.1995.070570515

[29] Irving HM, Rossotti HS (1954) The calculation of formation curves of metal complexes from pH titration curves in mixed solvents. J Chem Soc 2904 . https://doi.org/10.1039/jr9540002904

[30] Lång (Loukamo) S, Tuhkanen A, Nielsen EJ, Turunen E, Bjerrum J, Rautanen N (2008) Metal Ammine Formation in Aqueous Solution. VI. Stability and Light Absorption of Copper Ethylenediamine Ions. Acta Chem. Scand. 2:297–318

[31] Irving H, Rossotti HS (1953) 680. Methods for computing successive stability constants from experimental formation curves. J Chem Soc 3397 . https://doi.org/10.1039/jr9530003397

[32] Zhang Y, Liu B-L, Wang L-J, Deng Y-H, Zhou S-Y, Feng J-W (2019) Preparation, Structure and Properties of Acid Aqueous Solution Plasticized Thermoplastic Chitosan. Polymers (Basel) 11:818 . https://doi.org/10.3390/polym11050818

[33] Brugnerotto J, Lizardi J, Goycoolea F., Argüelles-Monal W, Desbrières J, Rinaudo M (2001) An infrared investigation in relation with chitin and chitosan characterization. Polymer (Guildf) 42:3569–3580 . https://doi.org/10.1016/S0032-3861(00)00713-8

[34] Hiemenz PC, Rajagopalan R (1997) Principles of Colloid and Surface Chemistry. CRC Press

[35] Nič M, Jirát J, Košata B, Jenkins A, McNaught A (2009) Transition Element. In: IUPAC Compendium of Chemical Terminology. IUPAC, Research Triagle Park, NC

[36] Mosmann T (1983) Rapid colorimetric assay for cellular growth and survival: Application to proliferation and cytotoxicity assays. J Immunol Methods 65:55–63 . https://doi.org/10.1016/0022-1759(83)90303-4

[37] Tan BH, Tam KC, Lam YC, Tan CB (2005) Osmotic Compressibility of Soft Colloidal Systems. Langmuir 21:4283–4290 . https://doi.org/10.1021/la047430d

[38] Krężel A, Maret W (2016) The biological inorganic chemistry of zinc ions. Arch Biochem Biophys 611:3–19 . https://doi.org/10.1016/j.abb.2016.04.010

[39] Gomes JRB, Jorge M, Gomes P (2014) Interaction of chitosan and chitin with Ni, Cu and Zn ions: A computational study. J Chem Thermodyn 73:121–129 . https://doi.org/10.1016/j.jct.2013.11.016

[40] Kurita K, Sannan T, Iwakura Y (1979) Studies on chitin. VI. Binding of metal cations. J Appl Polym Sci 23:511–515 . https://doi.org/10.1002/app.1979.070230221

[41] Vold IMN, Vårum KM, Guibal E, Smidsrød O (2003) Binding of ions to chitosan—selectivity studies. Carbohydr Polym 54:471–477 . https://doi.org/10.1016/j.carbpol.2003.07.001

[42] Khoder M, Tsapis N, Domergue-Dupont V, Gueutin C, Fattal E (2010) Removal of residual colonic ciprofloxacin in the rat by activated charcoal entrapped within zinc-pectinate beads. Eur J Pharm Sci 41:281–288 . https://doi.org/10.1016/j.ejps.2010.06.018

[43] Thanasarakhan W, Liawruangrath S, Wangkarn S, Liawruangrath B (2007) Sequential injection spectrophotometric determination of zinc(II) in pharmaceuticals based on zinc(II)-PAN in non-ionic surfactant medium. Talanta 71:1849–1855 . https://doi.org/10.1016/j.talanta.2006.08.034

Chapter 5: Synthesis of a block copolymer containing a short chitosan block for the non-covalent conjugation to siRNA

5.1. Introduction

Chitosan is the only polysaccharide naturally presenting cationic moieties on its backbone. It is obtained from chitin, a polymer composed of 1,4-linked N-acetyl-D-glucosamine (GlcNAc) residues. The N-deacetylation of chitin provides chitosan which is based on D-glucosamine (GlcN) residues carrying cationic charges in slightly acid solutions. Chitosan is the object of a large number of studies covering several fields. For instance, chitosan is studied for its antimicrobial and antioxidative properties for food packaging applications [1, 2] but also in the field of medicine in tissue engineering [3] and for drug delivery applications [4], particularly gene delivery applications [5]. The chemical modification of chitosan is widely investigated in order to enhance its remarkable native properties. Chitosan can be used to condense DNA molecules through electrostatic interaction with the negatively charged nucleic acids. This phenomenon allows the formation of nanoparticles for the gene delivery. Chemical routes have been investigated to improve the properties of chitosan for such electrostatic complexes. Mainly, the modification of the amines on the chitosan backbone is the privileged pathway to incorporate new chemical functions. The modification of the cationicity of the polycation at physiological pH has been largely investigated with the introduction of Schiff bases [6] or the quaternisation of the amines [7]. It has also been proposed to chemically modified amine groups with the grafting of PEG, resulting in the formation of a chitosan-*g*-PEG [8, 9]. It was shown that the introduction of a PEG block could enhance the gene delivery efficiency by improving the complex stability and the biocompatibility of the complexes [10]. However, this approach based on the introduction of PEG can be problematic when the number of charged units is low, i.e. for chitosan of high DA and/or of low molecular weight. Moreover, the distribution of PEG blocks and their absolute number per chitosan chain is hardly controllable. From this point of view, the formation of linear diblock copolymers based on the reaction of the chitosan reducing end with end-functionalized PEG allow to preserve the amine groups of chitosan and to better stabilize the complexes. Therefore, the end-modification of chitosan with PEG accounts for a better control of the complexation of chitosan with nucleic acids.

The synthesis of such diblock copolymers, which was scarcely studied, has gained interest in the last years and different approaches have been developed to obtain chitosan-*b*-PEG copolymers. For instance, one of the earliest synthesis of chitosan-based block copolymer reported relies on the reaction of a PEG macromer introduced during the radical depolymerization process of chitosan with potassium persulfate as initiator [11]. The other approaches developed aimed to take advantage of the reducing end of the chitosan which is a reactive aldehyde in equilibrium with the hemiacetal form. This aldehyde moiety enables

modification methods such as thioacetylation [12] or reductive amination allowing the introduction of clickable moieties for alkyne/azide chemistry [13, 14], oxyamines [15] or hydrazides [16]. However, these reactions are relatively slow [16] which has led to the development of another reaction pathway. Indeed, the depolymerization of a fully de-N-acetylated chitosan through the nitrous acid (HONO) deamination process leads to low molecular weight chitosans or chitooligosaccharides (COS) with a 2,5-anhydro-D-mannofurannose (AMF, or M-unit) at the new reducing end (Figure 5.1-1) [17, 18]. This new reducing end, bearing a more reactive and available aldehyde group under its hydrated gem-diol form, has been found to react with various compounds for further modifications towards the formation of COS-based block copolymers. The reaction of this M-unit with aniline derivatives could lead to the synthesis of a library of COS-based building blocks ready for further conjugation [19]. The reaction of this terminal residue thanks to a thioacetylation process with a "triskelion" approach using a linker bearing three thiol moieties could also lead to a thiol end-functionalised COS block ready for further reaction with any thiol-reactive species such as a PEG blocks, ligands or sufaces through Michael type addition or the formation of disulfide bridges [20]. Finally, the successful reaction of the terminal residue with dioxyamines and dihydrazides could lead to terminally activated COS blocks that are ready for the formation of diblock oligosaccharides [21]. This reaction, seems particularly advantageous for the formation of COS-*b*-PEG copolymers since PEG functionalized with hydrazide are commercially available and only two steps would be necessary (Figure 5.3-1): 1) the reaction between the aldehyde of the M residue at the reducing end of COS with the PEG hydrazide function leading to the formation of the hydrazone and 2) the irreversible reduction of the hydrazone bond with sodium cyanoborohydride ($NaCNBH_3$) or less toxic reducing agent like picoline borane. Moreover, the reduction of the hydrazone bond after reaction seems more efficient and faster than oxime reduction [21]. One can also remark that the reaction of the M residue with amines is much slower than with hydrazide. Hence, the self-branching reaction resulting from the formation of a Schiff base by reaction of the aldehyde of the M unit with the amines of the COS, should be avoided or at least minimized in presence of hydrazide [17].

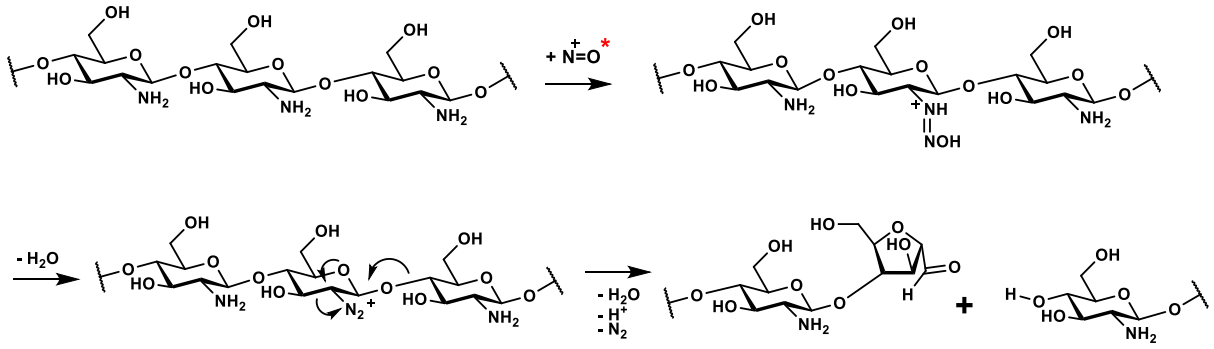

Figure 5.1-1. Mechanism of the nitrous deamination of chitosan [18]. *Nitrosonium ion is formed in acidic solution after the introduction of sodium nitrite ($NaNO_2$) in the chitosan solution.

Regarding the complexes obtained from COS-*b*-PEG copolymer and siRNA, a particular attention was paid to their characterisation. Indeed, the structure expected from the electrostatic assembly of a COS-*b*-PEG can be either a PIC micelle [22, 23] or a structure of conjugate type as described by Kataoka and al. [24, 25] and earlier by DeRouchey and al. [26]. The assembly in one of the two structures should be determined by the length of the complexing block use for the assembly, the COS block in our case. Indeed, for a same PEG block length, a long COS block should favour the formation of PIC micelles with the formation of inter-siRNA bridges due to a polycationic block longer than the siRNA strand whereas a shorter COS block is expected to favour the assembly in a conjugate-like structure. Therefore, particular attention should be paid to the choice of the length of the polycationic block, as it must be also long enough to ensure efficient binding to siRNA [27]. Moreover, the addition of a PEG block to the complexing COS block should reduce the strength of the interaction between the polycationic block and the siRNA compared to the polycationic block alone. It was decided to use a COS with a DP of 16 to 20 for the synthesis of the COS-*b*-PEG copolymer with the goal obtain a structure of the conjugate type. Indeed, we demonstrated in the chapter 2 that a COS with a DP of 20 should efficiently bind siRNA and the length of such a COS should approximately match the length of the siRNA [27].

5.2. Materials and methods

Chemicals. mPEG hydrazide (M_w = 5 000 g/mol) was provided by Interchim (Montluçon, France). Sodium cyanoborohydride ($NaCNBH_3$) (95%) was obtained from Sigma Aldrich, Sodium carbonate (> 99.8%) (Na_2CO_3) from Roth and other chemicals were of analytical grade.

siRNA. The siRNA duplex was provided by Kaneka Eurogentec S.A. (Seraing, Belgium) and received as lyophilisate after purification by reverse phase HPLC. The sense sequence was 5'-[Phos]GUCUCAGCCUCUUCUCAUUCCUG[dC][dT]-3' (M = 7807.6 g/mol) and the antisense was 5'-AGCAGGAA[mU]G[mA]G[mA]A[mG]A[mG]G[mC]U[mG]A[mG]A [mC][mA][mU][dT][dT] (M = 8999.6 g/mol). The molar masses were determined by MALDI-TOF analysis. The annealing step was performed by Eurogentec according to standard procedures in a buffer 50 mM TRIS-HCl, 100 mM NaCl, pH 7.6. Fluorescently labeled siRNA was provided from the same supplier, presenting the same sequence and purification protocol. The fluorescent probe Cy 5.5 was attached to the 5' of the sense strand.

Chitosan oligosaccharide (COS). A COS with a polymerisation degree of 20 (COS20) was synthesised according to the nitrous acid depolymerization process previously described by Allan and Peyron [18, 28] on a de-N-acetylated chitosan (DA < 1%) with M_n = 90 000 g/mol and Đ = 2.1 provided by Mahtani Chitosan. Chitosan was dissolved at 3 wt % in water with a stoichiometric amount of HCl relative to the GlcN residues for the full protonation of the amine functions. After 1 day of stirring, sodium nitrite was added to the chitosan solution at a GlcN/$NaNO_2$ molar ratio of 9 to obtain a DP of 20. After 24h of reaction at room temperature, the solution was filtered on a 1.0 µm pore size glass fibre membrane and freeze-dried. The lyophilizate was dissolved in a minimum volume of ultrapure water and the COS was precipitated in a ethanol:acetone (1:1 v:v) mixture and the precipitate washed three times with the same solvent and centrifuged. The swollen pellet was then dissolved in ultrapure water and freeze dried, three times. According to this protocol the hydrochloride form of COS was obtained which allowed its solubilization in water without addition of acid.

Preparation of a COS20-*b*-PEG5k. The protocol was developed at IMP@Lyon laboratory in the framework of a joint ANR project with LCPO (project TANGO, 2016-2020). COS (0.05 g, 0.014 mmol, M_w = 3 500 g.mol^{-1}, 1 eq) was dissolved in deionized water as a 1.0 % (w/v) solution. The pH was increased to 4.5-5.0 by addition of Na_2CO_3. mPEG-hydrazide (0.210 g, 0.042 mmol, M_w = 5 000 g.mol^{-1}, 3 eq) was then added to the reaction media. After 2 h of reaction at RT, $NaCNBH_3$ (~ 4.4 mg, 0.07 mmol, 5 eq) was added and the reaction was left for 12 h under stirring. In order to remove the residual COS, insoluble in alkali conditions, pH was raised above 9 with ammonium hydroxide (NH_4OH) and the precipitate was centrifuged at 15,000 rpm for 15 min. The precipitate was re-dissolved by lowering the pH with HCl and residual COS were re-precipitated three times with NH_4OH. The supernatants, containing the excess of PEG and the copolymer, was freeze-dried. The solid was washed three times against dichloromethane to remove PEG excess. The precipitate was then solubilised in deionized water dialysed by membrane dialysis (regenerated cellulose, MWCO 1000 Da) against water for 24 h to remove $NaCNBH_3$.The dialysate was finally freeze-dried

to retrieve COS20-*b*-PEG5k. The different steps of the synthesis were monitored by ^{1}H NMR: PEG (-CH3, 3.4 ppm, -O-CH2, 3.6-3.8 ppm), COS (N-CO-CH3, 2.1 ppm; H-1(D), 5.1 ppm; H-2(D), 3.1 ppm; H-3(D), H-4(D), H-5(D) and H-6(D), 3.6-4.2 ppm), H-1(AMF) imine formation (d, CH=N, 7.4-7.7 ppm) and reduction (disappearance). The final product was analysed by SEC and NMR.

NMR spectroscopy. The chemical structures were determined at 298 K from proton nuclear magnetic resonance (^{1}H-NMR) spectroscopy on a Bruker AVANCE III HD 400 MHz spectrometer using a 5 mm Bruker multinuclear z-gradient direct probe. The ^{1}H NMR spectra were calibrated from the signal of HOD at 4.79 ppm.

All DOSY (Diffusion Ordered Spectroscopy) [29, 30] measurements were performed at 298K on a Bruker Avance NEO 400 spectrometer operating at 400.33 MHz and equipped with a 5 mm Bruker multinuclear z-gradient direct cryoprobe-head capable of producing gradients in the z direction with strength 53.5 G cm^{-1}. Sample was dissolved in D_2O (Volume 80 µL) for internal lock in capillary tubes. The dosy spectra were acquired with the *ledbpgp2s.mod* pulse program_from Bruker topspin software without spinning. The duration of the pulse gradients and the diffusion time were adjusted in order to obtain full attenuation of the signals at 95 % of maximum gradient strength. The values were 5.0 ms for the duration of the gradient pulses and 100 ms for the diffusion time. The gradients strength was linearly incremented in 16 steps from 5% to 95% of the maximum gradient strength. A delay of 5 **s** between echoes was used. The data were processed using 8192 points in the F2 dimension and 128 points in the F1 dimension with the Bruker topspin software. Field gradient calibration was accomplished at 25°C using the self-diffusion coefficient of H_2O+D_2O at 19.0 x 10^{-10} m^2.s^{-1} [31, 32].

Analytical Size Exclusion Chromatography (SEC). The mass-average molar mass (M_w), the number-average molar mass (M_n) and the dispersity (Đ) of the products were determined by high-performance size exclusion chromatography (SEC) (UltiMate 3000 HPLC, Thermofisher, Waltham, MA, USA) with a multiangle laser light scattering detection (MALLS) (Dawn Heleos, Wyatt, Santa Barbara, CA, USA) operating at λ_0 = 658 nm and a differential refractive index detector (Optilab rEX, Wyatt) operating at the same wavelength. Two sets of columns were used for the separation of the samples: Tosoh TSK gel columns (G6000PWXL and G2500PWXL) or TSK gel columns (G4000PWXL and G3000 PWXL). A degassed 0.3 M acetic acid/0.2 M sodium acetate buffer (pH 4.5) was used as eluent after filtration on a 0.22 µm pore size membrane (Millipore). The flow rate was maintained at 0.6 mL/min, and the amount of sample injected was 100 µL at a concentration of 5 mg/mL.

Preparative Size Exclusion Chromatography. Preparative size exclusion chromatography (SEC) was used for fractionation of products. The system was composed of the ÄKTA purifier 100 equipped with a HiLoad 16/600 Superdex 75 prep grade column (16 mm × 60 cm) continuously eluting acetate buffer (0.3 M acetic acid/0.2 M sodium acetate, pH = 4.5) after filtration on a 0.22 µm pore size membrane (Millipore). The fractionation was monitored online using a UV detector at λ = 280 nm and fractions of 4 mL were collected and pooled according to elution times. The flow rate was maintained at 1mL/min for a sample at a concentration of 5 mg/mL after filtration on a 0.22 µm cellulose acetate membrane. The pooled fractions were dialysed (MWCO = 100−500 Da) against ultrapure Milli-Q (MQ) water and freeze-dried. The preparative SEC experiments were realised at the ENSTBB in Bordeaux with the associate professor Charlotte Cabanne from the CBMN.

UV-visible measurements. Full spectra and measurements at a fixed wavelength were recorded on a Cary 100 UV-visible spectrophotometer (Agilent technologies, CA, USA). Full spectra were obtained by the mean of three acquisitions. Measurements at a fixed wavelength for turbidimetry experiments were done in triplicate and are represented as the mean of the 3 measurements with the standard deviation.

Fluorescence Correlation Spectroscopy. Fluorescence correlation spectroscopy (FCS) measurements were performed on an IX83 confocal laser scanning microscope (Olympus, Tokyo, Japan) equipped with a FLIM/FLCS upgrade kit (PicoQuant GmbH, Berlin, Germany). The samples were excited by a laser at an excitation wavelength of 640 nm, driven by a PDL 828 Sepia II driver in picosecond pulsed mode at a 20 MHz repetition rate (both devices: PicoQuant). An Olympus UPlanSApo water immersion objective (60x, 1.2 NA) delivered the excitation light into a diffraction-limited spot and collected the emitted fluorescence. The fluorescence signal passed through a Semrock 690/70 nm BrightLine emission filters and was detected by a hybrid photomultiplier (PMA Hybride-40 from PicoQuant) operated in photon counting mode. Photon counts were recorded using a PicoHarp300 TCSPC module in a T3 time tagging mode. The measurements were performed at 23 ± 1 °C over a period of 10 or 20 min. The SymPhoTime64, ver. 2.1 software (PicoQuant) was used for data acquisition and FCS autocorrelation function calculation. These measurements were performed at the Institute of Macromolecular Chemistry (Prague, Czech Republic) in the team of Pr. Petr Štěpánek with the great help of Dr. Jiří Pánek.

The autocorrelation function in the case of FCS is of the form:

$$G(t) = \frac{1}{N}\left(1 + \frac{t}{\tau_D}\right)^{-1}\left(1 + \frac{t}{\kappa^2\tau_D}\right)^{-1/2}$$

Where N is the average number of fluorescent species in the focal volume and $\kappa = {w_z}/{w_{xy}}$ with w_{xy} and w_z being the width of the focal volume in the $x - y$ plane (perpendicular to the optical axis) and along the z-axis. τ_D is the diffusion time such as $\tau_D = {w_{xy}^2}/{4D}$ where D is the diffusion coefficient.

κ is a constant obtained after calibration of the experimental setup, using fluorescent species with a known diffusion coefficient. Moreover, the contribution of the triplet - specific to the fluorescent probe used - in the autocorrelation function can be taken into account and removed from the final autocorrelation curve describing the dynamics of the objects of interest [33].

Finally, knowing the instrumental parameter κ after calibration, the diffusion coefficient D and the number of fluorescent objects N in the focal volume can be derived from a fitting of the experimental autocorrelation curve.

The measurements were done in duplicate on two different samples. Each autocorrelation curve could be fitted by a single component model, addition of a second component didn't modify the result, confirming the relevance of a single component model.

Optimisation of fluorophore concentration in solution were carried to obtain the best signal. In order to keep an initial concentration of 0.1 g/L of siRNA for the formation of complexes (final concentration of 0.05 g/L after complexation), the dilution of the fluorescent siRNA solution (at 0.1 g/L) was achieved by the addition of a non-labelled siRNA solution at 0.1 g/L.

Dynamic Light Scattering. Routine Dynamic Light Scattering experiments were performed on a ZetasizerUltra (Malvern Panalytical Ltd., Malvern, UK) at 25 °C, equipped with a laser working at λ = 632.8 nm and using a back scattering angle detection (173°). Further, three to five measurements were performed for each condition of complexation. The particle size distribution was determined using a non-negative least squares (NNLS) algorithm for the fitting of the correlation function. The parameters Z-average and the PdI are obtained by means of the cumulant analysis of the correlation function.

Formation of complexes. The complexes between siRNA and the copolymer were formed by mixing 50 µL of the copolymer solution with 50 µL of siRNA solution, both prepared in RNase free water. The copolymer solution is adjusted to pH = 4 prior to use to ensure full protonation of the glucosamine residues (the volume of HCl added is taken into account for concentration calculations). The concentration of the siRNA solution was set to 0.1 g/L (0.294 mM in phosphate groups), while the copolymer concentration in protonated glucosamine residues was varied according to the targeted nitrogen to phosphate (N:P) ratio. The copolymer solution was filtered on 0.22 µm mixed cellulose membrane prior to use. The

complexation was carried out by a one-shot addition with a micropipette of the copolymer solution to the siRNA solution for N:P < 1. The opposite order of addition was used for N:P > 1. By doing so the component in default was always added to the one in excess. Hence the system avoided the experience of the neutral state at charge stoichiometry. The fast-mixing conditions were obtained by achieving the complexation reaction in a 1.5 mL plastic microtube placed in a VXR basic Vibrax (IKA) set at 1000 rpm.

5.3. Results and discussion

5.3.1. Strategy for the synthesis of the COS-*b*-PEG

As introduced, the reaction chosen to obtain a copolymer of the type chitosan-*b*-PEG is the reductive amination based on the reaction of the aldehyde at the reducing end of the chitosan with a hydrazide at the PEG chain end. It has been demonstrated that the reducing end of a COS (the M-unit) obtained from the depolymerization of a long chitosan leads to a much more reactive aldehyde than the classical reducing end of polysaccharides [16, 21]. The first step considered is therefore the synthesis of a COS composed exclusively of D residues, with a reactive M-unit at the reducing end through a nitrous deamination (HONO) depolymerization process of a fully deacetylated chitosan (Figure 5.3-1 step 1).

The conjugation of the COS with a methoxy PEG functionalised with a hydrazide is expected to take place by the formation of an imine (hydrazone) which can be monitored by ^{1}H NMR (Figure 5.3-1 step 2). The kinetics of this reaction is described in the literature as pH-dependent, with an optimal pH between 4 and 5, a pH of 5 leading to faster kinetics but a pH of 4 yielding a more efficient reducing step [21].

Finally, the hydrazone can be reduced. This reduction leads to the formation of a stable secondary amine between the two blocks (Figure 5.3-1 step 3). This reduction can also be monitored by ^{1}H NMR with the disappearance of the imine peak appeared in the previous step.

This strategy presents a few advantages such as the use of water as solvent and reactions are performed in mild conditions. However, this reaction had not been performed yet with a COS of DP ~ 20 and a PEG of 5 kDa, i.e, two relatively long blocks. Similar coupling reactions reported in the literature usually involved shorter polysaccharide blocks [21] or longer chitosan blocks coupled with non-polymeric hydrazide molecule [34]. Here, the case of longer

blocks could be a problem with regards to the probability of encountering the two reactive ends, which could result in low conversions.

The purification step to recover the expected copolymer structure is critical and difficult to implement as described in the section 5.2.

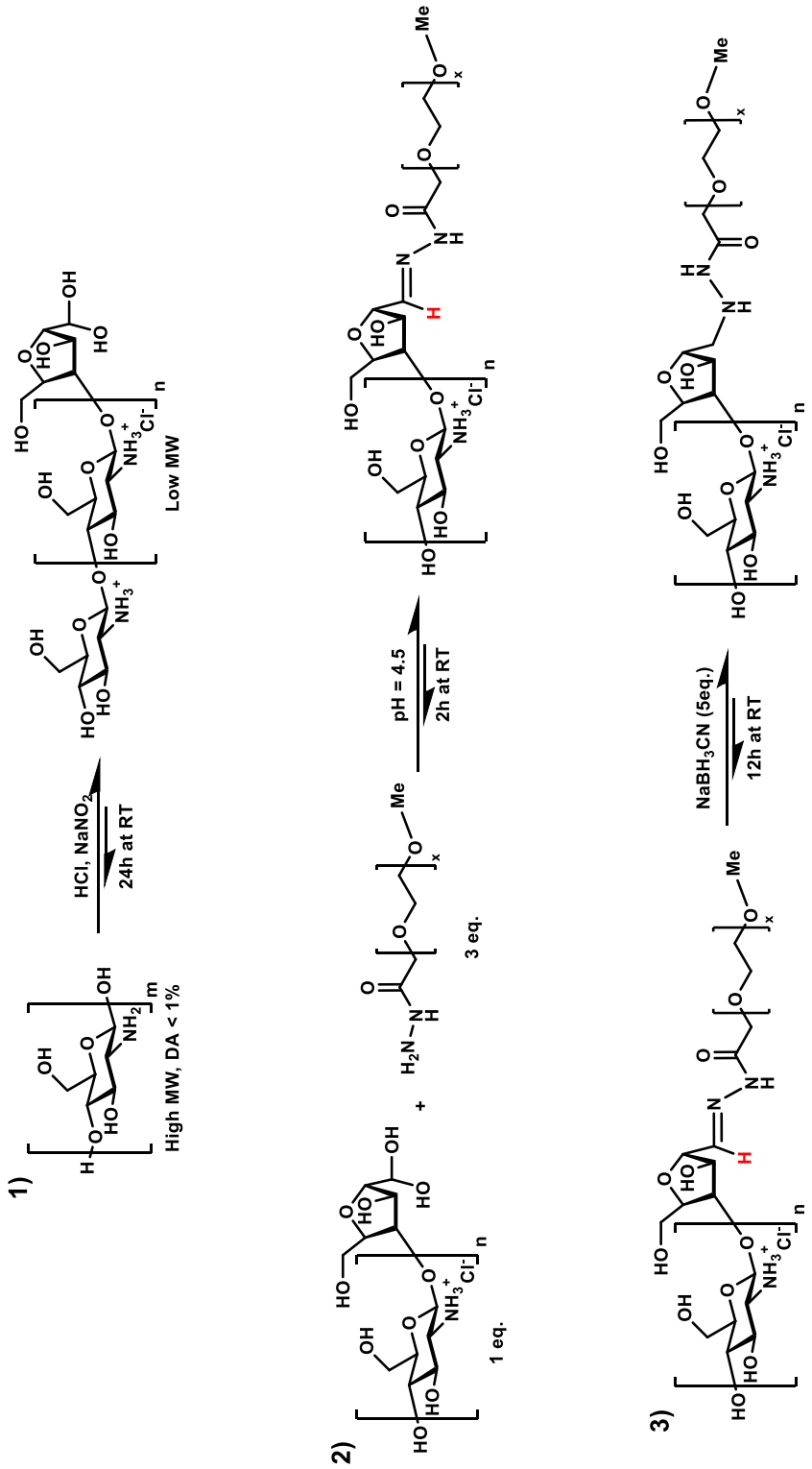

Figure 5.3-1. Strategy for the synthesis of a COS-*b*-PEG copolymer. 1) Synthesis of the COS block by depolymerization with the HONO process of a high molecular weight chitosan with a DA < 1%. 2) Hydrazone formation between the aldehyde of the COS M-residue and the PEG hydrazide function. 3) Reduction of the hydrazone with the reducing agent $NaCNBH_3$. The presence of the imino proton (in red) can be monitored by ^1H NMR (hydrazone formation, at 7.4 ppm and disappearance after the reduction step).

5.3.2. Synthesis of the COS20-*b*-PEG5k

Preparation of COS. Chitosan oligosaccharide of DP = 20 (COS20) was prepared by depolymerization of an almost fully N-deacetylated chitosan (DA < 1%) of 9×10^4 g/mol with nitrous acid. In this reaction, the number of broken glycosidic linkages is approximately stoichiometric to the amount of nitrous acid used. After several purification steps, the COS was obtained under the water-soluble hydrochloride salt form. All chemical shifts could be assigned on ^{1}H NMR spectra obtained in D_2O (Figure appendix 16). In particular, the signal at 5.11 ppm was assigned to the gem diol group of the terminal 2,5-anhydro-D-mannofuranose (M-unit). Importantly, no trace of hydroxymethylfurfural (HMF), the main degradation product of the M-unit through reaction with amine groups, was evidenced by the absence of the characteristic peaks of HMF at 9.52, 7.52, 6.66 and 4.68 ppm [35].

Conjugation of a COS with mPEG hydrazide. The conjugation of a COS bearing the M-unit at the reducing end with a methoxy PEG bearing a hydrazide function leads to the formation of the targeted block copolymer. The formation of the imine bond was monitored here with a shorter COS of DP = 13.5 during 2h30 by ^{1}H NMR with the corresponding chemical shift at 7.4 ppm which is complementary to the decrease of the H-1 proton of the M-unit at 5.1 ppm (Figure 5.3-2). The integrations were calculated by using the signal at 3.2 ppm as reference which corresponds to the H-2 of the D-unit of chitosan. Besides, the PEG signal at 3.4 ppm corresponds to the methoxy group at the chain end (an integral of 9 is expected in the reaction medium where 3 equivalents of PEG were introduced). It can be noted that the reaction is very fast as expected from the literature and seems to lead only to the *E*-form of the hydrazone, predominant for this reaction [21]. The *Z*-form of the imine might be present but was not detected, being in too low proportions. The hydrazone peak integrating for 1, it was considered that the conversion was almost full after 2h.

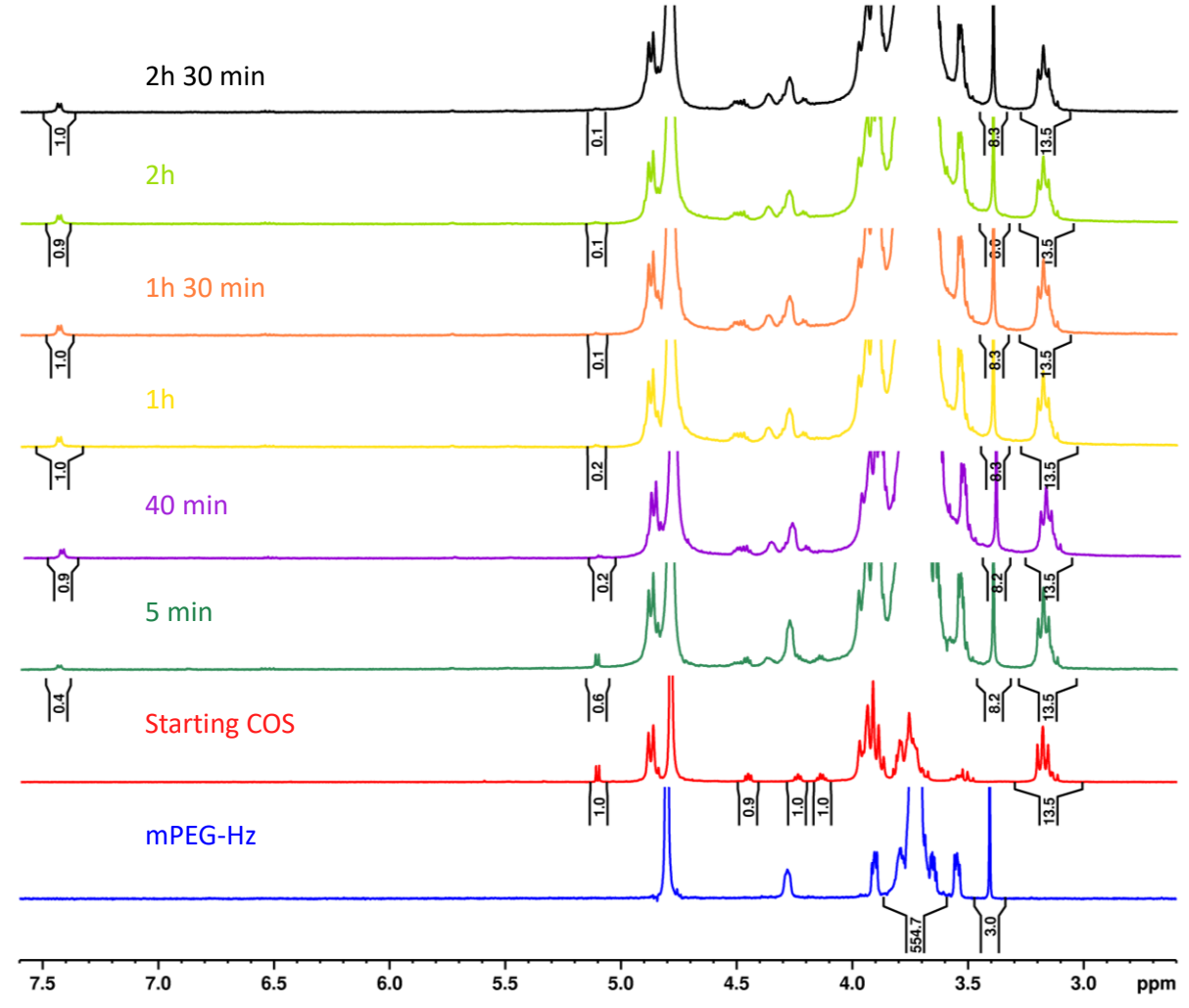

Figure 5.3-2. ^{1}H NMR spectra of the reaction medium of COS of DP = 13.5 with mPEG-Hz (D_2O, 400 MHz, 298 K). The reaction was followed during 2h30. The formation of the hydrazone bond can be monitored through the increase of the peak at 7.4 ppm and by the complementary decrease of the signal at 5.1 ppm corresponding to the H-1 of the M-unit. The integrals at 7.4 ppm and 5.1 ppm are obtained with the integrals of the H-2 protons (3.1 ppm) set to the COS DP.

The successful reduction with 5 equivalents of $NaCNBH_3$ during 12 hours at room temperature was verified through the disappearance of the hydrazone peak at 7.4 ppm and the disappearance of the peak corresponding to the H-1 protons of the M-unit under its gem-diol form at 5.1 ppm (Figure 5.3-3).

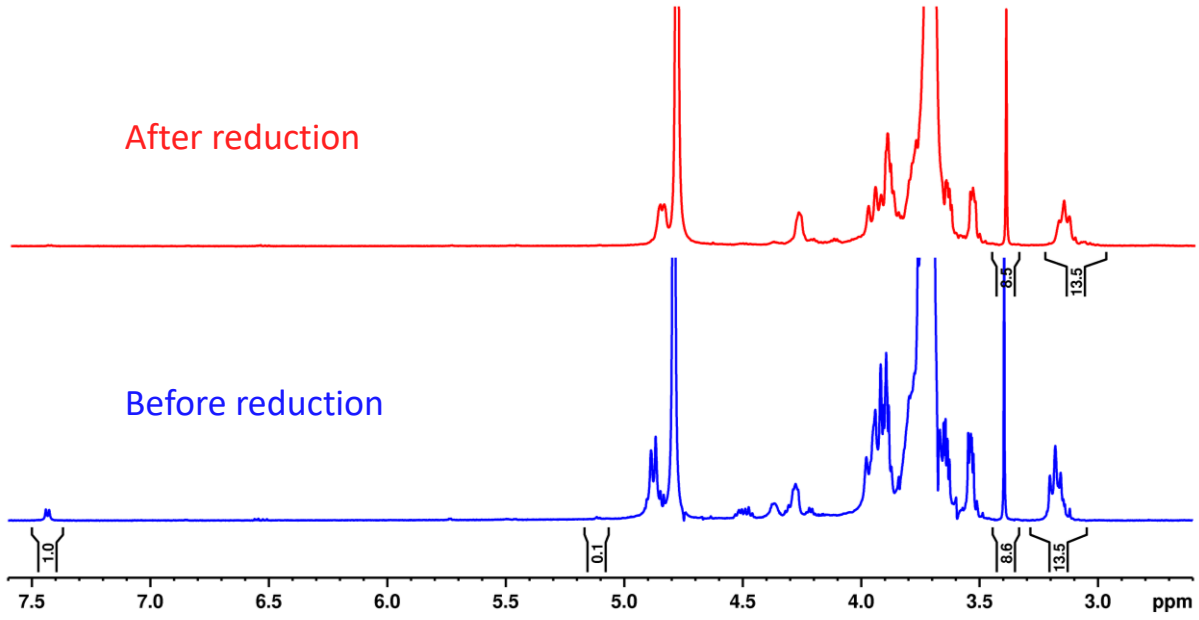

Figure 5.3-3. ^{1}H NMR spectra of the reaction medium of COS with a DP = 13.5 with mPEG-Hz (D_2O, 400 MHz, 298 K) after 2h30 of reaction (blue) and after the reduction with $NaCNBH_3$ (red). Integration of the signals at 7.4 ppm and 5.1 ppm are obtained by setting the signal of the H-2 of the D-unit (3.1 ppm) to the COS DP.

After the purification described in the experimental section, one can compare the SEC chromatograms of the two initial polymers (COS20 and mPEG-Hz) with the purified product. A clear shift to the shorter retention times was observed, indicating the successful conjugation of the two starting blocks (Figure 5.3-4.a). Moreover, the ^{1}H NMR spectrum of the copolymer showed the expected integrations of a block copolymer based on a COS20 and a methoxy PEG. Indeed, when setting the integral of the methoxy protons of PEG to 3, the resulting integral of the H-1 protons of D-units corresponded to the expected DP of 18 for the COS (Figure 5.3-4.b). Similar results were obtained for the conjugation of a shorter COS block (DP = 13) with the same mPEG-Hz of 5 kDa (Figure appendix 18). The characteristics of the starting products and the copolymer obtained are reported in Table 5.3.1. Unfortunately, the purification method led to very low mass yields (< 20%) because a large amount of block copolymer probably precipitated with free chitosan. The purification will be discussed in more detail in the section 5.3.3.3.

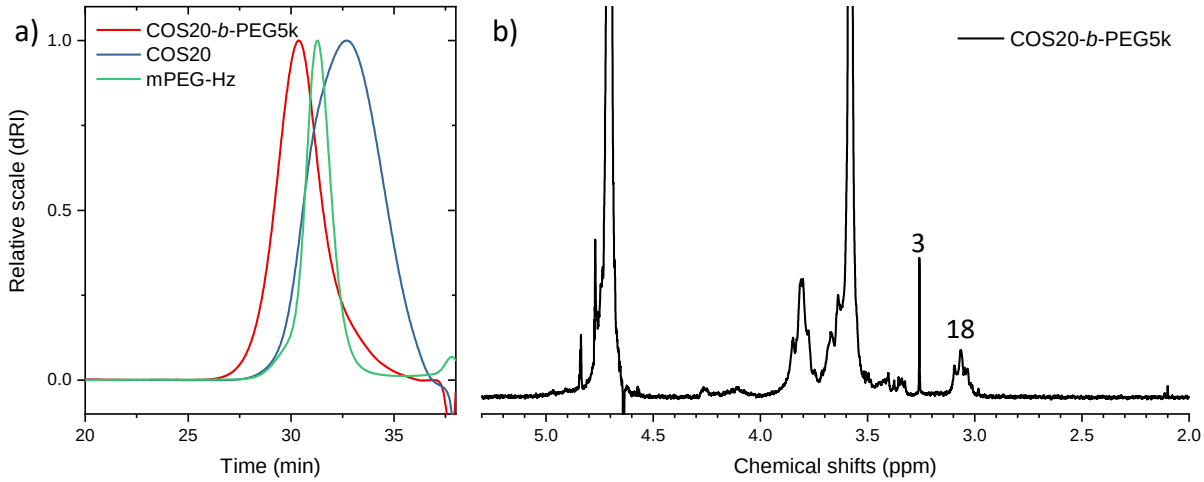

Figure 5.3-4. Characterisation of the COS20-*b*-PEG5k copolymer. a) Chromatograms (dRI trace) of the copolymer (red) and the two starting blocks: COS20 (blue) and mPEG-Hz (green). (chromatography conditions: Tosoh G6000Pwxl and G2500Pwxl columns, acetate buffer pH 4.5 as eluent). b) ^{1}H NMR spectrum of the final copolymer. The integral of the methyl group at the PEG chain end is set to 3. (D_2O, 400 MHz, 298 K).

Table 5.3.1. Characterisation of the COS-*b*-PEG copolymer and initial blocks by SEC-MALLS.

Product	M_n (g/mol)	M_w (g/mol)	Đ	DP_n
COS20[1]	3 033	4 110	1.35	18[4]
mPEG hydrazide[2]	5 433	5 479	1.009	121
COS20-*b*-PEG5k[3]	9 095	10 080	1.187	/

[1]dn/dc of 0.1860 mL/g measured previously
[2]dn/dc taken as 0.1350 mL/g [36]
[3]dn/dc taken as 0.157 mL/g, (weight-average average of the dn/dc of the two blocks)
[4]Corresponds to the number of GlcN units exclusively

A way to verify the purification and the successful obtention of the block copolymer is to measure the solubility of the copolymer compared to that of the COS alone as a function of the pH. Turbidimetry can be an efficient way to assay the solubility of the polymers in solution, the Optical Density (OD) increasing when the solubility of the polymer decreases. As seen in the chapter 2, the solubility of a COS will strongly depend on the pH of the solution, leading to aggregates when the critical pH of solubility is reached. It is expected for the COS-based copolymer to obtain an apparent solubility over a larger range of pH thanks to the introduction of a long hydrophilic PEG block. Figure 5.3-5 shows indeed a critical pH of

solubility for the homopolymer COS20 below pH = 7 whereas the copolymer seems to be soluble in the whole range of pH.

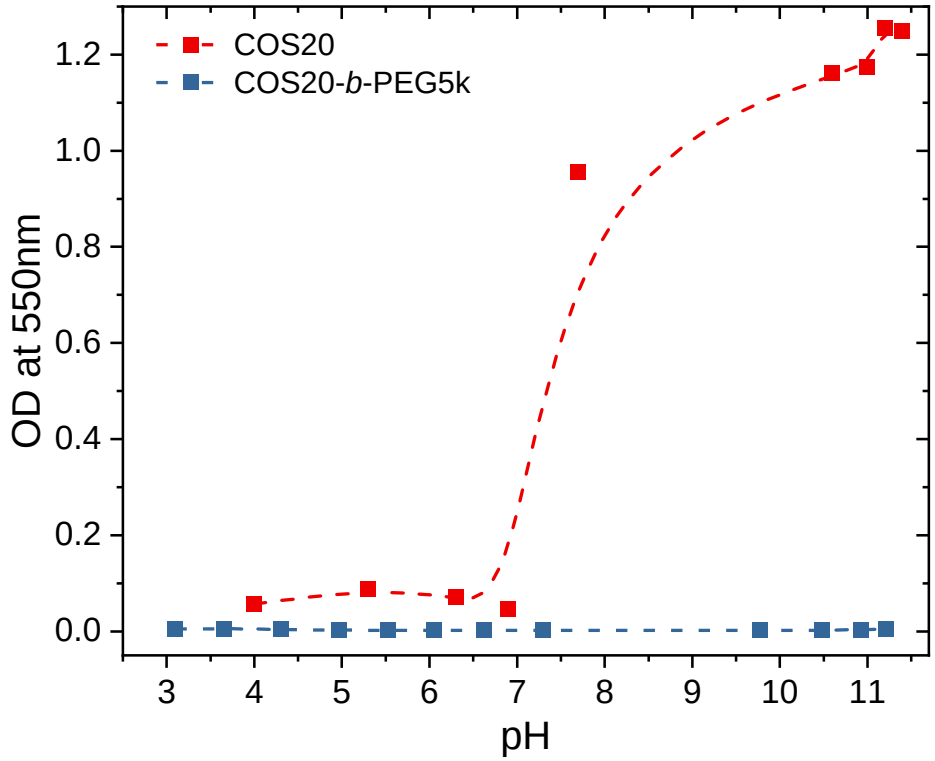

Figure 5.3-5. Turbidimetry of solutions of COS20 and COS20-*b*-PEG5k at 2 g/L as a function of pH. The optical density of the solution is measured at λ = 550 nm.

5.3.3. Complexation of COS-*b*-PEG copolymer with siRNA

The COS-*b*-PEG block copolymer is expected to form a conjugate structure with siRNA for N:P ratios equal or higher than 1 [26]. Indeed, the use of a COS block whose length matches the number of charges of one strand of the siRNA should lead to the formation of a conjugate structure. In these conditions, it is expected that two copolymer chains can attach to the siRNA at the charge neutrality of the system [24]. The morphology of the complexes was mainly studied by dynamic light scattering and fluorescence correlation spectroscopy.

5.3.3.1. Analysis of complexes by Dynamic Light Scattering (DLS)

Dynamic Light Scattering analysis was performed on complexes formed between siRNA and COS-*b*-PEG copolymers having COS blocks varying in DP from 13 to 27 and PEG blocks of 2kDa or 5kDa. The idea of testing different block copolymer compositions and molar masses was to better understand the influence of molecular parameters on the morphology of complexes. One of the difficulties encountered in the preparation of complexes and their characterization was the low amount of block copolymer available. This prompted us to develop complexation protocols where everything was 'micro', from the microtube for the mixing step to the microcell for the characterization.

The DLS data summarized in Figure 5.3-6 shed light on the morphology of complexes in a very clear manner. First, one must notice that more than one population can be detected on the PSD of the siRNA and the block copolymers. This emphasized the presence of additional relaxation modes, probably related to the electrostatic properties of the two polyelectrolytes. However, these additional modes vanish when the PSD is weighted by the number of scattering objects. The peaks corresponding to the relaxation of polymer chains were usually observed close to 10 nm or slightly below for the siRNA and the copolymer. For N:P = 0.5, the PSD was very similar to the PSD of siRNA and the scattering intensity was almost unchanged (Figure 5.3-6.a). For many PEC systems the complexation at a charge ratio of 0.5 is by far sufficient to form colloidal particles of complex with strong scattering properties. Therefore, the fact that complexes obtained at N:P = 0.5 scatter little light suggests that they contain a limited number of polymer chains, which is in agreement with the picture of a conjugate structure (Figure 5.3-6). For N:P values of 1 and 3 (or 2.5), a main population in the 50 nm range could be detected on the PSD of all block copolymer systems. This is also coherent with a conjugate structure. However, looking closer to the data, one can notice important differences in the scattered intensity between systems containing PEG 5k which scattered very little light and the system containing PEG 2k for which there was a very strong increase in scattered intensity from N:P = 1. This suggests that blocks of PEG 2k are too short to effectively stabilize the conjugate structures, and consequently, the complexes have probably aggregated into small colloidal particles (Figure 5.3-6). For N:P equal or higher to 5, the scattering intensity remain low and almost constant for all systems containing PEG 5k, which clearly supports the formation of conjugate structures (Figure 5.3-6.a). The new peaks detected on the PSD likely arises from the presence of a large excess of block copolymer. Hence, the specific relaxation of conjugates can be hardly resolved. It is noticeable that a single peak was detected on the PSD of complexes based on PEG 2k. It is clear that the

scattering intensity of the complex particles totally mask the scattering of copolymer in excess. Therefore, this was also an indirect evidence of the successful formation of conjugates for copolymers containing PEG blocks of 5 kDa. In contrast, PEG blocks of 2kDa were probably too short to stabilize the conjugate structure, thus favouring the formation of complex particles.

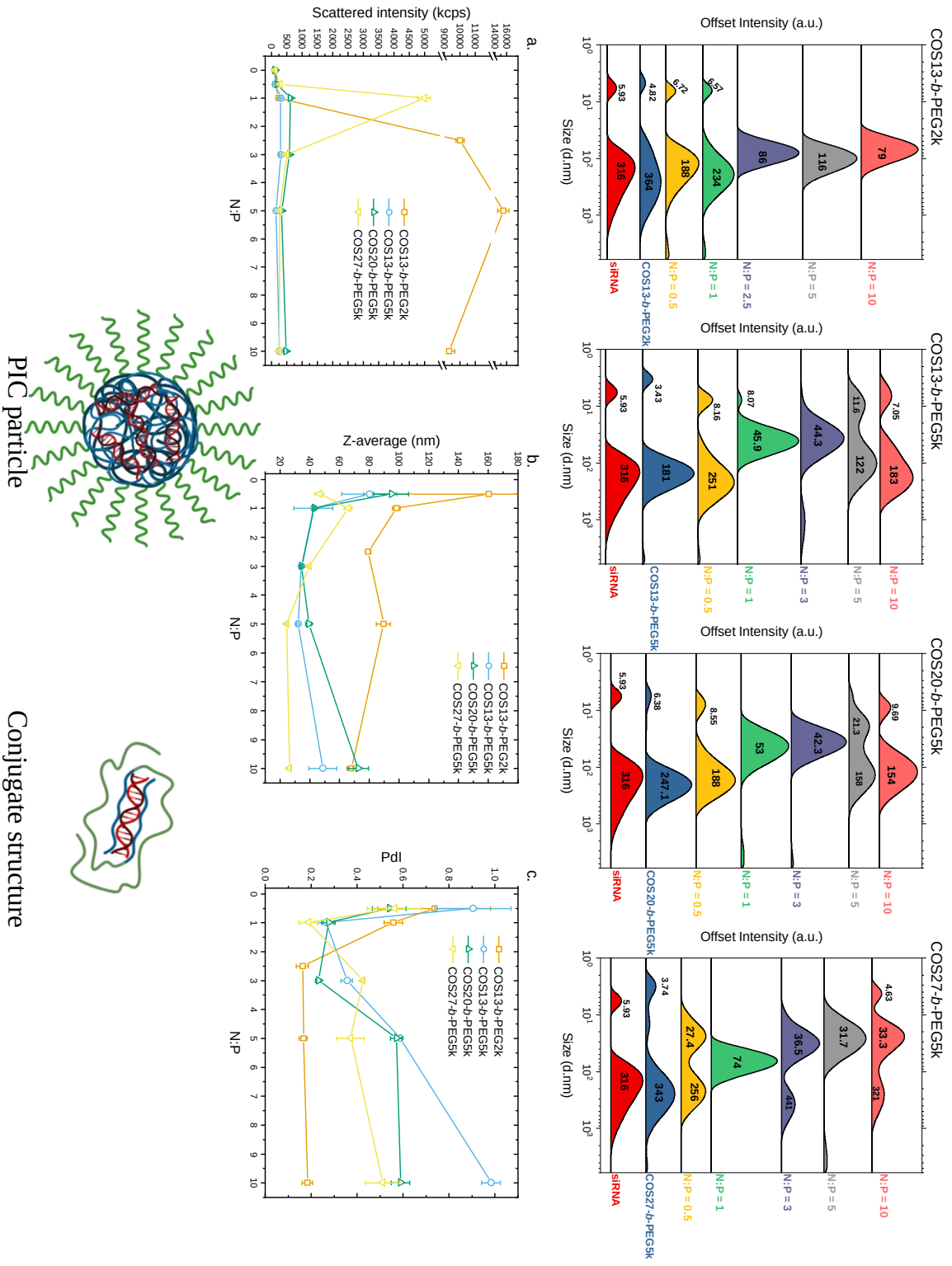

Figure 5.3-6. Dynamic light scattering analysis of the complexes of siRNA with copolymers COS-*b*-PEG5k having COS blocks varying in DP from 13 to 27 and PEG blocks of 2kDa or 5kDa at various N:P ratios. (Top panel) PSD (D_h in nm) of the siRNA alone, the copolymer alone and the assemblies obtained at different N:P ratios. a) Scattered light intensity from the complexes as a function of N:P. b) Z-average (D_h) and c) PdI of the objects formed at the different N:P obtained from the cumulant analysis of the correlation data. (Bottom) Scheme of a PIC particle and a conjugate structure.

5.3.3.2. Study of the assemblies by Fluorescence Correlation Spectroscopy (FCS)

Fluorescence Correlation Spectroscopy (FCS) is a relevant technique to assay the size of the targeted conjugate structure. Indeed, the size expected for such a structure being in the same order of magnitude of size as siRNA alone, the diffusion coefficient differences of the objects would be more precisely followed and not affected by the self-associating nature of the polyelectrolytes. By using a fluorescently labelled siRNA (Cyanine 5.5), the size of the structures containing the siRNA can be accurately measured. The optimisation of concentrations led to the conclusion that the labelled siRNA had to be diluted by 2000 in order to reach around one fluorophore in the volume of observation (see 5.2 for the procedure). By doing so, the average number of fluorescent molecules in the volume was between 1 and 2, allowing a good signal and autocorrelation data for siRNA alone (Figure 5.3-7). Additionally, the block copolymer alone was measured at the highest concentration investigated during the study and did not give any fluorescent signal. The fitting of the correlation data led to a diffusion coefficient for the siRNA alone of 69.9 ± 2.98 µm²/s which corresponds to the expected hydrodynamic diameter for siRNA alone of around 7 nm [26].

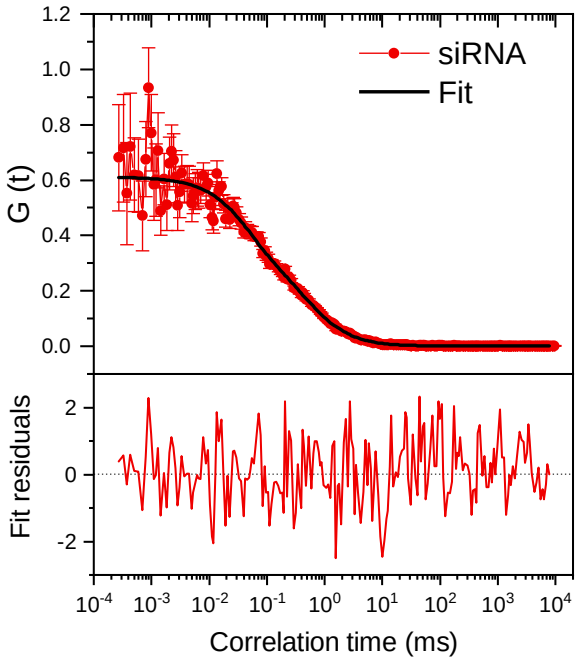

Figure 5.3-7. Autocorrelation curve and fit residuals of siRNA alone tagged with Cy5.5 obtained by FCS analysis.

The addition of COS20-*b*-PEG5k copolymer to the siRNA solution at increasing N:P ratios is expected to gradually increase the size of the monitored fluorescent object. Indeed, the siRNA will be gradually decorated by the copolymer thanks to the electrostatic interaction between the positively charged COS block and the phosphate groups carrying negative charges. The charge neutralisation state at N:P = 1 is expected to correspond to the siRNA completely decorated by the copolymer describing the targeted 'conjugate-like' structure. Therefore, the diffusion coefficient of the fluorescent object should decrease until reaching this state and remain constant. Indeed, the full decoration of the siRNA surface should prevent any further complexation of copolymer to the nucleic acids.

The Figure 5.3-8 presents the variation of the diffusion coefficient of the labelled siRNA as a function of the amount of copolymer introduced, expressed as the N:P ratio. As expected, a gradual decrease of the diffusion coefficient was observed with the increase of the amount of copolymer introduced. The diffusion coefficient decreased until reaching a minimal value at a N:P ratio of 2, corresponding to objects with a hydrodynamic diameter of 50 nm. The lowest diffusion coefficients obtained for N:P ratios of 1 and 2 were associated to autocorrelation curves for which the coefficient 1/N – derived from the y intercept at t = 0 – was greater than 1 (Figure appendix 17.c and d). This phenomenon corresponds to an aggregation where several fluorescent siRNAs are condensed in the same object. In this case, the siRNAs behave as fluorescent particles, thus decreasing the number of fluorescent objects in the focal volume [38].

Further addition of copolymer led to the expected size for a conjugated structure, around 16 nm in diameter [24, 39] at N:P = 4. The conjugate size was similar at N:P = 8. The autocorrelation curves at these N:P ratios have coefficient $1/N$ below 1, thus confirming the absence of aggregation phenomena (Figure appendix 17.e, f and g). Very similar results were obtained from the COS13-*b*-PEG5k copolymer (see Figure appendix 19 and Figure appendix 20) with hydrodynamic diameter of 40 nm at N:P = 2 characterised by an aggregation state (Figure appendix 20.d) and a hydrodynamic diameter of 16 nm at N:P = 8.

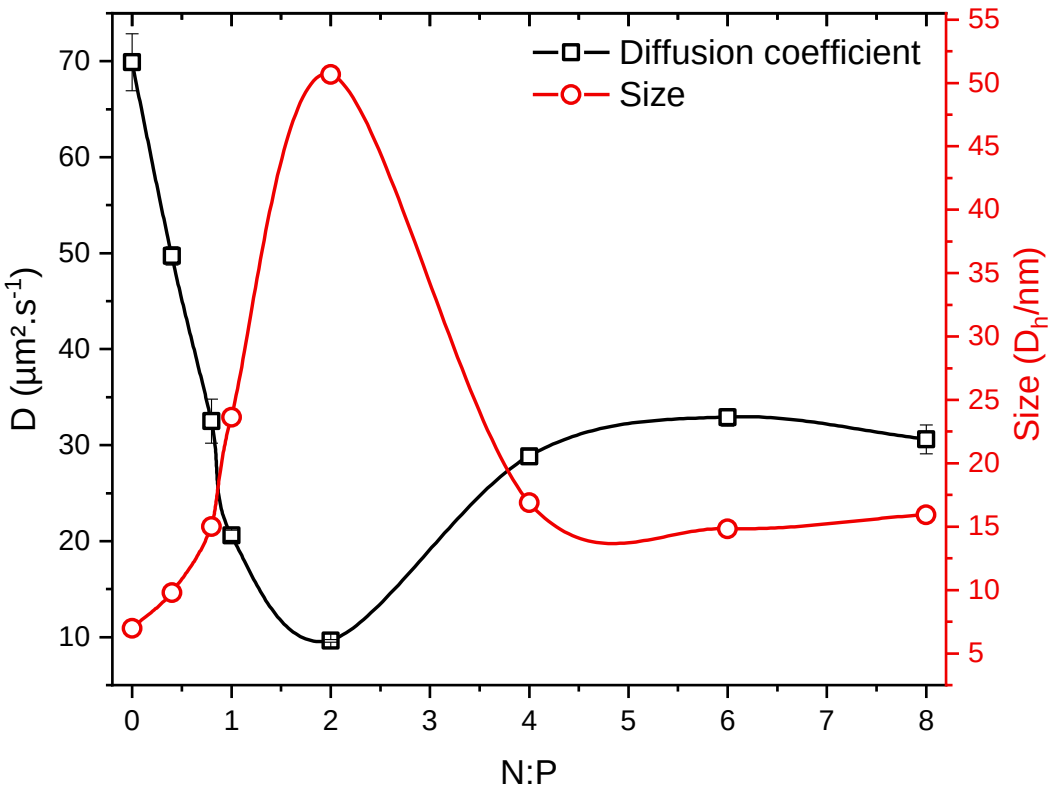

Figure 5.3-8. Variation of the diffusion coefficient of the siRNA-Cy5.5 with increasing amounts of COS20-*b*-PEG5k (increasing N:P ratios) (black) and corresponding sizes (hydrodynamic diameter) (red).

5.3.3.3. Discussion

The characterisation of the complexes obtained from siRNA and the COS-*b*-PEG copolymer by DLS and FCS lead to the conclusion that two structures were obtained with this system depending on the block copolymer composition. For the copolymers containing COS having a DP between 13 and 27 and a PEG of 5kDa, complexes with a conjugate-like structure that can be also referred as 'monomolecular' or 'unimolecular' complexes in the sense of they contain a single molecule of siRNA, were obtained for N:P values above 1. According to the FCS analysis which provides number-averaged diffusion coefficients, the hydrodynamic diameter of the conjugate is below 20 nm. The hydrodynamic size provided by DLS is larger, i.e. in the 50 nm range due to the R^6 dependency of the scattered light in the Rayleigh regime. For block copolymers containing PEG of 2kDa, the PEG block was likely too short to well stabilize the conjugate structure. As a consequence, complexes aggregate into colloidal particles in the 50 nm size range. Such complex particles of small size might be also of interest for the delivery of siRNA as they can better interact with the cell membrane. In addition, the siRNA payload is also higher than in conjugates. However, the main disadvantage of the

complexes forming particles is their early recognition by the reticuloendothelial system followed by their degradation by the macrophages. It is believed that the conjugate-like structure allows the complexes to better escape the immune system.

5.3.4. Additional purification of the COS-*b*-PEG copolymer

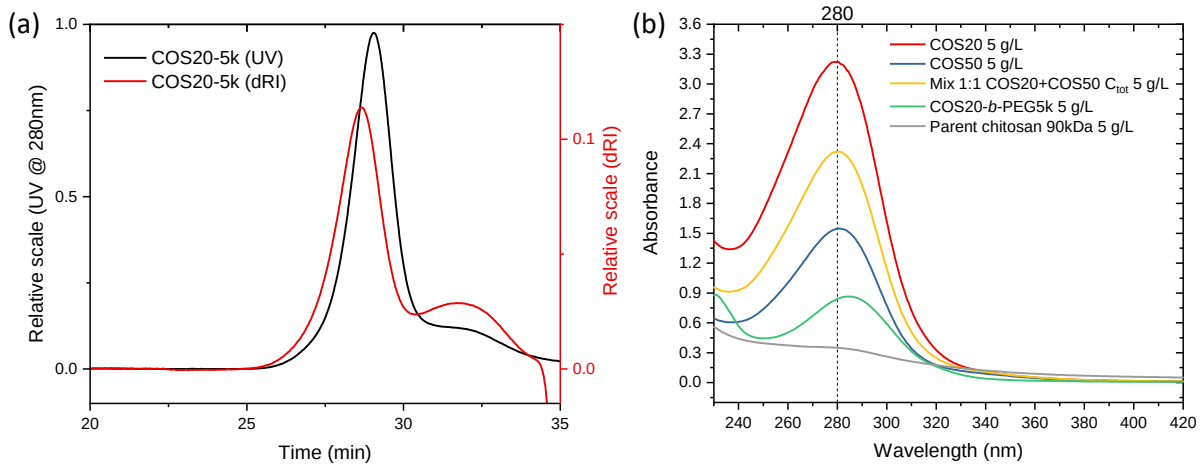

Figure 5.3-9. a) Chromatogram of the COS20-*b*-PEG5k copolymer, dRI trace in red and UV trace at λ = 280 nm in black. Chromatography conditions: Tosoh G4000Pwxl and G3000Pwxl columns, acetate buffer pH 4.5 as eluent. b) UV spectra in acetate buffer (blank measured accordingly) of the COS20 (red), COS50 (blue), a mixture of COS20 and COS50 (1:1 w:w) (yellow), COS20-*b*-PEG5k (green) and the parent chitosan before depolymerization (grey). The polymer concentrations were 5 g/L.

In a new chromatographic analysis of the copolymer COS20-*b*-PEG5k, it was noticed that there is a large shoulder on the low molecular weight side. This would suggest the presence of a non-negligible fraction of free COS that had not been detected in the first chromatographic analyses (Figure 5.3-9.a). Furthermore, it could be noticed during these analyses that the copolymer and the supposed free COS strongly absorbed UV at 280 nm (Figure 5.3-9.b). Additional characterisation by spectrophotometry suggests that the activity of the COS in the UV range can be attributed to its M-unit with a maximum of absorbance at λ = 280 nm. Indeed, the absorbance of COS20 is higher than that of COS50 at similar mass concentration (Figure 5.3-9.b, red and blue), suggesting the presence of UV absorbing-end group. The parent chitosan presents almost no absorbance at same concentration. The remaining free COS in the product might be explained by several hypothesis. First, the synthesis itself: the ^{1}H NMR spectrum before the reduction step (Figure 5.3-3) suggested the presence of unreacted COS from the remaining signal as a trace at 5.1 ppm. Secondly, from

the purification procedure where it is possible that small COS chains may have remained in the supernatant when the pH is increased at the end of the reaction. Moreover, some of the free COS chains may also be trapped in the micelles of block copolymer that can also form at high pH.

The purification of the copolymer was attempted through fractionation by preparative chromatography. The chromatogram obtained with the preparative SEC was very similar to the one obtained from analytical SEC with the presence of the same two distinct populations: the first attributed to the copolymer at smaller eluted volume and the bump at larger eluted volumes attributed to the free COS (Figure 5.3-10.a). The fractions corresponding to the copolymer with elution volumes between 48.8 and 68.8 mL were pooled together and dialysed against water to remove ions of the acetate buffer and finally freeze dried. The deconvolution of the chromatogram to estimate the distribution of the populations revealed the possible presence of remaining COS in the final product (Figure 5.3-10.b). Indeed, the population attributed to the free COS (green) seems to go beyond the elution volume of 68.8 mL.

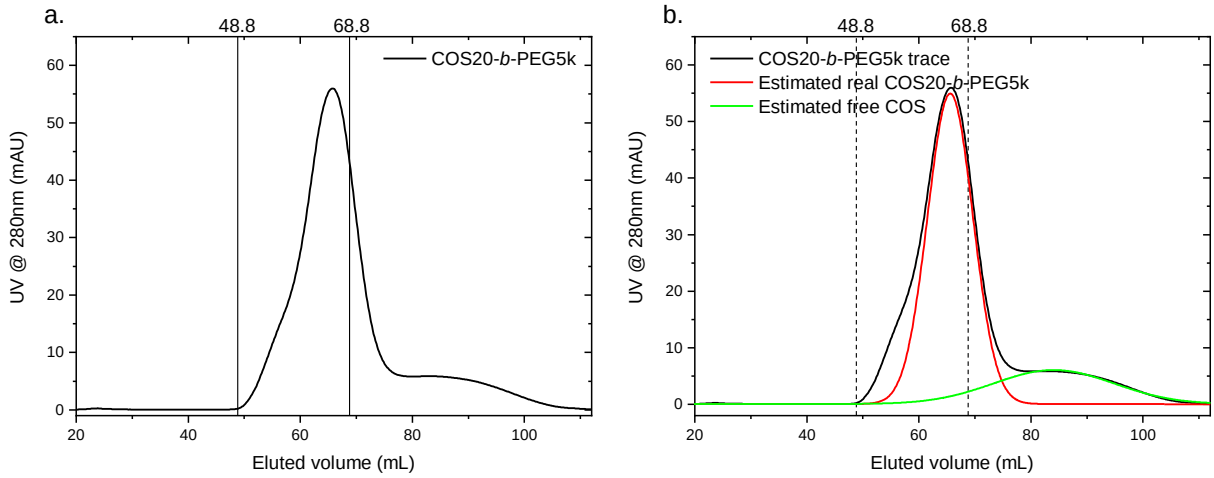

Figure 5.3-10. Preparative SEC chromatogram of COS20-*b*-PEG5k. a) Chromatogram with a UV detection at 280 nm. The fractions between 48.8 and 68.8 mL were selected and pooled. b) Deconvolution of the chromatogram to estimate the distribution of the two populations.

The polymer recovered from the preparative SEC was characterised by SEC and ^{1}H NMR. The purified copolymer presents a COS block with a lower DP than the targeted one. Indeed, the ^{1}H NMR spectrum in Figure 5.3-11.b indicates a DP around 13. This decrease in DP is due to the removal of some of the excess COS. Unfortunately, a shoulder in the UV trace of the chromatogram was still detected (Figure 5.3-11.a, red). It might correspond to a small fraction of free COS as feared after the deconvolution of the chromatogram of the preparative SEC (Figure 5.3-10.b). However, this shoulder did not appear on the trace of the dRI and LS

signals. This suggests that only a very low amount of free COS remained in the copolymer for which the UV detection is particularly sensitive.

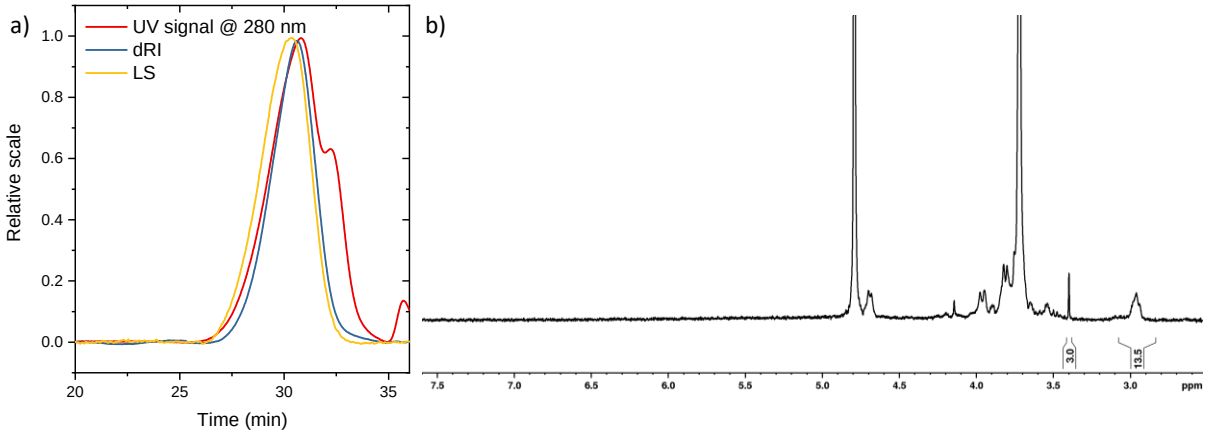

Figure 5.3-11. Characterisation of the COS20-*b*-PEG5k purified by preparative SEC. a) Chromatograms, UV trace of the signal at λ = 280 nm (red), dRI trace (blue) and LS signal (yellow) of the copolymer. Chromatography conditions: Tosoh G4000Pwxl and G3000Pwxl columns, acetate buffer pH 4.5 as eluent. b) ^{1}H NMR spectrum of the final product, the integration of the methyl at the PEG end is fixed, corresponding to 3 protons (D_2O, 400 MHz, 298 K).

5.3.5. siRNA complexation with the fractionated copolymer

5.3.5.1. Analysis by Dynamic Light Scattering

Complexes from siRNA and the purified COS13-*b*-PEG5k copolymer were prepared at various N:P ratios under similar conditions as described previously. The complexes were characterized by DLS using a new instrument from Malvern Panalytical, the Zetasizer Ultra. For N:P values less than or equal to 1, the relaxation of free siRNA was well evidenced in the PSD. For N:P = 2 and above, a unique relaxation was detected with a hydrodynamic diameter in the 50 nm range. Contrary to the data obtained with the non-purified copolymer, the scattering due to the copolymer in excess could not be detected at high N:P ratios. It is likely that the scattering of the complexes is much higher this time and completely masks that of the copolymer. As the purified copolymer consists of a shorter COS block (DP 13 vs. 20 before purification), the siRNA molecules are probably decorated by a larger number of copolymer molecules. Similarly, the fact that there was less free COS after purification also allowed more copolymer molecules to complex with siRNA (free COS did not compete). It can also be noticed that even if the scattered intensity was more important than before, it did not reach the scattering levels of complexes with a particle morphology as with COS13-b-PEG2K

(Figure 5.3-6). This supports the hypothesis of the formation of a conjugate-type structure with a larger number of copolymer molecules decorating siRNAs.

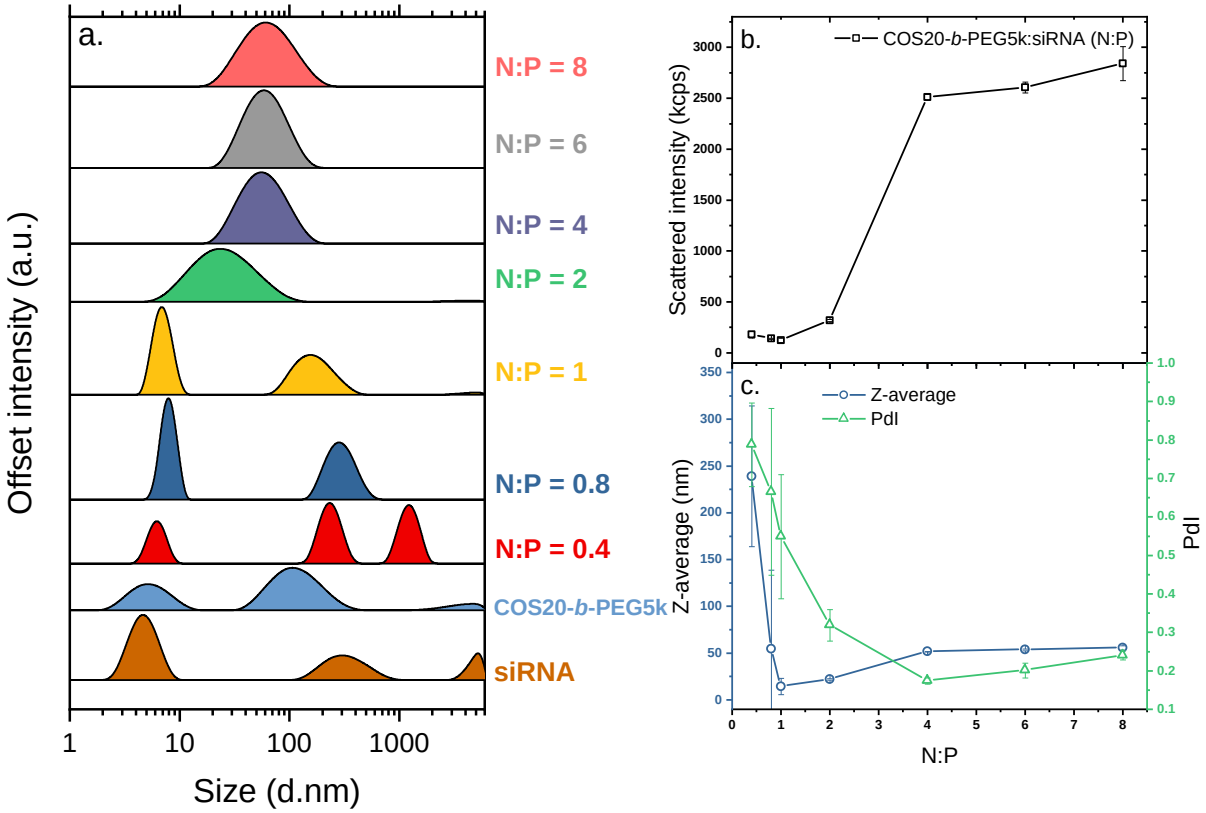

Figure 5.3-12. Dynamic light scattering analysis of siRNA/COS-b-PEG complexes with the copolymer fractionated by preparative SEC. a) PSD (D_h in nm) of the complexes at various N:P. b) Scattered light intensity from the complexes as a function of N:P. c) Z-average (D_h) and PdI of the objects formed at various N:P obtained from the cumulant analysis of the correlation data.

The stability of these structures over time was evaluated by analysing the samples after 13 days of storage in the fridge. The ageing of the samples was characterised by a systematic increase of the size of the complexes (Figure 5.3-13). Nonetheless, the complexes after 13 days of incubation kept a narrow size distribution and relatively low PdI. This was especially the case for the ratio N:P = 4 where the PdI under 0.2 was preserved with a slight increase of the size to a Z-average of 70 nm. In order to explain this instability of the complexes over time, it is hypothesized that the absorbing blocks, i.e. the COS blocks were too short to maintain the integrity of the conjugate structure. As shown previously, a DP between 8 and 13 is required to form stable complexes between COS and siRNA but this threshold could be shifted to higher DPs for block copolymer due to the entropy penalty resulting from the PEG block coupled to the COS.

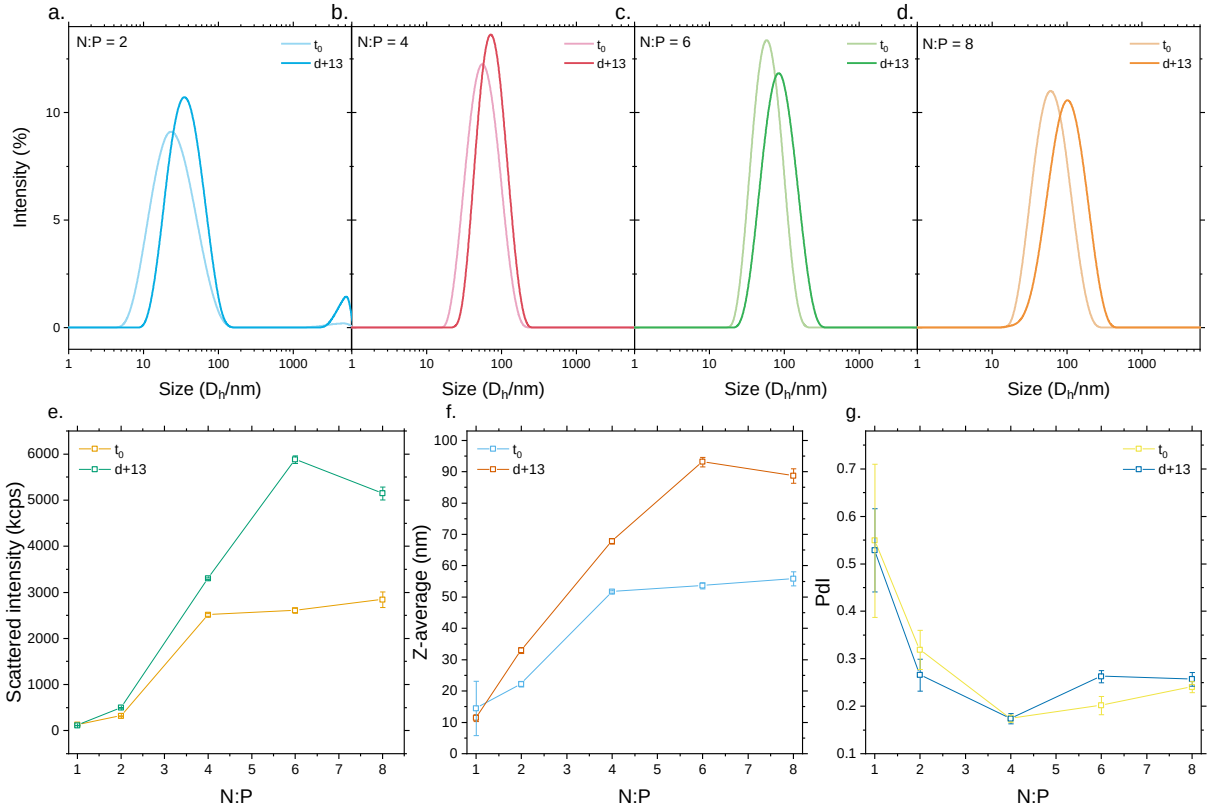

Figure 5.3-13. Stability evaluation of the complexes formed with the purified COS20-*b*-PEG5k. PSD of the complexes at t_0 (light colour) and after 13 days (dark colour) at various N:P ratios a) N:P = 2, b) N:P = 4, c) N:P = 6 and d) N:P = 8. e) Scattered light intensity from the complexes at t_0 and after 13 days as a function of N:P. Evolution of the parameters derived from the cumulant analysis of the correlation data as a function of N:P: f) Z-average (D_h) and g) PdI.

5.4. New strategy in the purification of the COS-*b*-PEG copolymer

5.4.1. Introduction

The synthetic approach developed in the previous section suffers from two disadvantages related to the purification process of the copolymer: the low yield and the presence of a significant amount of free COS in the copolymer. In the procedure used, the reaction medium was precipitated in a basic medium at the end of the synthesis and the supernatant was recovered. It was assumed that the copolymer was mostly in the supernatant but the low yields obtained suggest that this may not be the case. Furthermore, the fact that the DP of COS in the purified copolymer was lower than the DP of the original COS tends to show that only copolymers containing COS of low DP are soluble in the supernatant and that those with

higher DP would precipitate with the vast majority of the excess COS. In other words, the hydrophilicity of the PEG of 5kDa could be not high enough to keep the copolymer in solution. The product remaining in the supernatant of the reaction medium after centrifugation would then be mostly the PEG in excess, the copolymer with the shortest COS block and the shortest free COS. Therefore, the majority of the copolymer and free COS must be in reality in the precipitate. The copolymer could then be isolated from the free COS by means of preparative SEC.

A reaction was therefore performed in a small quantity and followed by ^{1}H NMR and SEC, to verify the formation of the copolymer and the amounts of each product remaining in the supernatant and the precipitate after centrifugation.

5.4.2. Monitoring the block copolymer formation and purification

A reaction at a reduced scale (2 mL) was run in D_2O in the same conditions as described in section 5.2. The ^{1}H NMR spectra of the starting products, the reaction medium after 4h30 and the reaction medium after 12h of reduction with $NaCNBH_3$ are depicted in Figure 5.4-1.d. The starting products as well as the reaction medium after reduction of the hydrazone were also analysed by SEC (Figure 5.4-1). A new batch of methoxy PEG hydrazide was used. It was composed of two fractions as shown by chromatographic analysis (Figure 5.4-1.a): one fraction corresponding to the desired 5 kDa mPEG-Hz and another one corresponding to a fraction of approximately 10 kDa which suggests that dimerization of PEG occurred during the functionalization step of PEG. Assuming that PEG-hydrazide has been synthesized by hydrazinolysis of a PEG ester, dimerization may result from insufficient hydrazide being introduced [41]. This dimer was evaluated to be 10% of the product in mass according to the integral of the corresponding peak (Figure 5.4-1.a). Moreover, only the PEG dimer was active in UV at 280 nm, supporting the hypothesis of the dimerization pathway and the absence of reactivity of this population. The reaction medium was analysed by SEC after 4h30 of reaction but the analysis was considered not reliable due to the reversibility of the hydrazone linkage in acidic conditions (acetate buffer pH = 4.5 as eluent) [42].

As described in the previous synthesis, the reaction allowed a conversion up to 90 % with the formation of the hydrazone illustrated by the signal at 7.4 ppm (Figure 5.4-1, green). On the 2 spectra of the reaction mixture, the presence of 3 equivalents of PEG were verified with the respective integrations. The successful reduction of the hydrazone linkage after 12h was verified with the disappearance of the corresponding signal at 7.4 ppm (purple).

SEC analysis led to overloaded chromatograms. However, the analysis of the dRI trace in Figure 5.4-1.b clearly indicates the formation of the copolymer. Indeed, after coupling and reduction, all the small chains of COS (blue trace) were no longer present in the reaction mixture. This was also verified with the UV detection (Figure 5.4-1.c). Moreover, a shift of the chromatogram peak of the reaction mixture towards shorter retention times compared to the COS or the PEG also corroborate the formation of the copolymer.

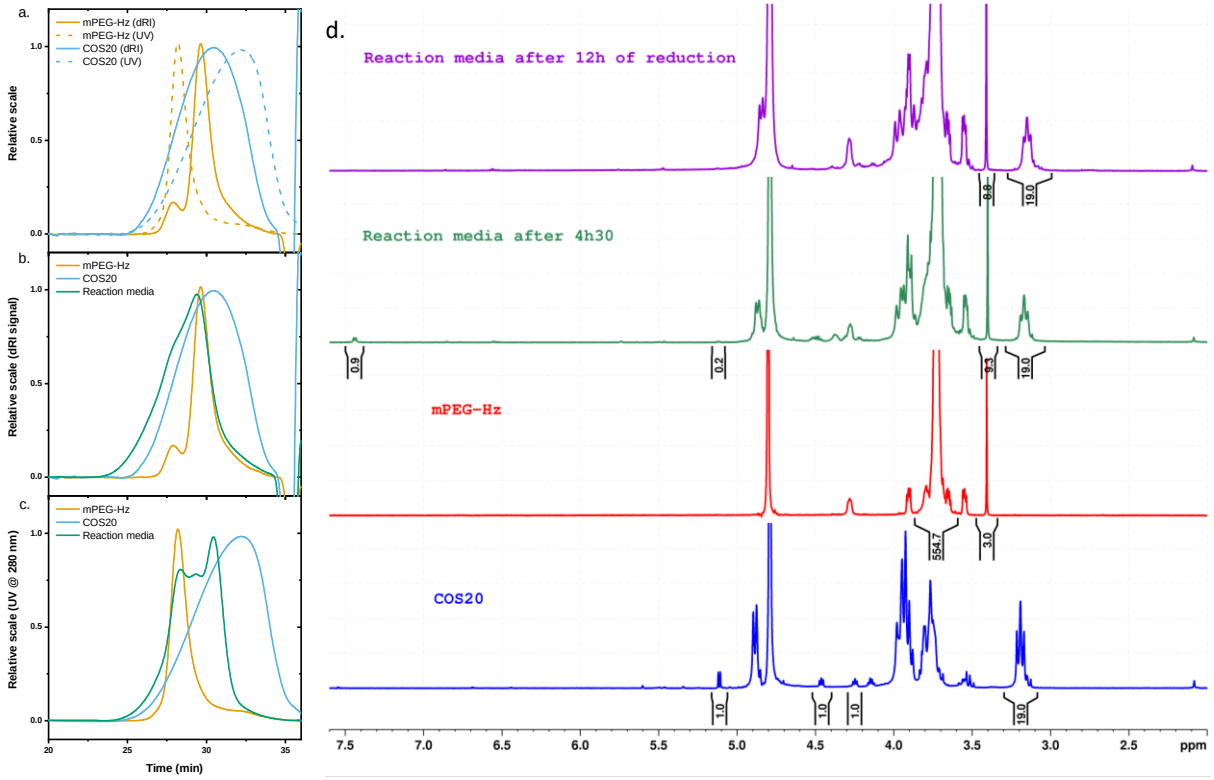

Figure 5.4-1. Characterisation of the starting products and the coupling reaction media. The columns used for SEC analysis were the G4000 and G3000. a) dRI and UV trace of the starting blocks. Trace of the starting blocks superimposed with the reaction media after reduction, b) dRI trace and c) UV trace. d) ^{1}H NMR spectra of the starting blocks COS20 (blue) and mPEG-Hs (red) and reaction media after 4h30 of reaction (green) and after 12h of reduction (purple).

After precipitation by increasing the pH of the solution above 9 and centrifugation, the supernatant and the precipitate were analysed by ^{1}H NMR (the precipitate was re-acidified to fully solubilize the chitosan). The spectra are represented in Figure 5.4-2. The spectrum of the supernatant (Figure 5.4-2, blue) presents a shift of the H-1 protons of the D-unit due to the increase of the pH [43]. The integral put in evidence the presence of a large excess of PEG, much more than the 3 equivalents introduced for the reaction. Indeed, almost 16 PEG chains are present in the supernatant for one COS chain. On the contrary, the analysis of the precipitate (Figure 5.4-2, red) almost reached the integral values expected for the targeted block copolymer with a small excess of COS compared to the PEG but this may be considered

within the margin of error. From this analysis, we can estimate that 86% of the COS and 28% of the PEG initially introduced were recovered in the precipitate. Therefore, the majority of the copolymer precipitates with the free COS. Clearly, this explains the low yield in block copolymer from the previous purification protocol.

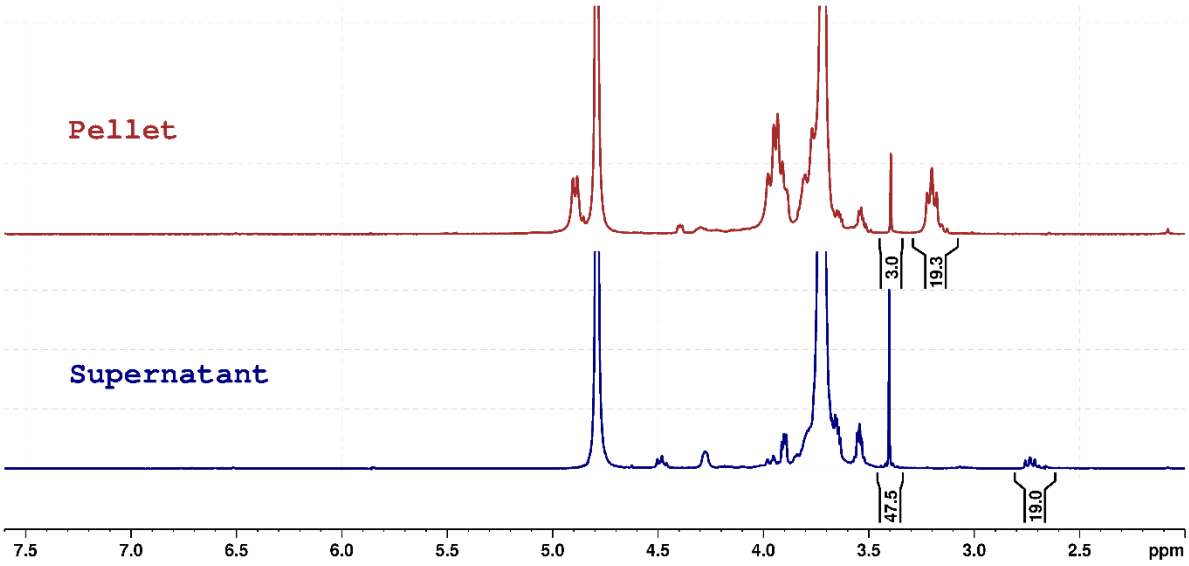

Figure 5.4-2. ^{1}H NMR spectra in D_2O of the supernatant and precipitate after precipitation in alkali conditions. The precipitate was re-acidified prior to analysis.

5.4.3. Synthesis of the COS-*b*-PEG copolymer at larger scale

The block copolymer synthesis was performed and followed at a larger scale following the same procedure as previously. Mainly, 250 mg of COS20 and 1.07 g of mPEG-Hz were dissolved in 25 mL of D_2O, so that the reaction could be followed by ^{1}H NMR at the key steps: after 2h30 of reaction and after complete reduction of the hydrazone bond (Figure 5.4-3.a). NMR spectra of the reaction media confirmed that the reaction performed as well as on a small scale. The precipitate was washed with a NaOH solution to remove the residual PEG. The analysis of the supernatant revealed a slightly smaller excess of PEG compared to the test at smaller scale (Figure 5.4-3.a, green *vs* Figure 5.4-2). The precipitate was analysed by SEC and the chromatogram compared to the COS alone (Figure 5.4-3.b). The two populations detected on the chromatogram can be attributed to the copolymer and the free COS (see the shoulder of the main peak). The two populations are even more visible on the UV trace, with a clear distinction of the two peaks attributed to the copolymer at shorter retention times and the free COS at longer retention times.

Therefore, the precipitate was purified by preparative SEC with UV detection in order to isolate the peak attributed to the copolymer population (Figure 5.4-3.c). The chromatogram obtained by preparative SEC was similar to that obtained by analytical SEC, with the clear distinction between the two populations (copolymer and free COS). The peak attributed to the copolymer was collected in 4 fractions as shown in the Figure 5.4-3.c. Each fraction was recovered and purified by dialysis as described in the Materials and methods section.

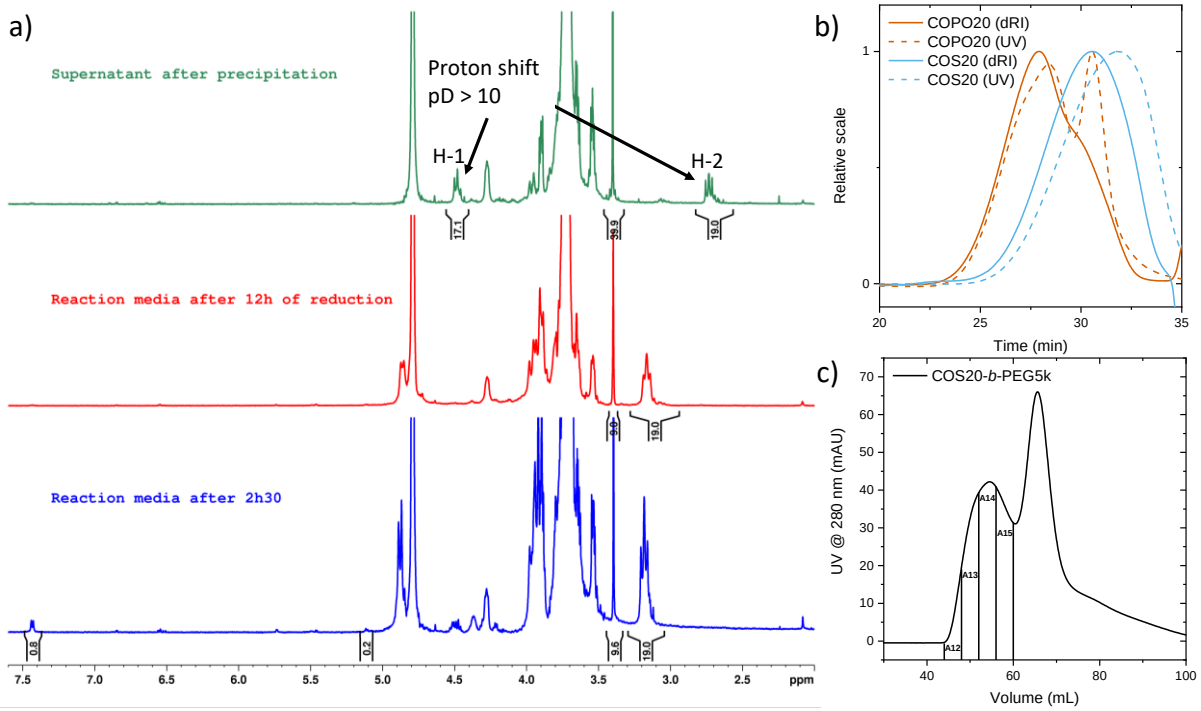

Figure 5.4-3. a) Key steps of the reaction between the COS20 and the mPEG-Hz at a larger scale studied by ^{1}H NMR: before the reduction (blue), after complete reduction (red) and analysis of the supernatant after precipitation by increasing pH. b) Chromatogram of the washed precipitate (orange) compared to the starting COS20 (blue). Solid line corresponds to the dRI signal and the dashed line to the UV one. Set of columns: G4000 and G3000, eluent: acetate buffer, pH 4.5. c) Preparative SEC of the precipitate: four fractions corresponding to the copolymer were collected (A12, A13, A14 and A14).

Each fraction was then characterised by analytical SEC (Figure 5.4-4 and Table 5.4.1), except for the fraction A12 that contained a very small amount of polymer. The purification by preparative SEC led to copolymer fractions with a narrow dispersity. However, the overlapping of the peaks of the COS20 and the different fractions of copolymer suggests that free COS may be still present in the copolymer fractions (Figure 5.4-4.a). A similar conclusion can be drawn from the chromatograms obtained with a UV detection (Figure 5.4-4.b). Moreover, the fractionation favoured the recovery of the copolymer with relatively long COS blocks. Indeed, as seen in the Table 5.4.1, the molar masses of the different fractions of

copolymer were high (the molar mass of the PEG is only 5 kDa). It turns out that the DP of the COS block must vary from 31 in the fraction A15 to 89 in the fraction A13. A similar value was indeed found by ^{1}H NMR for the fraction A13 (Figure appendix 21). Additionally, and this was at least good news, no free PEG or free COS was detected by DOSY NMR in the fraction A13 (Figure appendix 22).

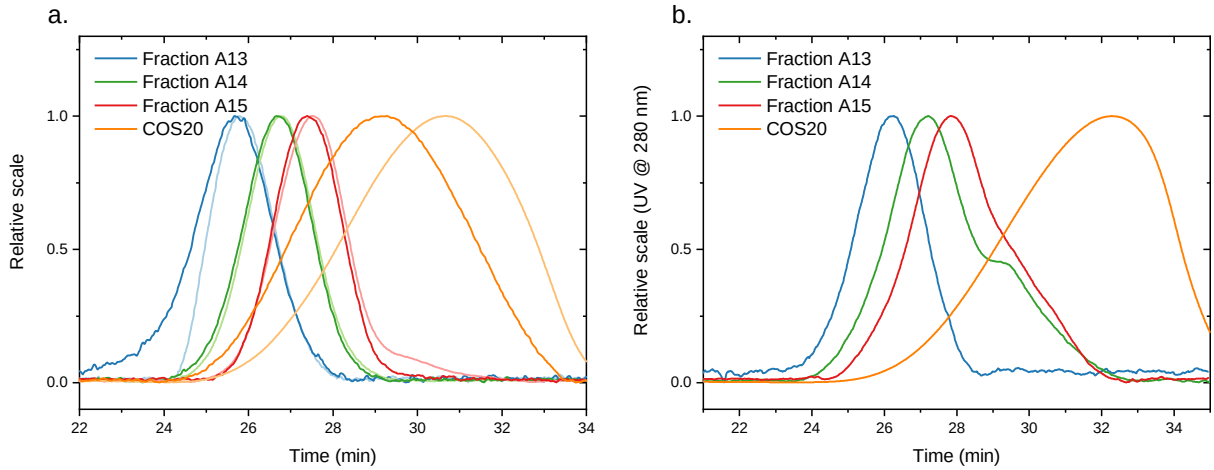

Figure 5.4-4. Analytical SEC chromatograms of the fractions recovered from preparative SEC compared to the starting COS20. a) LS signal (dark colour) and dRI signal (light colour). b) UV trace with the detector set at 280 nm.

Table 5.4.1. Characteristics of the copolymer fractions and starting COS20 determined by SEC-MALLS.

Sample	M_w (g.mol^{-1})	M_n (g.mol^{-1})	Đ
COS20[1]	4 110	3 033	1.35
Fraction A13[2]	21 920	19 720	1.112
Fraction A14[2]	12 910	12 810	1.008
Fraction A15[2]	10 570	10 450	1.012

[1]dn/dc of 0.1860 mL/g measured previously

[2]dn/dc taken as 0.157 mL/g, the weight-average dn/dc of the two blocks.

5.4.4. Discussion

The fractionation of the reaction medium after precipitation in alkali conditions, although effective, did not allow the recovery of a copolymer having a short COS block without the presence of free COS in the product. This downside of the approach originates from the limited separation efficiency of the column used for preparative SEC. By extension, this downside is also related to the fact that the targeted block copolymer and COS have almost similar molecular weights. Therefore, the COS-free fractions of copolymer that could be recovered by preparative SEC mostly contained chitosan blocks of high DP. One can also remark that the precipitation of the reaction medium mostly favoured the recovery of copolymer composed of long cationic blocks due to their low solubility at high pH.

The improvement towards a copolymer containing a short cationic block can be tackle at various levels. First, the dispersity of the starting COS is an important parameter since the solubility behaviour of the longest chains is different from the shortest ones when the pH increases above 7. Moreover, the size dispersity of the COS blocks is somewhat retrieved in the block copolymer structure after the coupling reaction. Therefore, the COS could be fractionated by preparative SEC before use in coupling reactions with PEG hydrazide. It is also believed that the coupling of a longer PEG (~10 kDa) to the chitosan should allow a more efficient separation of the block copolymer by preparative SEC. In addition, it is expected that the COS-PEG block copolymer containing a PEG block larger than 5 kDa should remain in solution at high pH, probably as micelles, which would allow its easier recovery after reaction (by assuming that the free COS fully precipitates under such conditions).

5.5. Conclusion and perspectives

This chapter was devoted to two aspects: the synthesis of a new block copolymer structure and the use of the copolymer in the electrostatic complexation with siRNA.

The conjugation of a PEG bearing a hydrazide function with a chitosan oligosaccharide presenting an aldehyde function at its reducing end is an efficient reaction, reaching conversions up to 90%. However, it appeared that if the coupling reaction worked well, the purification of the copolymer to remove unreacted COS and excess PEG was a nightmare. A first purification based on the extraction of the PEGylated species after precipitation of the free COS by increasing the pH led to a poor yield. In addition, the purified copolymer was still contaminated by some traces of free COS. However, we could demonstrate, by using

DLS and FCS, that the complexes obtained with siRNA have the expected conjugate-like morphology for N:P ratios equal or higher to one.

Further characterisation of the copolymer revealed an unexpected UV absorbance of the COS and the copolymer, which is related to the M-unit. Then, the purification of the copolymer was attempted by means of preparative size exclusion chromatography with a UV detection – the only available for our experiments – as traditionally used in the purification of proteins. The fractionation of the copolymer worked well even though some traces of free COS could be still detected in the copolymer. The complexes obtained with siRNA and the fractionated copolymer have a conjugate morphology with similar characteristics as those obtained with the non-fractionated copolymer. However, the relatively high scattering intensity found for these conjugates suggests that more copolymer molecules were complexed with siRNA. The shorter COS blocks in the fractionated copolymer might explain this.

Finally, a new purification method was investigated based on the precipitation of the copolymer in alkali conditions followed by its fractionation by means of preparative chromatography. This method allowed the obtention of a product with a narrow size distribution but it was limited by the close values of the molar masses of the copolymer and the COS. Indeed, a copolymer COS-*b*-PEG5k formed with short COS blocks has more or less the same molar mass as the long COS chains. The fraction of copolymer obtained without free COS contained rather long COS blocks with regards to the size required to form a conjugate structure with siRNAs.

The purification protocol of the copolymer could be improved by modifying several aspects:

1) The fractionation of the starting COS which has a rather high dispersity ($Đ = 1.35$) would allow a better control over the solubility behaviour of the COS chains as well as a more precise control over the length of the cationic block in the final DHBC structure. Moreover, this would allow a better separation of the copolymer and free COS by preparative SEC.
2) The coupling of COS with a longer PEG, i.e 10 kDa also should allow a better separation of the copolymer and free COS by preparative SEC. Moreover, copolymers with longer PEG blocks are expected to form micelles in alkaline conditions and only unreacted COS must precipitate under such conditions. This should considerably facilitate the purification of the copolymer.

These two points could either be applied separately or combined depending on the cost of COS and PEG hydrazide. In any case, the use of preparative SEC would be recommended to obtain a copolymer having a narrow molar mass dispersity and a defined length of the cationic block.

The control over the length of the cationic block drives the complexation of the copolymer with siRNA in either a conjugate structure or a PIC micelle. It was observed in this chapter that a conjugate structure can be obtained from copolymer with a short cationic block. However, the presence of free COS chains of various lengths may favour the formation of complex with a different morphology. This justifies that pure COS-*b*-PEG copolymer with short COS blocks is the prerequisite towards the formation of complexes with a true conjugate structure.

5.6. References

[1] Portes E, Gardrat C, Castellan A, Coma V (2009) Environmentally friendly films based on chitosan and tetrahydrocurcuminoid derivatives exhibiting antibacterial and antioxidative properties. Carbohydr Polym 76:578–584 . https://doi.org/10.1016/j.carbpol.2008.11.031

[2] Chapelle C, Quienne B, Bonneaud C, David G, Caillol S (2021) Diels-Alder-Chitosan based dissociative covalent adaptable networks. Carbohydr Polym 253:117222 . https://doi.org/10.1016/j.carbpol.2020.117222

[3] Croisier F, Jérôme C (2013) Chitosan-based biomaterials for tissue engineering. Eur Polym J 49:780–792 . https://doi.org/10.1016/j.eurpolymj.2012.12.009

[4] Hsu CW, Hsieh MH, Xiao MC, Chou YH, Wang TH, Chiang WH (2020) pH-responsive polymeric micelles self-assembled from benzoic-imine-containing alkyl-modified PEGylated chitosan for delivery of amphiphilic drugs. Int J Biol Macromol 163:1106–1116 . https://doi.org/10.1016/j.ijbiomac.2020.07.110

[5] Cao Y, Tan YF, Wong YS, Liew MWJ, Venkatraman S (2019) Recent Advances in Chitosan-Based Carriers for Gene Delivery. Mar Drugs 17:381 . https://doi.org/10.3390/md17060381

[6] Shi B, Zhang H, Shen Z, Bi J, Dai S (2013) Developing a chitosan supported imidazole Schiff-base for high-efficiency gene delivery. Polym Chem 4:840–850 . https://doi.org/10.1039/C2PY20494K

[7] Dehousse V, Garbacki N, Jaspart S, Castagne D, Piel G, Colige A, Evrard B (2010) Comparison of chitosan/siRNA and trimethylchitosan/siRNA complexes behaviour in vitro. Int J Biol Macromol 46:342–349 . https://doi.org/10.1016/j.ijbiomac.2010.01.010

[8] Guţoaia A, Schuster L, Margutti S, Laufer S, Schlosshauer B, Krastev R, Stoll D, Hartmann H (2016) Fine-tuned PEGylation of chitosan to maintain optimal siRNA-nanoplex bioactivity. Carbohydr Polym 143:25–34 . https://doi.org/10.1016/j.carbpol.2016.01.010

[9] Rudzinski WE, Palacios A, Ahmed A, Lane MA, Aminabhavi TM (2016) Targeted delivery of small interfering RNA to colon cancer cells using chitosan and PEGylated chitosan nanoparticles. Carbohydr Polym 147:323–332 . https://doi.org/10.1016/j.carbpol.2016.04.041

[10] Shi Q, Fernandes J, Winnik F, Benderdour M, Zhang, Qiu, Dai (2012) Low molecular weight chitosan conjugated with folate for siRNA delivery in vitro: optimization studies. Int J Nanomedicine 7:5833 . https://doi.org/10.2147/IJN.S35567

[11] Ganji F, Abdekhodaie MJ (2008) Synthesis and characterization of a new thermosensitive chitosan–PEG diblock copolymer. Carbohydr Polym 74:435–441 . https://doi.org/10.1016/j.carbpol.2008.03.017

[12] Pickenhahn VD, Darras V, Dziopa F, Biniecki K, De Crescenzo G, Lavertu M, Buschmann MD (2015) Regioselective thioacetylation of chitosan end-groups for nanoparticle gene delivery systems. Chem Sci 6:4650–4664 . https://doi.org/10.1039/C5SC00038F

[13] Rosselgong J, Chemin M, Almada CC, Hemery G, Guigner J-M, Chollet G, Labat G, Da Silva Perez D, Ham-Pichavant F, Grau E, Grelier S, Lecommandoux S, Cramail H (2019) Synthesis and Self-Assembly of Xylan-Based Amphiphiles: From Bio-Based Vesicles to Antifungal Properties. Biomacromolecules 20:118–129 . https://doi.org/10.1021/acs.biomac.8b01210

[14] Guerry A, Bernard J, Samain E, Fleury E, Cottaz S, Halila S (2013) Aniline-Catalyzed Reductive Amination as a Powerful Method for the Preparation of Reducing End-"Clickable" Chitooligosaccharides. Bioconjug Chem 24:544–549 . https://doi.org/10.1021/bc3003716

[15] Novoa-Carballal R, Müller AHE (2012) Synthesis of polysaccharide-b-PEG block copolymers by oxime click. Chem Commun 48:3781 . https://doi.org/10.1039/c2cc30726j

[16] Vikøren Mo I, Feng Y, Øksnes Dalheim M, Solberg A, Aachmann FL, Schatz C, Christensen BE (2020) Activation of enzymatically produced chitooligosaccharides by dioxyamines and dihydrazides. Carbohydr Polym 232:115748 . https://doi.org/10.1016/j.carbpol.2019.115748

[17] Tømmeraas K, Vårum KM, Christensen BE, Smidsrød O (2001) Preparation and characterisation of oligosaccharides produced by nitrous acid depolymerisation of chitosans. Carbohydr Res 333:137–144 . https://doi.org/10.1016/S0008-6215(01)00130-6

[18] Allan GG, Peyron M (1995) Molecular weight manipulation of chitosan I: kinetics of depolymerization by nitrous acid. Carbohydr Res 277:257–272 . https://doi.org/10.1016/0008-6215(95)00207-A

[19] Moussa A, Crépet A, Ladavière C, Trombotto S (2019) Reducing-end "clickable" functionalizations of chitosan oligomers for the synthesis of chitosan-based diblock copolymers. Carbohydr Polym 219:387–394 . https://doi.org/10.1016/j.carbpol.2019.04.078

[20] Pickenhahn VD, Grange M, De Crescenzo G, Lavertu M, Buschmann MD (2017) Regioselective chitosan end-group activation: the triskelion approach. RSC Adv 7:18628–18638 . https://doi.org/10.1039/C7RA01348E

[21] Mo IV, Dalheim MØ, Aachmann FL, Schatz C, Christensen BE (2020) 2,5-Anhydro-D-Mannose End-Functionalized Chitin Oligomers Activated by Dioxyamines or Dihydrazides as Precursors of Diblock Oligosaccharides. Biomacromolecules 21:2884–2895 . https://doi.org/10.1021/acs.biomac.0c00620

[22] Harada A, Kataoka K (1995) Formation of Polyion Complex Micelles in an Aqueous

Milieu from a Pair of Oppositely-Charged Block Copolymers with Poly(ethylene glycol) Segments. Macromolecules 28:5294–5299 . https://doi.org/10.1021/ma00119a019

[23] Matsumoto S, Christie RJ, Nishiyama N, Miyata K, Ishii A, Oba M, Koyama H, Yamasaki Y, Kataoka K (2009) Environment-Responsive Block Copolymer Micelles with a Disulfide Cross-Linked Core for Enhanced siRNA Delivery. Biomacromolecules 10:119–127 . https://doi.org/10.1021/bm800985e

[24] Watanabe S, Hayashi K, Toh K, Kim HJ, Liu X, Chaya H, Fukushima S, Katsushima K, Kondo Y, Uchida S, Ogura S, Nomoto T, Takemoto H, Cabral H, Kinoh H, Tanaka HY, Kano MR, Matsumoto Y, Fukuhara H, Uchida S, Nangaku M, Osada K, Nishiyama N, Miyata K, Kataoka K (2019) In vivo rendezvous of small nucleic acid drugs with charge-matched block catiomers to target cancers. Nat Commun 10: . https://doi.org/10.1038/s41467-019-09856-w

[25] Yi Y, Kim HJ, Zheng M, Mi P, Naito M, Kim BS, Min HS, Hayashi K, Perche F, Toh K, Liu X, Mochida Y, Kinoh H, Cabral H, Miyata K, Kataoka K (2019) Glucose-linked sub-50-nm unimer polyion complex-assembled gold nanoparticles for targeted siRNA delivery to glucose transporter 1-overexpressing breast cancer stem-like cells. J Control Release 295:268–277 . https://doi.org/10.1016/j.jconrel.2019.01.006

[26] DeRouchey J, Schmidt C, Walker GF, Koch C, Plank C, Wagner E, Rädler JO (2008) Monomolecular Assembly of siRNA and Poly(ethylene glycol)−Peptide Copolymers. Biomacromolecules 9:724–732 . https://doi.org/10.1021/bm7011482

[27] Delas, Mock-Joubert, Faivre, Hofmaier, Sandre, Dole, Chapel, Crépet, Trombotto, Delair, Schatz (2019) Effects of Chain Length of Chitosan Oligosaccharides on Solution Properties and Complexation with siRNA. Polymers (Basel) 11:1236 . https://doi.org/10.3390/polym11081236

[28] Allan GG, Peyron M (1995) Molecular weight manipulation of chitosan II: prediction and control of extent of depolymerization by nitrous acid. Carbohydr Res 277:273–282 . https://doi.org/10.1016/0008-6215(95)00208-B

[29] Johnson CS (1999) Diffusion ordered nuclear magnetic resonance spectroscopy: principles and applications. Prog Nucl Magn Reson Spectrosc 34:203–256 . https://doi.org/10.1016/S0079-6565(99)00003-5

[30] Stilbs P (1981) Molecular self-diffusion coefficients in Fourier transform nuclear magnetic resonance spectrometric analysis of complex mixtures. Anal Chem 53:2135–2137 . https://doi.org/10.1021/ac00236a044

[31] Holz M, Weingartner H (1991) Calibration in accurate spin-echo self-diffusion measurements using 1H and less-common nuclei. J Magn Reson 92:115–125 . https://doi.org/10.1016/0022-2364(91)90252-O

[32] Longsworth LG (1960) THE MUTUAL DIFFUSION OF LIGHT AND HEAVY WATER. J Phys Chem 64:1914–1917 . https://doi.org/10.1021/j100841a027

[33] Pánek J, Loukotová L, Hrubý M, Štěpánek P (2018) Distribution of Diffusion Times Determined by Fluorescence (Lifetime) Correlation Spectroscopy. Macromolecules 51:2796–2804 . https://doi.org/10.1021/acs.macromol.7b02158

[34] Moussa A, Trombotto S (2016) Octanoic Hydrazide-Linked Chitooligosaccharides-2,5-Anhydro-d-Mannofuranose. Molbank 2016:M904 . https://doi.org/10.3390/M904

[35] Chapelle C, David G, Caillol S, Negrell C, Durand G, Desroches le Foll M, Trombotto S (2019) Water-Soluble 2,5-Anhydro-D-mannofuranose Chain End Chitosan Oligomers of a Very Low Molecular Weight: Synthesis and Characterization. Biomacromolecules 20:4353–4360 . https://doi.org/10.1021/acs.biomac.9b01003

[36] Refractive increment data-book for polymer and biomolecular scientists. Nottingham : Nottingham University Press

[37] Christie RJ, Miyata K, Matsumoto Y, Nomoto T, Menasco D, Lai TC, Pennisi M, Osada K, Fukushima S, Nishiyama N, Yamasaki Y, Kataoka K (2011) Effect of Polymer Structure on Micelles Formed between siRNA and Cationic Block Copolymer Comprising Thiols and Amidines. Biomacromolecules 12:3174–3185 . https://doi.org/10.1021/bm2006714

[38] Albuquerque LJC, Annes K, Milazzotto MP, Mattei B, Riske KA, Jäger E, Pánek J, Štěpánek P, Kapusta P, Muraro PIR, De Freitas AGO, Schmidt V, Giacomelli C, Bonvent J-J, Giacomelli FC (2016) Efficient Condensation of DNA into Environmentally Responsive Polyplexes Produced from Block Catiomers Carrying Amine or Diamine Groups. Langmuir 32:577–586 . https://doi.org/10.1021/acs.langmuir.5b04080

[39] Naito M, Chaya H, Toh K, Kim BS, Hayashi K, Fukushima S, Nagata T, Yokota T, Kataoka K, Miyata K (2021) Structural tuning of oligonucleotides for enhanced blood circulation properties of unit polyion complexes prepared from two-branched poly(ethylene glycol)-block-poly(l-lysine). J Control Release. https://doi.org/10.1016/j.jconrel.2021.01.001

[40] Zalipsky S (1995) Functionalized Poly(ethylene glycols) for Preparation of Biologically Relevant Conjugates. Bioconjug Chem 6:150–165 . https://doi.org/10.1021/bc00032a002

[41] Sonawane SJ, Kalhapure RS, Govender T (2017) Hydrazone linkages in pH responsive drug delivery systems. Eur J Pharm Sci 99:45–65 . https://doi.org/10.1016/j.ejps.2016.12.011

[42] Strand SP, Tømmeraas K, Vårum KM, Østgaard K (2001) Electrophoretic Light Scattering Studies of Chitosans with Different Degrees of *N* -acetylation. Biomacromolecules 2:1310–1314 . https://doi.org/10.1021/bm015598x

Conclusion and Prospects

The aim of this PhD project was to study the interaction between chitosan and siRNA with the idea to develop new approaches for siRNA delivery. Several aspects were addressed concerning the electrostatic interaction itself and the formation of the resulting complexes. The variety of parameters having a role in the formation and stability of the complexes was discussed and some of them were the focus of this work. The formation and colloidal stability of the complexes have been studied using different approaches. The influence of the chitosan chain length on the complexation and colloidal properties of complexes with siRNA was addressed. The approaches developed to enhance the stability were the modification of the acetylation degree of chitosan, the introduction of metallic ions in the formulation and a new approach for the PEGylation of the chitosan.

The first study of the thesis was devoted to the role of the chitosan chain length on a variety of properties. For this purpose, N-deacetylated chitosan oligosaccharides (COS) with different degree of polymerization were synthesised based on the depolymerization of a fully deacetylated chitosan presenting a high molar mass. The precise control of this process led to a library of COS varying in degree of polymerization (DP) and presenting a good dispersity. First, the properties of the COS chains alone in solution were investigated in terms of solubility and electrostatic properties in relation with the pH of the solution. It was found that the length of the COS chains plays a critical role on the solubility properties. Mainly, the shorter the COS chain, the higher the pH where chitosan begins to precipitate. This is related to the protonation state of chitosan where the pK_a of chitosan decreases as the chain length increases. More generally, the electrostatic properties of chitosan vary with the chain length, as seen from the complexing behaviour of chitosan with siRNA under conditions of full protonation (pH = 4). Indeed, it was found that the binding affinity of COS for siRNA increased sharply between DP5 and DP13 and that, on the other hand, the pK_a of COS decreased just as abruptly between the same DP values. This has been attributed to the existence of a critical DP in which electrostatics plays a major role, resulting in important repulsions between neighboring charged residues (increase of the pK_a) and a strong interaction with the oppositely charged siRNA. However, it was evidenced that despite good complexation properties, short COS chains should have a minimum chain length in order to provide good stability to the complexes.

Metallic ions were used to strengthen the interaction between chitosan and siRNA at physiological pH where chitosan is almost unprotonated. Unexpected cytotoxicity data obtained for this type of complexes has led us to better understand the interaction between

siRNA and metallic ions, Mg(II), Zn(II), Fe(II) and Fe(III). It led to investigations at the molecular and colloidal level. Two types of interactions were evidenced depending on the divalent cation studied. An electrostatic interaction and an interaction of the coordinating type, the first type involving the charged phosphate groups of the siRNA whereas the second, the nucleobases. The electrostatic interaction between the divalent cations and the phosphate groups seemed to be present for all the ions studied whereas the second varying in intensity was almost not observed with Mg(II). Electrostatic interactions with the phosphate groups were evidenced by thermal stability measurements and infrared spectroscopy. The interaction of metal ions with nucleobases leads to the formation of colloidal structures observable by DLS and AFM. Limited-size clusters of siRNA were formed in the presence of the divalent ions, Zn^{2+} and Fe^{2+} and where related to their relative affinity with the nucleobases. For example, a higher concentration of Zn^{2+} ions was needed to aggregate siRNA into clusters whereas only a small amount of Fe^{2+} ions lead to this aggregation phenomena. The affinity of the cations with the bases was evidenced by ethidium bromide displacements and infrared spectroscopy. A metallic form of the siRNA, the so-called 'M-form', was attributed to the A-type structure conserved in presence of Zn(II).The presence of the annealing buffer, Tris-HCl with the siRNA resulted in infrared spectrum with an important number of signals. The removal of this buffer by a dialysis step would allow a better allocation of the IR bands to the siRNA functions and more reliable interpretation of their changes in presence of metal ions.

The introduction of zinc ions in the formulation of colloidal polyelectrolyte complexes between chitosan and siRNA was considered to enhance the stability properties of the complexes in physiological conditions. In particular, the challenge tackled with this new formulation pathway was the stability at physiological pH and salt concentration. For this purpose, the interaction between zinc and chitosan was studied by means of potentiometric titrations, infrared spectroscopy and light scattering experiments. It was found by potentiometry that complexes of the form [Zn(-NH_2)] were formed during the deprotonation of the chitosan with the maximal amount of glucosamine residues involved at pH = 6. The solubility of chitosan at high pH was enhanced by its interaction with zinc ions. Moreover, this effect was also visible with a conservation of the cationicity for the same chitosans of low DA at increased pH. In a second part, efforts were made to improve the stability of the chitosan-siRNA complexes under physiological pH and ionic strength. This led to the observation that the stability could be increased at physiological ionic strength thanks to the increase of the DA of chitosan. The stability at physiological pH was tackled by the introduction of the zinc ions. The chelation of zinc ions by chitosan preserved the interaction with siRNA and the stability of the complexes at physiological pH. The chitosans used in this study varied in molar mass and DA. A deeper investigation of the role of these two parameters

on the complex stability in presence of zinc ions could allow to better understand the interaction at play and how to improve the long-term stability of complexes in PBS buffer or biological media.

A new synthetic pathway taking advantage of the reducing end of chitosan after its depolymerization by nitrous acid was investigated. PEG hydrazide could be successfully coupled through reductive amination to the very reactive reducing end, with conversions up to 90%. However, the procedures investigated for the purification of the synthesised copolymer led to residual free COS in the final product. Nonetheless, the complexation of the copolymer with siRNA was studied. Complexes having a conjugate-like morphology were obtained with copolymers having a chitosan block of DP 13 to 27 and a PEG block of 5 kDa. Copolymer containing shorter PEG blocks led to more aggregated complexes having a morphology of particle. The different structures were mainly characterized by dynamic light scattering and fluorescence correlation spectroscopy. The purification of the copolymer containing a short cationic block was not entirely solved in this thesis. However, several leads can be considered to improve this purification. Mainly, the decrease of the initial dispersity of COS blocks and the increase of the PEG length should provide a better separation between the copolymer and the unreacted COS. In any case, the use of preparative SEC would be recommended to obtain COS-*b*-PEG copolymers of low dispersity containing a short block of COS (DP < 30) without any trace of free COS.

Appendix

Chapter 2 supporting information

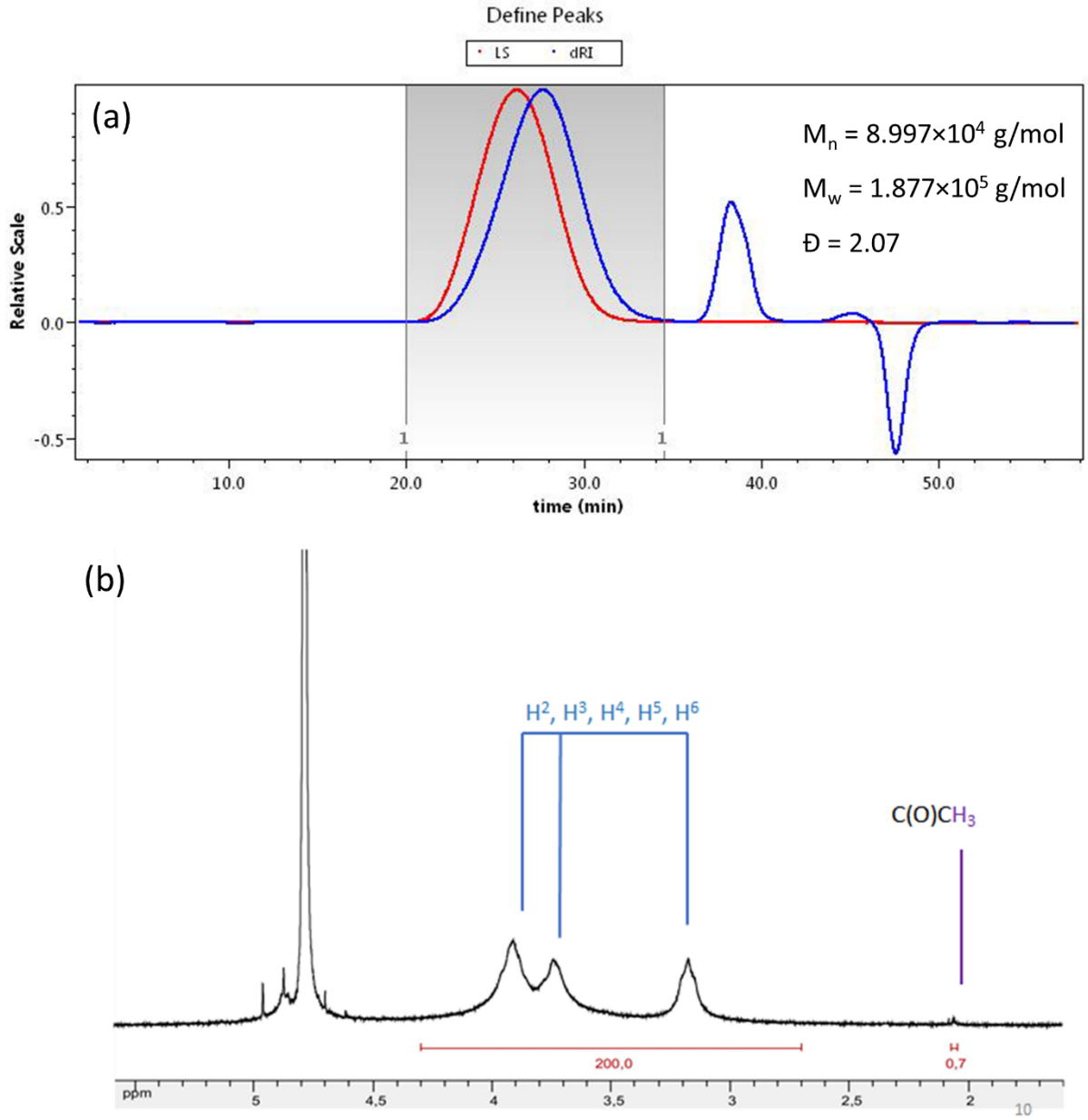

Figure appendix 1. (a). SEC-MALLS analysis of the starting chitosan with a light scattering detection (red) and a differential refractometer (blue). (b) ^{1}H NMR analysis of the starting chitosan in D_2O.

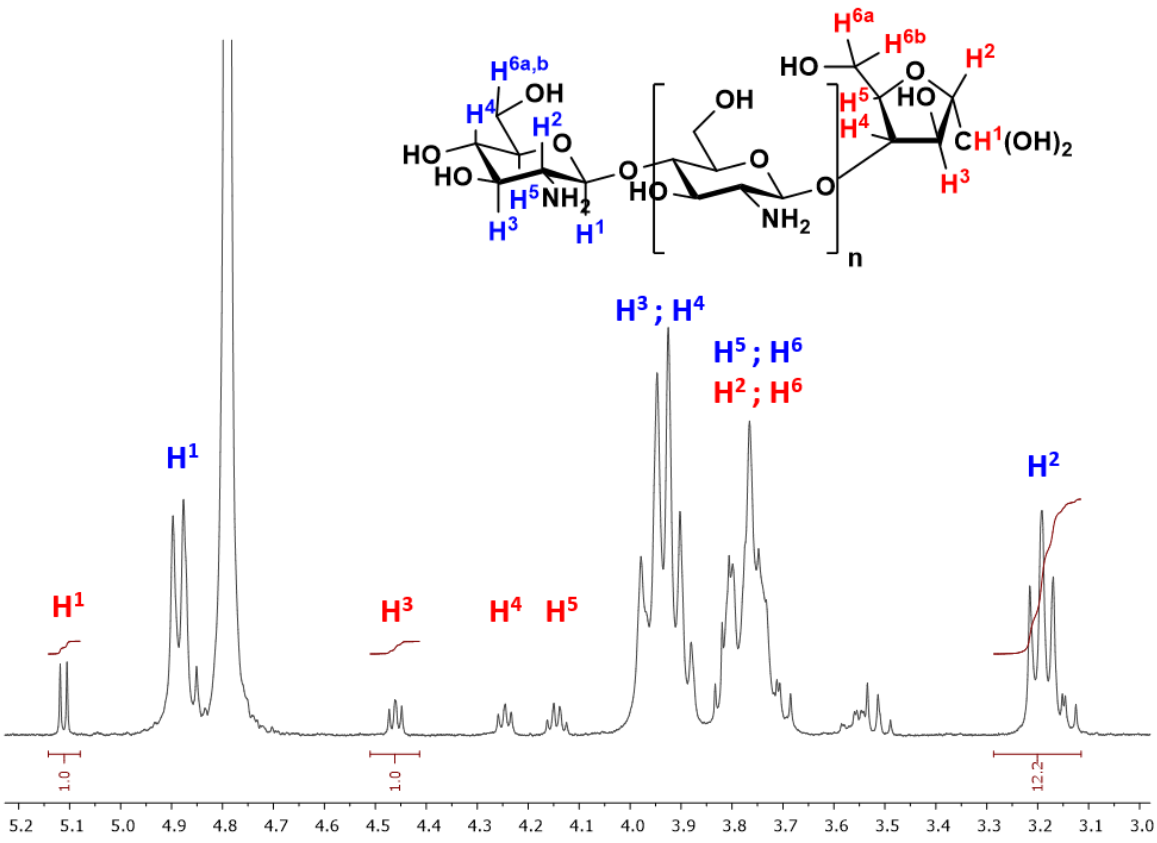

Figure appendix 2. ^{1}H NMR analysis of the COS-13 (hydrochloride form) in D_2O.

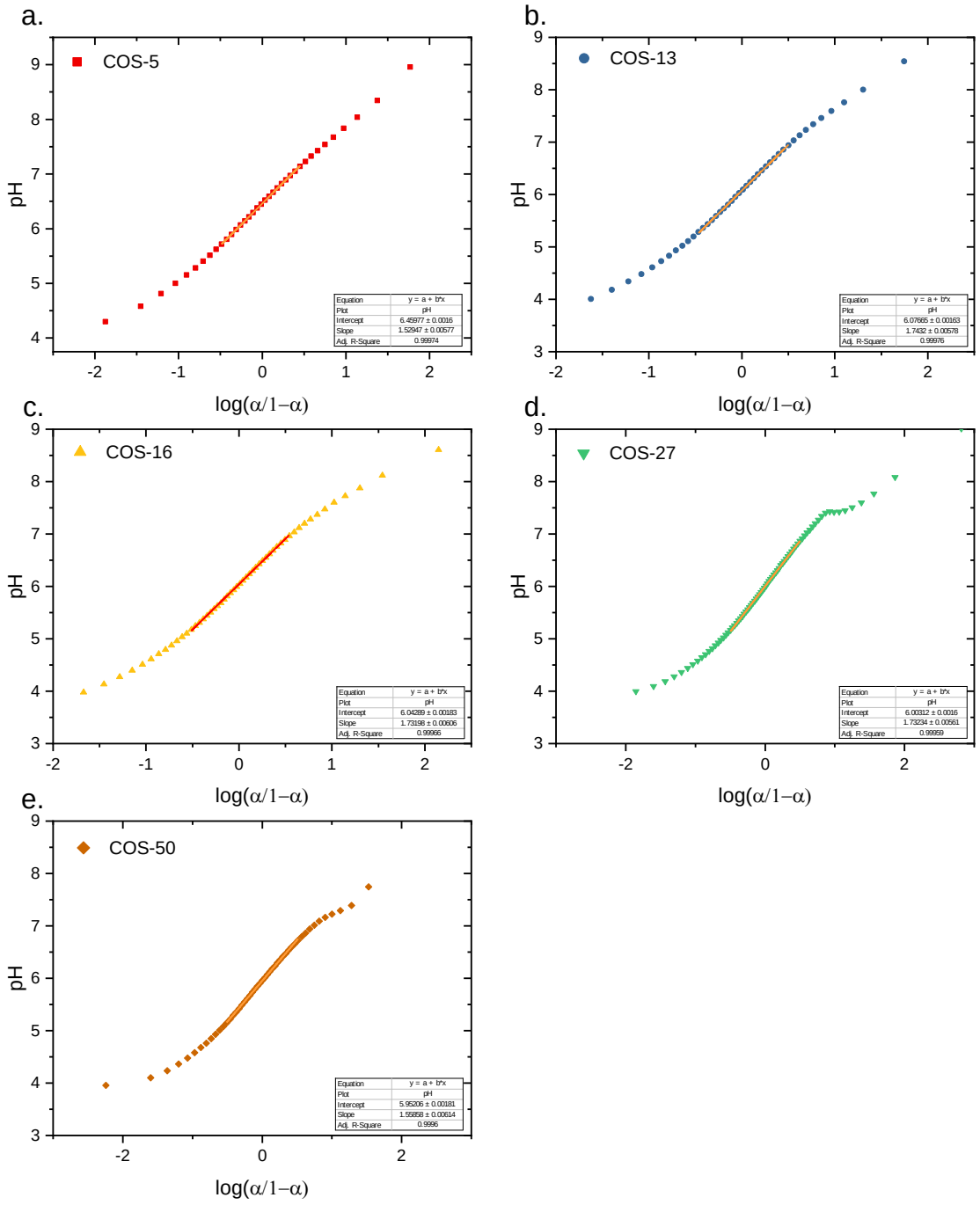

Figure appendix 3. Determination of the $pK_{1/2}$ and n values of the extended Henderson-Hasselbalch equation, $pH = pK_{1/2} + n \log [\alpha/(1- \alpha)]$ from a linear regression in the interval $-0.5 < \log [(\alpha/(1- \alpha)] < 0.5$.

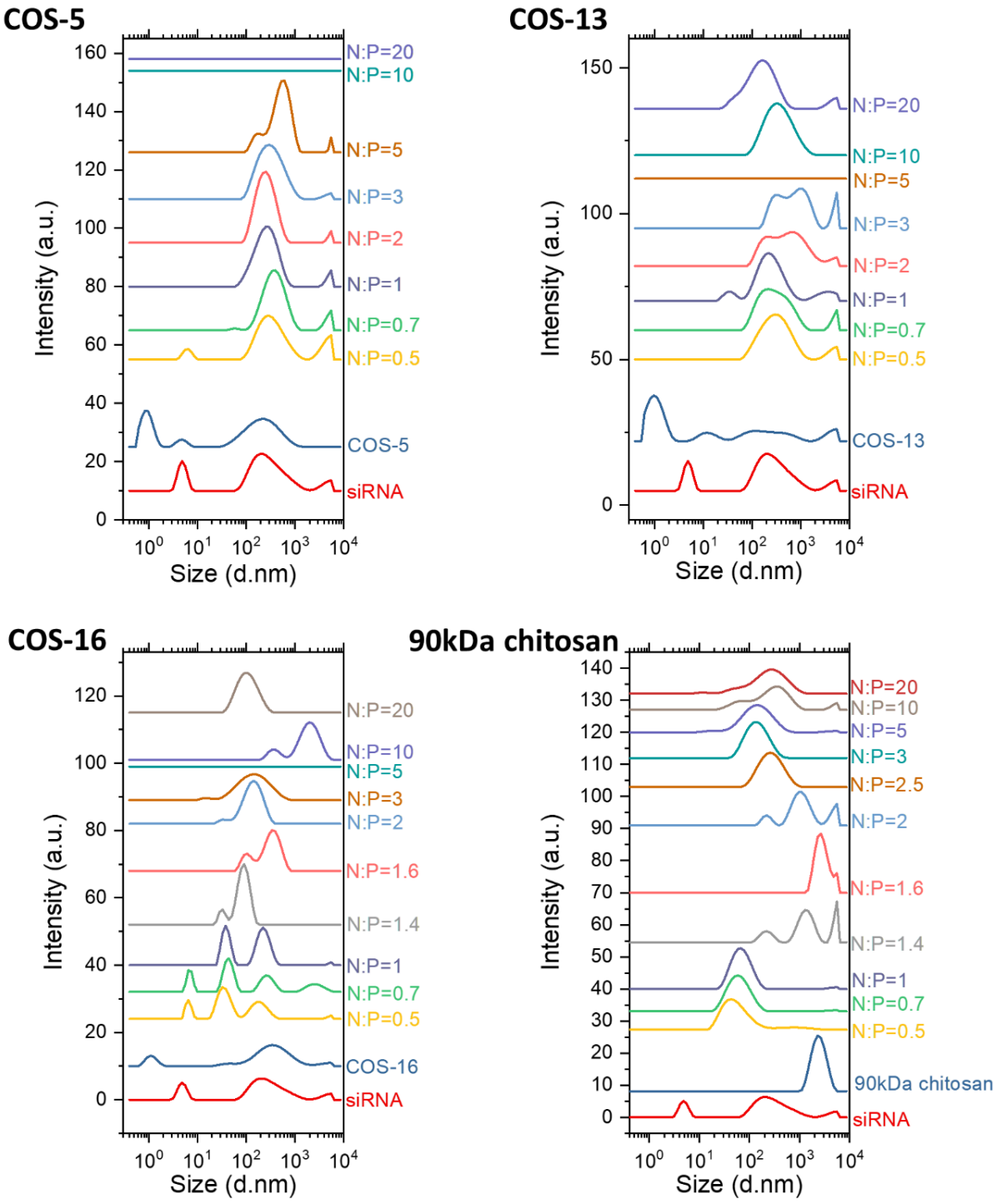

Figure appendix 4. Intensity-average particle size distributions of COS/siRNA complexes in RNase-free water by dynamic light scattering with a 173° angle detection at various N:P ratios using a siRNA concentration of 0.1 g/L. Complexes were prepared by fast addition of the polyelectrolyte in default (COS for N:P < 1, siRNA for N:P > 1). Note that the sizes of the aggregates are out of range for COS-5 at N:P = 10 & N:P = 20 and for COS-13 at N:P = 5.

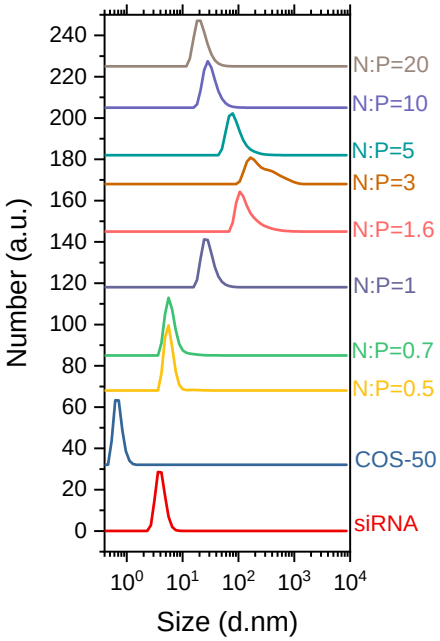

Figure appendix 5. Number-average particle size distributions of COS-50/siRNA complexes by dynamic light scattering with a 173° angle detection at various N:P ratios using a siRNA concentration of 0.1 g/L. Complexes were prepared by fast addition of the polyelectrolyte in default (COS for N:P < 1, siRNA for N:P > 1).

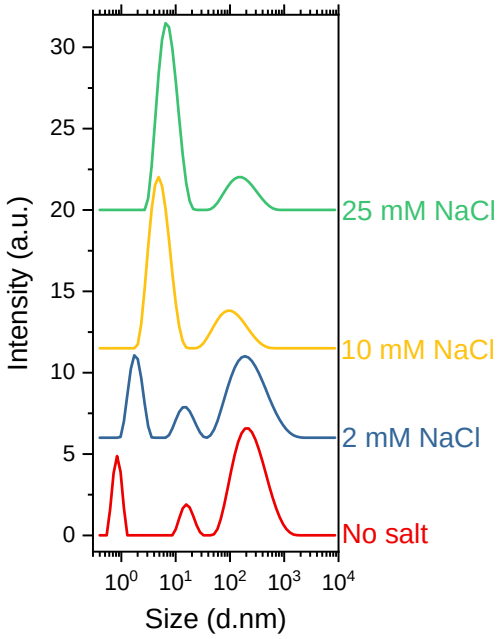

Figure appendix 6. Intensity-average size distributions of COS-50 (hydrochloride form) in presence of various amounts of salt by dynamic light scattering with a 173° angle detection. The COS concentration is 1 g/L.

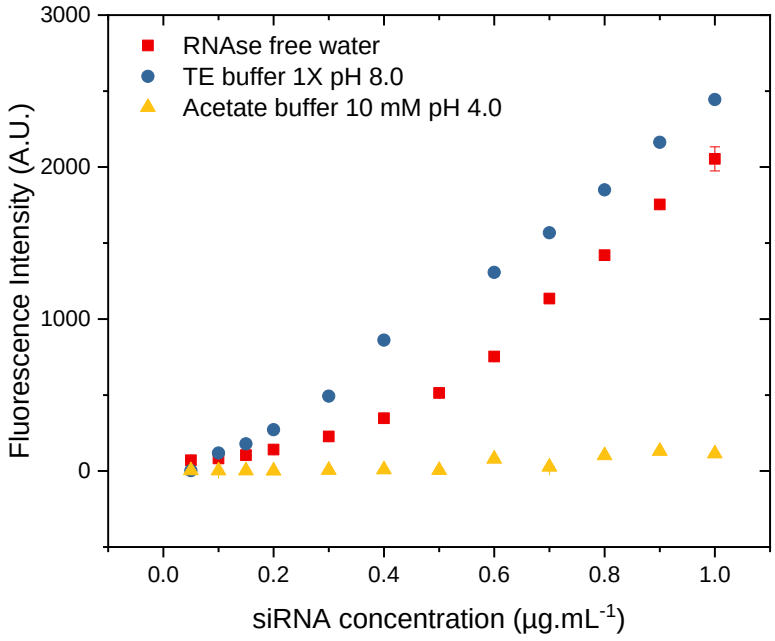

Figure appendix 7. siRNA assay with RiboGreen in various solvent conditions (λ_{ex} = 480 nm, λ_{em} = 520 nm).

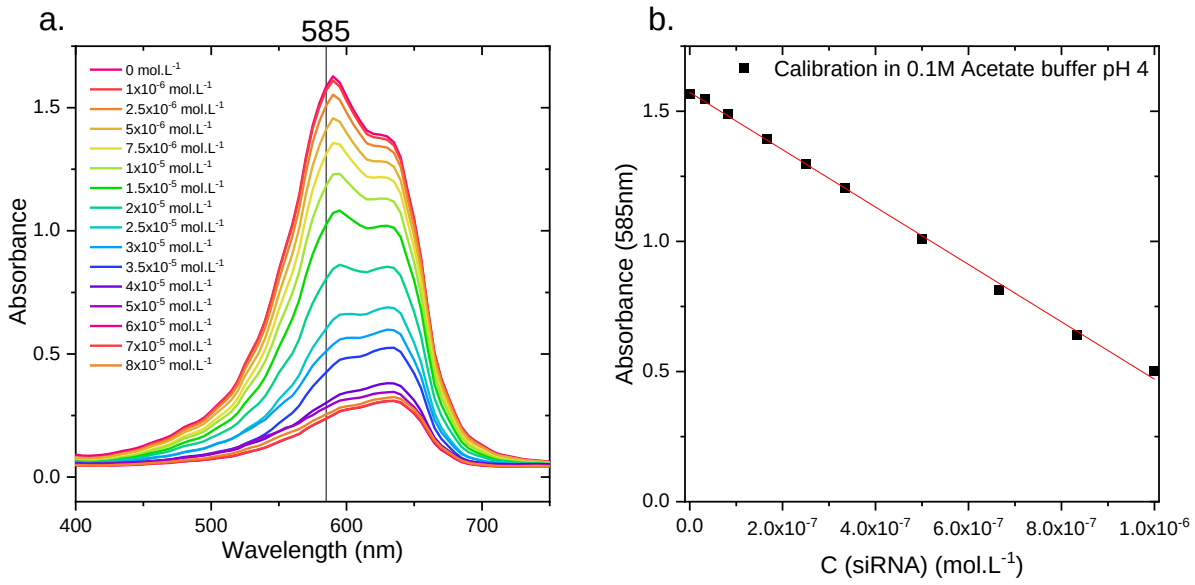

Figure appendix 8. siRNA assay in 0.1 M acetate buffer pH 4.0 in presence of excess Toluidine Blue (TB). a) Overlay of the absorbance spectra of the supernatants after centrifugation of the siRNA/TB dispersions. b) Calibration curve of siRNA with TB at λ = 585 nm.

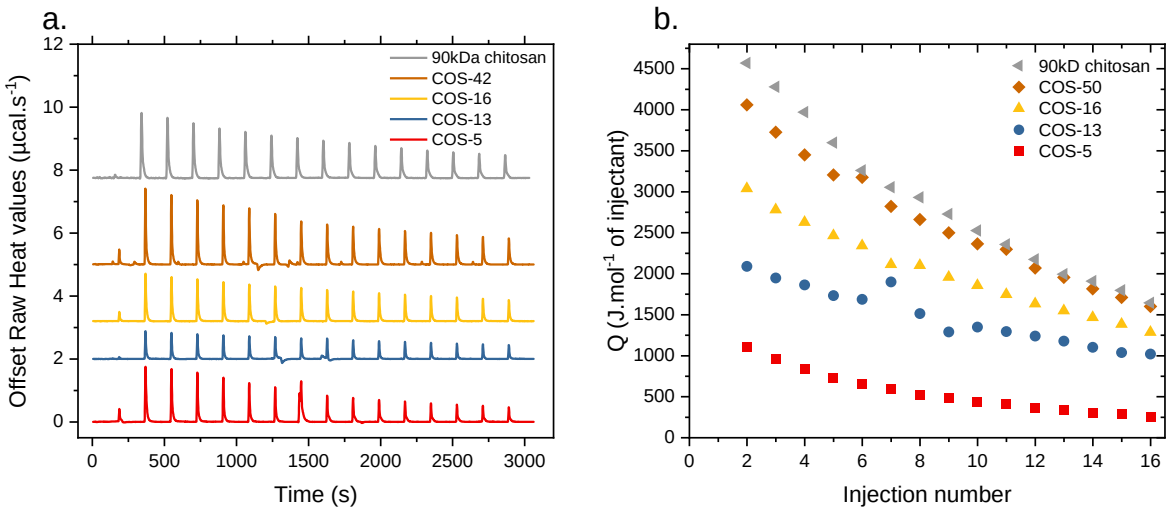

Figure appendix 9. Heat flow per injection versus time (a) and integrated heats (b) for the isothermal dilution of COS varying in DP in 10 mM acetate buffer pH 4.5.

ITC modelling

With the exception of the parent chitosan of 90 kDa presenting a classical sigmoidal ITC isotherm, the COS of lower DP (5, 13, 16, 50) showed a more or less pronounced exothermic peak before the equivalency. A second aggregative process hindering/counterbalancing the classical ion-pairing process should then be assumed to rationalize these titration experiments. Following the approach put forward recently by Vitorazi et al. [1], the heat exchange

measured during the complexation of the COS with siRNA was considered to be the sum of two distinct contributions, $\Delta H_{IP}(Z, n_{IP}, r_{IP})$ for the electrostatic ion pairing process and $\Delta H_{Agg}(Z, n_{Agg}, r_{Agg})$ for the aggregation process, with both contributions being of the form of equation 1 derived from the Multiple Non-Interacting Sites (MNIS) model [2, 3]:

$$\Delta H(Z, n, r) = \frac{1}{2}\Delta H_b \left(1 + \frac{n - Z - r}{\sqrt{(n + Z + r)^2 - 4Zn}}\right) \quad (1)$$

This approach supposes that the siRNA to be titrated have several anchoring sites to which COS can bind with a probability independent of the rate of occupation of the other sites on the same siRNA molecule. The complexation between siRNA and COS comes then with either an absorption or a release of heat proportional to the amount of binding. The reaction is characterized by a binding constant K_b, a binding enthalpy ΔH and a reaction stoichiometry n. In equation 1, $r = 1/K_b[M]$ with $[M]$ the molar concentration of siRNA and Z the N:P ratio. It is then assumed that the total enthalpy change during titration can be written as:

$$\Delta H(Z) = \Delta H_{IP}(Z, n_{IP}, r_{IP}) + \alpha(Z)\Delta H_{Agg}(Z, n_{Agg}, r_{Agg}) \quad (2)$$

where the function $\alpha(Z)$ is the fraction of the aggregate phase at Z. $\alpha(Z)$ is considered to be of the form: $\alpha(Z) = \left(1 + exp\left((Z - Z_0)/\sigma\right)\right)^{-1}$ which corresponds to a step function centered at Z_0 and of lateral extension σ (with $Z_0 = n_{IP}$ and $\sigma = 0.3$ for all isotherms). The isotherm of the parent chitosan showing a classical sigmoidal variation, the binding enthalpy was fitted with a unique ion pairing process. For the chitosans of lower DPs, the two-step model was used in order to take into account the aggregation process superimposed on the ion-pairing process.

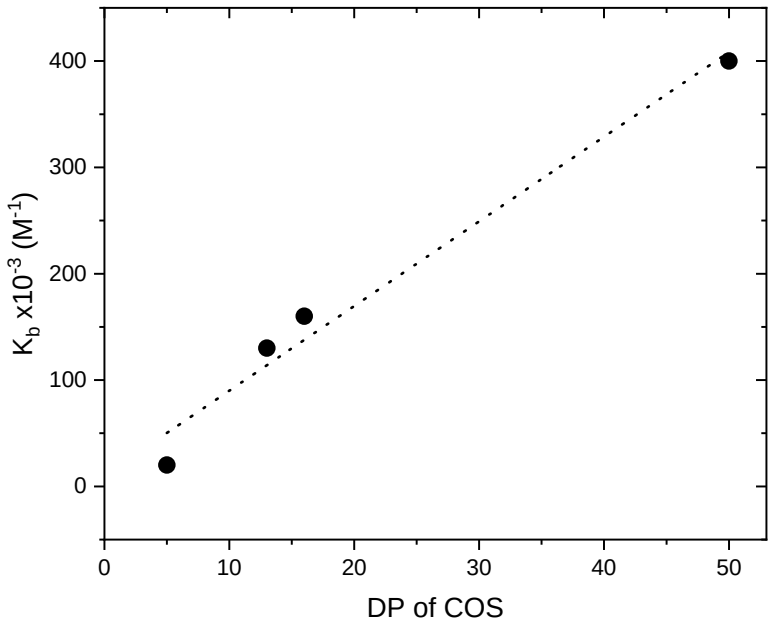

Figure appendix 10. Binding constant related to the ion pairing as function of the DP of COS (from data in

Table 2.4.3). The dotted line was plotted to guide the eye.

References

[1] Vitorazi L, Ould-Moussa N, Sekar S, Fresnais J, Loh W, Chapel J-P, Berret J-F (2014) Evidence of a two-step process and pathway dependency in the thermodynamics of poly(diallyldimethylammonium chloride)/poly(sodium acrylate) complexation. Soft Matter 10:9496–9505 . https://doi.org/10.1039/C4SM01461H

[2] Pierce MM, Raman CS, Nall BT (1999) Isothermal Titration Calorimetry of Protein–Protein Interactions. Methods 19:213–221 . https://doi.org/10.1006/meth.1999.0852

[3] Wiseman T, Williston S, Brandts JF, Lin L-N (1989) Rapid measurement of binding constants and heats of binding using a new titration calorimeter. Anal Biochem 179:131–137 . https://doi.org/10.1016/0003-2697(89)90213-3

Chapter 4 supporting information

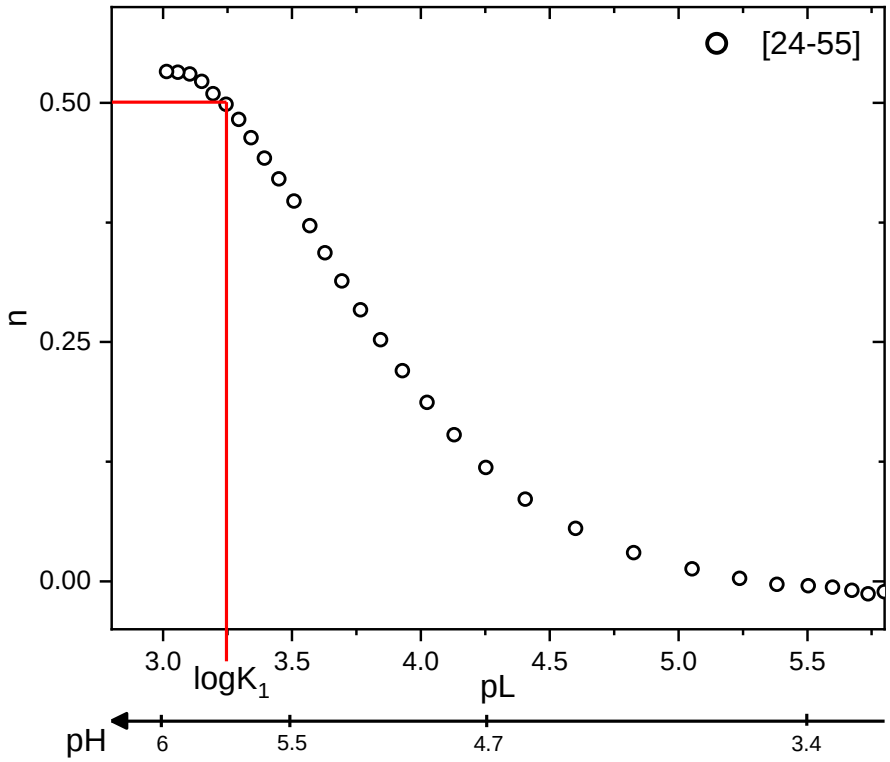

Figure appendix 11. Determination of complexation constant between glucosamine residues and Zn^{2+} from interpolation of pL at half n values. Example given for the chitosan [24-55].

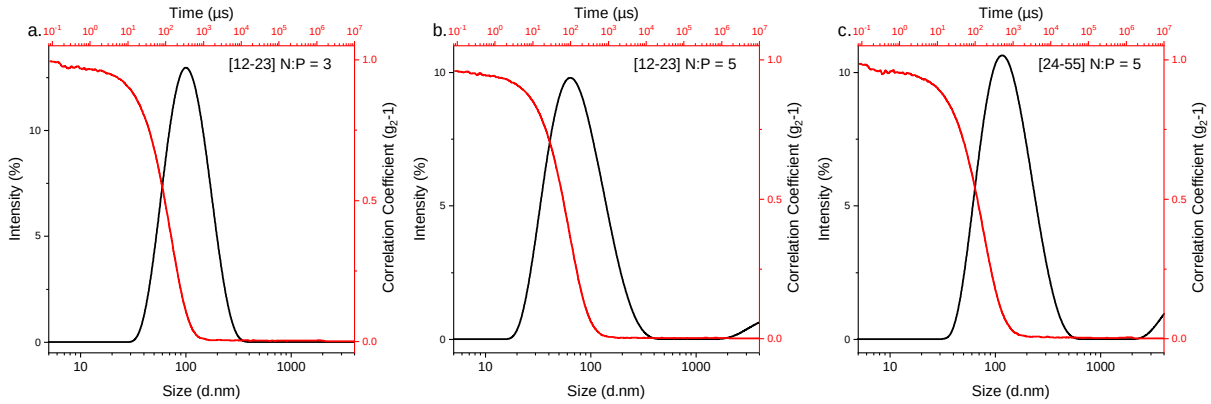

Figure appendix 12. Intensity-averaged size distributions (D_h in nm) and correlation data of polyplexes obtained with (a) Chitosan [12-23] at a ratio N:P = 3, (b) Chitosan [12-23] at a ratio N:P = 5 and (c) Chitosan [24-55] at a ratio N:P = 5.

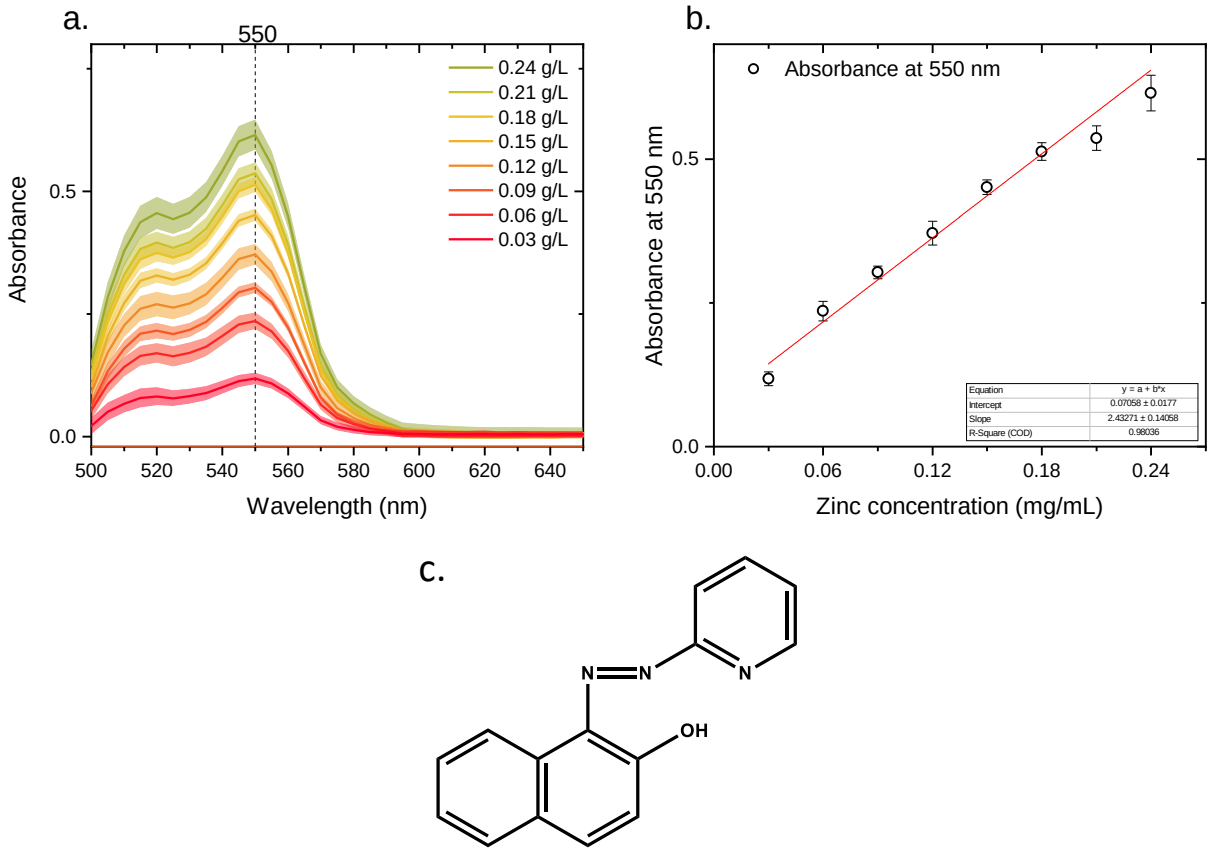

Figure appendix 13. Calibration realised with 1-(2-pyridylazo)-2-naphthol (PAN). (a) Absorbance spectrum between 500 and 650 nm at various zinc concentrations for a fixed PAN concentration. (b) Calibration obtained from the absorbance measured at 550 nm. (c) Chemical structure of PAN.

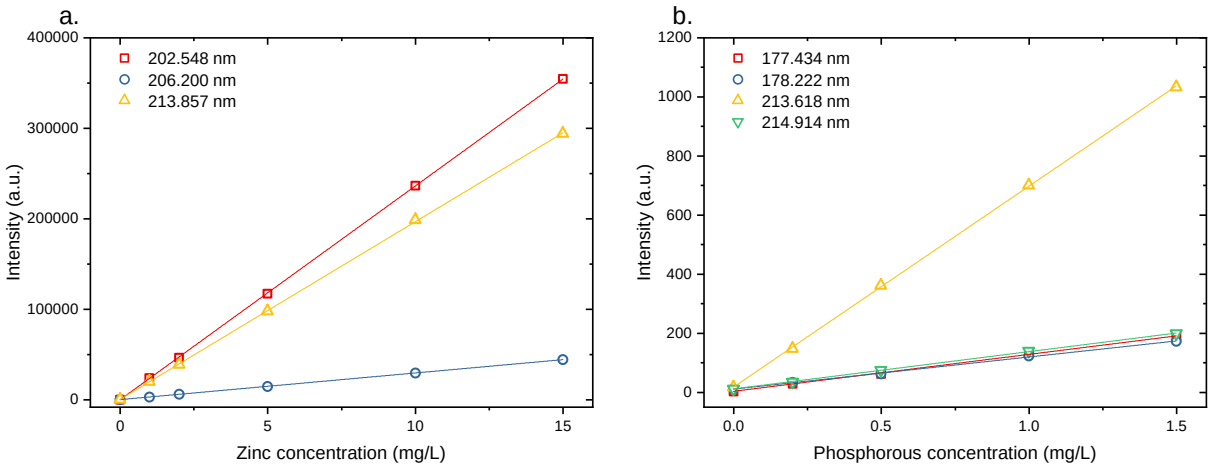

Figure appendix 14. Calibration curves obtained for ICP-EOS measurements for (a) Zinc and (b) Phosphorous.

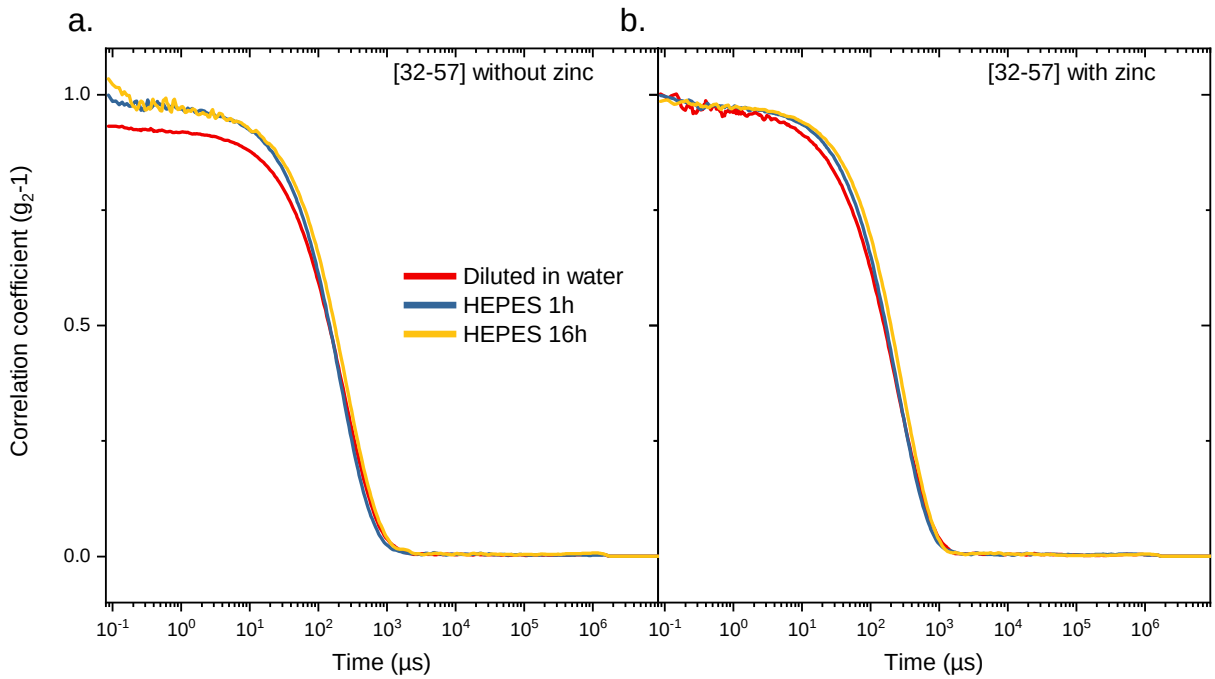

Figure appendix 15. Correlation data of the polyplexes formed with [32-57] and diluted in water (red) or incubated in HEPES for 1h (blue) and 16h (yellow). (a) Polyplexes formulated without zinc and (b) Polyplexes formulated with zinc.

Chapter 5 supporting information

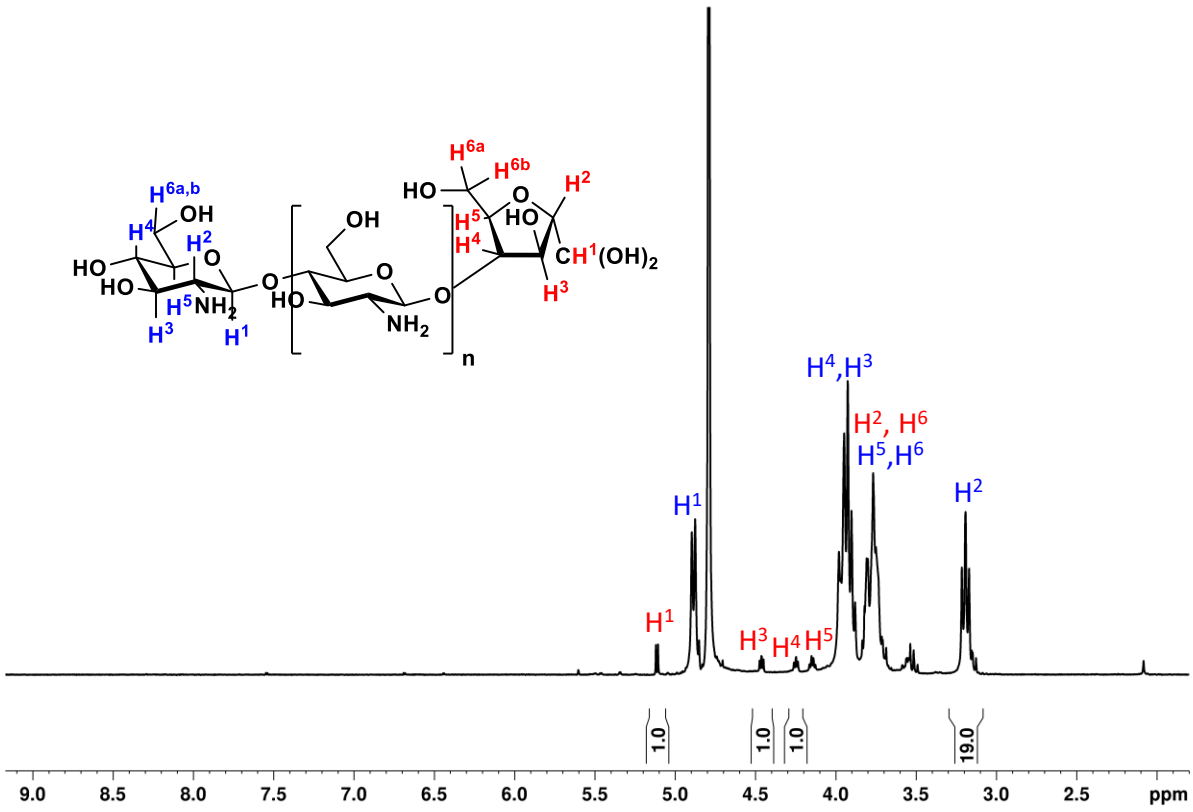

Figure appendix 16. ^{1}H NMR spectrum of the initial COS20 (D_2O, 400 MHz, 298K).

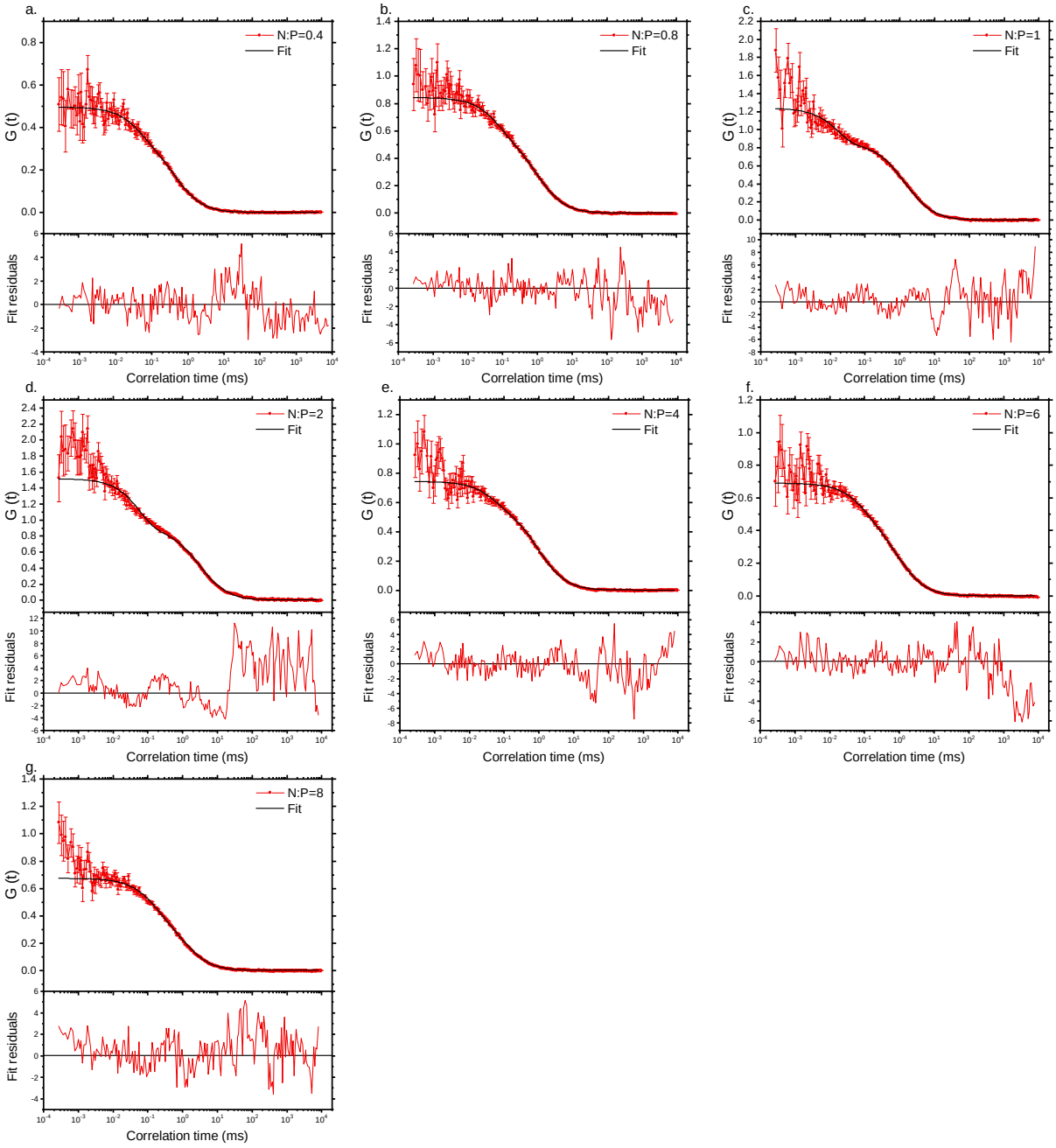

Figure appendix 17. Autocorrelation data (red) and corresponding fits (black) from FCS measurements performed at various N:P ratios with a COS20-*b*-PEG5k. a) N:P = 0.4, b) N:P = 0.8, c) N:P = 1, d) N:P = 2, e) N:P = 4, f) N:P = 6 and g) N:P = 8.

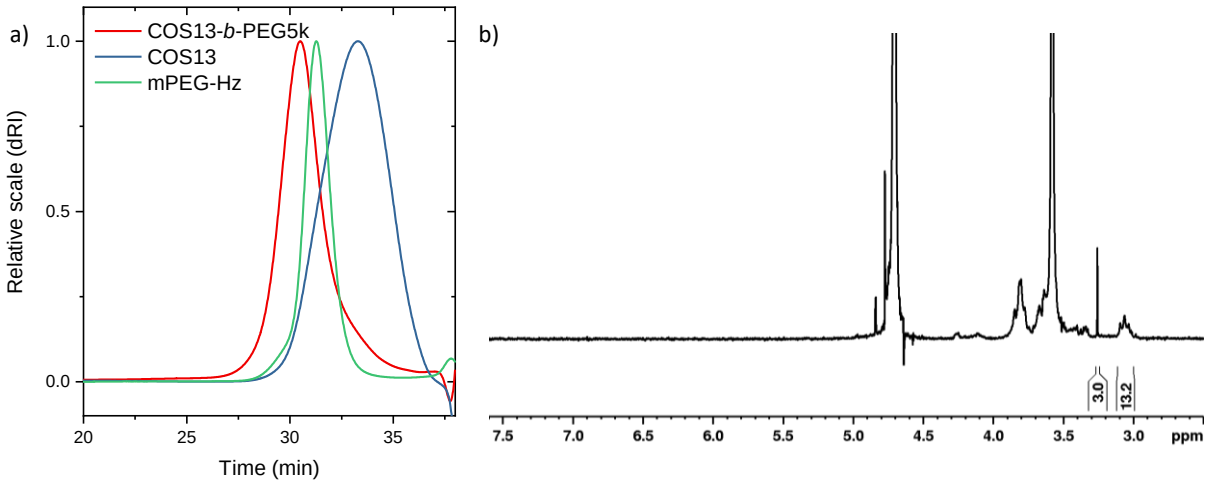

Figure appendix 18. Characterisation of the COS13-*b*-PEG5k. a) Chromatograms (dRI trace) of the copolymer (red) and the starting blocks: COS13 (blue) and mPEG-Hz (green). (Tosoh G6000Pwxl and G2500Pwxl columns, acetate buffer pH 4.5). b) ^{1}H NMR spectrum of the final copolymer. The integral of the methyl group at the PEG chain end is set to 3. (D_2O, 400 MHz, 298 K).

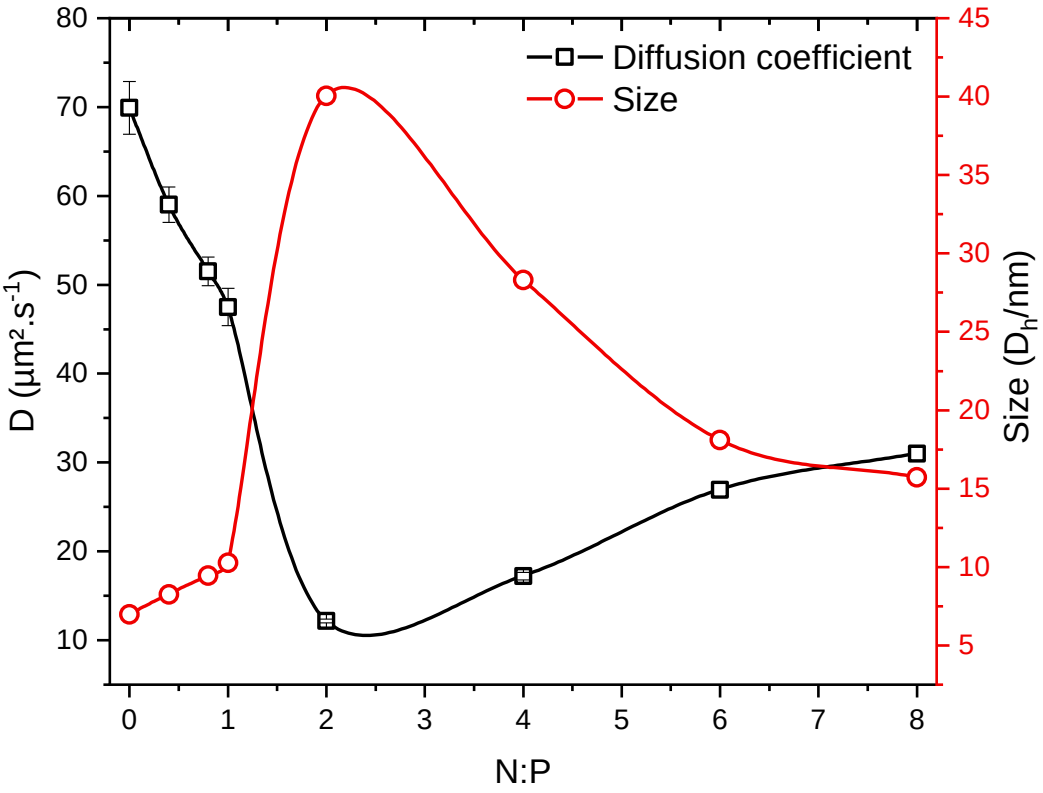

Figure appendix 19. Variation of the diffusion coefficient of the siRNA-Cy5.5 with increasing amounts of COS13-*b*-PEG5k (increasing N:P ratios) (black) and corresponding sizes (hydrodynamic diameter) (red).

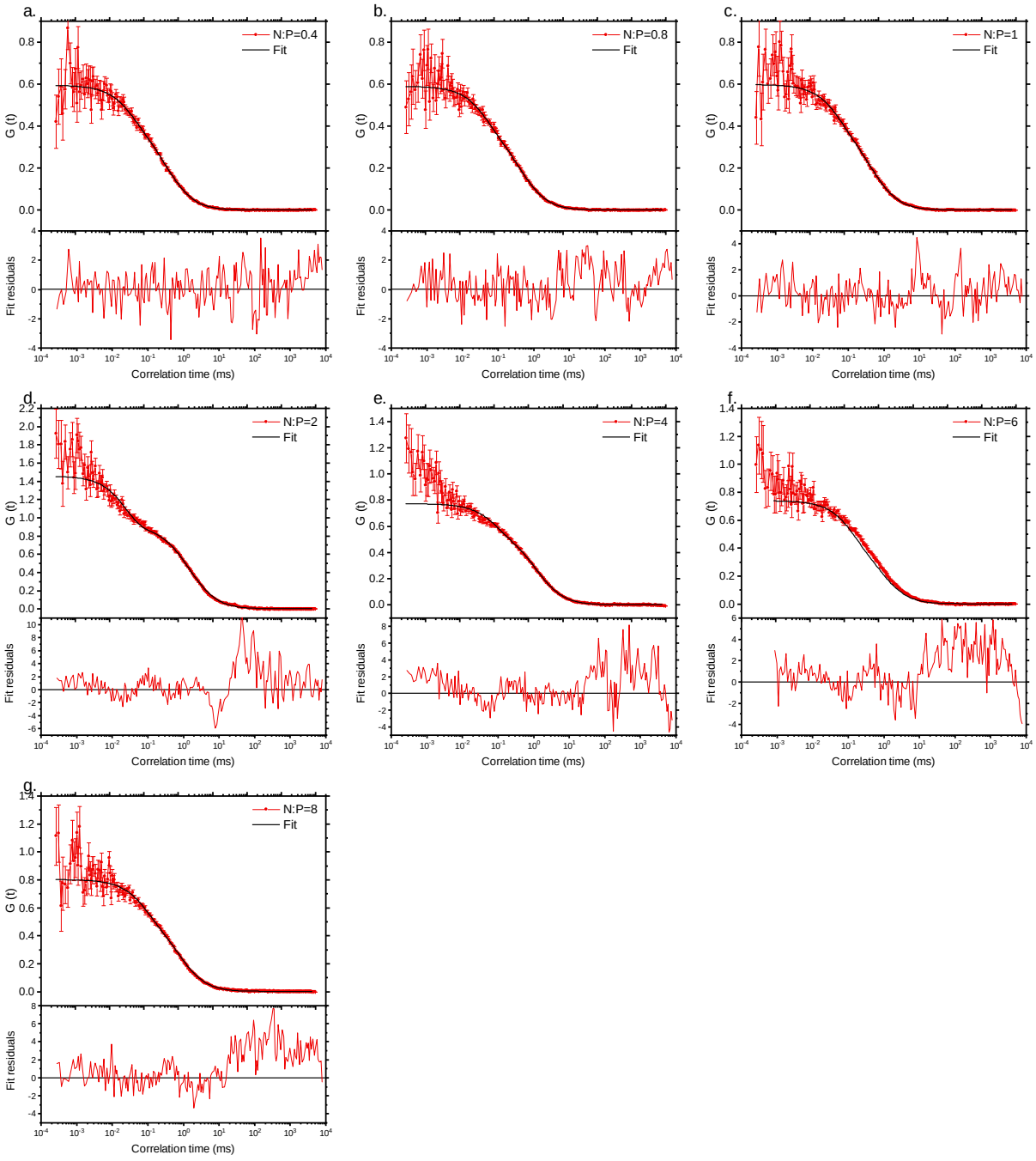

Figure appendix 20. Autocorrelation data (red) and corresponding fits (black) from FCS measurements performed at various N:P ratios with a COS13-*b*-PEG5k. a) N:P = 0.4, b) N:P = 0.8, c) N:P = 1, d) N:P = 2, e) N:P = 4, f) N:P = 6 and g) N:P = 8.

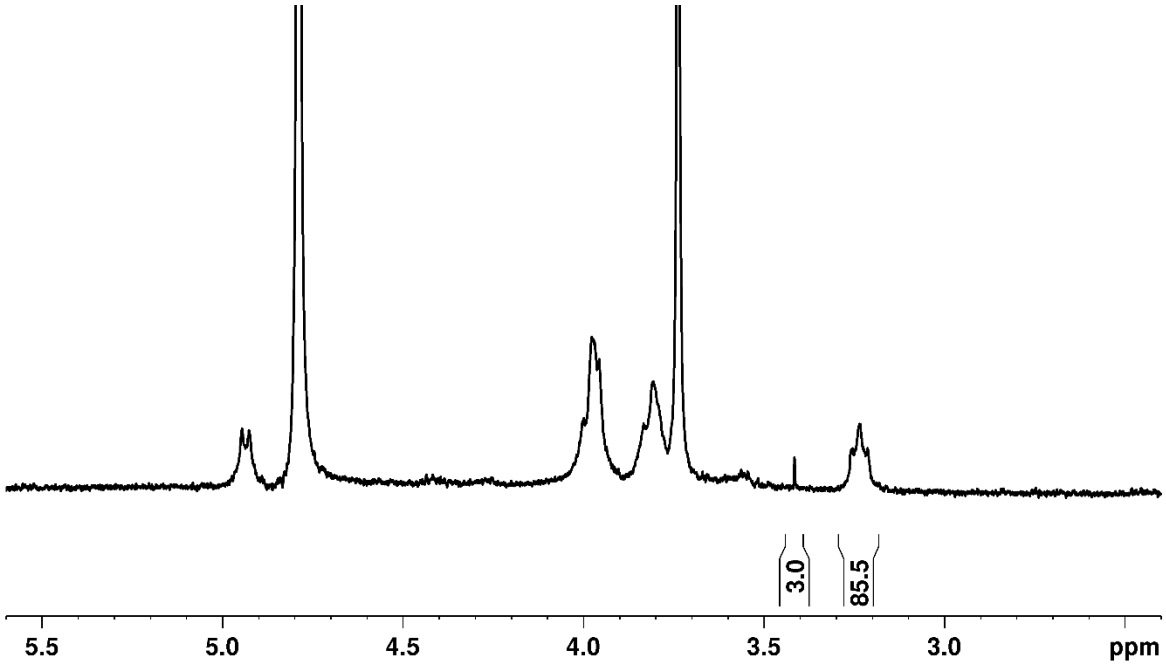

Figure appendix 21. ^{1}H NMR spectrum of the fraction A13 (D_2O, 400 MHz, 298K).

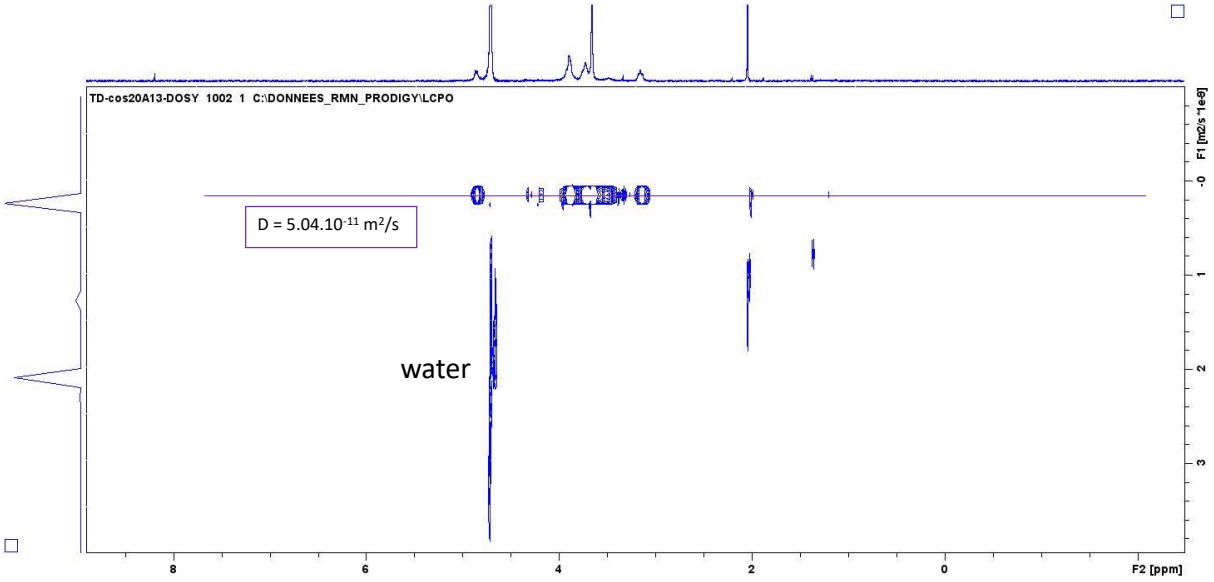

Figure appendix 22. DOSY NMR spectrum of the fraction A13 and determination of the main diffusion coefficient.

Titre : Formulation et stabilisation de complexes de polyélectrolytes à base de chitosane et de siRNA

Résumé : La présence de fortes interactions électrostatiques entre les acides nucléiques tel que l'ADN, l'ARN et des polycations permet l'élaboration de particules colloïdales appelées complexes de polyélectrolytes (PECs). Cette approche permettant la formation de vecteurs non-viraux pour la délivrance de matériel génétique a fait l'objet de nombreuses études basées sur l'utilisation de chitosane comme polycation. Dans le cadre de cette thèse, ce dernier a été étudié pour ses propriétés de complexation avec des petits ARN interférents (small interfering RNA, siRNA).

Dans un premier temps, des oligosaccharides de chitosane (COS) ont fait l'objet d'une étude quant à leurs propriétés en solution et de complexation avec des siRNA. L'effet de longueur de chaîne sur la solubilité du chitosane et leur comportement complexant a pu être étudié. Par la suite, la stabilité colloïdale en conditions physiologiques des PECs formés à partir de chitosane et de siRNA a été abordée. La déprotonation du chitosane étant un élément rédhibitoire quant à la stabilité des complexes, l'introduction d'ions zinc lors de la formulation des complexes a permis une amélioration de la stabilité à pH physiologique. De plus, l'augmentation du degré d'acétylation du chitosane a également permis une nette amélioration de la stabilité des complexes à des concentrations physiologiques en sel. Avec l'introduction de zinc, une étude portant sur les interactions entre des ions métalliques et le siRNA a également été menée. Finalement, une nouvelle synthèse menant à la formation d'un nouveau copolymère à base de chitosane a été réalisée, permettant d'obtenir des structures encore inexplorées à base de chitosane telles que des micelles ou des structures de type conjugués.

Mots clés : chitosane, oligosaccharide, siRNA, interactions électrostatiques, complexes de polyélectrolytes, stabilité colloïdale, conjugué

Title: Formulation and stabilization of colloidal polyelectrolyte complexes of chitosan and siRNA

Abstract: The presence of strong electrostatic interactions between nucleic acids such as DNA, RNA and polycations leads to the formation of colloidal particles called polyelectrolyte complexes (PECs). This approach, which allows the formation of non-viral vectors for genetic material delivery, has been the subject of numerous studies based on the use of chitosan as polycation. In the framework of this thesis, the latter was studied for its complexing properties towards small interfering RNA (siRNA).

First, chitosan oligosaccharides (COS) were studied for their solution properties and complexation properties with siRNA. The effect of chain length on the solubility of chitosan and their complexing behaviour was demonstrated. Subsequently, the colloidal stability of PECs formed between chitosan and siRNA under physiological conditions was addressed. As the deprotonation of chitosan is redhibitory for the stability of the complexes, it was shown that the introduction of zinc ions in the formulation of complexes allowed to improve their stability at physiological pH. Moreover, the increase in the degree of acetylation of chitosan also allowed a clear improvement in the stability of the complexes at physiological salt conditions. With the introduction of zinc, a study of the interactions between metal ions and siRNA was also carried out and was able to highlight the strong interactions involved between metal ions and siRNA. Finally, a new synthesis leading to the formation of a new chitosan-based copolymer was carried out, making it possible to obtain as yet unexplored chitosan-based structures such as micelles or conjugate-type structures.

Keywords: chitosan, oligosaccharide, siRNA, electrostatic interaction, polyelectrolyte complexes, colloidal stability, conjugates

---

Tim DELAS 2021